Faculty of Engineering
Department of Mechanical Engineering

7th INTERNATIONAL SCIENTIFIC CONFERENCE ON ADVANCES IN MECHANICAL ENGINEERING (ISCAME 2019)
7-9 November, 2019 Debrecen, Hungary

CONFERENCE PROCEEDINGS
(BOOK OF EXTENDED ABSTRACTS)

organized by
Department of Mechanical Engineering
Faculty of Engineering, University of Debrecen
and
Working Commission in Mechanical Engineering
Specialized Committee in Engineering
Regional Committee in Debrecen, Hungarian Academy of Science

Edited by **Tamás MANKOVITS PhD**

Technical editor **Szandra SITKU**

Publisher: **Department of Mechanical Engineering**
Faculty of Engineering
University of Debrecen
2-4 Ótemető str. Debrecen, Hungary
Phone: +36 52 512 900
Web page: https://mecheng.unideb.hu/

ISBN 978-963-490-168-6

CONFERENCE PROCEEDINGS
(BOOK OF EXTENDED ABSTRACTS)

7th INTERNATIONAL SCIENTIFIC CONFERENCE ON ADVANCES IN MECHANICAL ENGINEERING (ISCAME 2019)

7-9 November, 2019

Debrecen, Hungary

Chair of ISCAME 2019

Tamás MANKOVITS, University of Debrecen, Hungary

Scientific Program Committee of ISCAME 2019

Piroska AILER, University of Debrecen, Hungary
†Ágnes BATTÁNÉ GINDERT-KELE, University of Debrecen, Hungary
Sándor BODZÁS, University of Debrecen, Hungary
Gábor BOHÁCS, Budapest University of Technology and Economics, Hungary
István BUDAI, University of Debrecen, Hungary
Levente CZÉGÉ, University of Debrecen, Hungary
Igor DRSTVENSEK, University of Maribor, Slovenia
János Péter ERDÉLYI, University of Miskolc, Hungary
Lajos FAZEKAS, University of Debrecen, Hungary
Csaba GYENGE, Technical University of Cluj-Napoca, Romania
Sándor HAJDU, University of Debrecen, Hungary
György JUHÁSZ, University of Debrecen, Hungary
Gábor KALÁCSKA, Szent István University, Hungary
Ferenc KALMÁR, University of Debrecen, Hungary
Imre KOCSIS, University of Debrecen, Hungary
Ákos LAKATOS, University of Debrecen, Hungary
Daniel LATES, Petru Maior University of Targu Mures, Romania
Stanislav LEGUTKO, Poznan University of Technology, Poland
János LÍSKA, John von Neumann University, Hungary
Zoltán MAJOR, Johannes Kepler University Linz, Austria
József MENYHÁRT, University of Debrecen, Hungary
Ljubica MILOVIC, University of Belgrade, Serbia
Imre Norbert ORBULOV, Budapest University of Technology and Economics, Hungary
Sándor PÁLINKÁS, University of Debrecen, Hungary
Tibor POÓS, Budapest University of Technology and Economics, Hungary
Milan RACKOV, University of Novi Sad, Serbia
Istvánné RÁTHY, Óbuda University, Hungary
Tamás SZABÓ, University of Miskolc, Hungary
Ferenc SZODRAI, University of Debrecen, Hungary
Edit SZŰCS, University of Debrecen, Hungary
György THALMAIER, Technical University of Cluj-Napoca, Romania
Zsolt TIBA, University of Debrecen, Hungary
László TÓTH, University of Debrecen, Hungary
Matej VESENJAK, University of Maribor, Slovenia
Zoltán WELTSCH, John von Neumann University, Hungary
László ZSIDAI, Szent István University, Hungary

Technical Assistance of ISCAME 2019

Szandra SITKU, University of Debrecen, Hungary
Lilla CSONKÁNÉ DÓRÓ, University of Debrecen, Hungary

CONTENTS

THE EFFECT OF BENTONITE ON THE PROPERTIES OF LIGHTWEIGHT EXPANDED CLAY AGGREGATES

ABDELFATTAH Mohamed, KOCSERHA István PhD, GÉBER Róbert PhD
Institute of Ceramic and Polymer Engineering, University of Miskolc
E-mail: madatow@yahoo.com, istvan.kocserha@uni-miskolc.hu, robert.geber@uni-miskolc.hu

Keywords: bentonite, expanded clay, aggregates

Lightweight aggregates (LWA) are one of the most vital materials which, it can be used in the construction and building materials. Lightweight aggregates are produced from natural and synthesized materials. Production of lightweight aggregates in industry is needed to rotary kilns, where the raw materials are fired at temperatures reached up to 1300 ^{o}C [1]. The expansion is the essential factor control on the validity of these aggregates. Chemical analysis was the vital key for defining the expansion of the aggregates. Silica, alumina oxide and total flux are the important oxides that effect on the expansion [2].

This work is focused on studying the effect of firing and bentonite on the physical, and expansion properties and the phases which be formed in the expanded clay minerals. Bentonite was formed by weathering effect on volcanic materials mainly consists of montmorillonite with different compositions of other minerals like quartz, sodium, and calcium feldspar [3]. Bentonite is divided into two types such as, Na-bentonite, which is as high swelling clay while CA-bentonite has less swelling capacity upon hydration with water [4]. From this property the bentonite material can be swelled or expanded. The mineral phase changing is an abundant effect on the physical and mechanical properties of the lightweight aggregates, like, mullite phase can be enhanced the compressive strength of the aggregates after firing [5].

The Expansion properties of the clay samples were measured by heating microscope. The samples were analyzed by XRF and XRD. The bulk density of the clay aggregates was measured according to relating standards. From XRF measured, the three oxides of the different three clay samples existed in the zone of the bloating, so these three samples can be expanded according to Riley [2].

The mineral phases of raw materials were studied by XRD. The mineral phases of the three clay sample were quartz, illite, vermiculite and illite-Montmorillonite group. At 1225 ^{o}C, the mineral phases were studied by XRD. The mineral phases of blue clay sample were quartz, hematite, and anorthite whilst the mineral phases of yellow clay sample were quartz, hematite, anorthite and mullite mineral

The height expansion of the blue clay sample with 0% of bentonite was enhanced to 138% (Fig. 1a), in addition, the height expansion of the yellow clay sample was 122% (Fig. 1a). Besides, the height expansion of the grey sample was 123% (Fig. 1a). Whilst, the height expansion of the blue clay sample with 10% of bentonite was enhanced to 164% (Fig. 1b), in addition, the height expansion of the yellow clay sample was 13% (Fig. 1b). Besides, the height expansion of the grey sample was enhanced to 135% (Fig. 1b).

Table 1 Chemical analysis of the clay samples

Sample	SiO_2, wt%	Al_2O_3, wt%	TF, wt%
B	62.2	17.7	19.3
Y	64.9	17.3	17.4
G	62.9	17.9	18.3

TF: total flux (Fe_2O_3 + MgO + CaO + Na_2O + K_2O); B: blue clay; Y: yellow clay and G: grey clay

The results were showed the changing in the properties and mineral phases of the clay aggreagres after adding the bentonite to the expanded clay aggregates. So, adding 10% of bentonite had great effect on the compressive strength, bulk density and expansion properties of the expanded clay samples. The bulk density of the clay samples without bentonite was lower than 1.2 g/cm^3. Which was started from 0.57 g/cm^3 for blue sample to 1.2 g/cm^3 for yellow sample at 1225°C. Whilst, after adding 10% of bentonite, The bulk density of the clay samples with 10% of bentonite was started from 0.55 g/cm^3 for the blue sample of 0.95 g/cm^3 for yellow sample at 1225°C. So, 10% of bentonite with LWA is crucial values can be decreased the bulk density of the LWA in addition can be increased the height expansion of the aggregates by 5% to20% compared with the values without bentonite.

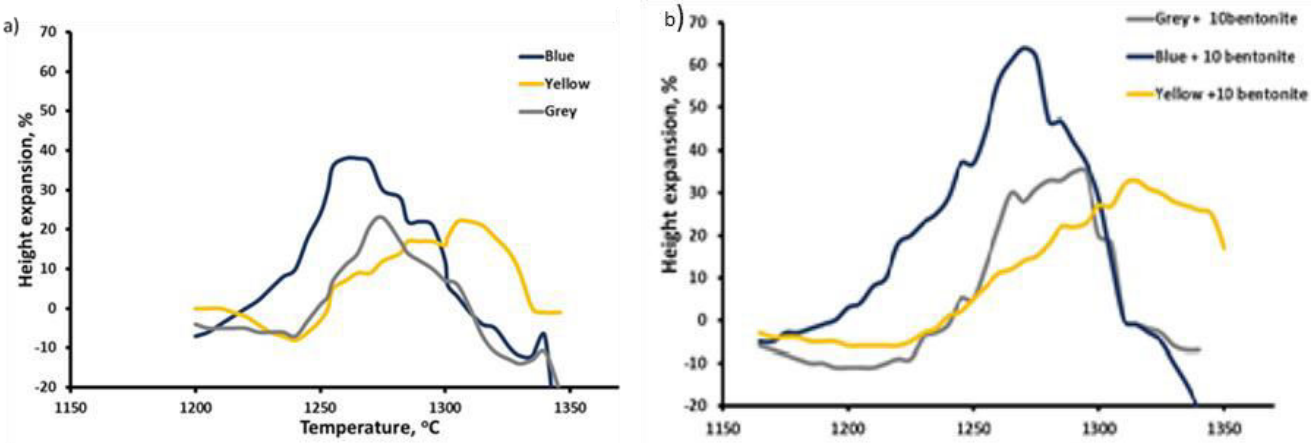

Figure 1. a) The relation between height expansion of clay samples with the temperature before adding bentonite. b) The relation between height expansion of clay samples with the temperature after adding 10% of bentonite

REFERENCES

[1] J. A. Bogas, R. Nogueira, G. A. Nuno, *Influence of mineral additions and different compositional parameters on the shrinkage of structural expanded clay lightweight concrete*, Mater. Des. 56 1039– 1048. 2014.

[2] Riley, C.M.: *Relationship of chemical properties to bloating of clays.* J. Am. Ceram. Soc. 34 121–128. 1951.

[3] B. Abu-Jdayil, *Rheology of sodium and calcium bentonite–water dispersions: effect of electrolytes and aging time*, Int. J. Miner. Process. 98 208–213. 2011.

[4] V. Kelessidis, R. Maglione, *Yield stress of water–bentonite dispersions, Colloids Surf. A Physicochem.* Eng. Asp. 318 217–226. 2008.

[5] M. Abdelfattah, I. Kocserha, R Géber: *effect of firing on mineral phases and properties of lightweight expanded clay aggregates.* XXXIII. microCAD International Multidisciplinary Scientific Conference University of Miskolc, 23-24 May ISBN 978-963-358-177-3 2019.

FUNDAMENTAL CONSIDERATIONS FOR FINITE ELEMENT MODELING OF A POLYURETHANE FOAM JOUNCE

[1]*AL Jweijati Mustafa,* [1,2]*HURI Dávid*
[1]*University of Debrecen, Faculty of Engineering, Department of Mechanical Engineering*
[2]*University of Debrecen, Doctoral School of Informatics*
E-mail: mus.jw1991@mailbox.unideb.hu, huri.david@eng.unideb.hu
https://orcid.org/0000-0002-4782-1610

Keywords: polyurethane foam, jounce bumper, hyperelastic foam model, finite element analysis

The aim of this research is to find the best material model to predict the behaviour of Jounce bumper under the work conditions. The Jounce bumper made by polyurethane elastomer [2], the behaviour of this material is non-linear elastic, and it will be under big compression loads during the work, so the deformation will be large. The best model for this material is the hyperelastic model, which is made for incompressible and compressible material too. Our material is compressible, so we will focus on the compressible hyperelastic models. Our part Jounce bumper or bump stops, it is a part used to absorb the noise, vibration and harshness in the suspension system under the full compression circumstances. Jounce bumpers act as an assistant compression spring when the maximum load is approached *figure (1)*. Thus, jounce bumpers can provide a smoother ride and can improve handling over a wide range of driving and load conditions. Jounce bumper is commonly made from polyurethane.

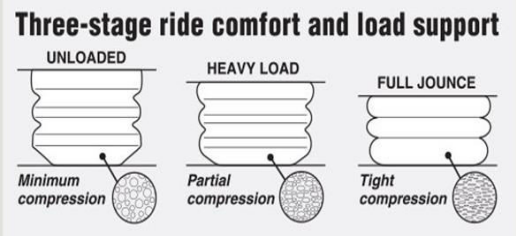

Figure 1 Three stages for Jounce bumper compression [3]

When we want to predict the mechanical behaviour of the rubber material, we have two main classes, Linear elasticity, and hyperelasticity models. The main difference between the elastic and hyperplastic model is that an elastic model is valid for small strain values. In the other side hyperelasticity suitable for large strain values and the materials that has non-elastic behaviour. When we want to study the foam, which is considered compressible material, we face some problems with the Hyperelastic material model. Since the foam goes under high volume change during processes, as we see in this *figure (2)* the predicted Poisson's ratio becomes odd in compressive loading when the bulk modulus is similar in magnitude to the shear modulus. This problem happened when modelling foams since foams often have a small bulk modulus and a small positive Poisson's ratio. On the other hand, in *figure (3)* we see the alternative model which take the volumetric response into consideration, we will use slightly different models of Helmholtz free energy and a different set of experimental data. We have two models, the first one is Blatz-Ko Foam model and Hyperfoam model, in the next I will represent both.

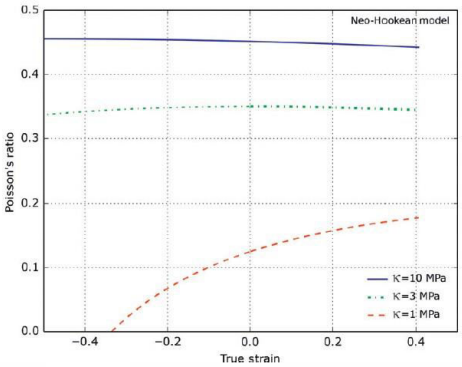

Figure 2 Predicted Poisson's ratio for the standard NH model [1]

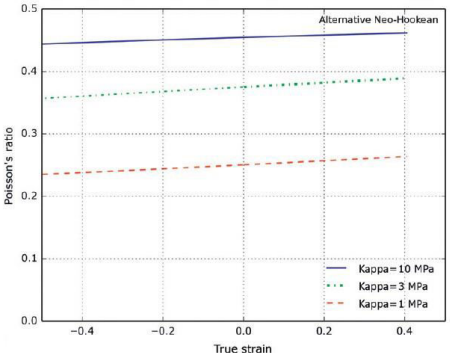

Figure 3 Predicted Poisson's ratio for the alternative NH model [1]

Blatz-Ko Foam model was developed for porous materials with a known shear modulus, Poisson's ratio, and volume fraction of voids. We usually set the void volume fraction parameter f=0, and by sitting Poisson's ratio ν= 0.25, we will gate the Blatz-Ko model, the ψ strain energy density will be [1]

$$\psi = \frac{\mu}{2}\left(\frac{I_1}{I_3} + 2I_3^{0.5} - 5\right)$$

As shown, this model only has one material parameter, the shear modulus μ. The Cauchy stress for this model given by

$$\sigma = \frac{\mu}{J_3}[I_1 b - b^2 - (I_2 - J^3)I]$$

The second model is Hyperfoam model, in this model we will not use the total deformation gradient in combination with the volumetric response. In this model the Helmholtz free energy is given the following expression [1]

$$\Psi = \sum_{k=1}^{N} \frac{2\mu_k}{\alpha_k^2}[(\lambda_1)^{\alpha_k} + (\lambda_2)^{\alpha_k} + (\lambda_3)^{\alpha_k} - 3 + \frac{1}{\beta_k}(J^{-\alpha_k\beta_k} - 1)]$$

Where $[\mu_k, \alpha_k, \beta_k], k = 1 \dots N$ are material parameters, $J = det[F], \lambda_i$ are the principal stretches. We can notice in this equation that hyperfoam model is very similar to the Ogden model. But the difference is the energy function for a volumetric response. We need the volumetric response to get a constant Poisson's ratio in uniaxial loading. The Cauchy stress can be derived from Equation giving [1]

$$\sigma = \sum_{k=1}^{N} \frac{2\mu_k}{J\alpha_k}\left[\sum_{i=1}^{3}(\lambda_i)^{\alpha_k} - J^{-\alpha_k\beta_k}\right]\tilde{n} \times \tilde{n}$$

The G small strain shear modulus and κ small strain bulk modulus can be written as [4]

$$G = \frac{1}{2}\sum_{k=1}^{N}\mu_k\alpha_k \qquad \kappa = \sum_{k=1}^{N}(\beta_k + \frac{1}{3})\mu_k\alpha_k$$

If all the β_k are equal, then the ν Poisson's ratio is related to β using [4]

$$\beta = \frac{\nu}{1 - 2\nu}$$

We will use the uniaxial compression to determine the material parameter, for this process the relevant standard is ISO 3386-1:1986 (Polymeric materials, cellular flexible - Determination of stress-strain characteristics in compression Part 1: Low-density materials). In this test we will use a compression platen, the limitation in this test is that we have an interface friction between the test specimen and the loading platens this will cause a nonhomogeneous deformation state. The friction also affects the stress response during unloading. It is changing the response during the initial unloading part of the experiment. After taking the curves from our test, we will use the stress-strain curve to make a curve fitting in FE software, by making the curve fitting we will be capable to calibrate the material model for the investigated polyurethane. In ANSYS, we can find a Blatz-Ko Foam Model and Ogden Compressible Foam Hyperelasticity supporting foam model, in FEMAP we see the Hyperfoam Model, I will try the two models that I mentioned in the literature to find the most appropriate prediction.

ACKNOWLEDGMENTS

The described work was carried out as part of a project supported by the EFOP-3.6.1-16-2016-00022 project. The project is cofinanced by the European Union and the European Social Fund. This research is partly supported by the ÚNKP-19-3 New National Excellence Program of the Ministry for Innovation and Technology.

REFERENCES

[1] C. Jörgen Bergström, *Mechanics of Solid Polymers Theory and Computational Modelling William Andrew publications*, 218-290. 2015.

[2] YuanlongWang, Zheng-dong Ma and LiangmoWang., *A finite element stratification method for a polyurethane jounce bumper*. Proceedings of the Institution of Mechanical Engineers Part D Journal of Automobile Engineering, 983–992. 2015.

[3] Air Lift Company website., *Jounce Bumpers: Everything You Need to Know*. https://www.airliftcompany.com/workshop/jounce-bumper.

[4] NX Nastran 11, *Advanced Nonlinear Theory and Modelling Guide*, Siemens Product Lifecycle Management Software Inc. 2019.

NUMERICAL SIMULATION STUDY ON THE RESIDUAL STRESS DISTRIBUTIONS IN DISSIMILAR PIPE WELDED

ALHAFADHI Mahmood, KRÁLLICS György PhD
Institute of Physical Metallurgy, Metal Forming, and Nanotechnology, University of Miskolc
E-mail: mahmoodhs199@gmail.com

Keywords: Numerical simulation, Residual stress, Welding pipe, Hardness test

This study used finite element techniques (FEM) to residual stresses in dissimilar welded pipes. Based on this study, a three dimensional (3D) and two dimensional (2D) modelling procedures with reasonable accuracy were developed. As compared to the 3D analysis, the 2D model significantly reduced the time and cost of the FE computation. A 2D thermo-mechanical FEM model finite element model using MSC Marc software to calculate the temperature distribution, hardness, and the distribution of residual stress during multipass welding of dissimilar material and different thickness pipes as shown in *figure 1(a) and (b)*. The results of the numerical simulation were compared with hardness measured data to evaluate the accuracy of the finite element modelling. The result show good agreement between simulated and experimental hardness in the weld. The axial and hoop residual stresses in dissimilar pipe joints of different thickness for V-groove shape were simulated in outer and inner surfaces. It is shown that the welding material has a significant effect on the magnitude and distribution of residual stresses in the pipe side of the joints. The welding parameters for weld joints and weld shape pool are given in Table 1. Goldak's double ellipsoidal heat source model shown in *figure 2.*[1]

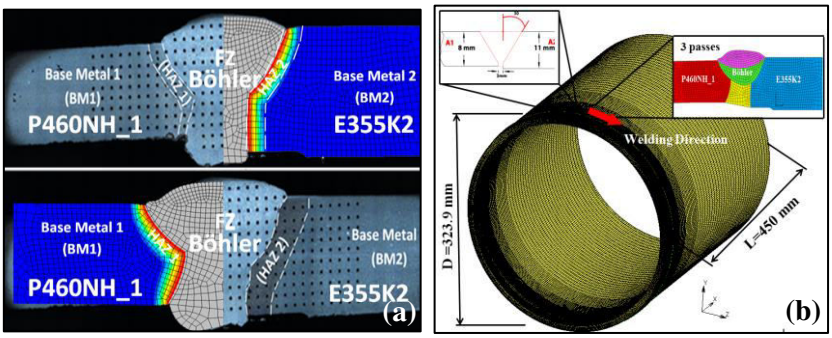

Figure 1 (a) Temperature profile in dissimilar welds joints with hardness measurement location (b) 3D model and 2D model dimensions and welding direction

Dissimilar metal joints between pipes of E355K2 and P460NH_1 steels are widely used in engineering structures, for instance, steam generators of power plants, pipeline, etc. Residual stresses distributions in and around the the heat-affected zone (HAZ) and (in the fusion zone, FZ) might lead to brittle fracture, cracking, and produced residual stress. Residual stresses present in the pipe weld are shown to be the reason for the failures.Moreover, the residual stresses in dissimilar joints are complex and difficult to predict, because of differences between mechanical and physical properties of the materials involved. Numerical simulation methods are also used to calculate residual stresses, due to the complexity of the problem or shape of the structure. Nowadays, it is possible to use numerical simulation techniques, such as finite element methods, to satisfactorily predict the residual stresses in welded structures [2-5].
This work aims to develop a validation model for the simulation model in multi-pass welds using a hardness test and compare the results with numerical simulation.the development of residual stresses in a dissimilar pipe weld joint made of E355K2 and P460NH_1 is studied by using 2D finite element method (FEM).The variation of stresses fields in the dissimilar joints is delineated in comparison to joints. In this work, the development of residual stresses in a dissimilar pipe weld joint made of E355K2 and P460NH_1 is studied by using 2D finite element method (FEM). The variation of stresses fields in the dissimilar joints is delineated in comparison to joints.

Table 1 Welding parameters

Pass No.	Current *(A)*	Voltage *(V)*	Speed mm/s	Efficiency	Welding pool parameters			
					a *(mm)*	b *(mm)*	c_1 *(mm)*	c_2*(mm)*
1	80	23.2	2	0.8	4	3	5	8
2	90	23.6	2	0.8	4	3	5	8
3	100	24	2	0.8	4	3	5	8

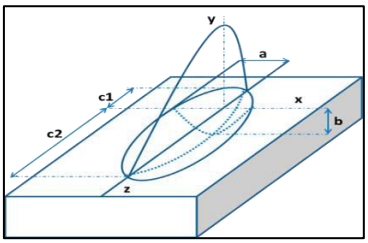

Figure 2 Goldak's double ellipsoidal heat source model

The axial and hoop residual stress distribution of the dissimilar welded joint on outer and inner surfaces shows in *figure 3*. It can see that the residual stress distribution in the dissimilar pipe weld joint is different due to the two different materials presented. The maximum tensile axial residual stress is located at the interface between welded metal and base metal P460NH_1 on inner surface. The maximum tensile hoop residual stress is located at the interface in (FZ) between the base metals E355K2 and P460NH_1. The hoop residual stresses are decreased away from the weld metal and HAZ.

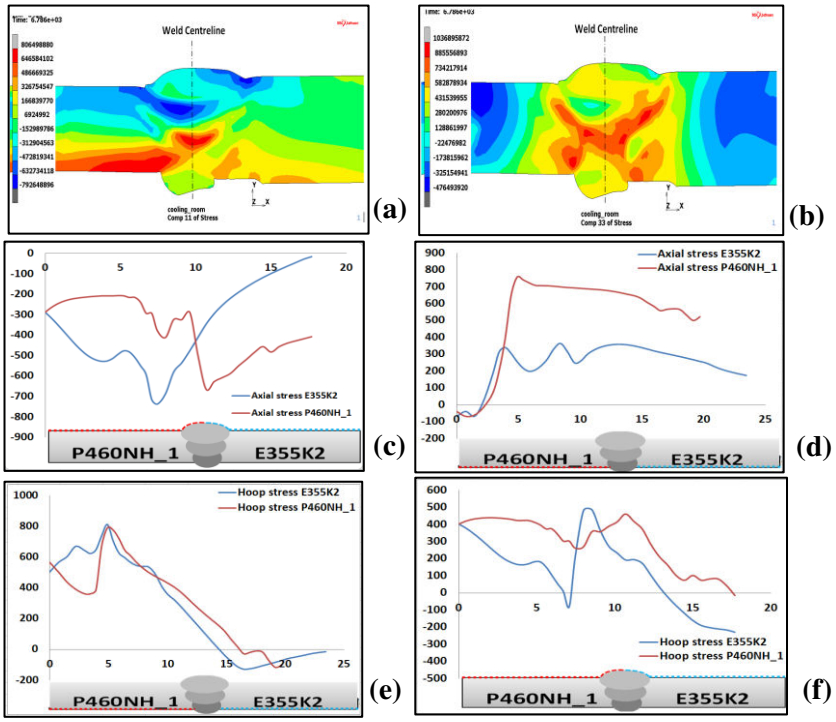

Figure 3 Axial residual stress distribution and hoop residual stress disribution on outer and inner surface

In this paper, it shows the methodology of the simulation of welding. The work presents the mock-up and the material properties and welding technologies that are needed to create a finite element simulation also to build a correct finite element model to copmare the result with hardness test mesurement. The result shows close agreement between simulated and experimental hardness in the weld.After that, perdicte residual stresses with differnt diracrtion on outer and inner surface of dissmiler weld pipe.

REFERENCES

[1] J. Goldak, A. Chakravarti, M. Bibby, *A new finite element model for welding heat sources*. Metallurgical transactions 15(2), 299-305. 1984.

[2] M. Alhafadhi, G. Krallics, *Numerical simulation prediction and validation two dimensional model weld pipe*. Machines.Technologies. Materials. 13 (10), 447-450. 2019.

[3] Sz. Szávai, Z. Bezi, and C. Ohms, *Numerical simulation of dissimilar metal welding and its verification for determination of residual stresses*. Frattura ed Integritá Strutturale 10 (36), 36-45. 2016.

[4] Sz. Szávaia, Z. Bezi, and P. Rózsahegyi, *Material Characterization and Numerical Simulation of a Dissimilar Metal Weld*. Procedia Structural Integrity 2 (10), 23-1030, 2016.

[5] M. Alhafadhi, G. Krallics, *The Effect of Heat Input Parameters on Residual Stress Distribution by Numerical Simulation*. IOP Conference Series: Materials Science and Engineering. 613 (1). 2019.

RECYCLING OF POLYETHYLENE TEREPHTHALATE BOTTLES WASTE (PET)

[1]AL-MOSAWI Ali I., [2]AL-MAAMORI Mohammed H., [3]ABED Maytham A., [1]ABDULSADA Shaymaa Abbas
[1]Faculty of Materials Science and Engineering, University of Miskolc
E-mail: qkoali76@uni-miskolc.hu, qkosha86@uni-miskolc.hu
[2]College of Engineering Materials, University of Babylon
E-mail: mat.mohammed.hamzah@uobabylon.edu.iq
[3]General Tires Company/Babil, IRAQ
E-mail: maytham_babil@yahoo.com

Keywords: polyethylene terephthalate, waste, road bumps, styrene-butadiene rubber

Every year, hundreds of scientific studies are published and highlighting a complex environmental problem which is pollution by plastics waste, because the quantities of these wastes are increasing annually. This environmental problem has made many scientific institutions around the world demands the adoption of laws to preserve the environment and human health and identify safe ways to dispose of these wastes. Therefore, we must look for applications that enable us to use this waste after recycling and one of these important applications is the road bumps [1-4] (see Fig.1). This artical addresses two major industrial problems, the first is an environmental problem considering these substances polluting the environment, and the second problem is an economic problem considering that road bumps are imported from abroad at high prices. Where we mentioned that any consumption of an industrial product is generated from solid residues such as with plastic bottles, which are thrown after consuming their beverages, which negatively affects the environment as a result of their accumulation and without benefiting from them, and most of them have a long life and also decompose when exposed to the sun, resulting in bitter Landfills cause environmental and health problems. In order to produce bumps locally and at low cost and with high mechanical properties and no less quality than imported bumps where these bumps were made of rubber added waste bottles, which can be recycled again when damaged unlike the imported, which cannot be recycled because they are made from materials used for once only (thermosetting plastic).

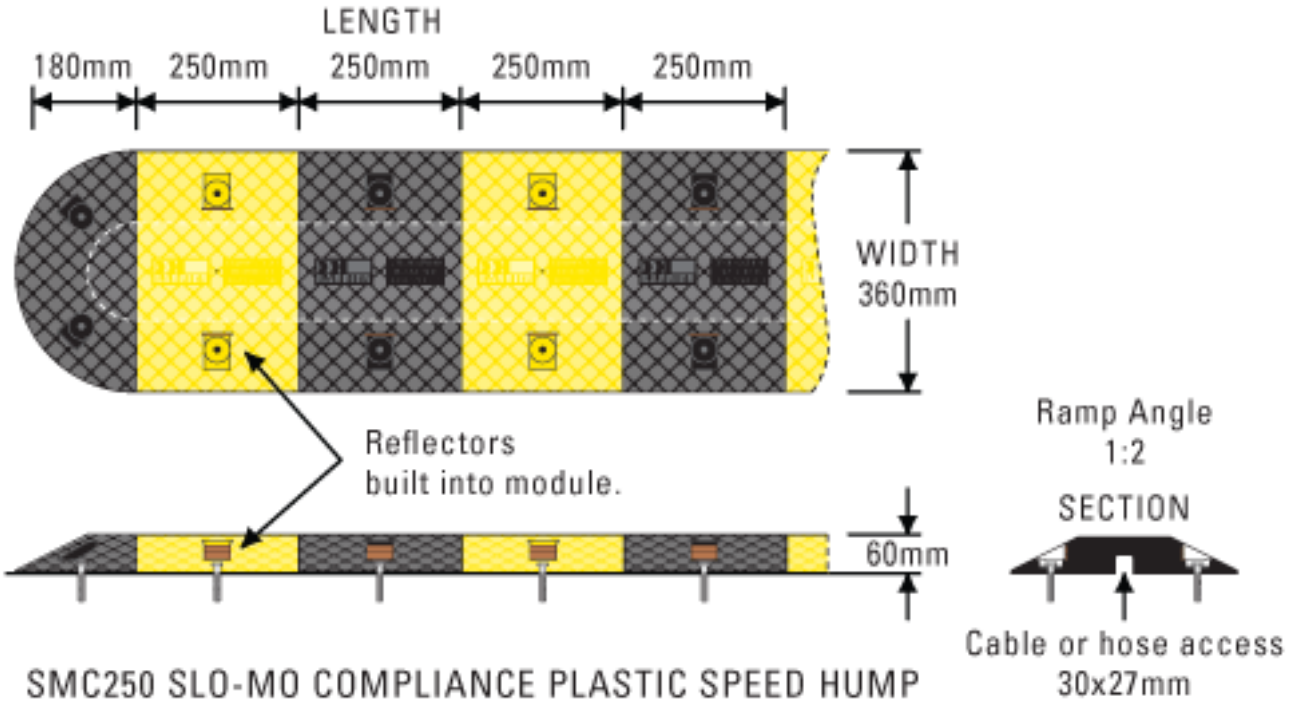

Figure 1 A standard plastic road bump [5]

In current artical, a strips of polyethylene terephthalate bottles (PET) waste with (0-100pphr) volume fraction was added to styrene-butadiene rubber for manufacture road bumps. Wear resistance, shear resistance, and adhesive tests were done after adding PET strips waste, and compare them with the results before adding this waste. The results

indicated the efficiency and high value of the mechanical properties of the manufactured rubber bumps, and better than the standard bumps properties currently available. The best results were obtained with the 80pphr PET waste addition.

REFERENCES

[1] I. Al-Mosawi, Ali, A. Hashim, Abbass, and H. Al-Maamori, Mohammed, *Production of high performance mountings by using rubber-polymer waste*, Open Access Library Journal, 6, 1-6. https://doi.org/10.4236/oalib.1105368,2019.

[2] W. d'Ambrières, *Plastics recycling worldwide: current overview and desirable changes*, Field Actions Science Reports, 19, 12-21. 2019.

[3] I. Al-Mosawi, Ali, A. Abdulsada, Shaymaa and M.A. Rijab, *Recycling Procedure of Plant Waste for Manufacturing Green Composite Material*, International Journal of Engineering Technology, Management and Applied Sciences, 5(4), 211-214. 2017.

[4] G. Faraca, T. Astrup, *Plastic waste from recycling centres: Characterisation and evaluation of plastic recyclability*, Waste Management, 95, 388-398. https://doi.org/10.1016/j.wasman.2019.06.038,2019.

[5] Technical report, *Heavy Duty Speed Hump Compliance – Polyethylene*, RJ COX Company. 2016.

NIL-STRENGTH TEMPERATURE AND HOT TENSILE TESTS ON S960QL HIGH-STRENGTH LOW-ALLOY STEEL

ALSALAMAH Bassel, KUZSELLA László PhD
Department of Mechanical Technologies, University of Miskolc
E-mail: bassel.alsalamah@gmail.com, kuzsella@uni-miskolc.hu

Keywords: Physical simulation, weldability, Nil-Strength Temperature (NST), hot tensile test, high-strength low-alloy (HSLA) steel

Temperature dependence crack initiation is a very critical point of the mathematical modelization of a part of a mechanical design. Therefore it is extremely important to know the temperature dependence of a material during the process of mathematical modelization when forming the design. Additionally, the forming limit at a certain temperature is a key parameter to know for the design. Two parallel ways appear to determine the formability limit of a material at a certain temperature. The first way is a physical simulation which is fully precise. It aims to simulate all the physical circumstances and execute the forming. It also records all the important parameters such as the force, the strain also the temperature as a function of the time. The second way is to find a mathematical model of the forming starting with all the boundary conditions of the tests and all the needed physical parameters of the material. The best way is to apply both methods parallel to have the real formability of the material to make the deliberated design. The welding processes have developed a lot thanks to the physical simulation. The paper introduces the connection between weldability and physical simulation, hot-cracking sensibility, the Gleeble 3500 thermo-mechanical physical simulator, respectively, and early experiments on the S960QL high-strength low-alloy (HSLA) steel. Identification of the Nil-Strength Temperature (NST), furthermore the results of the hot tensile tests (on heating and on cooling parts of the welding simulation curve are also investigated) will be introduced. As well as, the future plans and ideas for upcoming research will be revealed too.
The strain induced crack initiation of steel has a standardized testing method; the so called SICO test. The first step is to produce the standardized samples and to perform the experiments using the GLEEBE system. Our method to perform SICO test is fully fulfills the standard and just added to the standard four thermocouple records the temperature during the experiments and it gives opportunities to draw the temperature distribution during the whole experiment along the sample. All the experiments are made at different temperature isotherms and different strain rates. Cross section and metallographic (including grinding, polishing and etching) preparation will be applied to all the samples. All the experiments are repeated with mathematical modellisation, so under DEFORM with the same circumstances too. For this step, all the boundary conditions have to be established and all the physical parameters of the material have to be optimized based on the results of the physical simulation.
NIL-Strenghth temperature will be used to reach the maximum temperature that SICO test specimen can reach without melting and shattering out of the jaws as it happened with K100 the first tool steel grade that we used.

Figure 1 Gleeble 3500 thermo-mechanic physical simulator installing at the Department of Mechanical Technology at the University of Miskolc

Figure 2 Specimens after the NST tests have been performed

REFERENCES

[1] L. Kuzsella, J. Lukács, K. Szűcs: *NIL-Strength Temperature and Hot Tensile Tests on S960QL High-Strength Low-Alloy Steel,* Production Processes and Systems, vol. 6. No. 1., pp. 65-76. 2013.

[2] Pohle C.*: Zerstörende Werkstoffprüfung in der Schweisstechnik. Deutscher Verlag für Schweisstechnik DVS-Verlag GmbH*, Düsseldorf, 1990.

[3] DUNAÚJVÁROS REGIONAL MATERIAL SCIENCE AND RESEARCH KNOWLEDGE CENTER DURATT 25-DRTT/2009 — Irt.: 2009/10/1 15th February, Dunaújváros. 2009.

[4] J. Lukács, Gy. Nagy, I. Harmati, F. R. Koritárné, K. Zs. Kuzsella Lászlóné: *Szemelvények a mérnöki szerkezetek integritása témaköréből*, Miskolci Egyetem, Miskolc, 210-218. 2012.

THE POSSIBILITY OF DETERMINATION THE DEFORMATION OF THE PRODUCT AFTER DRYING

ANTAL Tamás PhD, KEREKES Benedek CSc, KISS Zsolt Péter PhD
Institute of Engineering and Agricultural Sciences, University of Nyíregyháza
E-mail: antal.tamas@nye.hu, kerekes.benedek@nye.hu, kiss.zsolt@nye.hu

Keywords: *food, drying, material deformation, 2 and 3D imaging*

Shrinkage of food materials has a negative consequence on the quality of the dehydrated product. When shrinkage is not uniform during the drying process leading to the formation of unbalanced stresses and failure of the material. Changes in shape, loss of volume and increased hardness cause in most cases a negative impression in the consumer [1].
Dewatering of foods during drying results in dimensional changes [3]. The change in size is greatly influenced by the moisture content and the method of heat-transfer. Measuring dimensional change and shrinkage in industry practice is a very important task due to material quality and sales. Measuring of shrinkage is a real challenge today.
The purpose of this study is to determine the degree of deformation of fruits preserved by various drying methods using a special digital microscope. This is a new way of approaching the problem.

MATERIALS AND METHODS

The pear material (*Pyrus communis* L.) was dried by various drying methods, i.e., lyophilization (FD), vacuum drying (VD), mid-infrared drying (MIR) and hot-air drying (HAD). The following parameters were used for drying: FD (T=-30 - 20°C, p=50-90 Pa, dt=22 h), VD (T=80°C, p=7 kPa, dt=7 h), MIR (T=80°C, p= 1 bar, dt=20 min) and HAD (T=80°C, p= 1 bar, dt=7 h), respectively. The moisture content of the samples at the end of the drying process: FD – 1,45% (w.b.), VD – 1,59% (w.b.), MIR – 1,06% (w.b.) and HAD – 2,11% (w.b.), respectively. The drying was carried out to a constant weight of the material. Moisture content of the dried pear dices was determined by the gravimetric method (LP306, LaborMIM, Hungary). 50-50 g of sample was used for each drying methods. Weighing was performed on a digital balance (JKH-500, Jadever Co., Taiwan). The raw samples used in the experiment are cube-shaped – smooth surface – with an average of 10 mm each.
A digital image was taken of the dried material from a particular direction using a digital microscope (Keyence VHX-6000, Keyence Co., Osaka, Japan). The two- and three-dimensional image was sufficient to determine the degree of deformation (400×magnification). Digital imaging was performed on ten to ten samples with duplicate replication. In each case, the microscope detected the greatest difference between the upper edge of the product and the recess.

RESULTS

Figures 1 and 2 show two- and three-dimensional views of hot air-, mid-infrared-, vacuum-, and freeze-dried pears, respectively. The upper parts contains the three-dimensional image with the base points and the connecting lines, and the bottom part of picture the two-dimensional image with the distances (in µm) indicating the degree of deformation.

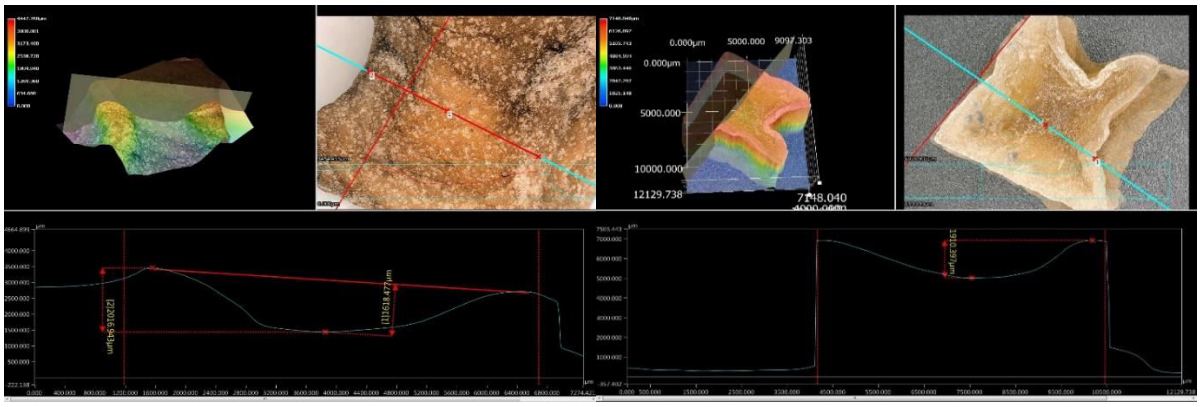

Figure 1 The 2 and 3D imaging of HAD and MIR dried material

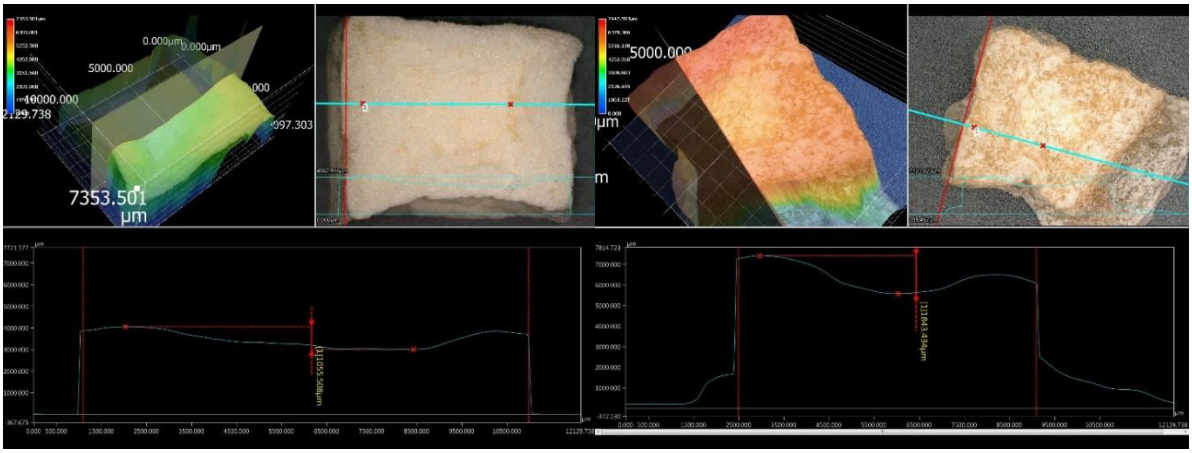

Figure 2 The 2 and 3D imaging of FD and VD dried material

The two-dimensional views of *Figures 1 and 2* clearly show that the lyophilized product is the least damaged and the greatest deformation is observed by the hot-air drying method.
The *Table 1* shows the degree of deformation caused by various drying methods.

Table 1 Deformation due to dehydration

Drying methods	Distance between the base point and the recess, H [mm]*×	Ranking
HAD: Hot-air drying	1,912-2,134	4
MIR: Mid-infrared drying	1,762-1,986	3
VD: Vacuum drying	1,714-1,966	2
FD: Freeze drying	0,923-1,104	1

*Average values from 10-10 samples.
×Marked with red in Figures 1 and 2.

According to *Table 1*, the lyophilized samples have the smallest size change (Based on two-dimensional images.). Ratti found that the shrinkage during freeze-drying is minimal (from 5% to 15%) while during hot-air drying is excessive (around 80%) [2].

CONCLUSIONS

Shrinkage of foods during drying has an impact on quality of the dehydrated material. Deformation of pear during hot-air drying was greater than vacuum-, mid-infrared- and freeze drying. The high material deformation during hot-air drying is due to the high temperature of the drying air (80°C) and uneven heat distribution. The rapid drying rate conditions are used at mid-infrared drying which contribute to relatively high shrinkage. There was minimal difference between the mid-infrared and vacuum dried samples, although the vacuum dried samples were favored by the low pressure. Less material deformation was observed at freeze drying. The effect of vacuum (p=50-90 Pa) and low drying temperature (T=-30 - 20°C) at freeze-drying, leads in general to much less deformation.
Further research is needed, that the digital imaging method is adequate to determine the deformation of dried products (for example, the possibility to measure volume loss).

ACKNOWLEDGMENTS

We would like to express our thanks to Mr. David Macsuga for his assistance in microscopic imaging.

REFERENCES

[1] L. Mayor, A.M. Sereno, *Modelling shrinkage during convective drying of food materials: a review*. Journal of Food Engineering 61, 373–386. 2004.
[2] C. Ratti, *Hot air and freeze-drying of high-value foods: a review*. Journal of Food Engineering 49, 311–319. 2001.
[3] N.J. Thakor, S.S. Sokhansanj, F. Sulski, S. Yannacopoulos, *Mass and dimensional changes of single canola kernels during drying.* Journal of Food Engineering 40(3), 153-160. 1999.

TRIBOLOGICAL PROPERTIES OF ION-IMPLANTED SILICON-NITRIDE CERAMICS

BABCSÁN K. Judit, MAROS B. Mária PhD
Institute of Materials Science and Technology, University of Miskolc
E-mail: metbab@uni-miskolc.hu, maria.maros@uni-miskolc.hu

Keywords: ion-implantation, SiAlON, tribology

Mechanical and tribological behaviour of ceramic materials depends strongly on the quality of the surface layer. Surface engineering methods, like ion-implantation, represent advanced techniques for improving these properties. Our former studies revealed, that during ion implantation of Si_3N_4 based ceramics in the vicinity of the surface layer a new amorphous region is developing, the microstructural characteristics of which is influenced by the energy of the implantation.
This paper deals with the investigation of the tribological property changes, which occur during the C^+ ion-implantation of a high-tech Si_3N_4 based ceramics material. The composition of the investigated material was Si_3N_4: 90 %, Y_2O_3: 6 % and Al_2O_3: 4 %, in mass percentage and the ceramics were produced by hot isostatic pressing. The ion-implantation was executed with C^+ ions at a fluence of 10^{17} ion/cm^2 and an energy of 500 keV, 1 MeV and 2 MeV.
The implantation resulted in an amorphous layer, near the surface. The depth and thickness of the expected amorphous layer was assessed by the so-called TRIM program.

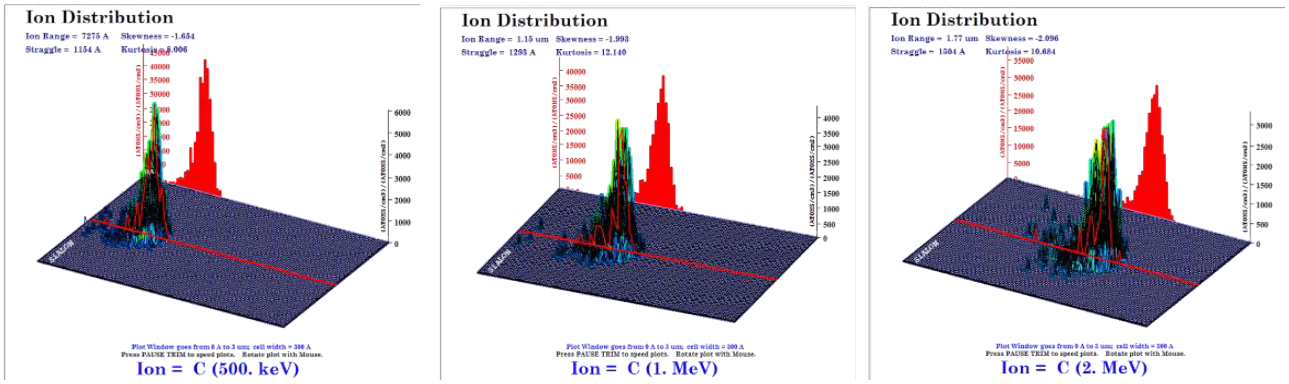

a b c

Figure 1 TRIM simulation for C^+ ion-implantation on to SiAlON ceramic with a) 500 keV, b) 1 MeV and c) 2MeV

The estimated amorphous layer of the implantation with 0.5 MeV, 1 MeV and 2 MeV implantation with C^+ ion in the case of Si_3N_4 substance were 0.73 µm, 1.15 µm and 1.77 µm respectively.
The surface layer, above the amorphous layer remained crystalline after the C^+ implantation, although the passed ions were partly built into the microstructure. Due to the revealed microstructural changes and the accompanying residual stresses the tribological behaviour of the investigated ceramics can be improved. An oscillating tribometer was used to accomplish the wear tests. The tribosystems consisted of a Si_3N_4 based prismatic bar (the testpiece) and a Si_3N_4 ball (the frictional counterpart, 10 mm diameter, commercial quality). The ball was fixed at the top of a lever with an integrated load cell for the measurement of friction force. The ball was not rotating, it was mounted on a vibrating table, loaded by a normal force. During the measurement the friction coefficient (COF) and the linear wear (W_l) was determined. The planimetric wear (W_q) was specified by a diamond stylus instrument crossing transversely the wear scar on the sample. The wear coefficient (k) was calculated to characterize the tribological behavior of the ion-implanted silicon nitride samples.

$$k = \frac{W_v}{\Delta x \cdot N \cdot F_n}$$

where W_v : the combined volumetric wear of the ball and the sample; Δx: stroke; N: number of cycles; F_n: normal load.

Table1 shows the test conditions during the wear test.

Table 1 Test conditions for the oscillating sliding wear test

Ball	Si_3N_4
Sample	SiAlON
Stroke	$\Delta x = 0.2$ mm
Frequency	$\nu = 20$ Hz
Normal force	$F_n = 5$ N
Number of cycles	$n = 5\times10^4$
Temperature	24 °C
Rel. humidity	50%

Figure 2 shows the results of the tribological measurements regarding to the untreated and the ion-implanted samples.

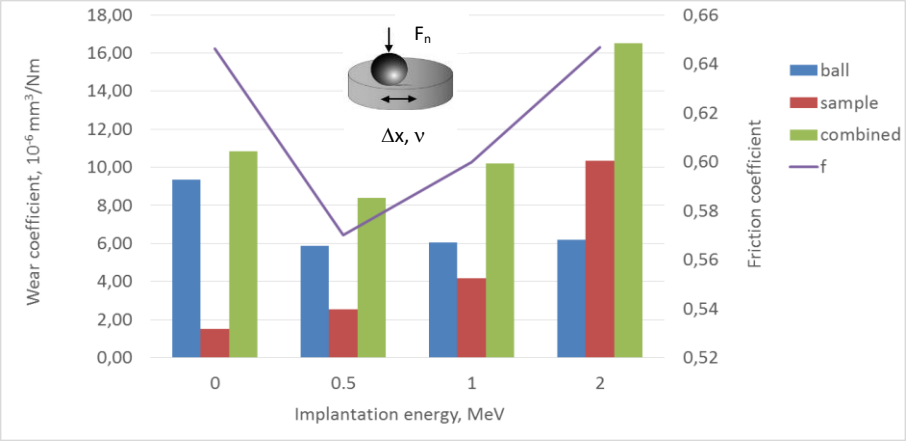

Figure 2 Wear coefficient of C^+ implanted silicon-nitride ceramics

The wear behaviour of tribosystems with the 0.5 and 1 MeV C^+ ion-implanted Si_3N_4 was improved in comparison with that of with the unimplanted reference material, and the related friction coefficients were also lower.

ACKNOWLEDGMENTS

This research was supported by the European Union and the Hungarian State, co-financed by the European Regional Development Fund in the framework of the GINOP-2.3.4-15-2016-00004 project, aimed to promote the cooperation between the higher education and the industry. The authors express their thanks to Helmholtz Zentrum Berlin for contribution to the ion-implantation and microstructural measurements; to Bundesanstalt für Materialforschung und –prüfung, Berlin for the tribological measurements, to P. Arato and Cs. Balazsi (Centre for Energy Research, Hungarian Academy of Sciences) for supplying the Si_3N_4 materials and for the mechanical tests.

REFERENCES

[1] F. Brenscheidt, W. Matz, E. Wieser, W. Möller, *Sur. and Coat. Techn.,* 110, p188, 1998.
[2] J.K. Babcsán, M.B. Maros, *Mat. und Werk.* 34, p343-348, 2003.
[3] J.P. Biersack and L. Haggmark, *Nucl. Instr. and Meth.,* 174, 257, 1980.
[4] J. K. Babcsán, B.M. Maros, P. Arató, *Microstructural features of the post heat-treated Si_3N_4 based ceramics*, Sil. Ind., 69 (7-8), pp199-203, 2004.
[5] P. Arató, F. Wéber, in: D. Huri (ed.), *Proceedings of ICCE/8, 8th Annual International Conference on Composites Engineering*, Tenerife, Spain, p35, 2001.
[6] D. Klaffke, R. Wäsche, N. Janakiraman, & F. Aldinger, *Tribological characterisation of siliconcarbonitride ceramics derived from preceramic polymers.* Wear, 260(7-8), p711–719. 2006.
[7] N. Nakamura, K. Hirao, Y. Yamauchi, *Eur. Ceram. Soc.*, 24 (2), p219, 2004.
[8] D.W. Oblas, V.K. Sarin, K.J. Ostreicher, *Mater. Res.*, Vol. 7, No. 9, p2579, 1992.

BATTERY INNOVATIONS AND CIRCULAR ECONOMY

BABCSÁN Norbert PhD
Innobay Hungary Ltd.
E-mail: norbert.babcsan@innobay.hu

Keywords: circular economy, aluminium, battery

The sustainable development of modern society requires new technological innovations in energy storage. Since the conversion of energy into kinetic energy is most effectively done by electric motors, it is obvious that the energy intended for motion is also stored in electrical form. By using alternative (non-fossil) energy sources, for example, sun, wind, nuclear, etc. the energy produced is also generated in the form of electrical energy. As a result, the emphasis on electrical energy storage is growing and batteries are playing an increasingly important role as the most efficient way of storing electricity. Society researchers estimate the proportion of electric cars in global car sales to 70% by 2050 [1]. To achieve these goals, humanity will need a fleet of about 50 TWh batteries [2]. Unfortunately, current battery solutions are inadequate for both the balancing of renewable energy production and the long-term storage of electrical energy needed for mobility (car batteries and charging or "fuel" station buffers). Reasons include lack of available raw material resources, inadequate battery parameters, and cost-effectiveness constraints. However, for aluminium-based batteries, it can be shown that aluminium-based electrical energy storage can be a solution for producing high specific energy batteries (2.5x higher capacity than Li batteries). Another advantage of aluminium is that it is the 3rd most common element in the earth's crust and is almost infinitely available and easy to integrate into the circular economy due to its simple recyclability.

One of the most advance aluminium battery innovation is pioneered by the Israeli company Phinergy [3] which is working on a new *primary nonrechargeable aluminum battery pack* (the aluminium battery is removed from the car and replaced with a new one) together with Alcoa (Arconic) but the production line will be established finally in China. Moreover, the current *rechargeable aluminum-ion batteries* can reach more than 2.5 times (1 kWh/kg) the lithium-ion battery theoretical maximum (300 Wh/kg) which can drastically change the future battery industry [4]. The recent Al-ion batteries are already capable to store 400 Wh/kg [5] energy. The Al-air battery theoretical energy density is 8.1 kWh/kg [6] (the value is similar than the density of the coil, the energy density of the natural gas or the gasoline, but three times as much per volume [7]). Unfortunately, primary aluminium production requires still 2 times the energy content of the theoretical Al-air battery. However, the best current Li-ion batteries have an energy density of only 0.25 kWh/kg [8]. The increased energy content of the batteries will revolutionize first the electric car industry and later at 400 Wh/kg density the manned electric aircraft industry [9]. At the moment, the Tesla Model S [10] is capable of running 539 km with a 100 kWh rechargeable battery pack (0.207 kWh/kg energy density, 0.19 kWh/km, 0.90 kg/km, 483 kg Li-ion battery). The new Alcoa-Phinergy electric car was able to drive 1750 km with the current 0.3 kWh/kg Al-air battery, which can easily be upgraded to 1 kWh/kg. Tesla Model S fueled with the improved Phinergy air battery technology would use only 100 kg of Al-air battery, which means that it will be enough to refuel with 100 kg Al for such distance. If the theoretical energy capacity of 8.1 kWh/kg Al can be utilized with the current electric power train, only 23 kg of aluminium should be refueled, which is only 8.5 liters of aluminium. To compare, this amounts at least 32 kg and 40 liters of petrol.

Aluminium is one of the most important contributors and playing the role of the main accelerator of the transition from a linear to a circular economy. The current approach to the circular economy oversimplifies the classification of materials and products as renewable or non-renewable, re-usable or non-reusable or even biodegradable or non-biodegradable. Aluminium is a permanent material which is more than a re-usable material, one for which the inherent properties do not change during use and following repeated recycling into new products. Aluminium is used in its permanent material form as a structural or functional material. As a structural material, aluminium is used in the building industry and mobility. As a functional material, it is used in the cable and the packaging industry. The *properties of the aluminium is mostly set by alloying* and traditional aluminium transformation technologies as solidification, casting, rolling, extrusion, wire drawing etc. The raw aluminium enters into the material cycle through a high temperature metallurgical process which transform the oxide of aluminium into aluminium metal. The aluminium material cycle contains four main steps. Aluminum is also expected to be a major part of the vehicle's materials. Very light car body structures can be constructed from hybrid aluminum which can be made from dirty (dross and or iron containing) aluminium melt. Depending on the complexity of the structure, we are talking about single (composite), double (foam) and triple hybrid (sandwich) aluminium (figure 1.).

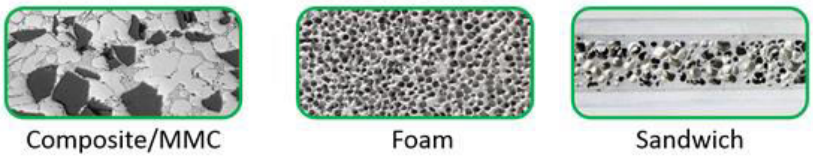

Figure 1 Hybrid aluminium classes

The production of aluminum from the ore (oxide) requires a significant amount of energy, and therefore aluminium smelting process is currently associated with low-energy price countries. New aluminium metallurgical technology has emerged, which will significantly improve the environmental friendliness and cost-effectiveness of primary aluminum production, as O_2 is a by-product instead of CO_2 [11]. In addition, technological advances in the field of secondary raw material manufacturers have produced environmentally-friendly salt-free waste recycling technology [12]. Due to the novel innovations (hybrid aluminium and battery) applications the two materials and the energy circles can be combined into one infinite loop. Summarizing, structuring and coupling the information listed previously an infinite aluminium circular economy diagram can be drawn (figure 2.).

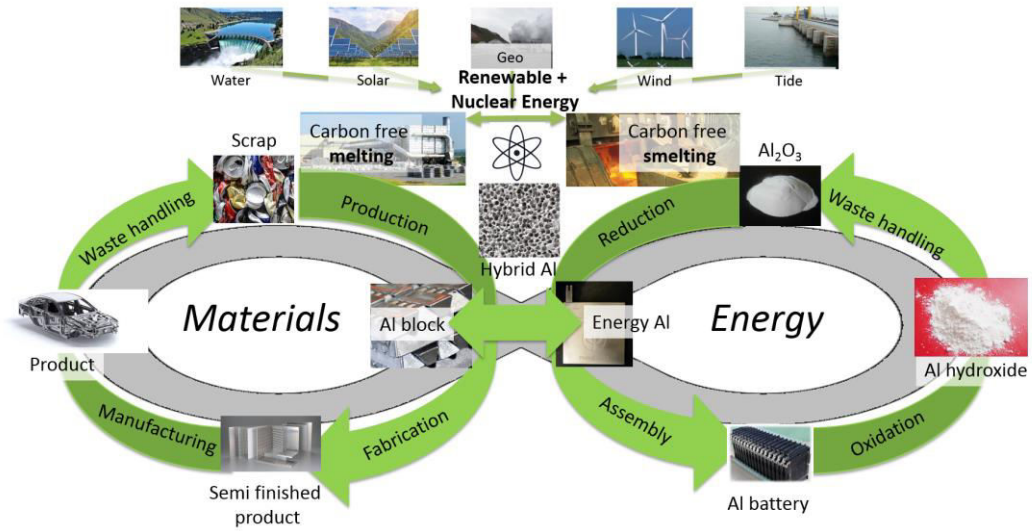

Figure 2 Aluminium Infinite Circular Economy

REFERENCES

[1] M. Stanley, *Electric Vehicles: On the Charge*, Morgan Stanley Research, August 31, 2017.
[2] http://science-and-energy.org/wp-content/uploads/2016/03/FPerdu_Houches_final-1.pdf
[3] http://www.phinergy.com/
[4] G. A. Elia, K. Marquardt, K. Hoeppner, S. Fantini, R. Lin, E. Knipping, W. Peters, J.-F. Drillet, S. Passerini and R. Hahn, *An Overview and Future Perspectives of Aluminium Batteries*, Advanced Materials, Volume28, Issue35, September 21, 2016, pp. 7564-7579.
[5] http://alionproject.eu/project/
[6] https://insideevs.com/alcoa-teams-with-phinergy-to-develop-claimed-1000-mile-aluminum-air-battery-technology-wvideo
[7] https://deepresource.wordpress.com/2012/04/23/energy-related-conversion-factors/
[8] https://en.wikipedia.org/wiki/Lithium-ion_battery
[9] https://www.idtechex.com/en/research-report/manned-electric-aircraft-2020-2030/672
[10] https://en.wikipedia.org/wiki/Tesla_Model_S
[11] https://www.riotinto.com/media/media-releases-237_25362.aspx
[12] https://www.riotinto.com/media/media-releases-237_25708.aspx

APPLICATION OF PATTERN RECOGNITION FOR ENGINEERING DATA CLASSIFICATION

BARKÓ György PhD, KALÁCSKA Gábor PhD
Institute for Mechanical Engineering Technology, Szent István University
E-mail: suestados@freemail.hu, kalacska.gabor@gek.szie.hu

Keywords: Pattern Recognition, data processing, sensor system engineering

Pattern recognition method using feature extraction is widely used to classify engineering data sets [1,2,3]. A computer program was developed for the measurement of the frequency changes of sensors and engineering data processing. This pattern recognition method using feature extraction was applied for classification of volatile substances, detected by different sensors. Four sensors were placed in an array and different compounds including organic solvents were classified.

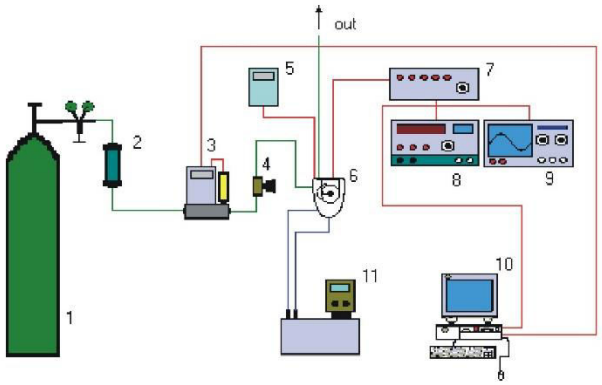

Figure 1 Experimental setup

The responses of four piezo sensors were investigated as an organic vapor sensor. Nitrogen (1) was filtered (2) and mass flow has been regulated (3). Temperature of the sensor array was regulated (11) and kept constant (5). A characteristic response was given by each sensor placed in the array. The reversibility, selectivity and sensitivity of the sensors to vapors rely on the coating materials covering the sensor surface. Sensor output was frequency change. The recorded frequency (7) was extracted from standard reference frequency (8). The flow rate was kept constant (20 L/h) for the reproducible responses.
The coating materials show different sensitivity to organic vapors. From the results four compounds were chosen for the characterization of the group of the organic materials. The benzene was applied as a representative compound of the aromatic hydrocarbons, acetone for ketones, n-pentane for the hydrocarbon groups, and chloroform for the chlorinated hydrocarbons. The frequencies characteristic to the compounds have been recorded. These values were used for the preparation of the data matrices. The frequency was converted to pattern with feature extraction. The feature extraction method consists of signal processing. The sensor signal can be processed by extraction of the most distinctive feature parts of the signal. The lowest and highest frequencies of four crystals were converted into the feature space. Not only the highest frequency change but does the lowest one contains valuable information concerning the reaction between the coating materials and analytes.

The feature space means a data files in the computer's memory. In the present case it consists of eight frequency values (two for each sensor). For classification of vapors the signals of the sensor array were transformed into a concentration independent plane. Linear transformation was applied for normalization of the signal. The process is shown by Equation 1. and 2.

$$X^+ = INT\left(\frac{\Delta F^+_{OV1}}{\Delta F^+_{OV1} + \Delta F^+_{ASI\,50} + \Delta F^+_{OV\,275} + \Delta F^+_{PPh-ether}} \cdot R\right)$$

Equation 1

$$Y^+ = 1$$

$$X^- = INT\left(\frac{\Delta F^-_{OV1}}{\Delta F^-_{OV1} + \Delta F^-_{ASI\,50} + \Delta F^-_{OV\,275} + \Delta F^-_{PPh-ether}} \cdot R\right)$$

Equation 2

$$Y^- = 1$$

where

X+	the position of the cluster at the highest value in rows (1....32)
Y+	the position of the cluster at the highest value in columns (1...4), (OV1=1, ASI50=2, OV275=3 and PPh-ether=4)
$\Delta F^+_{OV1}, \Delta F^-_{OV1}$	the highest and lowest value of the measured frequency on OV1 sensor
$\Delta F^+_{ASI\,50}, \Delta F^-_{ASI\,50}$	the highest and lowest value of the measured frequency on ASI 50 sensor
$\Delta F^+_{OV275}, \Delta F^-_{OV275}$	the highest and lowest value of the measured frequency on OV275 sensor
$\Delta F^+_{PPh-ether}, \Delta F^-_{PPh-ether}$	the highest and lowest value of the measured frequency PPh-ether sensor
R	the resolution of the feature extraction,(R=32)

It can be seen that each transformed response is calculated as the ratio of the summary of the four sensor replies. This method could eliminate the effects of absolute amounts of vapors on pattern recognition. The patterns were stored as binary data set. The data set gives a value of 1 when a cluster has been found in the column of a sensor. In any other case the values are 0. The size of the saved pattern file was about ten per cent of the file of frequencies recorded. The number of columns of the data set was equal to the number of the sensors (Fig. 4). The number of rows of the data set was proportional to the resolution of the feature extraction. With an increasing resolution the calculation time of pattern recognition should considerably be increased. However, large differences in the frequency changes are not necessary for the distinction of the patterns. The repeatability of the patterns has been found to be the most important criteria of the appropriate recognition.

At first, the computer program was learned. Sample of organic vapors was injected and the changes in the frequencies of the crystals were measured, converted to patterns and saved in the memory. After the teaching process, the unknown organic vapor was measured. The pattern of unknown compound was compared with the learned patterns. The two binary data sets were processed by K-nearest neighbor method. The unknown sample set has been grouped to its nearest neighbor learning point. During the learning process the data base of organic compounds can be formed by the given sample set. The maximum score was saved to the matched pattern and the unknown organic compound was identified.

REFERENCES

[1] B. Qiu, M. Zhang, Y. Xie, X. Qu, X. Li, *Mechanical Systems and Signal Processing*, Volume 128, 1 August 2019, Pages 429-445, 2019
[2] A. Bhateja, S. Sharma, S. Chaudhury, *Pattern Recognition Letters*, Volume 73, 1 April 2016, Pages 13-18, 2016
[3] G. Barkó and J. Hlavay, *Talanta*, Volume 42, Pages 475-482, 1995

OPTIMIZATION OF PICK AND PLACE TASK PROBLEM FOR A MANIPULATOR ARM

[1]BENOTSMANE Rabab, [1]DUDÁS László PhD, [2]KOVÁCS György PhD
[1]*Institute of Information Science and Technology*
E-mail: benrabab1@gmail.com, iitdl@uni-miskolc.hu
[2]*Institute of Logistics*
E-mail: altkovac@uni-miskolc.hu

Keywords: Manipulator arm, Industry 4.0, Pick and place, Singularity problem, Workspace

In recent years manipulator robots have play an important role in the revolution of production philosophy in factories and especially in the Industry 4.0 concept [1], due to their flexibility to execute tasks and cooperate with their environments. In this article we present an optimization approach regarding a pick and place application of an RV-2AJ Mitsubishi robot arm in order to execute a special task. This approach aims to build a card house using one manipulator arm and a support element. The optimization approach will create a solution for singularity problem of RV-2AJ arm which has five degrees of freedom that limit its workspace.

PROBLEM DESCRIPTION

The essential goal of our research is building a card house. This task to be achieved usually needs two hands. In our laboratory we try to execute this task using only one manipulator arm (RV-2AJ robot) and a simple support element. The task is executed in the real environment (Figure 1.a) and modeled in the virtual environment (Figure 1.b) using Solidworks software [2].

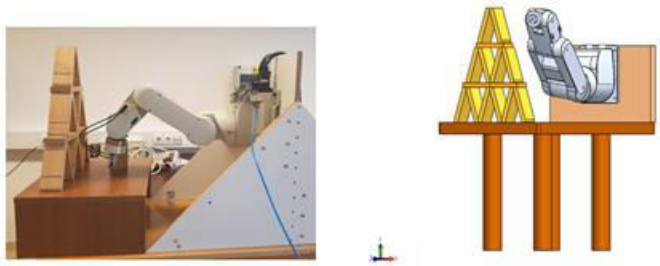

Figure 1 Card house building by RV-2AJ robot arm in the real environment (1.a) and in a virtual environment of Solidworks software (1.b)

We started at first by manufacturing all the elements needed for this operation presented in Figure (2).
The components of the card house are the following:

- 12 cards (slanted cards) having a special form (Figure 2.b) to create A shape and guarantee the stability of the structure,
- 3 cards in horizontal position having rectangular shape (Figure 2.c) located between the levels of the card house,
- one card which is a support element (Figure 2.d) to help fixing the single slanted cards.

The cards were manufactured from wood material using CNC machine.

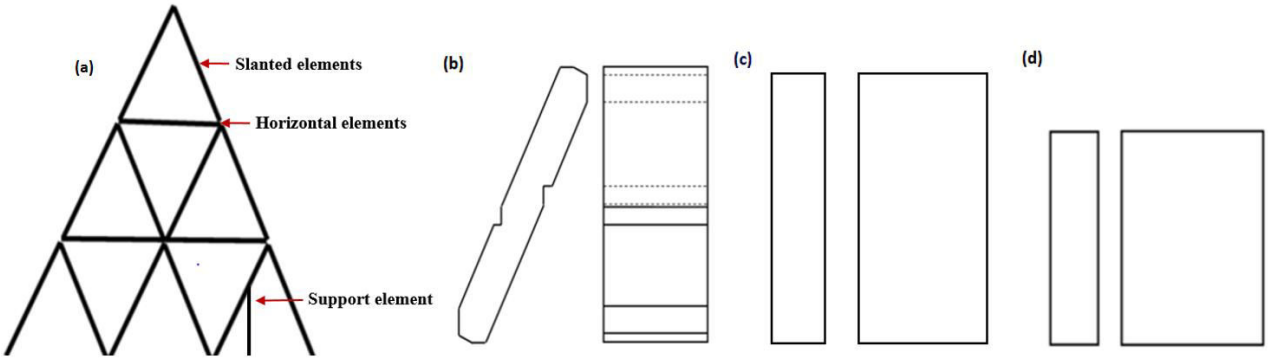

Figure 2 Elements needed for card house building

OPERATION IN THE REAL ENVIRONMENT

The robot arm is in vertical placement

The task is divided into subtasks starting by realizing the first small A shape composed by two cards where RV-2AJ executed the program clearly but the precision in the parallelism of two cards was not correct as presented in Figure (3). The problem was due to the normal vertical placement and the singularity of RV-2AJ arm which has 5 degree of freedom that limits its workspace to achieve some positions and cause the angle problem resulting instability (red rectangle in Figure 3).

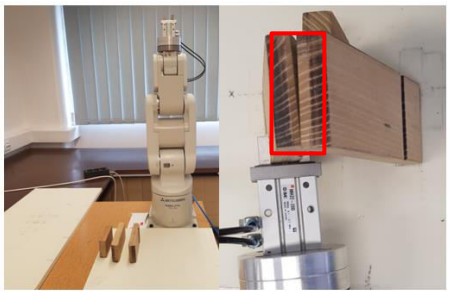

Figure 3 Executing the subtask by RV-2AJ arm (arm in vertical position)

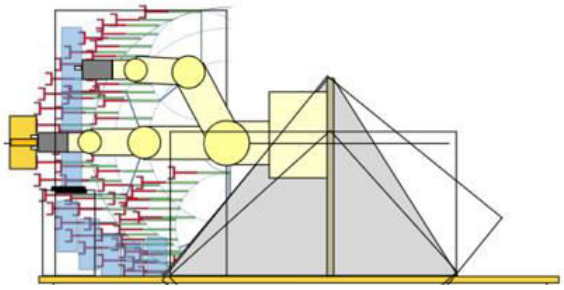

Figure 4 Optimal solution for singularity problem (arm in horizontal position)

The robot arm is in horizontal placement

The solution for this problem was based on the optimal formation of the workspace which means finding a new placement for RV-2AJ arm presented in Figure (4). Where the arm in the horizontal position can move and rotate the end effector more precisely to reduce the positioning errors providing stability of the card house.

Operation in the virtual environment (simulation)

The modeling of the card house in the virtual environment aimed to create at first the CAD model of RV-2AJ arm in Solidworks (Figure 1.b). In the future research we would like to optimize the motion of the robot arm by the application of our own program written in Python using the Tree search algorithm [3] which defines all the steps of the motion. Using V-rep software [4] we can synchronize the CAD model and our optimization program. The result of the optimization will be the reduction of total cycle time of the construction.

ACKNOWLEDGMENTS

This research was partially carried out in the framework of the Center of Excellence of Mechatronics and Logistics at the University of Miskolc. The described study additionally was carried out as part of the EFOP-3.6.1-16-00011 “Younger and Renewing University – Innovative Knowledge City – institutional development of the University of Miskolc aiming at intelligent specialization” project implemented in the framework of the Széchenyi 2020 program. The realization of this project is supported by the European Union, co-financed by the European Social Fund.

REFERENCES

[1] R. Benotsmane, G. Kovács, L. Dudás, *Economic, Social Impacts and Operation of Smart Factories in Industry 4.0 Focusing on Simulation and Artificial Intelligence of Collaborating Robots*. *Social Sciences*, *8*(5), 143, 1-21. 2019.

[2] G. Onwubolu, *A Comprehensive Introduction to Solidworks 2013*, SDC publications, USA. 2013.

[3] F. Torres, S. Puente, C. Diaz, *Control Engineering Practice Automatic Cooperative Disassembly Robotic System: Task Planner to Distribute Tasks Among Robots*. Control Engineering Practice, 17, 112-121. 2009.

[4] E. Rohmer, S. Singh, M. Freese, *V-REP: a Versatile and Scalable Robot Simulation Framework*. IEEE/RSJ International Conference on Intelligent Robots and Systems, Conference proceedings, 1321-1326. 2013.

DESIGNING AND ANALYSIS OF SPECIAL GEAR PAIRS BY GEARTEQ AND SOLIDWORKS SOFTWARES

BODZÁS Sándor PhD
Department of Mechanical Engineering, University of Debrecen
E-mail: bodzassandor@eng.unideb.hu

Keywords: GearTeq, Solidworks, software, gear, CAD

The GearTeq software is a unique designing program for many types of gear pairs (spur gears, helical gears, bevel gears, worm gears, elliptical gears, epicyclic gear trains, etc.). Knowing of the recommendation of the references an engineer can set the input parameters of several pinion and driven gears and after that this program can calculate the other necessary parameters. During the designing process the designing gear geometry could be followed by schematic figures.

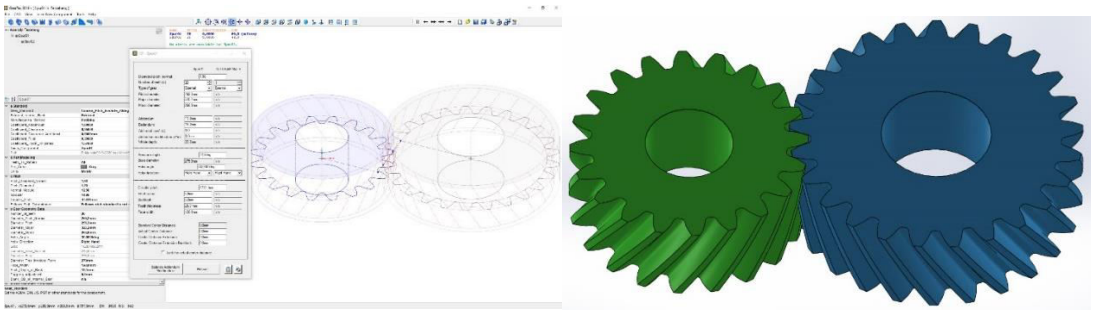

Figure 1 Designing of a helical gear pair by GearTeq and Solidworks softwares (m_{ax}=15 mm, z_1=20, z_2=25, β_0=30°, right hand, α_0=20°)

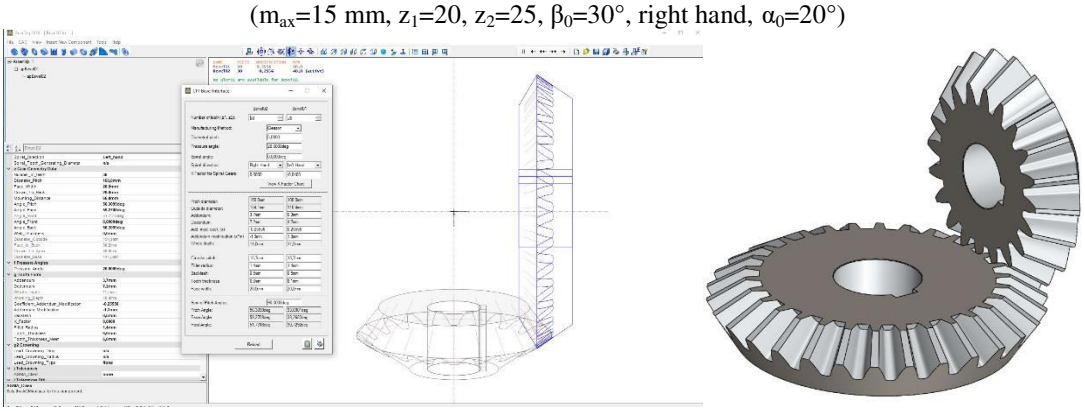

Figure 2 Designing of a bevel gear pair having straight tooth by GearTeq and Solidworks softwares (m_{ax}=5 mm, z_1=20, z_2=30, α_0=20°, Σ=90°)

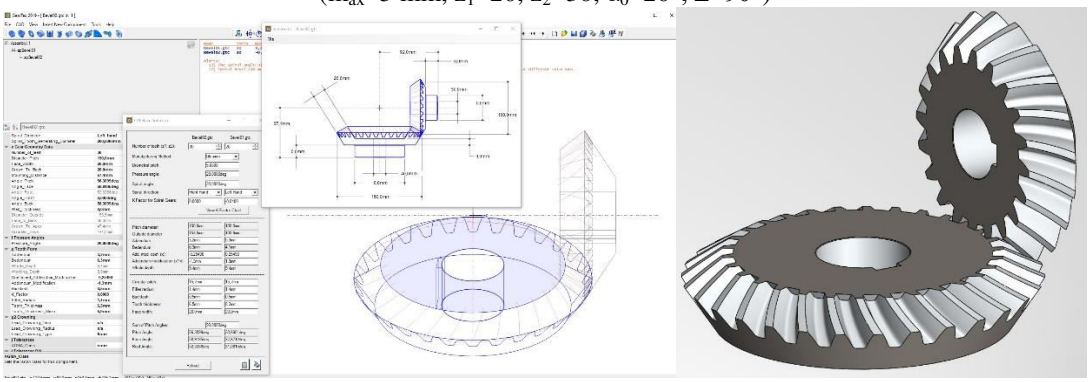

Figure 3 Designing of a helical bevel gear pair by GearTeq and Solidworks softwares (m_{ax}=5 mm, z_1=20, z_2=30, α_0=20°, Σ=90°, right hand, β_0=20°)

If we know the geometry of the pinion or the cutting tool this software can determine the connecting element by the kinematic track of the tool or double wrapping. Unique gear geometries could be designed by overwriting of the references. All of the determined parameters could be saved into Excel and the geometric shapes could be saved into

SolidWorks designer software for further utilization (motion simulations, CAM, CNC designing, TCA, etc.). In this topic some our-designed special gear pairs are shown.

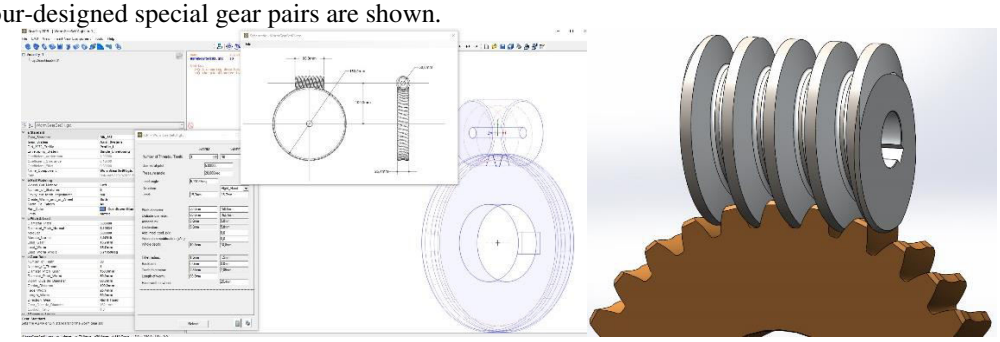

a) m_{ax}=5 mm, z_1=1, z_2=30, α_0=20°, Σ=90°, right hand

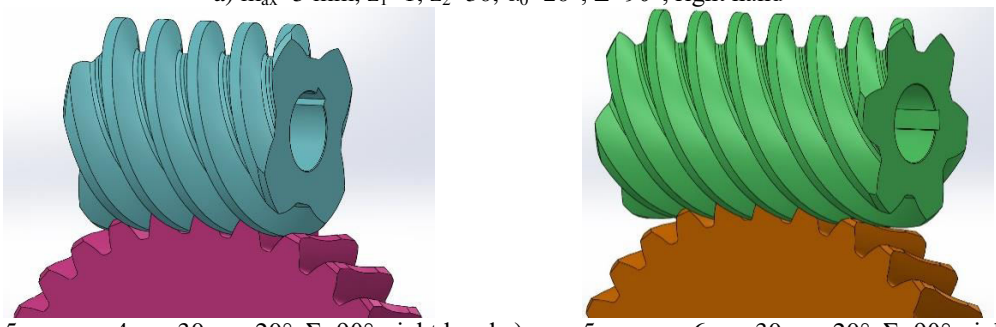

b) m_{ax}=5 mm, z_1=4, z_2=30, α_0=20°, Σ=90°, right hand c) m_{ax}=5 mm, z_1=6, z_2=30, α_0=20°, Σ=90°, right hand

Figure 4 Designing of cylindrical worm gear drive by GearTeq and Solidworks softwares

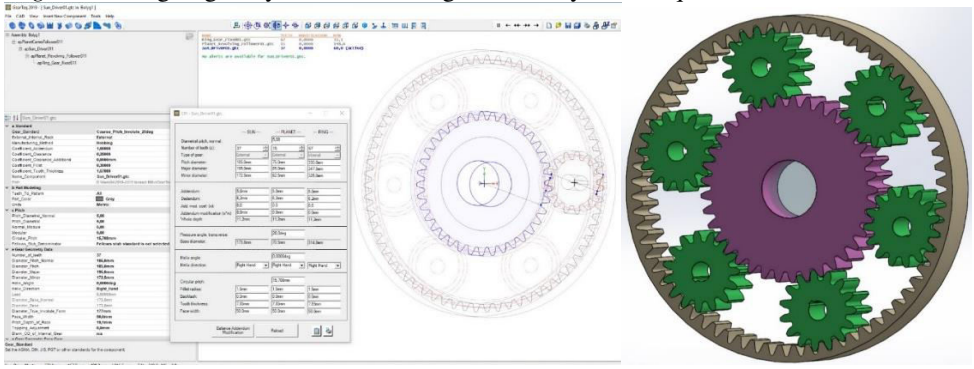

Figure 5 Designing of epicyclic gear train by GearTeq and Solidworks softwares (m_{ax}=5 mm, $z_{internalg}$=67, $z_{sungear}$=37, $z_{planetp}$=15, α_0=20°)

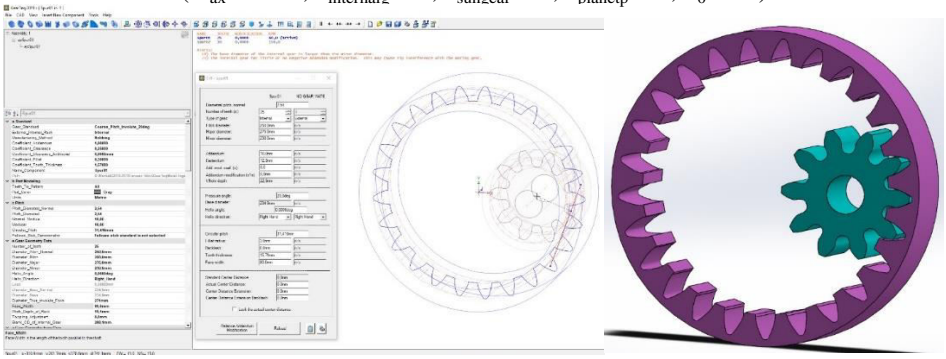

Figure 6 Designing of internal gearing by GearTeq and Solidworks softwares (m_{ax}=5 mm, z_1=20, z_2=10, α_0=20°)

ACKNOWLEDGMENTS

This research was supported by the **János Bolyai Research Scholarship of the Hungarian Academy of Sciences**.

DETERMINATION OF GTN PARAMETERS USING LOCAL APPROCH GURSON MODEL

CHAHBOUB Yassine, SZÁVAI Szabolcs PhD
University of Miskolc
E-mail: chahboubyassine@gmail.com, szavai.szabolcs@uni-miskolc.hu

Keywords: gurson model; sent specimen; ductile fracture**.**

The Gurson–Tvergaard–Needleman (GTN) model, is widely used to predict the failure of materials based on lab specimens, The direct identification of the GTN parameters is not easy and its time and money consuming.
The Gurson model based on micro-mechanical behavior of ductile fracture, containing void nucleation, growth and coalescence.
The most used method to determine the GTN parameters is the combination between the experimental and FEM results but its time consuming as we have to repeat the simulations for many times until the simulation data fits the experimental data in the specimen level (axisymmetric tensile bar and CT specimens), but there are also other methods used to determine the GTN parameters, the aim of these methods is to determine the parameters in short time as Artificial Neural Network, Hybrid Particle Swarm Optimization,. Metallographic Method.
In this paper, we determine the GTN parameters for the SENT specimen based on the fracture toughness test of CT specimen.
The reason behind choosing the SENT specimen is because it can be an excellent representative of the pipe for both uniaxial and biaxial loading conditions. [1]
The Results show that the GTN parameters concluded from CT simulations, predict very well the crack initiation and propagation of SENT specimen (Figure 1) which confirm the validity of this model, as already proved in the literature.

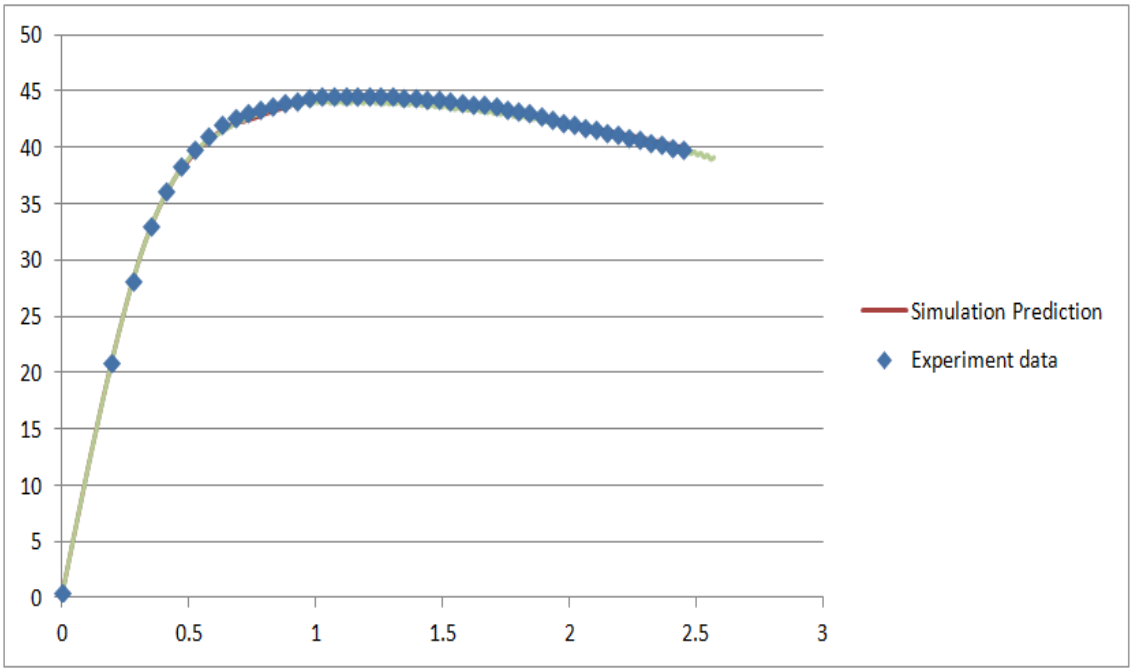

Figure 1 Force-COD curves of the predicted simulation and Experimental data

The main goal behind using the GTN model is to predict the crack initiation and crack propagation, and as we can see in figure 2 and figure 3 the GTN model was a powerful tool to predict the failure of the SENT specimen.

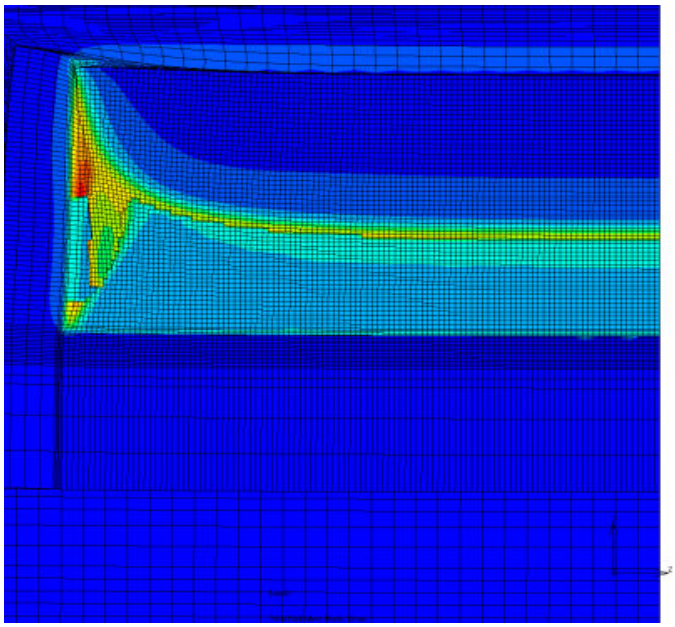

Figure 2 the contour plot of the void volume fraction of the deformed specimen

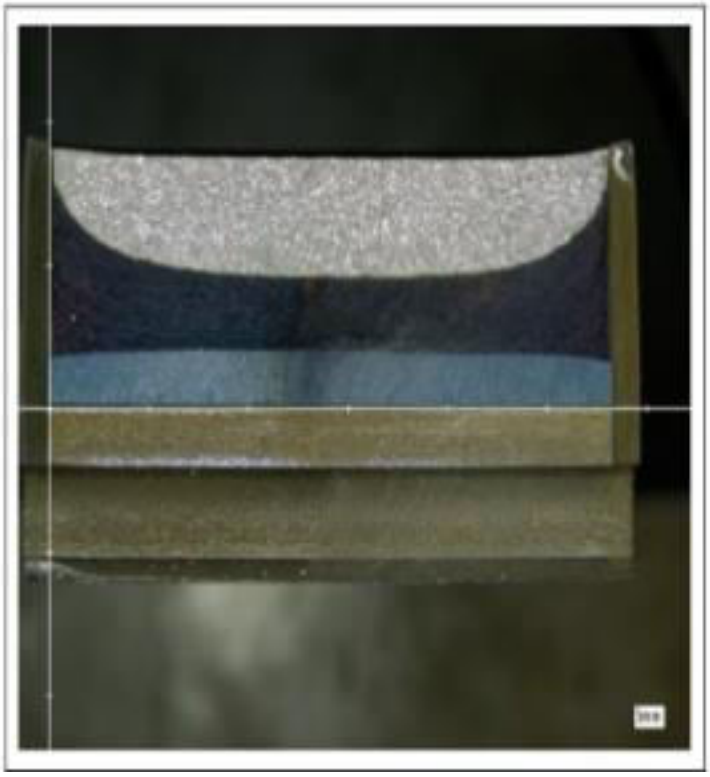

Figure 3 The crack propagation in the sent specimen

REFERENCES

[1] C. Soret, Y. Madi, J. Besson, V. Gaffard. *Use of the sent specimen in pipeline design*. 20th JTM - EPRG European pipeline research group, Paris, France. 34 p., 2015.

ALUMINUM PERLITE SYNTACTIC FOAMS

CSAPAI Alexandra, THALMAIER György PhD, SECHEL Niculina A. PhD, VIDA-SIMITI Ioan
Technical University of Cluj-Napoca
E-mail: Alexandra.csapai@gmail.com, Gyorgy.Thalmaier@sim.utcluj.ro, Niculina.SECHEL@stm.utcluj.ro, Vida.Simiti@stm.utcluj.ro

Keywords: syntactic foams, expanded perlite, aluminium, compression strength

Metallic foams combine numerous unique properties which makes them ideal for different engineering applications, such as lightweight structural sandwich panels, energy absorption devices, and heat sinks [1]. Interest in the porous metal field has increased in the last few decades, however, the most researched material is still aluminium, due to its capacity to produce a highly porous material (over 90% porosity), in large quantities, at low cost prices [2].
The aim of this research is to develop and characterize aluminium- expanded perlite syntactic foams with high porosity via spark plasma sintering (SPS). The main concern when processing metallic foams from solid state is the oxide layer formed on the surface of the aluminium particles. The SPS method has been chosen with the purpose of diminishing the effects of the oxide layer, providing a better control over the sintering process.
The materials used to carry out this research were fine aluminium particles, obtained by mechanical milling, with a flaky shape and a particle size range between 20 and 40 μm . The expended perlite, a natural, inorganic, granular material, had a size range of <500 μm and a density of 0.25 g/cm^3. Both materials have been characterized by Scanning Electron Microscopy (SEM), which showed that there are two types of perlite particles: fully expended particles and perlite particles in the beginning stages of expansion.
In the first step of the process, three batches of samples were prepared. One batch with aluminium powder in a ratio of 60% volume percentage of perlite, one sample with 70% volume percentage of perlite, and one with 80% volume percentage of perlite, respectively. The resulting mixtures were homogenized for 15 minutes, by shaking, during this step the aluminium powder covers the perlite particles. The second step consisted of sintering the mixtures by SPS in an argon atmosphere, at a temperature of 550 °C.

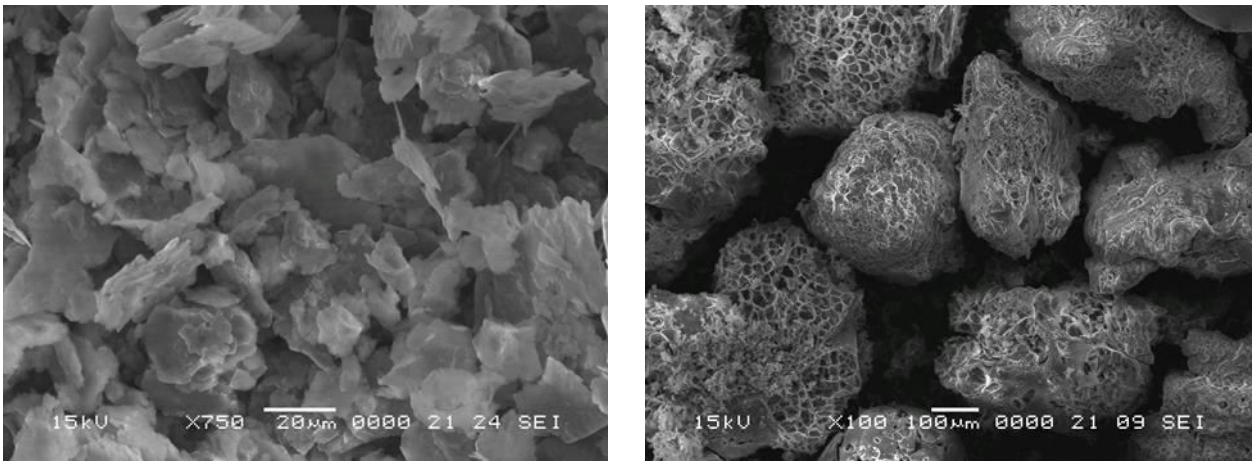

a). b).

Figure 1 SEM image of the starting powders: a). flaky aluminium and b). rounded expanded perlite

For this research, the sample's topography was characterized by Scanning Electron Microscopy and their mechanical properties by compression tests. The SEM images indicate a low sintering rate for the metallic foams obtained from the particles that were not fully expanded and better consolidation between particles in the samples obtained from fully expanded perlite. The compression tests showed that the foams with 60% volume percentage of perlite exhibit a similar behaviour as aluminium, while the 70% and 80% volume percentage of fully expended perlite samples present a more metallic foam-like behaviour.

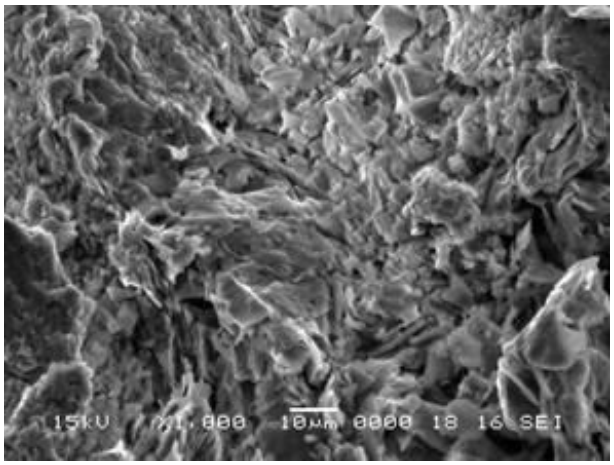

a).

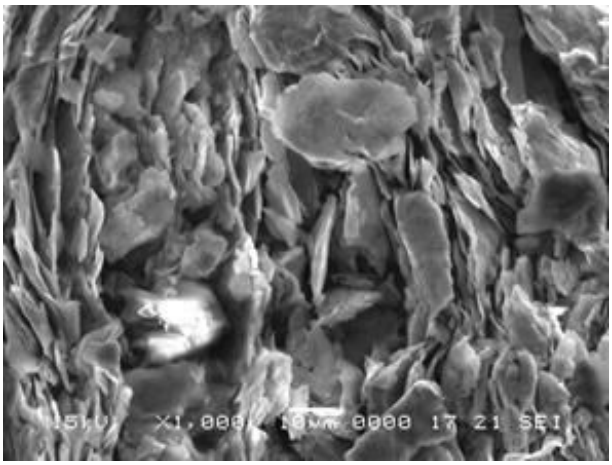

b).

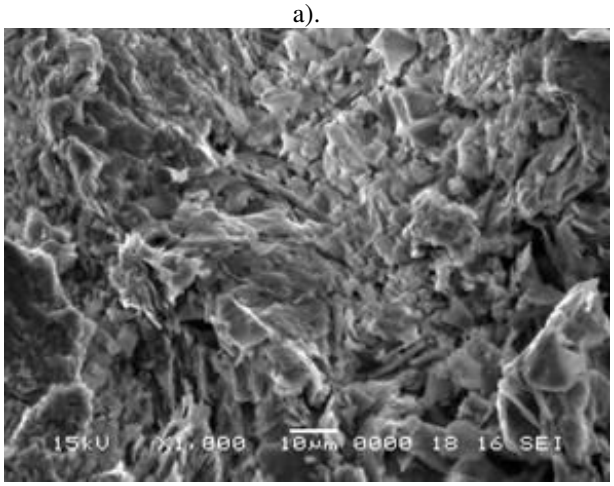

c).

Figure 2 SEM image of the sintered samples a). 60% perlite; b). 70% perlite and c). 80% perlite

The samples densities vary from 1.73 g/cm^3 to 1.16 g/cm^3.This values correspond to a weight reduction from 36% up to 57%. The compression strength for the samples containing 70 % perlite particles is around 18 MPa and decreases to around 13MPa for the samples containing 80% perlite. Energy absorption (W) and its efficiency (EW) calculations have been carried out using the Origin software. For the 70% volume percentage of perlite samples W= 3.22 MJ/m³ the efficiency was EW= 90%, and for the 80% volume percentage we obtain W= 4.79 MJ/m³ and EW= 70%.

REFERENCES

[1] L. J. Gibson: *Mechanical Behavior of Metallic Foams,* Annual Review of Materials Science, Vol. 30, 191–227. 2000.

[2] Mark A. Atwater, Laura N. Guevara, Kris A. Darling, Mark A. Tschopp: *Solid State Porous Metal Production: A Review of the Capabilities, Characteristics, and Challenges*- Advanced Engineering Materials, Vol. 20, 1-33. 2018.

INVESTIGATION OF THE GRANULOMETRIC AND MECHANICAL PROPERTIES OF INORGANIC USED SAND

DARGAI Viktória, VARGA László PhD
Institute of Metallurgical and Foundry Engineering, Faculty of Material Science and Engineering, University of Miskolc
E-mail: viktoria.dargai@gmail.com, ontvlaci@uni-miskolc.hu

Keywords: used sand, inorganic binder, granulometric, mechanical properties, sand testing

Nowadays foundry technologies are the main users of quartz sand, which is used as the base material of moulding and core making. Traditional sand technologies are still dominating all other foundry processes so much, that about 80% of the castings made worldwide are performed by this method [1] In recent years, foundry technologies have strongly developed, but they are still applying quartz sand as the main material for core production. Therefore, the application and reusability of sand plays an important role in the foundry world. The other major factor is the ever stricter environmental and health laws. These changes negatively affect the cost of depositing the used sand and the reclaimed sand as the procedures are becoming more and more expensive. Foundries are trying to recycle the used sand in the sand circuit system in order to save costs, thus in most cases, the used sand will be reclaimed. Reclamation of used sands can be defined as a conversion process of foundry sands into a moulding material which properties similar to new sand, by removing the residual binder. [2], [3] Generally applied reclamation processes are used practically for all foundry sands, but the reclamation is not always successful, especially when the binder materials are inorganic. The use of inorganic binders has been increased significantly in recent decades, because it is less harmful to the environment and health, due to zero emission and there is no unpleasant odour occurring during core production and casting. Hydrated sodium silicate is one of the most popular and commonly applied inorganic binder. [4] However, continuous research and development in the field of inorganic binder systems are required in order to ensure their problem-free application.

The aim of presented research was to determine the mechanical and granulometric properties of inorganic used sand. The inorganic used sand was recycled in multiple rounds using the same sand mixture recipe. As research materials, a Slovakian 3-components quartz sand and a modified inorganic binder were used. The applied amount of binder for each recycled round was 2,2m/m%. The used sand was thermal loaded at 150°C and 600°C for one hour. After lump crushing, the used sand was recycled for making the new mixture from which the new test piece was created. The bending samples were produced using Multiserw Universal Core Shooter laboratory machine. Table 1 shows the production parameters for bending samples.

Table 1 Default test parameters for samples

Core box temperature	180°*C*
Gassing temperature	100°*C*
Shoot pressure	3*bar*
Gassing time	30*s*

During the research, the granulometric properties of the recycled used sand were investigated after every cycle. Due to this process, it has been occurred, that the grain composition of used sands shifted towards the coarse grain fraction.
The mechanical properties were tested with the Multiserw Universal Strength Testing Machine. The results of the used sand, after being thermal loaded at 150°C for an hour, are shown in Figure 1.

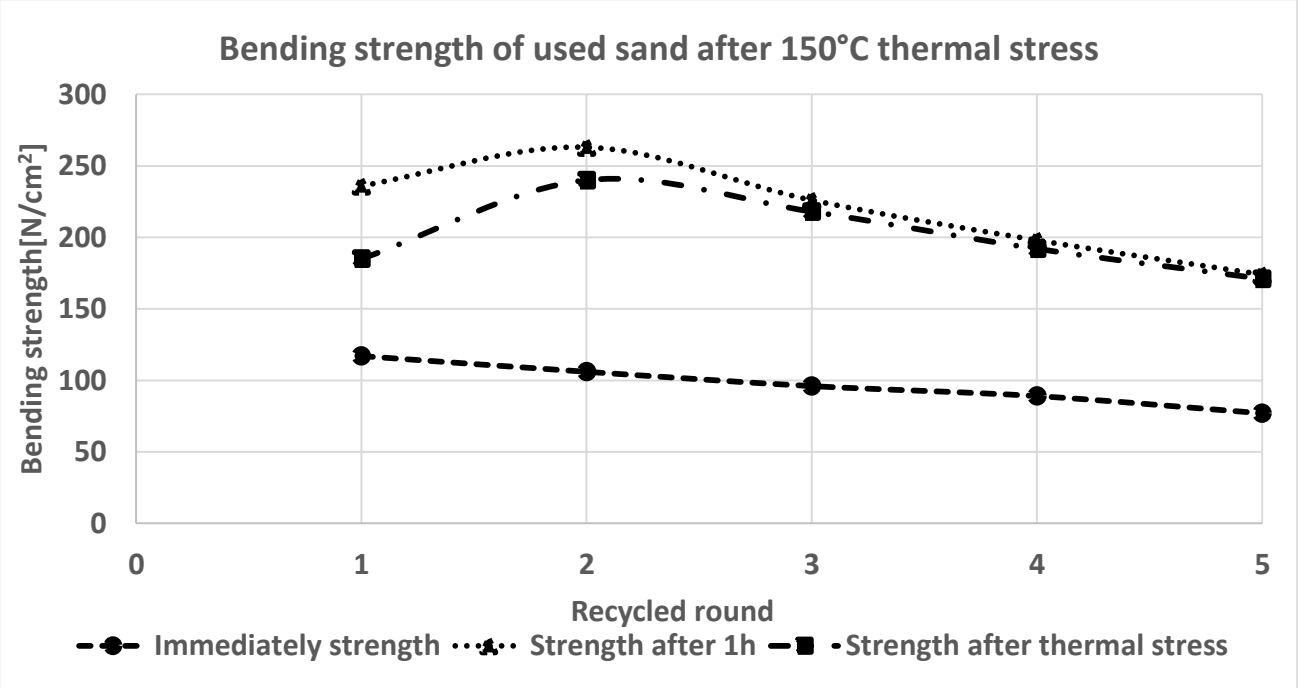

Figure 1 Bending strength of used sand after 150°C thermal stress

Figure 1 shows that in this case, there is a decrease in the immediate binding strength. In the second recycled round, a 10% strength value increase can be observed after one-hour preservation, however after the third recycled round this strength value is steadily decreasing. The residual strength value increased by 30% for second recycled round, but after that, even these residual strength values were started to decline.
Summarizing the results, all the data we collected were organised according to their process parameters, then measurements were made towards the connection between the ever coarsening sand particles during each cycle and the decline in strength properties.

REFERENCES

[1] Danko J., Danko R., Holtzer M., *Reclamation of used sands in foundry production*. Metalurgija 42 (3), 173-177, 2003.
[2] Polzin H., *Anorganische Binder zur Form- und Kernherstellung in der Giesserei*. Fachverlag Schiele und Schön GmbH, 2012.
[3] Danko J., Holtzer M., Dank O., *Factors influencing selection of effective reclamation techniques and assessment methods of the reclaimed material quality*. Archives of Foundry Engineering Volume 7 (4), 29-32, 2007.
[4] Izdebska-Szanda I., Kaminska J., Angrecki M., Palma A., Stefanski Z., *The Effect of Additive "B" on the Properties of Foundry Sands with Hydrated Sodium Silicate Made by Floster Technologie*. Archives of Foundry Engineering Volume 17, 31-34, 2017.

APPLIED DIAGNOSTIC METHODS IN ENGINE AND BEARING HEALTH MONITORING

DEÁK Krisztián, KOCSIS Imre PhD
Department of Mechanical Engineering, Faculty of Mechanical Engineering, University of Debrecen
E-mail: deak.krisztian@eng.unideb.hu, kocsisi@eng.unideb.hu

Keywords: wavelet, diagnosis, bearing, fault, engine, knocking detonation

Experiments are connected to the analysis of internal combustion engines with wavelet-based feature extraction. It has been investigated how the needle shape and position influence the vibration level of the engine with a defined main jet and pilot jet combination in the carburettor. With lean petrol-gas ratio the combustion develops detonation that produces a special knocking sound and vibration form that is harmful to the piston, rod and bearings of the engines but it is not easy to detect in the early cases especially in higher rpm's. In this experiment Keihin PWK 36S carburetor was used with constant setting of 165 main jet, 35 pilot jet, N2ZW needle #3 position, AS 1.75 turn out. Different fuels were used and the compression ratio was adjusted by the cylinder base gasket thickness from 0.2 mm up to 1.2 mm. Thicker gasket means higher compression.
To create more torque and power from the engine the pre-ignition angle could be increased and the compression in the cylinder head if it is changed to a high-compression head or milled to produce lower X dimension and squish. In both cases the risk of detonation is high even if high octane petrol is used. The knocking detonation was measured by wavelet methods using not only petrol but race fuel and methanol. As the part of technical maintenance and diagnostics it is important to reveal this phenomena and avoid it. Both methanol and ethanol burn at lower temperatures than gasoline, and both are less volatile, making engine starting in cold weather more difficult. Using methanol as a fuel in spark-ignition engines can offer an increased thermal efficiency and increased power output (as compared to gasoline) due to its high octane rating (114) and high heat of vaporization. However, its low energy content of 19.7 MJ/kg and stoichiometric air-to-fuel ratio of 6.42:1 mean that fuel consumption (on volume or mass bases) will be higher than hydrocarbon fuels. Besides the detonation phenomena the water pump bearing was checked by wavelet analysis with 12 different wavelets.

For effective fault detection it is critical to find a proper wavelet that matches well with the shape of the signal at a specific scale and location. Low transform value is obtained if the signal and the wavelet do not correlate well. Visual observation of contour plots is not appropriate for adequate wavelet selection. Thus, a more sophisticated method for wavelet selection is used in this experiment. Real valued wavelet is compared to complex Morlet wavelet according to the Energy-to-Shannon-Entropy ratio criteria to determine which is the most efficient for detecting the manufacturing fault. Complex Morlet wavelet is a kind of band-pass filter which has a good capacity for noise reduction and bearing fault frequency detection. The center frequency and bandwidth of complex Morlet wavelet is adjustable, thus, it has more flexibility for feature extraction. To determine the efficiency of the designed wavelet and compare to the other wavelets, a test-rig was constructed equipped with high-precision sensors and devices. The designed wavelet is found to be the most effective to detect the knocking phenomena of the internal combustion engines.

$$DWT(j,k) = \frac{1}{\sqrt{2^j}} \int_{-\infty}^{\infty} s(t) \cdot \Psi^* \left(\frac{t-2^j k}{2^j}\right) dt \qquad \psi(x) = \frac{1}{\sqrt{\pi\beta}} e^{2i\pi f_0 x} e^{-\frac{x^2}{\beta}} \qquad E(n) = \sum_i^m \left|C_{n,i}\right|^2$$

$$S(n) = -\sum_{i=1}^{m} p_i \log_2 p_i$$

NI 9234 DAQ is used in the experiment that delivers 102 dB of dynamic range with sampling rates up to 51.2 kHz per channel with built-in anti-aliasing filters. 32 bit AMD Athlon II X2 M300 2.0 GHz processor is used for data processing. PCB IMI 603C01 vibration transducer is applied with low noise level, high sensitivity of 100 mV/g, frequency range up to 10 kHz with top exit 2-pin connector. The accelerometer is placed on the surface of the cylinder by heat resistant Loctite glue after degreasing. KTM EXC 300 2-stroke dirt bike engine was analyzed in the experiment. Compression ratio was modified from 10:1 to 13:1 by adding thin base cylinder gaskets and milled cylinder head in case of the 13:1 highest compression. Water pump bearing was KTM grooved ball bearing 6901v c3. Measurements were executed at idle of 1350 1/min.

Figure 1 Knocking measurement with PCBIMI603C01 transducer (left), cylinder base gasket changing procedure (middle) and the water pump bearing (right)

Table 1 Energy-to-Shannon Entropy values with 95 octane fuel with 14:1 compression with knocking combustion

Compression knocking phenomena results				**Water pump bearing fault detection**			
Wavelet	**E/S**	**Wavelet**	**E/S**	**Wavelet**	**E/S**	**Wavelet**	**E/S**
Symlet-02	78.59	Mexican hat	68.74	Symlet-02	63.15	Mexican hat	79.42
Symlet-05	94.53	Coiflet-04	102.44	Symlet-05	74.56	Coiflet-04	88.46
Symlet-08	111.37	Meyer	98.65	Symlet-08	107.68	Meyer	53.47
Daub-02	81.45	Haar	57.34	Daub-02	64.67	Haar	51.98
Daub-05	97.56	Morlet	123.78	Daub-05	81.54	Morlet	103.45
Daub-08	109.43	**Cmor (452,1785)**	**161.36**	**Daub-08**	**120.42**	**Cmor (218,2856)**	**121.78**

Table 2 Vibration acceleration values [mm/s^2] and wavelet parameters of the engine analysis,

Fuel Type	**Compression ratios**				**Wavelet type with parameters**
	11:1	**12:1**	**13:1**	**14:1**	
95 octane	22.46	23.12	***124.87***	***157.79***	Cmor (452, 1785)
98 octane	20.47	22.74	22.54	***143.41***	Cmor (452, 1785)
100 octane	19.33	21.79	21.85	**63.69**	Cmor (452, 1785)
Race Fuel (106 octane)	18.77	20.12	20.78	21.47	Daubechies_14 and Cmor (452, 1785)
Methanol (114)	19.12	20.76	20.89	23.78	Cmor (452, 1785)

Knocking detonation was occurred with 95 octane and 98 octane petrols under 14:1 and 13:1 compressions. In case of 100 octane petrol we perceived partly detonation with increased value of 63.69 mm/s^2 vibration acceleration. They are highlighted in the Table 2. In the experiments Cmor (452, 1785) which was produced the best E/S ratio that means the highest efficiency to the knocking detection. For the waterpump fault detection Daub-08 and the designed Cmor (218,2856) wavelet appeared to be the most efficient. Faults on the bearing derived from operation wear processess. Four bearings were examined with different wear conditions counted in operational hours (21, 57, 111 and 218 hours). All bearing came from motorcycle repair workshops for the experiment and they were repaired in the motorbike in the experiment.

REFERENCES

[1] Patel, V. N., Tandon, N., and Pandey, R., K., *Defect Detection in Deep Groove Ball Bearing in Presence of External Vibration Using Envelope Analysis and Duffing Oscillator*, Measurement 45, p. 960. 2012.

[2] Al-Ghamd, A.M., Mba, D., *A Comparative Experimental Study on the Use of Acoustic Emission and Vibration Analysis fo r Bearing Defect Identification and Estimation of Defect Size*, Mechanical Systems and Signal Processing 20, p. 1537. 2006.

[3] Elforjani, M., Mba, D., *Accelerated Natural Fault Diagnosis in Slow Speed Bearings with Acoustic Emission*, Engineering Fracture Mechanics 77, p. 112. 2010.

PRINCIPLES OF THREE-DIMENSIONAL COMPUTER DESIGN FOR UNDERSTANDING IMPOSSIBLE FIGURES

DOVRAMADJIEV Tihomir PhD
Department of Industrial Design, Technical University of Varna
E-mail: dr.tihomir.dovramadjiev@gmail.com

Keywords: 3D, blender, logic

INTRODUCTION

Impossible figures are combinations of geometric elements positioned in specific compilations that create the illusion of completed objects, but at the same time have an extremely impossible vision. This is especially the case when certain details are interwoven in a particular order or position. Creating them requires a rich imagination and understanding of three-dimensional space. Impossible figures are a good tool for developing logical thinking, creating creativity in adolescents, and are often used in the educational process. Impossible figures are present in the visual arts, architecture and spatial form shaping. These types of figures are challenging for both the users and the authors of the compositions themselves. In the development of conceptual designs, various techniques are used, based on the knowledge related to conventional geometry, spatial vision and exact isometric coordinates. Some of the popular models of impossible figures were created as sculptures by Australian artist Brian Mackay and architect Ahmad Abbas [1 - 3].

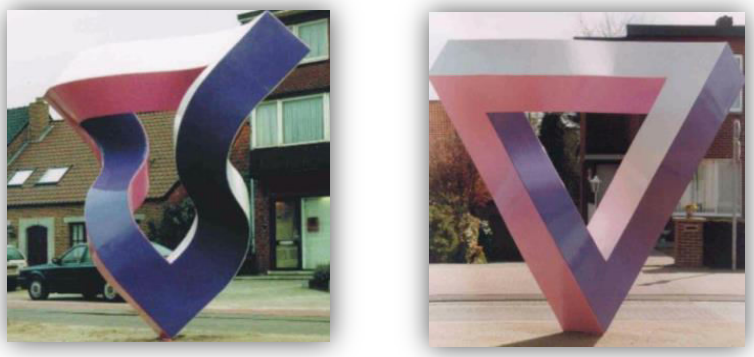

Figure 1 Popular sculptures of impossible figures [1-3]

The impossible figures are the inspiration of the Dutch graphic artist M.C. Escher, who has sketched the popular artworks “Waterfall”, “Belvedere”, “Ascending and descending”, and more [4-9].

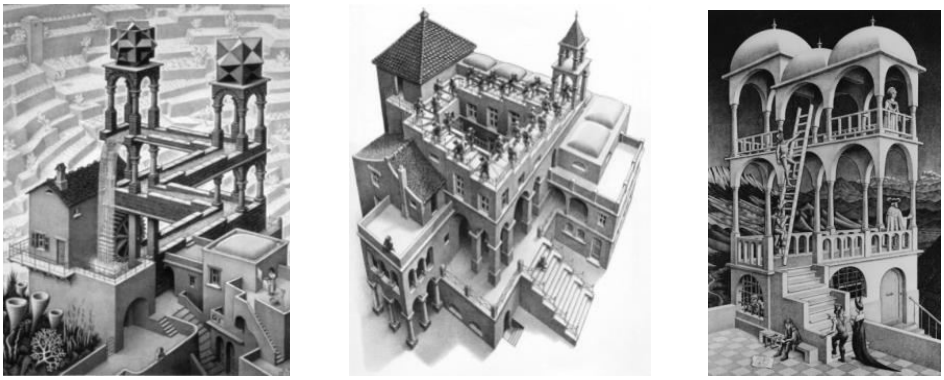

Figure 2 Popular works by the Dutch graphic artist M.C. Escher. From left to right: “Waterfall”, “Belvedere”, “Ascending and descending” [4-9]

Over time, impossible figures have become increasingly popular and interesting to a wide range of professionals, ordinary people, adolescents, and people with multiple interests. Impossible figures begin to be interpreted in architecture, in interior and exterior design, in computer and mathematical modeling. In certain cases elements are borrowed or involved in diverse compositions [10–19]. This is possible when conventional design, modeling and other design techniques are applied [20-25]. Based on these, hybrid models have been successfully implemented. In recent years, there has been a steady increase in video and animation and other types of interpretations of impossible figures in

combination with physical processes, where the emphasis is on the influential effect of perceptions in order to develop logical thinking and improve spatial-analytical memory [26-30].

MATERIALS AND METHODS

Creating three-dimensional geometry of impossible figures is a challenge not only logically but also technically and constructively. It is necessary to make the right selection of applicable software, knowing the technical capabilities of the program, in accordance with the approach applied by three-dimensional designers. A good solution is the 3D Blender program [31-37]. It has all the resources available to fulfill the set goals, and through it it solves the tasks related to the development of three-dimensional geometry. The following are relevant:

- The individual logical approach of the designer;
- Conventional Blender 3D Design Technique;
- Application of specialized modifiers in the work process.

Figure 3 shows the digitally realized 3D models of impossible Penrose triangle, Penrose Stairs, and Necker cub figure.

Figure 3 Computer made 3D models of impossible figures using open source Blender software 3D. From left to right: Penrose triangle; Penrose Stairs; Necker cub

In this study, the technique for visualizing a selected developed model (Penrose Triangle) is presented in a sequence that fully reveals the way in which it is possible to design an impossible model that actually has real correct geometric characteristics.

ACKNOWLEDGMENTS

The described work was carried out as part of the research “Advanced technologies in design”.

SPATIAL ROTARY COMBUSTION ENGINE

[1]DUDÁS László PhD, [2]BIRÓ Máté, [3]NOVÁK László Lajos, [1]KAPITÁNY Pálma
[1]University of Miskolc, Miskolc, Hungary
E-mail: iitdl@uni-miskolc.hu, kapitanypalma@gmail.com
[2]STEGA Ltd., Miskolc, Hungary
E-mail: biroomate@gmail.com
[3]Harman Ltd., Pécs, Hungary
E-mail: dariusz4424@gmail.com

Keywords: Rotary engine, internal combustion, spatial, rotor, rotary chamber

EVOLUTION OF ROTARY PISTON ENGINES

The evolution of rotary piston engines began at a distance and took place on two branches: from the screw compressor ancestors and from the progressive cavity pumps. The screw compressor branch is not analysed here because of the largely different build-up.

The progressive cavity pumps direction began in 1932 with the invention of the American inventor *Moineau* [1]. His design consisted of a rotor with two superimposed rotary motions, i.e. planetary motions, and a stationary chamber having an inner screw surface surrounding the rotor. *Moineau's* compact design induced the creation of several variants. The patented *Dudás motor* [2], unlike the previous designs, comprises continuously variable pitch screw surfaces, see Figure 1b. The goal of this analysis is to reveal its potential.

The famous construction (1951, see Figure 1a) of *Felix Wankel* [3], is a planar realization of the two rotary motion and the helical shape is missing. Under the name *Wankel engine* which in fact has so far represented the rotary piston engines alone, instead of the rotary piston and rotary chamber version the planetary piston version having stationary chamber suggested by *Hanns Dieter Paschke* [4] is known. All major car manufacturers have been experimenting with this design, but Mazda has got the furthest.

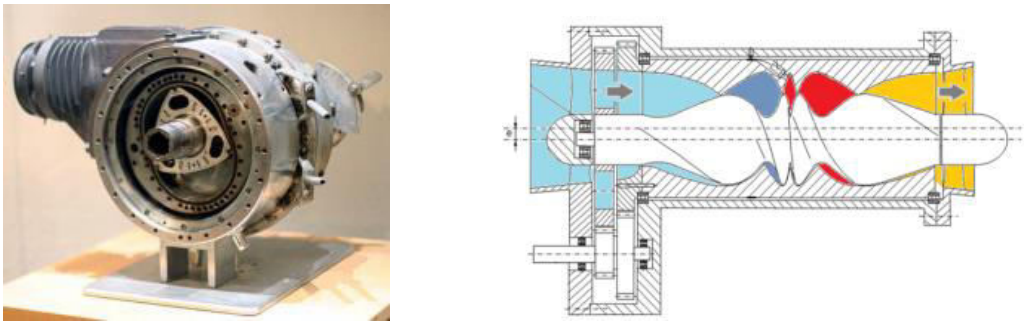

Figure 1 (a) Wankel-built DKM 54 clean rotary motor [3] and *(b)* the Dudás motor [2].

COMPARISON OF ADVANTAGES AND DISADVANTAGES OF PLANAR AND SPATIAL ROTARY PISTON INTERNAL COMBUSTION ENGINES

The advantage of rotary piston engines over alternative piston engines is their incredible smooth, quiet running and compact design. Due to their high rpm and very good power/weight ratio they are more suitable for racing cars. The main advantage of *Dudas engine* relatively to the *Wankel engine* is the **3 dimensional (3D) spatial construction** where the construction freedom in axial direction appears and allows parallel strokes and phases not only on different sides of the rotary piston but along the axis also. Additionally it makes possible optimizations through the thread pitch function.

Main Disadvantages The *Wankel engine* that has an extruded **planar (2D) construction** is similar to conventional two-stroke engines for flow control, where the openings are closed by the piston. The problem is similar, that is, the expanding gas is not completely burned when the spill gap opens. This causes fuel loss, power loss and environmental pollution. The very rapid cyclic temperature change at the rotor gaskets because of the constant temperature difference between the inlet and expansion sides of the housing imposes high demands on the material of the gasket. All these operational problems do not appear at first glance evaluating the brilliant geometric design. The lubrication with oil

injected into the suction cavity to lubricate the sliding edge and side seals results in high levels of pollutant and odor emissions.

Bearings Due to the eccentric shaft, *Wankel motors* usually have plain bearings, which are disadvantageous in operation due to mixed friction at start and stop. At the same time, dynamic loads are better tolerated. The *Dudás motor* without rotor friction is clearly fitted with ball bearings, which can be made of ceramic, do not restrict accessing very high speeds of up to 40,000 rpm at very high temperature.

Efficiency In terms of efficiency, the *Wankel engine* can be said to have a crank drive loss of about 1% and a 10% loss due to the fact that the compression ratio cannot be set to the required level. All these problems do not exist with the *Dudás engine* because it contains only rotating moving parts, the compression and expansion ratios are independently adjustable over a wide range, the sucked compressed mixture and the expanding working gas are completely separated. Even after-ignition can be used at any location in the expansion chamber. This great degree of freedom results from the fact that the construction is not planar (2D) but spatial (3D) in relation to the *Wankel engine*. However, the drawback of the *Dudás engine* is that it is longer in size, which requires dimensioning of the rotor deflection, and the manufacture of the shaped rotor and especially of the split chamber is demanding and complex, i.e. expensive. This justifies, among other things, the production of these parts from ceramics, which eliminates the need for cooling and heat loss.

Compactness, power/volume ratio The *Wankel engine* is more compact. The *Dudás engine* is less compact due to the larger length. With the better power/weight ratio, this engine boasts four longitudinal phases that are doubled on both sides of the rotor, when three strokes works at one time on the three sides of the rotor in the *Wankel engine*.

Engine Parts Since the gaskets appear as separate elements, the amount of parts of the *Wankel engine* may be larger.

Engine Assembling and Mantainability Assembling is partly related to the number of parts and affects the mantainability. To piece together the *Wankel engine* is easier. The *Dudás engine* requires more precision in assembly.

Engine Failure Probability The failure probability of a *Dudás engine* is clearly smaller, since the piston and rotary chamber are only rotating, there is not even contact, the main problem occurs with gears and bearings. The final version of the engine should be made of ceramic. Zirconium-based industrial gears and bearings can already be purchased. On the other side the *Wankel engine* needs frequent replacement of the edge seals.

CONCLUSION

The article analyzed the advantages and disadvantages of 2D *Wankel* and 3D *Dudás* rotary piston internal combustion engines. Opposite to advantageous compactness of *Wankel engine*, the exhaust imperfections, exhaust gas mixing with the intake mixture, and the high oil consumption due to the lubrication requirements can be mentioned. The full ceramic design would increase the chances of a *Dudás engine*, taking advantage of the friction-free operation, but it would require the development of a fuel component that does not generate harmful combustion products against to the gap sealing operation. In addition, one of the perspectives of converting hydrocarbons into motion energy, due to the extremely high operating temperatures and the extremely high speeds resulting from the design, is the motor that only rotates.

ACKNOWLEDGMENTS

This research was partially carried out in the framework of the Center of Excellence of Mechatronics and Logistics at the University of Miskolc. The described study additionally was carried out as part of the EFOP-3.6.1-16-00011 “Younger and Renewing University – Innovative Knowledge City – institutional development of the University of Miskolc aiming at intelligent specialization” project implemented in the framework of the Széchenyi 2020 program. The realization of this project is supported by the European Union, co-financed by the European Social Fund.

REFERENCES

[1] L. R. J. Moineau, *Gear Mechanism*, United States patent US 1892217 A. 1932.
[2] L. Dudás, *Rotary Piston Internal Combustion Engine*. Hungarian patent HU230082. 2015.
[3] Craig, *NSU Wankel rotary engines and cars*, http://cp_www.tripod.com/rotary/pg05.htm, Accessed: Oct. 12, 2019. 2001.
[4] *Der Wankelmotor und sein Erfinder*, http://www.nsuro80.ch/das-auto/der-motor/, Accessed: Oct. 11, 2019.

NEUTRAL INHOMOGENEITY IN CIRCULAR CYLINDER SUBJECTED TO AXIAL LOAD ON ITS LATERAL BOUNDARY

ECSEDI István PhD, LENGYEL Ákos József, BAKSA Attila PhD
Institute of Applied Mechanics, University of Miskolc
E-mail: mechecs@uni-miskolc.hu, mechlen@uni-miskolc.hu, mechab@uni-miskolc.hu

Keywords: circular cylinder**,** elastic inclusion, neutral inhomogeneity, antiplane shear deformation

In this study we consider the problem of single circular elastic inhomogeneity embedded within a circular cylinder whose curved boundary surface is subjected to surface traction acting on axial direction. We investigate the displacement neutrality of the coupled system of host body and inclusion. Neutral inhomogeneity (inclusion) does not disturb the displacement, strain and stress fields in the host body. The deformation of the considered inhomogenneous cylinder is antiplane shear deformation.
The antiplane shear deformation is a special case of the state of deformation in a solid body. This state is achived when the displacements in the body are zero in the plane of interest but nonzero in the direction perpendicular to the plane. If the plane of antiplane shear deformation is the plane *Oxy* of the rectangular Cartesian frame *Oxyz* and the displacement vector is represented as

$$\mathbf{u} = u\mathbf{e}_x + v\mathbf{e}_y + w\mathbf{e}_z,$$

where $\mathbf{e}_x$, $\mathbf{e}_y$, $\mathbf{e}_z$ are unit vectors in x, y and z directions, then the antiplane shear deformation is defined by the next equations [1,2,3]

$$u = 0, \quad v = 0, \quad w = w(x, y).$$

This means that if we consider a cylindrical body (Fig. 1) whose generators are parallel to axis z, all cross sections of this body have same deformations according to Eq. (2). The strain field of infinitesimal antiplane shear deformation is expressed as

$$\gamma_{xz} = \frac{\partial w}{\partial x}, \quad \gamma_{yz} = \frac{\partial w}{\partial y},$$

where $\gamma_{xz} = \gamma_{xz}(x, y)$ and $\gamma_{yz} = \gamma_{yz}(x, y)$ are the shearing strains, other strains are zero. The cross section of the cylindrical body is a simply connected bounded plane domain, it is denoted by A. The boundary curve of A is indicated by ∂A (Fig. 1). In our example A is a solid circular domain (Fig. 2). It is assumed that the material of the considered host body is homogeneous cylindrical orthotropic linearly elastic. The material of the cylindrical inclusion is isotropic, homogeneous and linearly elastic. The coupled system of host body and inclusion is shown in Fig. 2. The radius of cylindrical boundary surface of circular inclusion is a, and the radius of circular boundary of host body is R (Fig. 2). The connection between the host body and inclusion is perfect. The coupled system of host body and inclusion is called z-homogeneous cylindrical bar since the material parameters depend only on the cross sectional coordinates x, y. In this study we consider the problem of a single circular elastic inclusion embedded within a circular cylinder whose boundary surface is loaded by axial traction. We investigate the displacement neutrality of the coupled host body and inclusion. The netural inhomogeneity does not disturb the displacement, strain and stress fields in the host body.
During our investigation we derive the governing equations of the host cylinder and provide solution for the axial displacement and shear stress. Then the equations and solution are formulated for the host cylinder with inclusion. Some numerical examples illustrate the developed method. The study formulates the condition of existence of neutral inhomogeneity.

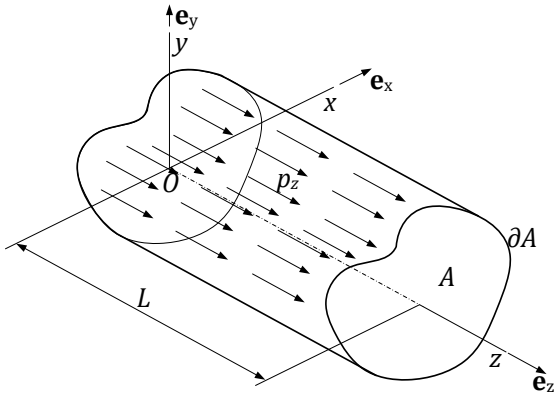

Figure 1 Cylindrical body with equilibrium surface traction

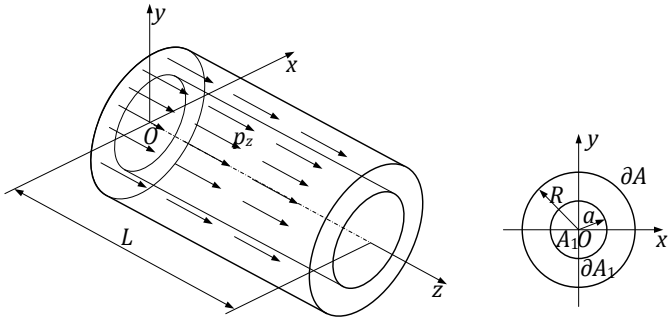

Figure 2 Circular cylinder with inclusion

ACKNOWLEDGMENTS
The described study was carried out as a part of the EFOP-3.6.1-16-2016-00011 "Younger and Renewing University – Innovative Knowledge City – institutional development of the University of Miskolc aiming at intelligent specialisation" project implemented in the framework of the Szechenyi 2020 program. The realization of this project is supported by the European Union, co-financed by the European Social Fund and supported by the National Research, Development and Innovation Office - NKFIH, K115701.

REFERENCES

[1] L. M. Milne-Thomson, *Antiplane Elastic Systems*, Springer-Verlag, Berlin. 1962.
[2] T. C. T. Ting, *Anisotropic Elasticity. Theory and Application*, Oxford University Press, Oxford. 1996.
[3] J. R. Barber, *Elasticity,* Springer-Verlag, Berlin. 2010.
[4] Y. Benveniste, T. Chen, *The Saint-Venant torsion of a circular bar consisting of a composite cylinder assemblage with cylindrically orthotropic constituents,* International Journal of Solids and Structures, 40(25), 7093-7107. 2003.

IMPROVE FIRE RESISTANCE OF DATE PALM TREE LEAFLET (*Phoenix Dactylifera L.*)

FATIMA ZOHRA Brahmia, ALPÁR Tibor PhD, HORVÁTH Péter György PhD
Simonyi Károly Faculty of Engineering, Wood Sciences and Applied Art, University of Sopron
E-mail: fatima.zohra.brahmia@phd.uni-sopron.hu, alpar.tibor@uni-sopron.hu, horvath.peter.gyorgy@uni-sopron.hu

Keywords: Date palm leaflet, Heat of Combustion, Fire Retardants, cement bonded particleboard.

Cement bonded particle boards are produced since 1928 [1] and are widely spread in building construction even until today. For cement bonded particleboard production not all, the wood species are suitable. Contrary to other materials wood is anisotropic, inhomogeneous and capillary diverse porous, and several studies emphasized that the measurable characteristics are wood species dependent [2]. Furthermore, within one species, the properties may differ according to the plantation characteristics and eventual clone variations of the same wood species [3-4-5]. Choosing the right wood species depends on the chemical structure of wood and on the type of wood cement composite produced, because the sugar and tannin content of the wood species is different [6]. It is important to choose the right wood species, the ratio of wood cement and ratio of cement water because the amount of extractives effects the cement hydration process [7]. In addition, the age, place of growth and season of harvesting are with influence also. The Scots pine is usually used in production of cement bonded particleboards because contains few extractives. Alpár and Rácz [8] proved that the poplar hybrid I214 is suitable for cement bonded particleboard production and more economic than Scots pine. Over time, many studies were made to find more alternatives for producing the cement bonded wood composites the date palm tree (*Phoenix Dactylifera L.*) was one of the interesting wood species especially on the Middle Eastern countries and north of Africa. For the wood-based industries in Algeria, more than 150 million tons of solid wood were used [9]. All part of date palm can be used in production like trunk rachis or leaflet. Haba et al [10] made new insulation material from date palm concrete. Ramadan et al [11] produced cement-bonded particleboard from date palm with positive results. This is why in our next study we want to produce CBPB from date palm tree leaflet. Before experimental board production we desired to enhance it's fire resistance. Fire retardation has many aspects, it could be related to many factors not just the type of fire retardants, but also concentration of fire retardants could make difference since wood is orthotropic material. In this study a date palm tree leaflet were used (*Phoenix Dactylifera L.*). It was broth from the oasis of oued souf, Algeria. The reason of using the date palm tree leaflet not the solid wood is that in parallel a CBPB were made from it. Two types of fire retardants have been used as test liquid: the boron compound Disodium-tetra borate ($Na_2B_4O_7$) known as Borax, and phosphorous compounds DSHP (Na_2HPO_4) in two concentrations: 25 g/l and 77g/l and DAHP ($(NH_2)_4HPO_4$) in two concentrations: 25 g/l and 300 g/l. For testing the fire retardancy of the fire retardants, a calorimeter test was made. Before the test, date palm leaflet kept at room climate of 65% RH and temperature of 20°C until reaching constant weight of 6% MC. 8g of date palm leaflet has been soaked into each fire retardant for 1 min, then drained and let to dry for 24 h, after that put to room climate till reached 6% of MC. The test has been made by Parr™ 6200 Compensated Calorimeter. The test has been repeated 5 times for each fire retardant. After measuring, the heat of combustion results showed (figure1) that Borax had no effect on fire resistance of the date palm leaflet and the same results for the other test liquids with low concentration. While PEG400 made the fire resistance worst. In other hand the fire resistance of the date palm tree leaflet increased with 5,37% for DAHP with concentration of 77g/l. and it increased with 19,80% for DAHP with concentration of 300g/l. According to previous studies, phosphorus compounds are well known as fire retardants of wood because it reduce the thermal degradation of wood. In general, phosphorus compounds forms acids that decrease the wood temperature and as result increase, its dehydration and char formation in this study two of the phosphorus compounds were used the DAHP and DSHP. In fire test, DAHP and DSHP barely improved the fire resistance of the date palm leaflet but when the concentration was increased, they were very effective as fire retardants. DAHP and DSHP with the high concentration form a thin white layer on the treated samples surface. That layer worked as protective layer from the fire. The DAHP and DSHP proved that are suitable fire retardants for wood but only if the concentration is high. The aim of next study is producing CBPB with particles of date palm leaflet treated with these fire retardants. Moreover, test the fire resistance of boards and testing the effect of fire retardant on the density and mechanical properties of boards.

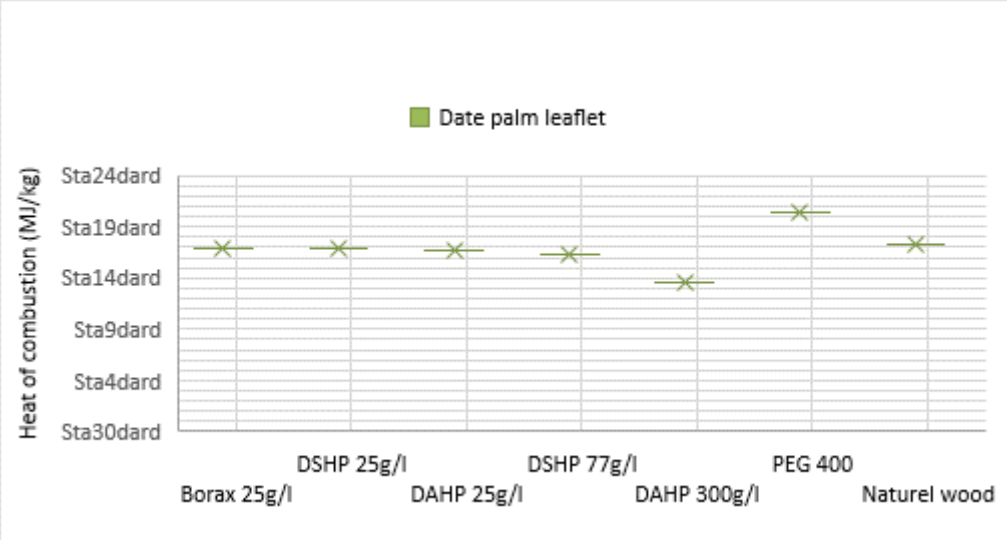

Figure 1 Heat of combustion (MJ/Kg) of date palm leaflet

ACKNOWLEDGMENTS

This article made in frame of the „EFOP-3.6.1-16-2016-00018 – Improving the role of research+ development+ innovation in the higher education through institutional developments assisting intelligent specialization in Sopron and Szombathely".

REFERENCES

[1] T.M. Malloney, *Composition board materials: properties and testing of modern particle and dry process fibreboard, Manifacturing.* 120-128. 1989.

[2] I. Variodina, N. Kosichenko, N. Nedelina, *Wood porosity depending on his tological structure.* Wood the best material for mankind J. Kudela and M. Babiak (eds). 7-10. 2013.

[3] I. Istok, T. Sedlar, B. Sefc, T. Sinkovic, T. Perkovic, *Physical properties of wood in poplar clones 'I-214' and 'S1-8'*. DRVNA IndustRiJa 67 (2). 163-170. 2016.

[4] J. Y. Zhu, C. T. Scott, K. L. Scallon, G. C. Myers, *Effects of plantation density on wood density and anatomical properties of red pine (Pinus resinosa Ait.).* Wood and fibre science. Vol. 39, no. 3. 502-512. 2017

[5] L. Benomar, A. DesRochers, G.R. Larocque *The effects of spacing on growth, morphology and biomass production and allocation in two hybrid poplar clones growing in the boreal region of Canada.* Trees 26. 939-949, DOI 10.1007/s00468-011-0671-6. 2012.

[6] M. Fan, M.K. Ndikontar, X. Zhou, J.N. Ngamveng, *Cement-bonded composites made from tropical woods: Compatibility of wood and cement.* Construction and Building Materials 36. 135-140. 2012.

[7] A.W.C. Lee, Z. Hong, *Effect of Cement/Wood Ratios and Wood Storage Conditions on Hydration Temperature, Hydration Time, and Compressive Strength of Wood-Cement Mixtures.* Wood and Fiber Science 19(3). 262-268. 1987.

[8] T. Alpár, I. Rácz, *Production of cement-bonded particleboards from poplar* (Populus euramericana cv. „I 214"). DRVNA INDUSTRIJA 60 (3). 155-160. 2009.

[9] S. Amirou, A. Zerizer, A. Pizzi, I. Hadadou, X. Zhou, *Particleboards production from date palm biomass*. Eur. J. Wood Prod. (2013) 71:717-723 DOI 10.1007/s00107-013-0730-3, 2013.

[10] B. Haba, B. Agoudjil, A. Boudenne, K. Benzarti, *Hygric properties and thermal conductivity of a new insulation material for building based on date palm concrete.* Construction and Building Materials 154:963-971, 2017.

[11] A. Ramadan, N. Al-Mefarrej, H.A. Al-Mefarrej, *Midribs of Date Palm as a Raw Material for Wood-Cement Composite Industry in Saudi Arabia.* World Applied Sciences Journal 15 (12): 1651-1658, 2011.

SEPARATION OF A TERNARY MIXTURE WITH SEMI-BATCH DISTILLATION

FERCHICHI Mariem, HÉGELY László PhD, LÁNG Péter DSc
Department of Building Service and Process Engineering, Budapest University of Technology and Economics
E-mail: mariemferchichi90@gmail.com

Keywords: batch distillation, semi-batch distillation, specific energy demand, ternary mixture

INTRODUCTION

The principal disadvantage of distillation, which is the most commonly used method for the separation of liquid mixtures, is its very high energy demand. Continuous distillation (CD) is used where large quantities of liquids have to be distilled, in which the feed is continuously fed into the column at a specific location that may have a great influence on the energy demand. On the other hand, batch distillation (BD) is frequently used for the separation of mixtures of varying composition or amount. By BD, the whole amount of charge is filled into the reboiler. BD usually requires more energy compared to CD. By combining CD and BD, different policies of semi-batch distillation (SBD) can be performed. By SBD1, one part of the feed is continuously fed into the reboiler of the batch column [1] and by SBD2, the continuous part is fed into one plate of the batch column. For different binary mixtures, using SBD2 led to a decrease of the specific energy demand (SED) compared to the BD [2-3].
In the present work, semi-batch distillation policies for a ternary mixture are investigated for the first time by computer simulation using the flowsheet simulator ChemCad. Our aim is to compare the specific energy demands (SED) of the different policies defined as the reboiler duty divided by the amount of charge or the distillate (MJ/kmol). The composition of the mixture to be separated is 33.3 mol% n-hexane, 33.3 mol% n-heptane and 33.3 mol% n-octane. The prescribed purity for each component is 95 mol%. Soave-Redlick-Kwong (SRK) thermodynamic model was chosen for describing the phase equilibrium conditions. In this work, we compare the specific energy needed for the production of n-hexane (A) only.

PROCESS DESCRIPTION

For all processes, the purity (95 mol%) and the recovery (98%) of n-hexane are the same.
For continuous distillation, the separation of the ternary mixture is performed in two continuous columns in direct sequence. The majority of n-hexane is obtained in the distillate of the first column. The minimum energy requirement can be found by changing the feeding location or the purity criterion and the recovery of A specified. The n-hexane recovery was specified by fixing the amount of n-hexane lost in the bottom product of the first column.
By BD, the maximum liquid volume is filled into the still pot. After the heating-up of the column, a first cut is taken to obtain A as distillate in a product tank and B and C remains as still residue. This step is stopped when the purity of A in the tank decreases to its specified value. For this policy, the reflux ratio (R) is adjusted in order to reach the same recovery of A as by the CD.
By the SBD policies, the continuous feeding begins immediately after the heating-up. Similarly to BD, A is produced in the first cut, which is stopped when the purity of A decreases to its specified value. After this step, the continuous feeding must be stopped. For SBD1 (feeding into the reboiler) and SBD2 (feeding into the column at a fixed location), the value of R must be determined to ensure the prescribed recovery of A. For SBD2, the optimal feeding location, where SED is minimal, must also be determined.
The data of the column (operating at atmospheric pressure) are the same for all the policies studied. The number of theoretical plates (in the ChemCad model): N=32 (including the total condenser and reboiler). The feed is always liquid at its boiling point. For the BD and SBD policies, the following additional specifications are given. The volume of the reboiler: 10 m^3, the maximal liquid volume in it: 8 m^3. The hold-ups: condenser: 0.08 m^3, column (total): 0.08 m^3. The volumetric flow rate of distillate is 1 m^3/h. At the start, the reboiler is filled up always until its maximal volume. For the SBD policies the reboiler volumetric hold-up is kept constant (close to the maximum) so the flow rate of the continuous feeding equals to that of the distillate (1 m^3/h).

PROCESS MODELS

The separation of the ternary mixture is studied using rigorous simulation calculations with the ChemCad 6.4 professional flow-sheet simulator (‘CC-BATCH’, ‘CC-STEADY STATE’ modules [4]). For continuous distillation (*Fig. 1a*), the separation is performed with two SCDS distillation columns, n-hexane is obtained as distillate in stream number 3. For the BD (*Fig. 1b*), SBD1 and SBD2 (*Fig. 1c*), n-hexane is collected as distillate of the first step in tank number 2. The other tanks are used to collect the first off-cut (tank 3), the n-heptane cut (tank 4), and the second off-cut (tank 5). N-octane will be collected into the reboiler.

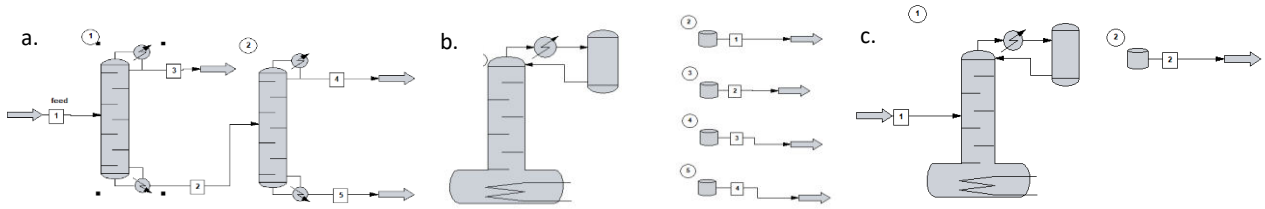

Figure 4 ChemCad flowsheets of the different policies: a. CD, b. BD and c. SBD 1 and 2

RESULTS

Continuous distillation

The flow rate of the saturated liquid feed is 1 kmol/h. The optimal feed plate of the first column (f_{opt}), where the reboiler duty (and the reflux ratio) is minimal, is determined: f_{opt}=14, R=1.42. The specific energy demand: SED=91.788 MJ/kmol distillate that is equivalent to 31.557 MJ/kmol feed.

Batch distillation

By this policy, the prescribed purity requires a much higher reflux ratio (13.2) compared to CD, which leads to an increase of the SED to 423.58 MJ/kmol distillate that is equivalent to 145.81 MJ/kmol charge. The duration of the first step is Δt=2.43h.

Semi-batch distillation with fixed feeding location into the reboiler (SBD1)

Due to the continuous feeding into the reboiler, a considerably higher reflux ratio is needed in order to reach the required n-hexane recovery: R=29.5. SED is very high compared even to BD, SED= 908.72 MJ/kmol distillate that is equivalent to 312.58 MJ/kmol charge. The duration of the first step is Δt=3.57h.

Semi-batch distillation with fixed feeding location into the column (SBD2)

The optimal feeding location is the 21th plate (counted from the top, including the condenser) with R=11.0. The specific energy demand is 363.76 MJ/kmol distillate, which is considerably lower than that of BD. The duration of the first step is Δt=3.57h which is equal to the duration of SBD1.

Table 1 SED for different policies

	CD	BD	SBD1	SBD2
f_{opt}	14	-	32	21
R	1.42	13.2	29.5	11.0
SED (MJ/kmol distillate)	91.788	423.58	908.72	363.76

CONCLUSION

From the equimolar ternary mixture n-hexane, n-heptane and n-octane, it was possible to obtain n-hexane in the specified purity (95 mol%) and with the recovery prescribed (98%) by all separation policies studied (CD, BD, SBD1 and SDB2), however, with different values of specific energy demand. SBD2 with the optimal feed plate and minimum reflux ratio, gave much lower SED values than BD, but these were still considerably higher than those of CD. The application of SBD1 is not recommended, since its SED was even higher than that of BD.

ACKNOWLEDGEMENTS

The research reported in this paper was supported by the Hungarian Scientific Research Fund (OTKA, project No.: K-120083) and by the Higher Education Excellence Program of the Ministry of Human Capacities in the frame of Biotechnology research area of Budapest University of Technology and Economics (BME FIKP-BIO).

REFERENCES

[1] P. Lang, M. Örsi, L. Hegely, *Comparison of Batch and Semi-batch Distillation*. ISCAME 2017, 12-13 October 2017, Debrecen, Hungary, 289-295. 2017.
[2] P. Lang, L. Hegely, *Different Feeding Policies for Semi-Batch Distillation*. Chemical Engineering Transactions, 69, 439-444. 2018.
[3] P. Lang, L. Hegely, *Different Semi-Batch Distillation Policies for Decreasing Energy Demand*. 22nd Conference on Process Integration, Modelling and Optimisation for Energy Saving and Pollution Reduction. 20-23 October 2019, Agios Nikolaos, Crete, Greece, article number: 366. 2019.
[4] Chemstations, *CHEMCAD Version 6 User Guide*. 2012.

MODERN APPLICATIONS OF ALUMINIUM FOAMS

GARAI Flórián
Department of Materials Technology, GAMF Faculty of Mechanical Engineering and IT, John von Neumann
E-mail: garai.florian@gamf.uni-neumann.hu

Keywords: aluminium foams, application areas, closed cell, open cell

The implementation of aluminium alloy foam has more and more attention. Application of closed cell aluminium foam has made an impact in automobile and aerospace applications where crash energy absorption, vibration and weight reduction is obligatory [1,2,3]. Figure 1 represents a possible application of closed cell aluminium foam as reinforcement element in a lightweight structure.

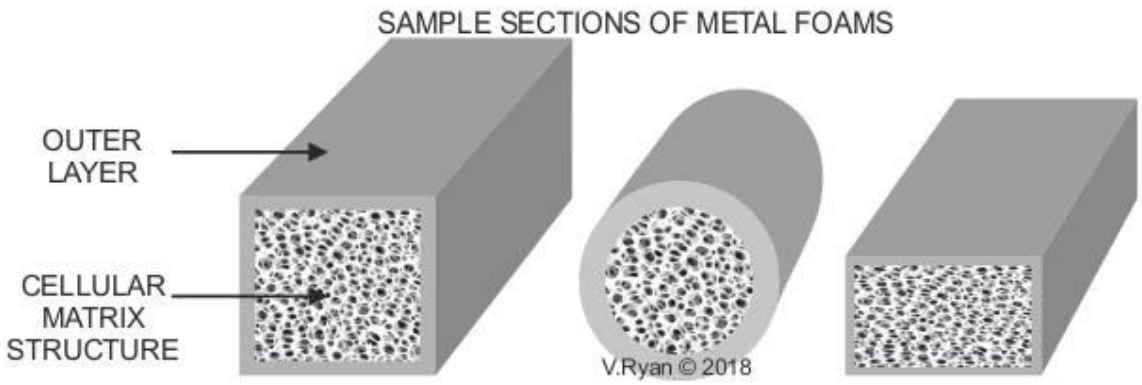

Figure 1 closed cell aluminium foam filled closed profiles
Source: www.technologystudent.com

The aluminium alloy foam is an advanced lightweight material providing high strength and stiffness at relatively low density. The technological use of aluminium alloy foam is difficult with the currently available technologies. In the case of open cell aluminium foams, the most common research areas for application are heat exchanger components, filters and sound damping elements [3]. Figure 2 represents open cell aluminium foams produced for filter elements.

Figure 2 open cell aluminium foams
Source: www.insertec-store.com

The manuscript focuses on the manufacturing techniques of the aluminium alloy foams according to the application areas. First step is the investigation of the requirements for the application: what are the loads and the circumstances and why can we use aluminium foams. Second step is the knowledge of the producing methods of the foam or the component. And the last step is the investigation of the possible testing methods.

ACKNOWLEDGMENTS
The project has been supported by the European Union, co-financed by the European Social Fund. EFOP-3.6.1-16-2016-00014

REFERENCES
[1] J. Banhart: *Manufacturing Routes for Metallic Foams, JOM: the journal of the Minerals, Metals & Materials Society 52*(12):22-2. 2012.
[2] D. Kumar Rajak, N. N. Mahajan, E. Linul: *Crashworthiness performance and microstructural characteristics of foam-filled thin-walled tubes under diverse strain rate*, Journal of Alloys and Compounds 775, 675-689. 2019.
[3] M.F. Ashby, A.G. Evans, N.A. Fleck, L.J. Gibson, J.W. Hutchinson, H.N.G. Wadley: *Metal Foams: A Design Guide, electric book*, Butterworth-Heinemann, ISBN: 9780080511467, 2000.

PROPERTY OF THERMOPLSTIC CORN STARCH REINFORCED WITH NATURAL FIBER AND FILLED WITH CALCIUM CARBONATE PRESPITATE

GEREZGIHER Alula Gebresas, SIMON Andrea PhD, SZABÓ Tamás PhD
University of Miskolc
E-mail: gebresas@gmail.com, femandi@uni-miskolc.hu, polsztam@uni-miskolc.hu

Keywords: thermoplastic starch, hybrid composites, biodegradable polymer

The shortage of oil and related minerals and also their extreme environmental drawback are the main reason for the quick growing interest in biodegradable polymer composites production. Biodegradable polymer composites are mainly produced from renewable resources which are biologically degradable. In this research, corn starch was plasticized with glycerol. The plasticized thermoplastic corn starch was reinforced with calcium carbonate powder as a filler and pine wood fiber. Free thermoplastic plasticized corn starch (FTPS), thermoplastic corn starch reinforced with calcium carbonate (CTPS), thermoplastic corn starch reinforced with pine wood (WTPS), thermoplastic corn starch reinforced with pine wood and calcium carbonate, hybrid composite (HTPS) were produced and compared for their mechanical properties like tensile strength and hardness. DSC, DMA analysis was also done for the samples produced. Water absorption test was also undertaken to understand their resistance to moisture.

PREPARATION OF TPS

Corn starch produced from Haas Naturals was weighed and mixed with glycerin produced from (company name and specification). 40 gram of glycerin was added to 60 gram of corn starch (2:3 weight percent) in a glass beaker. Then, it was mixed manually until it is plasticized. Next, for further homogenization, the mixture in the beaker was put in furnace at 120 oC for three minutes. Immediately after the solution is released from the furnace it was mixed by a mixer (name) for 5 minute at 600 rpm. The mixed solution was compressed by a compression machines in to thin sheets of 1 mm thickness under a compression of 20 Mpa and 160 oC for 5 minutes.

PREPARATION OF TPS COMPOSITES

Four samples are prepared, the table shows the ratio and composition of the samples prepared.

Table 1 Samples produced

S.No.	Sample Name	Description	Composition in weight percent	ratio
	FTPS (free)	Thermoplastic corn starch	60 % corn starch + 40% glycerin	6:4
	WTPS (wood)	Thermoplastic corn starch + wood fiber	55 % corn starch + 5% wood fiber +40% glycerin	5.5:0.5:4
	CTPS (clay)	Thermoplastic corn starch + calcium carbonate (micro, not fully nano)	55% corn starch + 5% CC + 40% glycerin	5.5:0.5:4
	HTPS (Hybrid)	Thermoplastic corn starch + wood fiber +calcium carbonate	50% corn starch + 5% CC 5% wood fiber + 40% glycerin	5:0.5:0.5:4

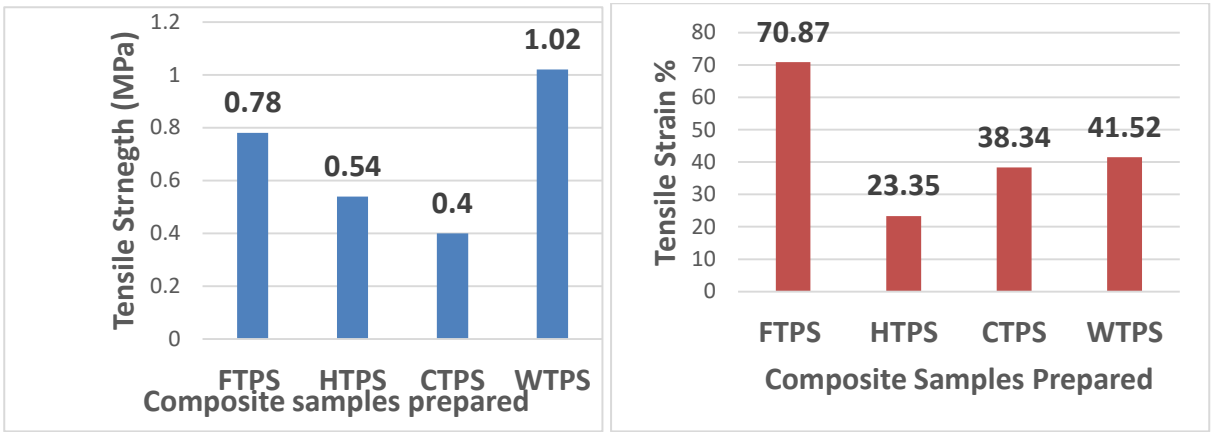

Figure1 Composite sample tensile test results

As can be shown in figures 1. WTPS has a greater strength due to the better homogeneity and compatibility (both are hydrophilic), CC composite is less strong as it is hydrophobic and due to agglomeration effect.

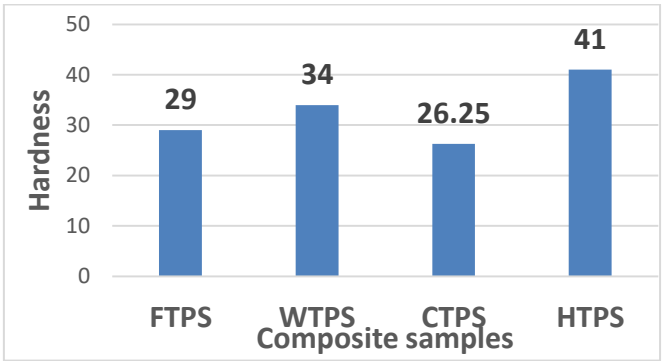

Figure 2 Hardness test result of composite samples

The graph in *Figure 2* Shows that the hybrid composite has greater hardness followed by wood reinforced TPS.

The samples SEM, DMA, DSC, Water absorption and Hardness Testing also show that pine wood fibre reinforced TPS has got better properties than precipitated calcium carbonate reinforced composites and the hybrid composites, this is due to the compatibility nature of wood fibre with TPS and hydrophobicity of calcium carbonate which leads to coagulation.

ACKNOWLEDGEMENT

I acknowledge BorsodChem chemical company for providing me inputs and technical support for the tests done in this report. I also want to appreciate Mr. Konya Csaba and other technical staffs of the company for their welcoming approach and support.

REFERENCES

[1] VK Thakur, AS Singha, IK Mehta, *Renewable resource-based green polymer composites: analysis and characterization.* Int J Polym Anal Charact 15:137–146. 2010.

[2] P González Seligra, F Nuevo, M Lamanna, L Famá, *Covalent grafting of carbon nanotubes to PLA in order to improve compatibility.* Compos B Eng 46:61–68. 2013.

[3] VK Thakur, MK Thakur, P Raghavan, MR Kessler, *Progress in green polymer composites from lignin for multifunctional applications: A Review.* ACS Sustainable Chem Eng 2:1072–1092. 2014.

[4] VK Thakur, D Grewell, M Thunga, MR Kessler, *Novel Composites from Eco-Friendly Soy Flour/SBS Triblock Copolymer.* Macromol Mater Eng 299:953–958. 2014.

INVESTIGATION ON DOUBLE OXIDE FILM INITIATED PORE FORMATION IN ALUMINUM CASTING ALLOYS

[1]GYARMATI Gábor, [1]FEGYVERNEKI György PhD, [1]TOKÁR Mónika, [2]MENDE Tamás PhD
[1]Foundry Institute, University of Miskolc
E-mail: gygabor007@gmail.com, gyorgy.fegyverneki@nemak.com, monika.tokar@uni-miskolc.hu
[2]Institute of Physical Metallurgy, Metalforming and Nanotechnology, University of Miskolc
E-mail: tamas.mende@uni-miskolc.hu

Keywords: Aluminum alloy, Casting, Porosity, Bifilm, Eutectic modification

In order to ensure adequate mechanical properties (tensile strength, elongation, fatigue life, etc.) of cast parts, the number of structural defects like porosity and inclusions must be minimized. Porosity is one of the most common defects, which can lead to inadequate mechanical properties and premature failure of cast parts. In the case of aluminum alloys, pore formation is mainly attributed to inadequate feeding of solidification shrinkage and the rejection of dissolved hydrogen during the solidification of the alloy. However, it was proposed in the literature, that double oxide films (bifilms) take a central role in pore formation as they can easily open up and inflate into pores due to hydrogen diffusion into their inner atmosphere and pressure drop in the mushy zone caused by the volumetric shrinkage during solidification (Fig. 1). This hypothesis is supported by experimental results and comprehensive theoretical calculations. Bifilm formation during the melt handling and processing techniques of aluminum alloys is mostly an unavoidable process as any disturbance of the melt surface leads to the entrainment of the surface oxide layer. In this way, numerous bifilms are introduced to the melts during common foundry activities like melting, alloying, fluxing and pouring.

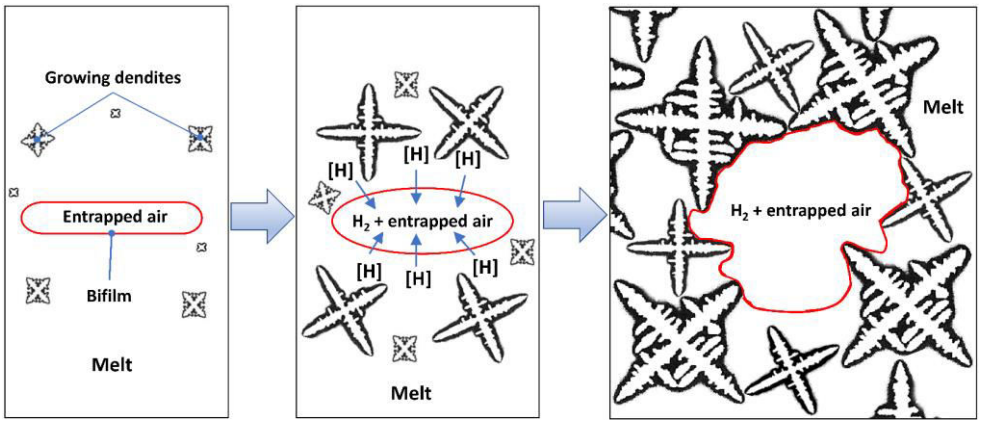

Figure 1 Schematic illustration of bifilm initiated pore formation processing

In order to produce high-quality castings, it is essential to assess and control the melt cleanliness. It was highlighted in the authors' previous research work, that the double oxide film content of liquid aluminum alloys, and thus the melt quality, can be characterized by computed tomography (CT) aided porosity analysis of reduced pressure test (RPT) specimens. In this work, this melt quality assessment technique is used for the characterization of the effects of different Sr concentrations on the bifilm content and the susceptibility to pore formation of Al-Si-Mg-Cu alloy melts.

Sr is generally used in the foundry industry to improve the mechanical properties of hypoeutectic Al-Si casting alloys, as small amounts of Sr (100-300 ppm, depending on the chemical composition of the alloy, cooling rate during solidification and melt cleanliness) causes the modification of the eutectic Si particles from a coarse flake-like morphology into a fine fibrous one. On the other hand, the modification-related research in the past decades demonstrated that Sr additions can lead to increased pore formation tendency. The increased volume fraction of porosity and higher pore number density in the cast parts is generally associated with Sr microalloying, especially at higher Sr concentrations (above 200 ppm). Despite the tremendous amount of research work aiming at the causes of this phenomenon, the mechanism underlying the effect of Sr on porosity formation is not fully understood. As bifilms are preferred sites for pore formation, it should be expected that Sr additions have a significant effect on the number and/or the structure of double oxide films present in the melt. Therefore, the aim of this research work is to study the effect of different Sr concentrations on the double oxide film content and the susceptibility of the alloy to pore formation.

Melt treatments consisting of rotary degassing with N_2 gas and flux addition were executed on AlSi7MgCu alloy melts. In order to raise the Sr concentration of the melts, in three treatment cycles, Al-10Sr master alloy rods were added to the melts. In the case of three additional experiments, no additional alloying was made. The elemental composition of the alloy was determined with optical emission spectrometry of samples cast at each stage of melt preparation. For the determination of eutectic modification level and, thus the quantity of Sr present in the melt in "active" form (in which it can take part in eutectic modification), thermal analysis was conducted before and following the melt treatments. The bifilm content of the melts was investigated by the evaluation of K-mold specimens and X-ray computed tomography (CT) of reduced pressure test (RPT) samples. During each melt preparation, specimens were cast two times. Samples were prepared from the melt in the holding furnace before and after the melt treatment. At each sampling step, 5 K-mold and 1 RPT specimens were cast. Based on the results of the CT analysis, the volume fraction and total surface area of pores, as well as the volumetric pore number density have been determined for each sample. Based on the optical emission spectrometry results, in the cases where higher Sr content was targeted, the average Sr concentration was 225 ppm. During the other three treatment cycles, an average Sr concentration of 183 ppm was achieved. Despite the relatively low difference in Sr content, the results of melt quality evaluation were significantly different from each other. The average volumetric pore number density values determined with the CT-aided porosity analysis of RPT samples are presented in Fig. 2.

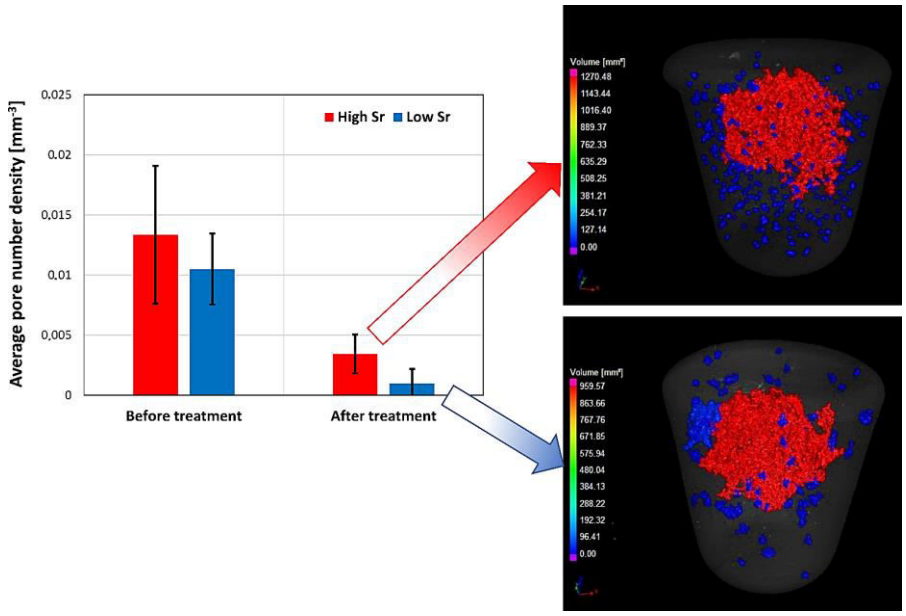

Figure 2 Pore number density results with representative reconstructed CT images

As can be seen in Fig. 2, significantly lower average pore number density results were attainable at lower Sr content, which is consistent with the experimental findings in the corresponding literature. The higher number of pores found in the RPT samples in the case of higher Sr concentration can be explained by the presence of a larger number of bifilm defects, which is confirmed by the results of the evaluation of K-mold specimens. The higher bifilm content is presumably the result of the effect of Sr additions on the oxidation rate of the alloy and its effect on the structure of oxides present in the liquid metal.

ACKNOWLEDGMENTS

SUPPORTED BY THE ÚNKP-19-3 NEW NATIONAL EXCELLENCE PROGRAM OF THE MINISTRY FOR INNOVATION AND TECHNOLOGY.

APPLICATION OF ADDITIVE TECHNOLOGY IN PRECISION CASTING

HALÁPI Dávid, VARGA László PhD
Faculty of Material Science and Engineering, University of Miskolc
E-mail: halapidavid@hotmail.com

Keywords: Additive manufacturing, 3D printing, precision casting, casting, SLA.

Nowadays, 3D printing is an extremely emerging and developing industry, one of the tools of Rapid Prototyping Technologies. Until the '80s, there were basically only two processes known as "RPT", and by the end of the decade a new revolutionary additive prototype manufacturing technology had emerged.
AM has more than 50 times the size of the market in the last decade than before and has exceeded the growth rate of 18% in the last 4 years (Wohler Report 2016). At the same time, AM's scope of application has expanded significantly, not only for prototypes, but also for tools and many other functional components, providing them high added value. It starts to outgrow itself and is slowly emerging as a production technology. Over the last 5 years, there has been a significant increase in applications for direct part production, especially in the space industry, medical technology and general engineering [3].
In many of these functional applications, AM's most sought capabilities are Design for Functionality (DFF), which focuses on maximizing the functions and performance of structures with minimal resource use (eg, materials, production time, failure, etc.). This, in turn, requires the users of AM technology to be fully aware of AM's design capabilities and limitations.
In this research, we investigate the feasibility of producing precision casting samples by 3D printing, and then the final products are certified on the basis of comparative analysis. Three manufacturing technologies and 3 different materials for each are compared.

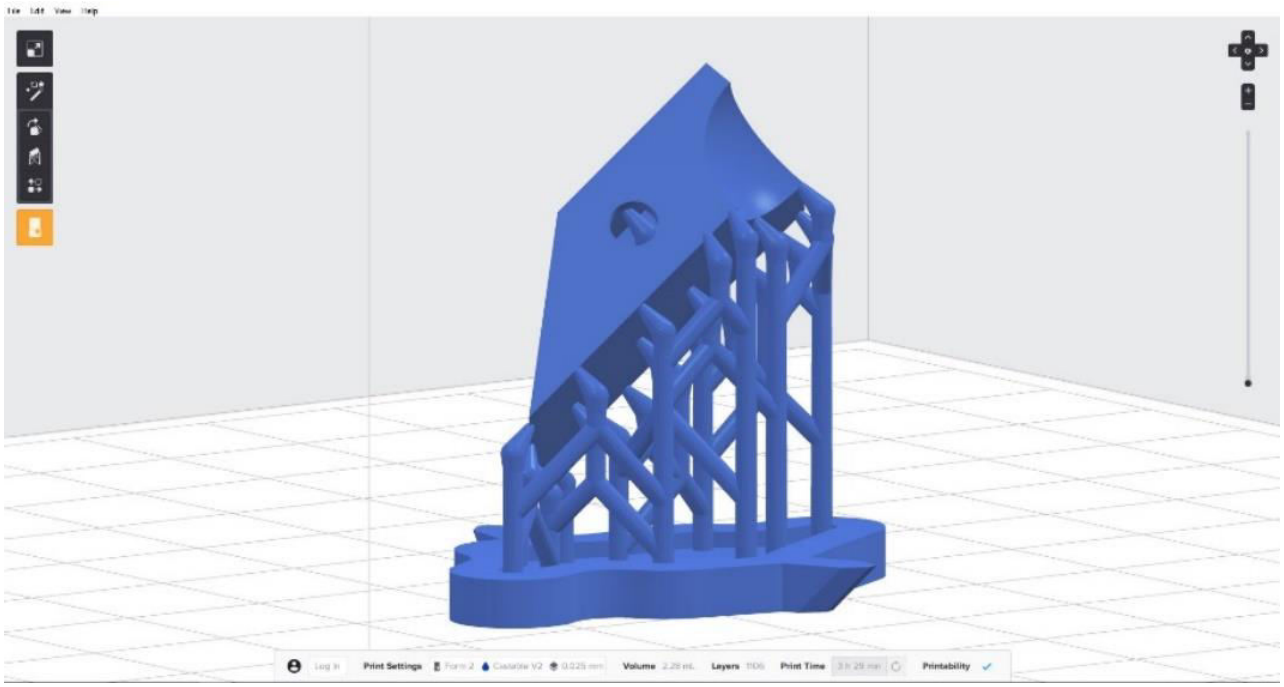

Figure 1 Assignment of the specimen within the slicer program

After studying the literature, the applicability of 3D printing in precision casting raises many questions. In my research I compared various 3D printing technologies from the field of rapid prototype production. As the applicability of the geometry allows, these were printing test specimens in the field of precision casting. Also experiments with the effect of printing orientation on the surface were conducted. In practical experiments, comparison were made between test specimens printed from different materials. Additionally, surface roughness were also tested, on the finished geometries and cast test specimens.

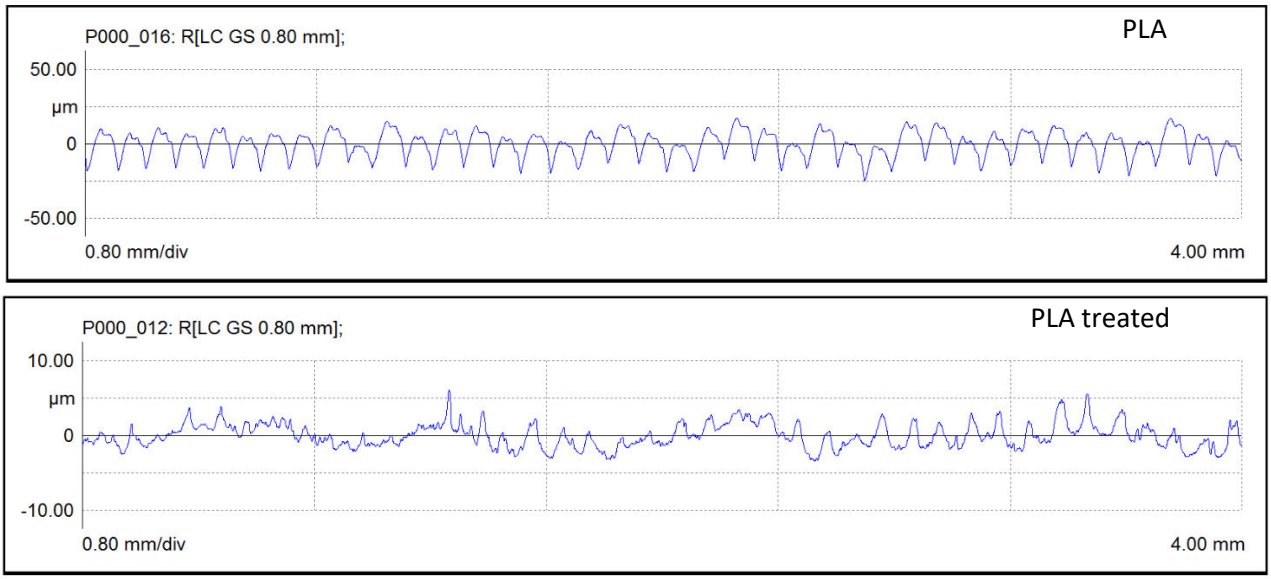

Figure 2 Surface roughness tests

The results of the surface roughness tests confirmed previous microscopic studies that the surface smoothness of PLA can be improved by ethyl acetate treatment. Figure 2 clearly shows the difference between "PLA" value and "PLA treated" value due to surface treatment.
The performed tests proved the possible usage of 3D printing in casting technologies. This dissertation only details the solutions used in precision casting, but many other areas of casting technologies can also benefit from 3D printing (design, sample making, sand forming, simulation testing, etc.). Constantly evolving industrial technologies allow for a bolder design and fabrication of structures that were previously unavailable. Rapid prototype manufacturing is a growing industry that can assist, facilitate and accelerate processes in all areas.

REFERENCES

[1] E. Pei, M. Monzón, and A. Bernard, *Additive Manufacturing – Developments in Training and Education*. 2018.
[2] L. Yang, *"Introducing the State-of-the-Art Additive Manufacturing Research in Education," in Additive Manufacturing -- Developments in Training and Education*, E. Pei, M. Monzón, and A. Bernard, Eds. Cham: Springer International Publishing, pp. 53–65. 2019.
[3] B. Redwood, F. Schöffer, and B. Garret, *"The 3D Printing Handbook," 3D Hubs*, p. 304, 2017.
[4] L. Ernő, *Precízziós öntés*. Budapest: Műszaki Könyvkiadó, 1967.

SIMULATION OF HOT ROLLING BY CELLULAR AUTOMATA

[1]HEGYES Tibor, [2]BARKÓCZY Péter PhD
[1]Antal Kerpely Doctoral School of Science, Arconic Köfém Kft
E-mail: hegyestibor1@gmail.com
[2]Faculty of Materials Science and Engineering-University of Miskolc, FUX Zrt.
E-mail: peter.barkoczy@gmail.com

Keywords: hot rolling, cellular automata, simulation, recovery, recrystallization

Our research is focusing to one of the most complex and important production step that is the simulation of hot rolling. During hot roling two phenomena as work hardening and the process of regeneration of cristals has strong influence for physical properties of microstructure of aluminium alloy. This has to be taking into account in case of rolling technology steps and developement. For example steel and aluminium is different and these work differently during hot rolling. When we talk about aluminium the dynamic softening in fact it is dynamic recovery that is followed by dynamic recrystallization. It goes in the same order of magnitude rate. But in steels the recovery has only a minor effect. Hot rolled and newly modified grain structure is influenced by these dynamic phenomena. Hot rolled grain structure goes througth significal changes under further production steps like cold rolling and heat treatments. But aside from these intermediate production steps the microstucture that we get after hot rolling has significat effect for mechanical and grains structure of the final flat rolled product. Proper technology planning is essential that for cellular automata simulation method can ensure useable and good solution. How did this idea come? In world wide millions of tons flat rolled aluminium sheets are produced per year for customers. For a technology engineer it is not easy task to build up a proper technology that fulfill product requirements. These requirements or we can call material properies like material thickness, grain size, mechanical properties, deep drawing capability etc.. These points are in focus for endusers and the rolled material has to achieve these specified customer requests. We are working on to find a simulation that could support industrial engineers in their daily practice to find the best optional production route. Our idea in first hand the simulation of material behavior and not the technology itself. For the rolling technology simulation from material workability, rolling passes etc. FEM simulations are more common solutions. It use continuous and deterministic functions. The space and time resolution are built in irregual units. The shape of units are changing during simulation. Cellular automata is different. It is better solution for recrystallization simulation. Space and time has steady resolution and the unit shape doesn't change during calcuation. is Both method has advantage and also disadvantage. Cellular automata working is easier and calculation time is shorter. For industrial application where time factor is important and material properties are in focus the cellular automata was the choosen tool. The simulation of Graingrowth and recrystallizaton by cellular automata method has been researched area for more than 20 years until today in Institute of Physical Metallurgy, Metalforming and Nanotechnology at University of Miskolc. At the beginning they focused on static recrystallization. Later researchers has introduced that their improved method can simulate hot rolling and dynamic recrystallization, but they focused on physical processes under annealing even so. Improved cellular automata has been simplified to 1D and they solved also the scale. In our lecture we report about further results of improvements of hot rolling 1D cellular automata simulation. We introduce the results of capability calculations. It is the main factor of this study. 1D cellular automata has the easiest structure, see in Figure 1.

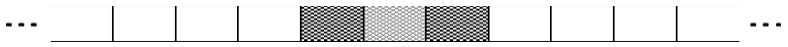

Figure 1 Chain of 1D cellular

Cells take place in neighborhoods to each other in chain. Every cell has two neighbours one at right and one at left side. Every cell has own state. According to the given mathematical algorithm these cells can calculate and based on the calculated result these can keep their state or they change it. We can define these cellular states as rolled, recovered, recrystallized etc.. Stored energy is the mutual point of workability, recovery and recrystallization. Our automata calculate with stored energy changing and finally it identifly the actual material state as a simulation of microstructure. In our research we could connect recovery and recrystallization calculation in one autamata. As a capability study we simulated a material that had height stored energy in the beginning than it is changed under annealing. These were not real physical measurement. We applied different state and alternate temperature for simulating annealing. Every applied temperature occured changing in stored energy in function of cellular autamat calculation steps Figure 2.

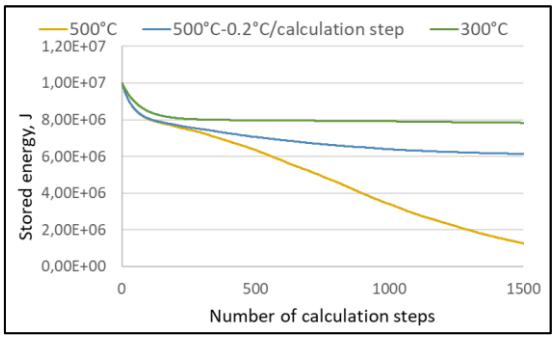

Figure 2 Stored energy changing in function of 1D cellular automata calculation steps

Results were extended and calculated into Avrami phase transformation. Character of curves are typical of real transformations and our automata can differentiate material states which is almost fully recrystallized or where we get only recovery at the end of calculation Figure 3.

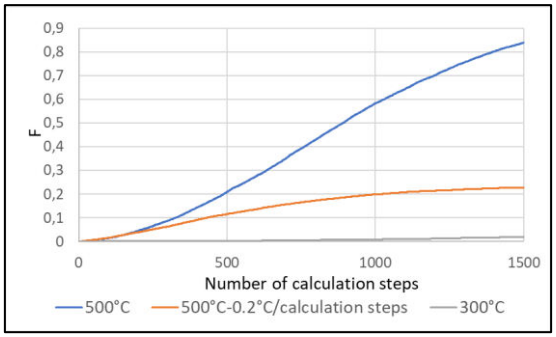

Figure 3 Avrami phase transformation with 1D cellular automata

Our automata can be used for hot rolling simulation. It is possible to determine calculational steps until metal forming phase and the time when the material is cooling on hot mill Figure 4.

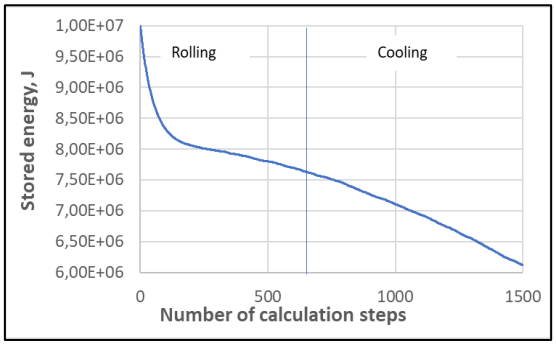

Figure 4 Stored energy changing in function of 1D cellular automata calculation steps (hot rolling)

1D cellular automata is proper solution for material structure simulation. It can calculate also with recovery not just recrystallization that is common in case of aluminium softening. This automata can handle static and dynamic process changing in the same time.

NUMERICAL INVESTIGATION OF SHEAR VELOCITY ON SHEAR FORCE IN DIRECT SHEAR BOX TEST USING DISCRETE SPHERICAL ELEMENTS

[1]HORVÁTH Dániel, [1]POÓS Tibor PhD, [2]TAMÁS Kornél PhD
[1]Budapest University of Technology and Economics, Department of Building Services and Process Engineering
[1]E-mail: horvath.daniel@mail.bme.hu, poos@mail.bme.hu
[2]Budapest University of Technology and Economics, Department of Machine and Product Design
E-mail: tamas.kornel@gt3.bme.hu

Keywords: direct shear box test, discrete element method, shear velocity, linear spring–dashpot contact model

In many areas of industry, granular materials are moved and processed. These processes need to be investigated because of efficiency gains. To estimate the operation of the analysed particulate bulk, it is essential to determine certain material properties of the particulate materials. These include, for example, the average particle size and shape, the particle and bulk density, the porosity and the internal friction angle of the bulk. The results can be useful for engineers and machine operators to select the right equipment, design and set operating parameters. The discrete element method (DEM) is a computer-aided modelling of particulate matter operations, which mathematical basis was created by Cundall and Strack [1]. DEM builds a set of particles from discrete elements with micromechanical material and interconnection properties. Many so-called contact models are available in the scientific literature to describe the collisions of the particles and their various relationships (cohesive, electrostatic, etc.). One of the most common is the soft-sphere linear spring – dashpot contact model consists of linear springs, viscous damping and friction slider [2]. With the advancement of the DEM method, researchers have developed rolling and twisting resistance coefficients, by means of which the rolling and twisting of contacting particles can be controlled by torques. They can be used to simulate – to a certain extent [3] – the movement of irregular particle shapes with regular spherical particles, and in the presence of cohesive bonds to change the direction and nature of their failure [4].
The aim of the research was to develop the mathematical background of a DEM contact model taking into account the models in the literature and to implement it in Yade open source DEM software [5], and finally to validate the model. For this, direct shear box test was used, the laboratory results of which have already been described in our previous studies [6], [7]. In the current research, a parameter sensitivity study was performed using the schematic contact model illustrated in *Fig. 1/a*, in which the effect of increased shear velocity (v) on the shear force was investigated to reduce DEM simulation time.

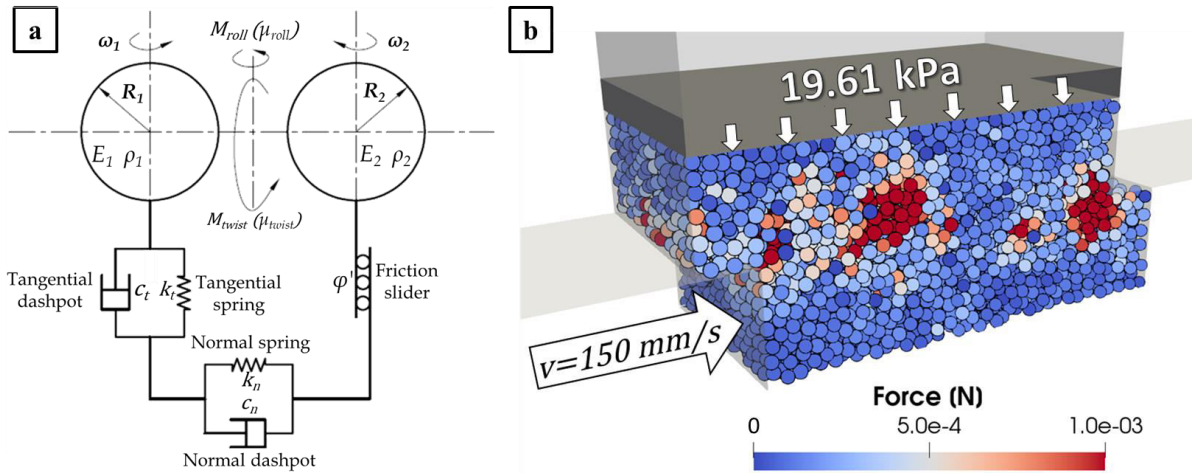

Figure 1 a: mechanical representation of the DEM contact model; b: the section of the direct shear box's DEM model in case of $v = 150\frac{mm}{s}$ shear velocity and 19.61 kPa normal stress (preload)

Fig. 1/b illustrates a section view of the 1:1 DEM model of a rectangular 60x60x30 mm direct shear box at shear velocity of $v = 150\frac{mm}{s}$, where the particles are colored according to the magnitude of the forces acting on them. *Table 1* summarizes the micromechanical parameters of the spherical particles of 1.8 ± 0.1 mm diameter used in the simulations and the parameters of the structure walls.

Table 1 Micromechanical DEM parameters of the particles and material parameters of the structure walls

Name	ρ [kg/m^3]	φ' [°]	E [MPa]	ν [1]	c_n [kg/s]	c_s [kg/s]	β_{kr} [1]	β_{kt} [1]	β_{cr} [1]	β_{ct} [1]	μ_{roll} [1]	μ_{twist} [1]

Particles	2000	20	3	0.2	0.2	0.2	0.25	0.5	0.25	0.5	0.05	0.05
Structure wall	7750	5.7	200000	0.3	0	0	0.25	0.5	0.25	0.5	0	0

In *Table 1*, ρ denotes the density, $\varphi'$the friction angle, E the elastic modulus, ν the ratio between the normal and the tangential contact stiffness, c_n the normal and c_s the tangential viscous damping coefficient, β_{kr} the rolling and β_{kt} the torsional spring stiffness ratio, β_{cr} the rolling and β_{ct} the torsional viscous damping coefficient ratio, μ_{roll} the rolling and μ_{twist} the twisting resistance coefficients. In the direct shear box simulations, the shear velocity was varied between $v = 0.02-200$ mm/s and a preload of 19.61 kPa was utilized. The resulted shear force – shear displacement results are shown in *Fig. 2*.

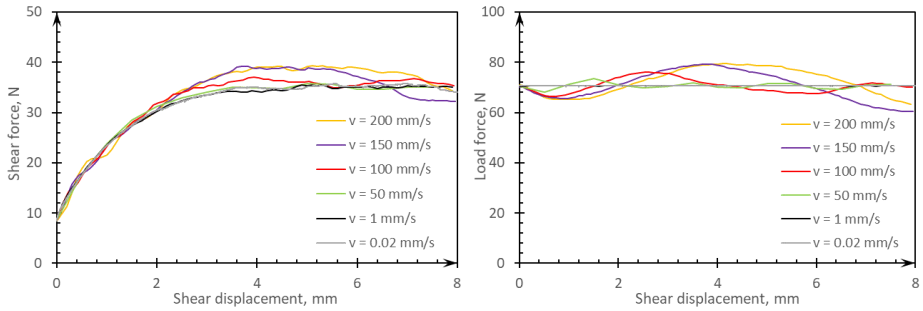

Figure 2 On the left, the shear force and on the right side, the force acting on the load plate by the particles as a function of shear displacement at different shear velocities

Based on the results it can be stated that the shear force did not change significantly, if shear velocity is $v \leq 50\ mm/s$, however, by using higher values different results were obtained. If the shear velocity is $v > 50\ mm/s$, the force exerted on the load plate was no longer so consistent. This is because, due to the effect of the high velocity difference between the two half of the shear box, the particles lift the load plate. Similar results were obtained by Saadat and Taheri [8], who also determined a shear velocity limit under the conditions they examined, but did not investigate the force acting on the load plate and its displacement. According to the results achieved, the shear force change resulting from the increase of shear velocity is related to the consistency of the force acting on the load plate in the used contact model. Thus, by examining the force acting on the load plate, it is possible to determine how much the shear velocity can be increased in the simulations – and thus decreasing the simulation time – so that the error in the numerical results of the direct shear box test is still acceptable.

ACKNOWLEDGMENTS
This work was supported by Richter Gedeon Talentum Foundation (19-21. Gyömrői street, 1103 Budapest, Hungary) and the ÚNKP-19-3 New National Excellence Program of the Ministry for Innovation and Technology.

REFERENCES

[1] Cundall, P. A., Strack, O. D. L. (1979), *Discrete numerical model for granular assemblies*. Geotechnique, 29(1), 47–65.
[2] Peng, B., *Discrete Element Method (DEM) Contact Models Applied to Pavement Simulation*. Master's thesis, Virginia Tech. 2014.
[3] Zhao, S., Evans, T. M., Zhou, X., *Shear-induced anisotropy of granular materials with rolling resistance and particle shape effects*. International Journal of Solids and Structures, 150, 268–281. 2018.
[4] Horváth, D., Poós, T., Tamás, K., *Modeling the movement of hulled millet in agitated drum dryer with discrete element method*. Computers and Electronics in Agriculture, 162, 254–268. 2019.
[5] Šmilauer, V. *et al.*, *Dem formulation. In Yade Documentation 2nd ed.*, Yade Project, 37. 2015.
[6] Poós, T., Horváth, D., Tamás, K., *Modeling the movement of the granular material in a static equipment with discrete element method*. Proceedings of the 5th International Scientific Conference on Advances in Mechanical Engineering (ISCAME 2017), Debrecen, Hungary, 418–421. 2017.
[7] Horváth, D., Poós, T., Tamás, K., *Comparison of the direct shear box test of two agricultural granular materials*. Proceedings of the 6th International Scientific Conference on Advances in Mechanical Engineering (ISCAME 2018), Debrecen, Hungary, 67–68. 2018.
[8] Saadat M., Taheri, A., *A cohesive discrete element based approach to characterizing the shear behavior of cohesive soil and clay-infilled rock joints*. Computers and Geotechnics, 114, 103-109. 2019.

POLYLACTIC ACID AS A POTENTIAL ALTERNATIVES OF TRADITIONAL PLASTIC PACKAGINGS IN FOOD INDUSTRY

HORVÁTH Tibor, SZABÓ Tamás J. PhD, MAROSSY Kálmán PhD
Institute of Ceramics and Polymer Engineering, Miskolc University
E-mail: horvath.tibor70@upcmail.hu, polsztam@uni-miskolc.hu, polkal01@uni-miskolc.hu

Keywords: PLA, PLLA, PDLA, PDLLA, PET, direct contact primary packaging

Huge quantity of synthetic polymers are used as packaging materials in different fields of food industries. A significant part of these polymers applied as a primary, direct food contact materials. The scoped application area is the sweet industry. In this field Polystyrol (PS), Polypropylene (PP) and Polyethylene-terephthalate (PET) have used but during the last fifteen years the usage of PET has been grown. In one hand the price of this material is efficient, form other hand the PET is the one of the most safe (for food industrial applications) petrol chemical plastic that can be used as primary or secondary food contact packaging material.
To maximize the customer safety and minimize the environmental impact of traditional PET, a new, bio-sourced and bio-degradable alternative polymer aimed to be used in this special food industrial segment.
One of the potential alternatives the Polylactic acid (PLA) would be a possible substitute which is compostable and made from renewable sources.

Table 1 Physical and chemical parameters of the PLA and PET foils [1]

Properties	PDLA	PLLA	PDLLA	PET
Crystalline structure	Crystalline	Semi crystalline	Amorphous	Amorphous and semi-crystalline
Melting temperature *(T_m)*	180 °C	180 °C	variable	260 °C
Glass transition temperature *(T_g)*	50-60 °C	50-60 °C	variable	67-81 °C
Half-life in 37°C normal saline	4-6 month	4-6 month	2-3 month	700 year
Elongation at break *(%)*	20-30 %	20-30 %	variable	230 %
Breaking strength *(g/d)*	4-5	5-6	variable	5,3

The mechanical and optical property of PLA is very similar to the PET, but the PLA and its alternatives like PLLA, PDLA and PDLLA is more fragile in case of rapid stress, and less heat-resistant compared to the PET. The appropriate mechanical properties of substitute material is quite important because the further usage of recently applied forming methods and costly tools are basic musts/requirements of the relevant industrial segment. In this work two commercial PLA foils (PLLA and PDLLA) have been compared to the commercial PET foil. During the laboratory tests the mechanical, thermal and barrier properties and the structures of materials were analyzed by tensile testing, differential scanning calorimetry and thermally simulated discharge analysis.

Table 2 Average molar mass of PET [2], PDLLA [3] and PLLA [4] foils

Properties	PET	PDLLA	PLLA
Average molar mass *(M_w)*	30 000 – 80 000 g/mol	100 000 – 180 000 g/mol	100 000 - 300 000 g/mol

The mechanical properties were determined with tensile test with application of INSTRON 5566 testing machine according to the ASTM D389 standard. 150%, 200% and 250% stretching levels were determined and adjusted, the test speed was 100 mm/min at room temperature (23±1°C). For purpose of further characterization of materials DSC131 evo machine was used with 10°C as heating/cooling rate.

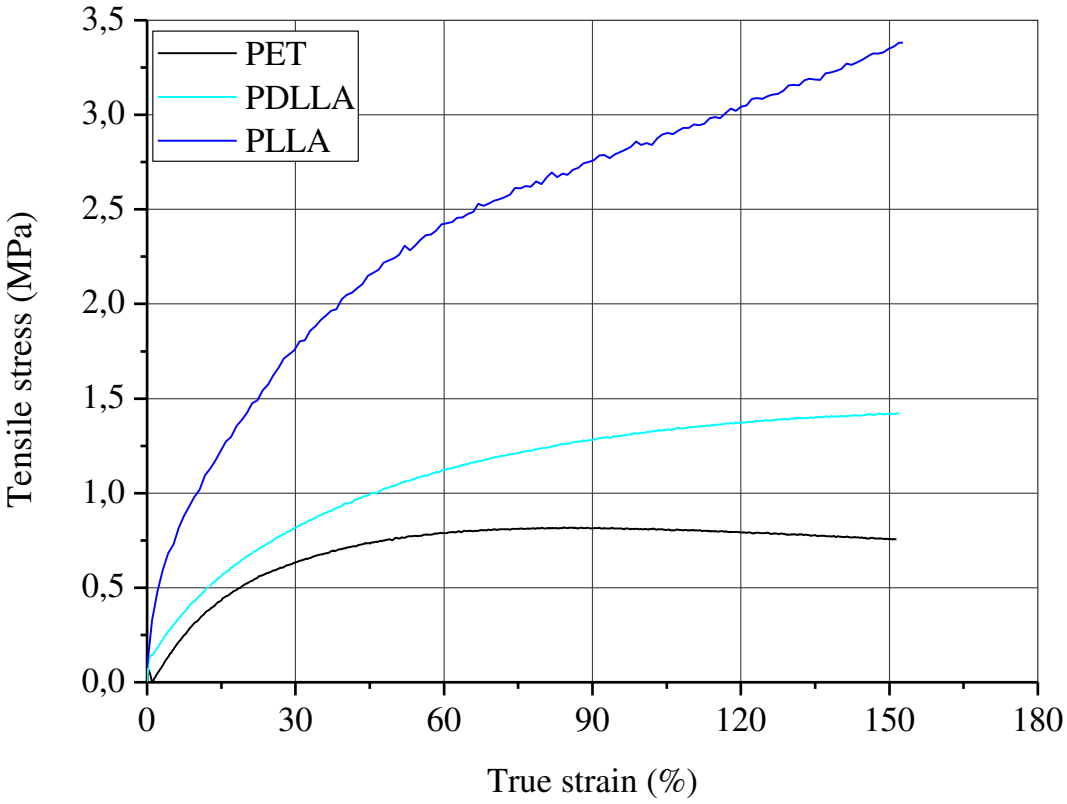

Figure 1 Results of tensile test of PET, PDLLA and PLLA foils at deformation of 250%

The comparison have been carried out and the final conclusion - as the application of PLA alternatives are recommended as primary and secondary packaging material for sweet industry - was taken based on the results of the analysis.

ACKNOWLEDGMENTS
The described work was carried out as part of a project supported by the National Research, Development and Innovation Office – NKFIH, K123456.

REFERENCES
[1] L. Xiao, B. Wang, G. Yang, M. Gauthier, *Poly(Lactic Acid)-Based Biomaterials: Synthesis, Modification and Applications.* Biomedical Science, Engineering and Technology, 247-282, 2012.
[2] Dr. Gy. Bánhegyi, *Poli(etilén-tereftalát) (PET) újrafeldolgozása a tulajdonságok javításával.* Műanyagipari szemle 5. 2005.
[3] http://www.bmg-inc.com/en/prod_and_res/bio_degmer/pdlla.html
[4] Y. Ikada, H. Tsuji, *Biodegradable polyesters for medical and ecological applications*. Macromol. Rapid Commun. 21, 117–132. 2000.

SYNTHESIS OF POLYLACTIC ACID (PLA) BY POLYCONDENSATION METHOD

HORVÁTH Tibor, SZABÓ Tamás J. PhD, MAROSSY Kálmán PhD
Institute of Ceramics and Polymer Engineering, Miskolc University
E-mail: horvath.tibor70@upcmail.hu, polsztam@uni-miskolc.hu, polkal01@uni-miskolc.hu

Keywords: PLLA, PDLA, PDLLA, polycondensation, capillary viscometry, solution rheology

According to the relevant literature polylactic acid (PLA) with 10^4-10^5 g·mol^{-1} molar mass can be synthetized by polycondensation. Over the normal thermal initiated polycondensation, microwave initiated method can be applied as an alternative approach of polymerization. The thermally initiated polycondensation is a quite time-consuming process to reach the above indicated molar mass of PLA. The microwave initiated alternative is a new, faster polycondensation method that can be used successfully as well [1].

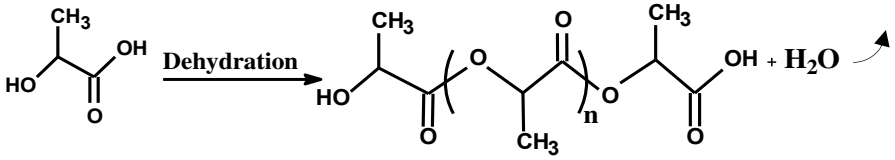

Figure 1 Direct polycondensation of Polylactic acid [2]

During the experiments polylactic acid alternatives (PLLA, PDLA, PDLLA) have been synthesized by both polycondensation methods. The applied two methods were compared based on time need of processes and the molar masses of synthetized polylactic acid alternatives. The L and D lactic acid raw materials have been ordered from Musashino Chemical Laboratory Ltd. The additive catalysator material was chosen as Stannous-Octoate that was ensured by University Of Miskolc. For the standard polycondensation experiments HEIDOLPH Laborota 400 efficient with joined Vacuubrand ME 1C type vacuum pump were used with various temperatures. In case of microwave initiated polymerization LG MB-3822G equipment with 700W nominal performance was applied.

Figure 2 HEIDOLPH Laborota 400 efficient with joined Vacuubrand ME 1C type vacuum pump

All synthetized polymers have been analyzed by Fourier-transform infrared spectroscopy (FTIR) and Differential scanning calorimetry (DSC). During the FTIR analysis BRUKER Tensor 27, in case of DSC measures DSC131 Evo equipment was used with dT/dt = 10°C min^{-1} heating/cooling rate.
The molar mass of polymer is a basic property that defines the appropriate processing method and the field of application of polymer. In light of this fact, the measurement of molar mass is a crucial point of polymer synthesis. By

evaluation of molar masses, the entire polymerization could be monitored and controlled, therefore PLA samples were periodically taken and measured during the process.
The proper measurement and definition of molar mass is an important and sensitive task. In absence of expensive analytical equipment an indirect rheology-based method can be used with reliable result. The polylactic acid samples (which were taken during the polycondensations) have been solved in chloroform in the first step, then prepared samples with different concentrations for further analysis. To measure the flow-times Ubbelohde capillary viscometer was applied. Based on the measured flow-time of polymer samples the relative viscosity (η_{rel}), the specific viscosity (η_{sp}) and the reduced specific viscosity (η_{red}) could be computed [3]. The intrinsic viscosities were graphically defined then with following the correlation of Mark – Houwink relation the molar masses of polylactic acid polymers have been calculated [4].

Table 1. Molar masses of synthetized PLA samples

Sample	Average molar mass *(M_v)*
$PLLA_{72\ hours}$	$6{,}97 \times 10^4\ g \cdot mol^{-1}$
$PDLA_{48\ hours}$	$1{,}88 \times 10^4\ g \cdot mol^{-1}$
$PLLA_{Micro\ wave\ initiated}$	$6{,}84 \times 10^4\ g \cdot mol^{-1}$

ACKNOWLEDGMENTS
The described work was carried out as part of a project supported by the National Research, Development and Innovation Office – NKFIH, K123456.

REFERENCES
[1] I. Bodnár, *Potenciálisan Biodegradábilis, Politejsav bázisú polimerek szintézise és vizsgálata.* Debreceni Egyetem, Alkalmazott Kémiai Tanszék. 2002.
[2] Milena S. Lopes*, André L. Jardini and Rubens M. Filho, *Synthesis and Characterizations of Poly (Lactic Acid) by Ring-Opening Polymerization for Biomedical Applications*. Chemical Engineering Transactions - VOL. 38, 2014.
[3] Q. Charlier, E. Girard, F. Freyermouth, M. Vandesteene, N. Jacquel, C. Ladavière, A. Rousseau, F. Fenouillot, *Solution viscosity – molar mass relationships for poly(butylene succinate) and discussion on molar mass analysis.* eXPRESS Polymer Letters Vol.9, No.5, 424–434. 2015.
[4] J.E. Mark, *Polymer Data Handbook.* USA: Oxford University Press; 629 p. 1999.

EFFECT OF THE CHANGES IN BULK DENSITY AND GRANULOMETRIC PROPERTIES ON THE STRENGTH PROPERTIES OF THE MOULDING SAND MIXTURES

HENRIETTA Hudák, LÁSZLÓ Varga PhD
Institute of Foundry, Faculty of Materials Science and Engineering, University of Miskolc
E-mail: ontheni@uni-miskolc.hu, laszlo.varga.mak@gmail.com, ontvlaci@uni-miskolc.hu

Keywords: quartz sand, granulometry, green sand, strength properties

Foundry technology use a lot of several natural materials. Sands use for preparing mixtures whereby making moulds or cores. Sand is defined as granular, refractory major portion of mixture (90 – 98% in dependence on used binder). Sand properties depend on it has chemical and mineralogical composition; mainly particle-size distribution and shape of grains and it size and sand surface texture. Quartz sand is the most frequently applied type of foundry sands not only because of its widespread use but also due to its low price. Based on the source materials, the sand core test specimens made of different surface quartz sands show even a double difference in their bending stress values [1-4].
Sands of almost the same granulometric but different micro surface properties can show variable behaviour in respect of the foundry use. The micro surface of the sands plays a very important role in the requirement for binders. Saving in the binder can be reached – achieving, however, the same strength, when choosing smooth surface sand [5].
A comparative measurement of two quartz sands with different surface quality was carried out. Green sand mixtures were prepared to measure their permeability, compression strength and wet tensile strength. The strength of green sand mixtures has two main components. One of them is the cohesion of the binder; the other one is the adhesion between the binder and the foundry sand. The aim of this research is to determine the ratio of cohesion and adhesion within the strength values.

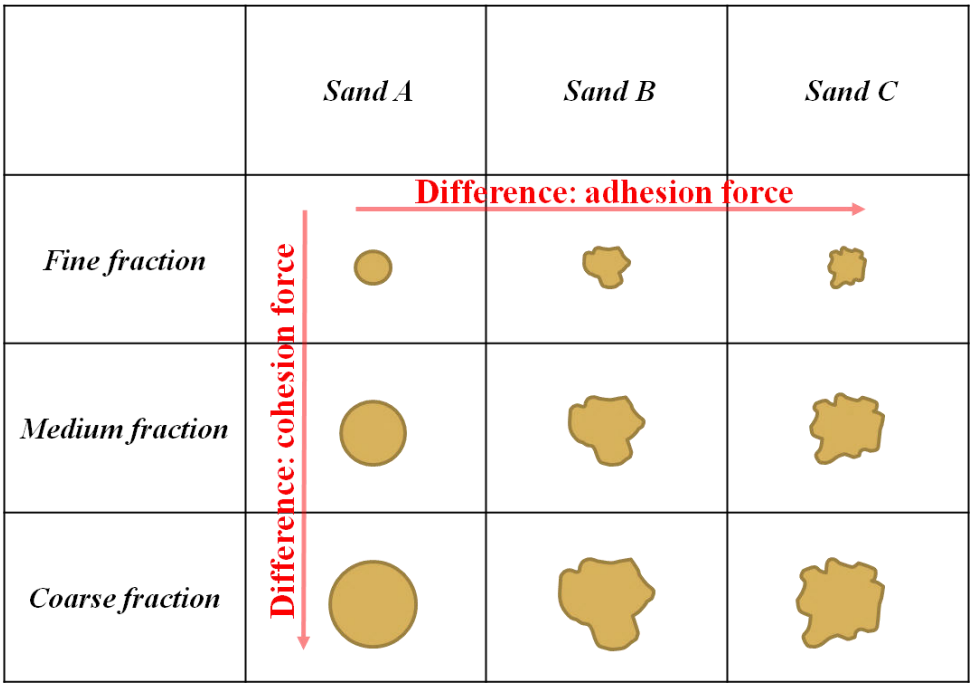

Figure 1 The method used for determining the cohesion and adhesion.

Quartz sand of two different surfaces was used for our tests (GBM 45 and SH 33). Figure 2 shows the grain morphology of different sands.

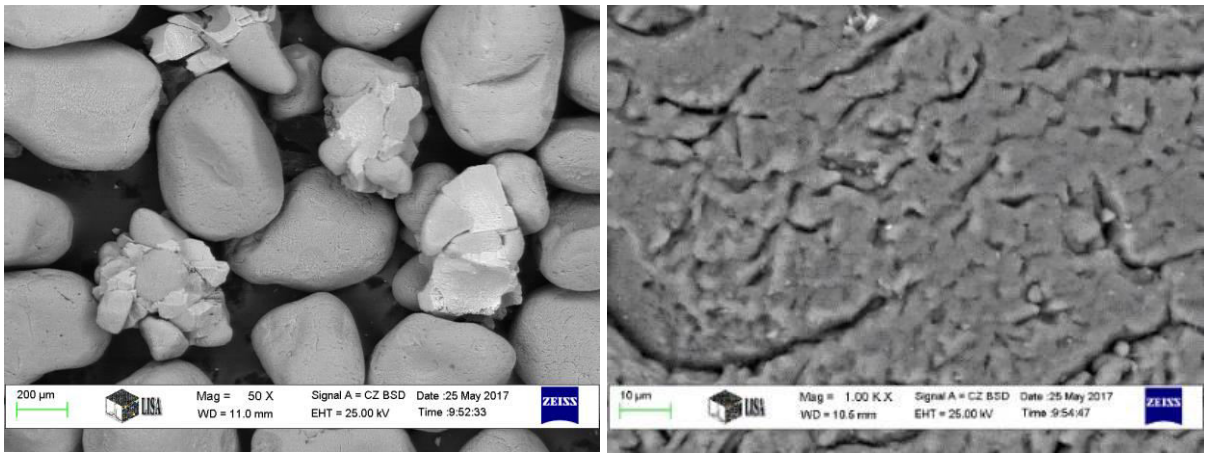

a)

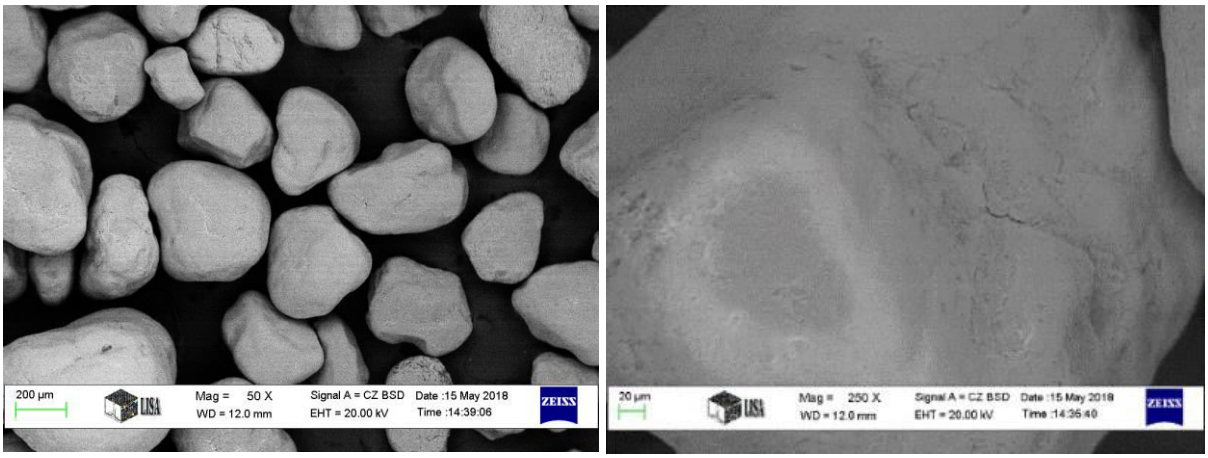

b)

Figure 2 Scanning electron microscopy (SEM) image of quartz sands.
GBM 45 (N=50x) and (N=1000x).
SH 33 (N=50x) and (N=250x).

Different bentonite binding sand mixtures were made from different type of sands. Sand were added to mixtures with and without fractionation and grain sizes were fine, medium and coarse. Bentonite quantity and quality were the same to ensure an equal number of the bond bridges which are the connection points of the sand grains.
Specimens for the investigation were prepared with stamping machine.
The ratio of cohesion and adhesion can be determined from the strength value results. In case of different surface qualities of samples with identical size distribution and binder quantity, equal bond strength developed. This means that the cohesion between sand grains was nearly the same. The difference between strength values may arise from the difference in the adhesion, which depends on the surface quality of the sand grains.

REFERENCES

[1] Löchte, K., *Working with the Cold Box Process in the Coremaking Department of a Foundry*. Internet. 1998.
[2] Bechný, V., *Zukünftige Herausforderungen an Gießereisande*. Giesserei-Rundschau, ¾, 81-83. 2012.
[3] Iden, F., Tilch, W., Wojtas, H. J., *Die Haftungsmechanismen von Cold-Box-Bindemitteln auf der Formstoffoberfläche*. Giesserei, 5, 24-36. 2011.
[4] Iden, F., Pohlmann, U., Tilch, W., Wojtas, H. J., *Strukturen von Cold-Box-Bindersystemen und die Möglichkeit ihrer Veränderung*. Giesserei Rundschau, ½. 3-8. 2011.
[5] http://giba.at/pdf/giba-de.pdf

CHARPY IMPACT TEST OF CLINCHED JOINTS

JÓNÁS Szabolcs, TISZA Miklós DSc
Institute if Mechanical Technology, University of Miskolc
E-mail: szabolcs.jonas@gmail.com, tisza.miklos@uni-miskolc.hu

Keywords: impact test, dynamical testing, clinch joint

A controlled body crushing zones are of considerable interest to automotive industry [1]. The Charpy V-notch test has been used for a century now as an indirect, cheap method of assessing fracture toughness properties. This dynamic test of a blunt notched specimen has been widely used to correlate material toughness behavior for quality control and material acceptance criteria for many industries [2]. This paper the authors would like to introduce the dynamic testing of clinched joints.
In this study a previous assumption [3] is proved through new tests. For the tests the used clamping device is originally developed for spot welds and presented in [3]. The specimens have a special form to be able to fix them in the device and prevent the impact hammer or pendulum to not get stuck in the testing machine (Figure 1 and 2.). For the tests six pieces of specimens were made by a TOX clinching machine controls by an MTS electro-hydraulic testing machine at the laboratory of University of Miskolc.


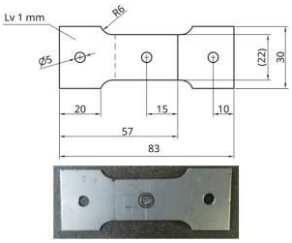

Figure 1 Preparation of a joint

Figure 2 Impact specimens

The presumption is that the dynamical resistance of clinch joints is depends on the direction of the impact. Two types of tests were performed, “normal” and “reversed” (Figure 3 and 4).

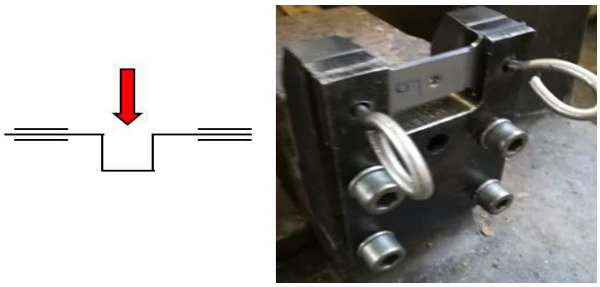

Figure 3 “normal” direction

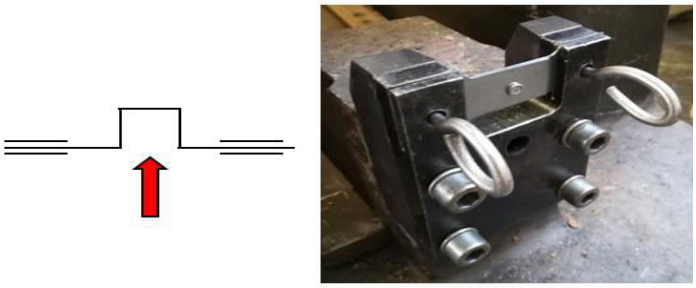

Figure 4 “reversed” direction

The results of the joining – t_B and F_{max} – and the modified Charpy tests for clinch joints can be seen in Table 1.

Table 1 Measured data

Orientation	Specimen ID	t_B [mm]	F_{max} [kN]	Impact energy [J]
Normal	#1	0.52	41.5	29.5
	#2	0.52	41.51	30
	#3	0.52	41.28	31
Reversed	#4	0.52	41.91	34
	#5	0.53	41.88	35.5
	#6	0.53	42.29	35

The comparison of the values for the two directions can be seen in Figure 5. The bar diagram shows that the “normal” direction is always less than the measured values of the “reversed” direction. When the impact (in this case an impact

hammer) comes from the protrusion side of the joint the measured impact energy is higher with ~15% for DP 600 steels. Which energy is quite high to be occasional. The cause of this phenomenon is that the impact hammer when hit the specimen in the holding equipment a very fast forming process sequence is done. From the total energy value, the ~1/3 is expended for bending of the jointed sheets. The rest of energy expended for the opening of the joint. In case of "normal" directional impacts this is the tearing of the neck, but in case of "reversed" directional impact the additional forming process (i.e. the hammer tries to push out the one sheet from the other during until the unbuttoning).

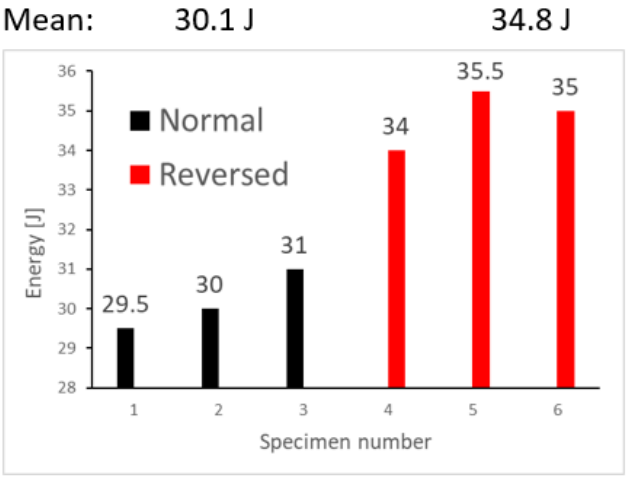

Figure 5 Comparison of the results of the impact tests

The results of the tests can be useful in automotive industry as a design proposal.

ACKNOWLEDGMENTS

SUPPORTED BY THE ÚNKP-19-3 NEW NATIONAL EXCELLENCE PROGRAM OF THE MINISTRY FOR INNOVATION AND TECHNOLOGY.

REFERENCES

[1] Z. Gronostajski, S. Polak, *Quasi-static and dynamic deformation of double-hat thin-walled elements of vehicle controlled body crushing zones joined by clinching*. Archives of Civil and Mechanical Engineering, 8(2), 57–65. 2008

[2] W.L. Server, *Instrumental Charpy test review and application to structural integrity*, European Structural Integrity Society, vol. 30. pp. 205-212. 2002.

[3] Sz. Jónás, M. Tisza, *Experimental study on DP600 clinched joints*, Metallurgy and Foundry Engineering, vol. 44, No. 1, 2018.

[4] Á. Dobosy, M. Gáspár, L. Prém, *Nagyszilárdságú acélok hegesztett kötéseinek műszerezett ütővizsgálatai* AGY, Miskolctapolca, 2016.

EFFECT OF THE FRICTION COEFFICIENT ON CLINCH JOINTS

JÓNÁS Szabolcs, TISZA Miklós DSc
Institute of Mechanical Technology, University of Miskolc
E-mail: szabolcs.jonas@gmail.com, tisza.miklos@uni-miskolc.hu

Keywords: clinch joint, frictional coefficient, surface, formability

Resistance to friction is one of the main factors limiting the sheet metal forming process. Friction between the sheet and tool during the forming process is influenced not only by the surface topography, but also by several parameters such as lubricant, surface chemistry, contact pressure, and sliding speed [1]. Due to the strong dependence of formability on the friction conditions between tools and blank as well as the resistance of material against deformation, reducing such friction and resistance becomes an important research topic to improve the processing [2].Two frictional laws are generally used in the metal forming field. One is Coulomb's law in which the frictional shear stress is proportional to the normal stress and the friction coefficient is used. Another one is frictional shear stress law in which the frictional shear stress is dependent on the flow stress of the bulk material and the friction shear factor is used [3].
Clinching is a joining method in which sheet metal parts are deformed locally, with a punch and a die by forming an interlock between them, without the use of any additional element and any thermal effects [4]. The neck thickness (t_N), the bottom thickness (t_B) and the undercut (C) are the most important geometrical parameters of the joints (Figure 1).

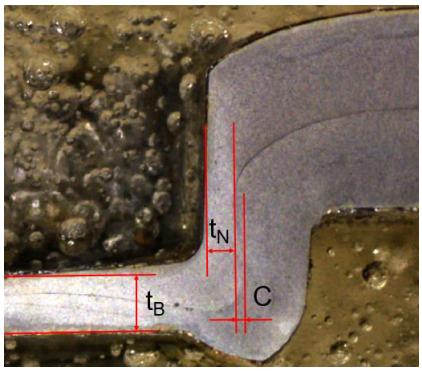

Figure 1 Main geometric parameters of clinch joints

As it described that the frictional condition is a highly affecting parameter of forming processes, so it has an effect also on the clinch joining process. To analyze the effect of the investigated DP600 joints in the point of view of friction experiments and FE simulations were performed. For the experiments the condition of the friction was modified. For small friction coefficient PTFA spray (signed with "C" on Figure 2) was used and for a higher frictional condition was reached with the modification of the surface roughness prepared with sandpaper (signed with "S" on Figure 2). Four joints were done for both the conditions. The results can be seen in Figure 3. The values are the average of the measured parameters. The highest impact of the frictional condition is on the undercut (so called C value as depicted on Figure 1). From the results it can be seen that the value of the undercut is lower in case of the rough surface condition. From which parameter the cross-tensile strength of the joint is depends.

Figure 2 Specimens (S – rough surface, C – PTFE coated)

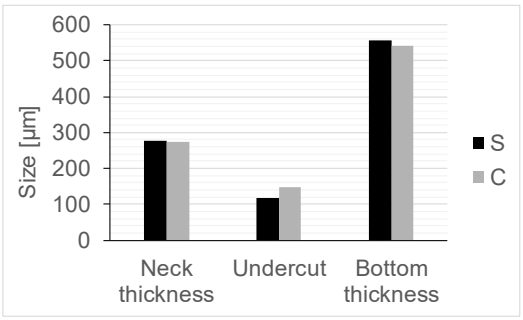

Figure 3 Averaged size parameter results

The FE calculations were performed with the calibrated model presented in [5]. Coulomb's friction law was used between the parts. Two simulations were carried out the modelling of the experimental case which were the friction

coefficient changed between the sheets, μ=0.03 for "C" and μ=0.2 for "S" respectively. In order to determine the possible behavior of the process all of the contacts were considered with the given values (dashed line on Figure 4.). The results were compared to the originally simulated F-d curve. It can be seen that the friction coefficient has a high impact on the forming force need of the process.

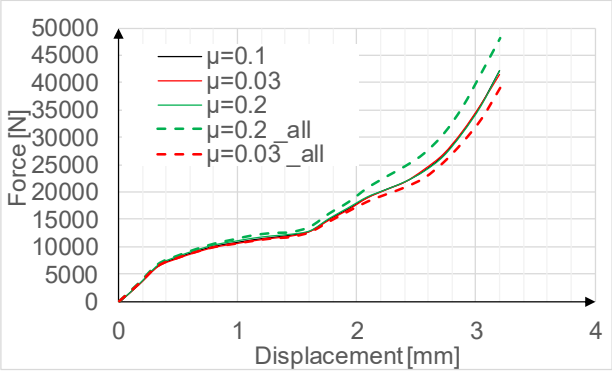

Figure 4 F-d curves with different frictional coefficients

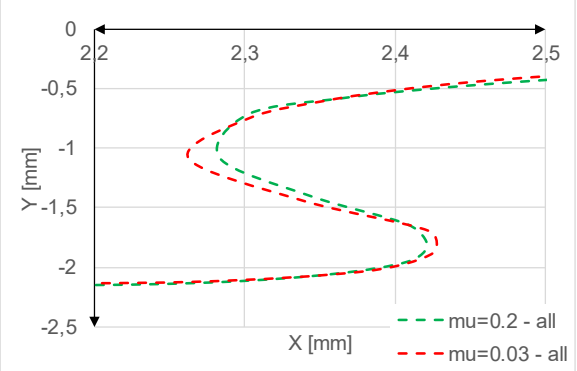

Figure 5 Comparison of the undercuts

From the FEA results it can be seen the same phenomena as measured. As a result, a well lubricated joining setup leads to better joints in the point of view of cross-tension type of loading with the lower forming force need which is favorable in serial production, but at the same time the higher frictional coefficient leads to a ~7% higher resistance against simple tension loading condition because of the small increase in the neck thickness [6].
As a result of the tests and the simulations is the condition of the surfaces is affects the strength of the joints.

ACKNOWLEDGMENTS

SUPPORTED BY THE ÚNKP-19-3 NEW NATIONAL EXCELLENCE PROGRAM OF THE MINISTRY FOR INNOVATION AND TECHNOLOGY.

REFERENCES

[1] T. Trzepiecinski, A. Bazan, H. G. Lemu, *Frictional characteristics of steel sheets used in automotive industry*, Int. J. of Autom. Tech. vol. 16, No. 5. Pp. 849-863. 2015.
[2] S. Olguner, A. T. Bozdana, *The effect of friction coefficient on punch load and thickness reduction in deep drawing process*, Int. J. of Materials vol. 3, 2016.
[3] T. Suzuki, Z. Wang, Y. Yoshikawa, *Effect of plastic deformation of bulk material on frictional behaviour in dry metal forming*, Procedia Engineering 81, 2014.
[4] T. Balawender, *Experimental Investigation of Clinch Joining Process*, Acta Mech. Slovaca 16 (1): 52 – 56, 2012.
[5] Sz. Jónás, M. Tisza, *Finite Element Modelling of Clinched Joints*, Adv. Techn. and Mat., vol. 43. No. 1., 2018.
[6] Sz. Jónás, M. Tisza, D- felhős, P. Z. Kovács, *Experimental and numerical study of dissimilar sheet metal clinching*, AIP Conference Proceedings 2113, 2019.

EFFECT OF THE PUNCHING TOOL GEOMETRY ON CLINCH JOINTS

JÓNÁS Szabolcs, KOVÁCS Péter Zoltán PhD
Institute if Mechanical Technology, University of Miskolc
E-mail: szabolcs.jonas@gmail.com, metkpz@uni-miskolc.hu

Keywords: clinch joint, technological parameter, effects, tool geometry

Clinching is a joining method in which sheet metal parts are deformed locally, with a punch and a die by forming an interlock between them, without the use of any additional element and any thermal effects [3]. The neck thickness (t_N), the bottom thickness (t_B) and the undercut (C) are the most important geometrical parameters of the joints (Figure 1).

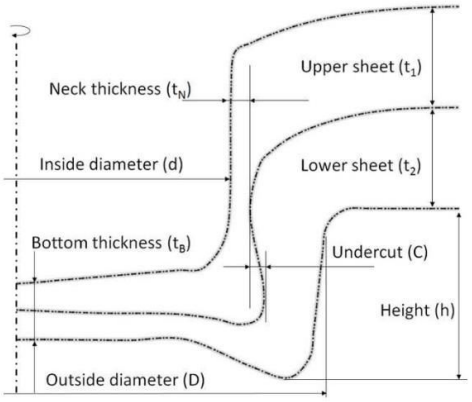

Figure 1 Geometrical parameters of a clinch joint

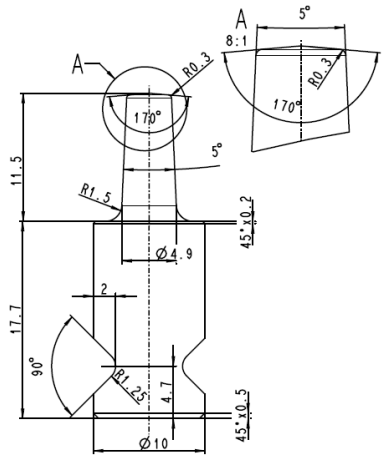

Figure 2 Punching tool geometry (original - #1. – developed for DP 600 steel)

The clinching process can be monitored via the registered force-displacement (F-d) curves. Every F-d curve can be divided three main phases (set up, elastic bending and die filling and plastic bending). For every pairs of sheets (material and/or thickness) has a specific F-d curve. The forming force of the technology is highly depending on the geometry of the tool, the friction between the sheets and the parts of the tool, the sheet thicknesses. The used TOX type clinching tool's maximum allowable load is around 50kN with the original tools. The process should be taken under the allowed maximum load because of the possibility of tool failure. In this study the F-d curves of 5 different tool geometry is presented. The aim of the study is to analyze the effect of the punching tool geometry on clinch joints. The used material is AA6082 solution heat treated type of aluminum alloy sheets with thickness of 1 mm. The desired bottom thickness is 0.75 mm instead of the previously presented papers [5]-[6] because of the possibility of compression of the tool. Several papers dealing with the effects of the tool on clinch joint via numerical analyses [5][6] and experiments [7].
The geometry of the punching tool can be seen in Figure 2. As it can be seen the analyzed geometrical parameters are the radius and the angle of the tool due to the results of the previous FE sensitivity analyses. The experiments were done with the following punching tool geometries (Table 1). The material of the newly produced punching tool is M1 type of steel with a heat treatment of quenching and tempering. The punching tool #1. is different in the material as the other four tools.

Table 1 Geometrical parametres of the punching tool variants

Number of tool geometry	Geometry	
	R [mm]	α [°]
#1. (original)	0.3	5
#2.	0.3	8
#3.	0.3	2
#4.	0.5	5
#5.	0.1	5

As it can be seen in Figure 3 the curves are similar, but the force need of the modified geometries is higher during the process. The maximal force is the lowest in case of the tool #2. (R=0.3 and α=8°) and the highest in case of tool #5.

(R=0.1 and α=5°). From the results it can be stated the increased angle of the tool can minimize the force need of the process, and the decreased radius increase the force. After all it can cause the failure of the sheets because the decreasing radius and the decreasing angle getting closer to a cutting process.

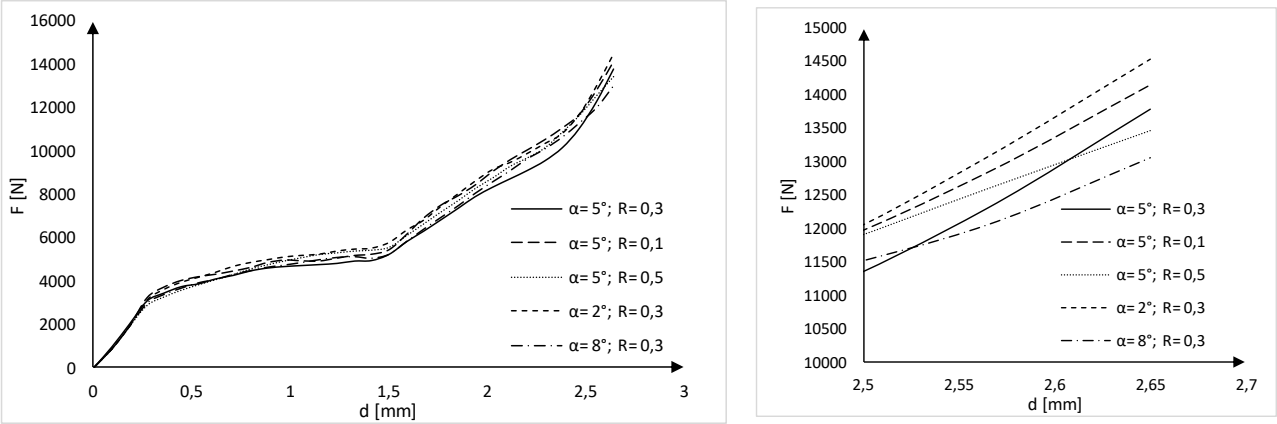

Figure 3 Measured F-d curves with different tools (maximal force - F_m is detailed)

The range of difference in maximal loads is ~1500 N which is not a high value, but measurable. For a deeper understand of the effects the cross sections of the joints will be investigated by microscopy as a next step of the research and compare with the FEA results.

ACKNOWLEDGMENTS

The authors would like to the thanks the support for this study.

Supported by the ÚNKP-19-3 New National Excellence Program of the Ministry for Innovation and Technology.

and

This research was supported by the European Union and the Hungarian State, co-financed by the European Regional Development Fund in the framework of the GINOP-2.3.4-15-2016-00004 project, aimed to promote the cooperation between the higher education and the industry.

REFERENCES

[1] T. Balawender, *Experimental Investigation of Clinch Joining Process*, Acta Mech. Slovaca 16 (1): 52 – 56, 2012.
[2] Sz. Jónás, M. Tisza, *Finite Element Modelling of Clinched Joints*, Adv. Techn. and Mat., vol. 43. No. 1. 2018.
[3] M. Tisza, G. Gál, A. Kiss, P. Z. Kovács, Zs. Lukács, *Alakítható nagyszilárdságú lemezanyagok klincs kötése*, Multidiszciplináris tudományok, 4. Kötet, 2014.
[4] Sz. Jónás, M. Tisza, D- felhős, P. Z. Kovács, *Experimental and numerical study of dissimilar sheet metal clinching*, AIP Conference Proceedings 2113, 2019.
[5] F. Lambiase, A. Di Ilio, *Optimization of the clinching tools by means of integrated FE modelling and artificial intelligence techniques*, Procedia CIRP 12, pp.163-168. 2013.
[6] F. Lambiase, A. Di Ilio, *An experimental study on clinched joints realized with different dies*, Thin-Walled Structures 85, 2014.
[7] S. Lee, C. Lee, J. Lee, B. Kim, D. Ko, *Influence of Tool Shape on Hole Clinching for Carbo Fiber-Reinforced Plastic and SPRC440*, Advances in Mechanical Engineering, 2015.

DIGITAL CONTROL OF CABLE VIBRATION DUE TO PERIODIC EXCITATION

KOLLÁR László E. PhD
Savaria Institute of Technology, Eötvös Loránd University
E-mail: kl@inf.elte.hu

Keywords: digital control, modelling, sampling delay, vibration

Suspended cable problems arise in engineering applications including power transmission lines and cable-stayed bridges. These structures are exposed to such natural phenomena as wind, icing, and ice shedding, which may induce cable vibration. The characteristics of the resulting vibration depends on the inducing mechanism. The interest of this paper is the high-frequency, low-amplitude vibration that develops due to vortex shedding in the wake, as is the case in aeolian vibration [1]. The frequency range may vary from 3 to 150 Hz, and the amplitude is in the range of the cable diameter [2]. Frequent occurrences of such vibration leads to reduced reliability and lifespan due to fatigue of the cable and other accessories of the structure. Damping devices have been applied for decades. They attenuate the vibration to a non-damaging level, but their application have limitations. An active vibration control, the electrical vibration absorber, was proposed in a recent research [3], which can be installed at any location of the cable and which is effective in a relatively wide frequency range. However, when active control is applied, the sampling delay must also be taken into account. The aim of the present study is to build a simplified model for active vibration control of a suspended cable exposed to periodic excitation, and examine the effect of time delay in the digital control. The time delay has a critical value above which the control becomes unsuccessful, and the excitation frequency significantly influences this critical delay.

The simplified model of the cable with the vibration absorber is a 2 degree-of-freedom (DOF) model as shown in Fig. 1. The parameters m, k and c denote mass, spring stiffness and damping, and the indices 1 and 2 refer to the cable and vibration absorber, respectively. Reduced-DOF models of conductor bundles with spacer at mid-span were proposed in [4]. However, the vibration absorber is usually placed at a position, which is close to one of the suspensions. Therefore, the calculation of the parameters of the cable model should be different from that presented in [4]. The spring stiffness k_1 of the cable is determined from the relationship of the force applied at the position of the vibration absorber and the displacement at the same position, see [4, 5] for more details. Although this relationship is nonlinear, a linear spring was assumed in the present model since small-amplitude vibration was considered. The cable damping c_1 is calculated from the geometrical and material properties of the cable [4] considering the vibration absorber in the mass per unit length of the cable. The mass m_2 of the vibration absorber was fixed, practically it is based on the design. The damping c_2 of the vibration absorber was neglected. The mass m_1 of the cable and the spring stiffness k_2 of the vibration absorber are determined together from the condition that the natural frequencies of the 2DOF system are equal to the first two natural frequencies, in vertical vibration modes, of the cable with the vibration absorber. The excitation considers wind effect in the form:

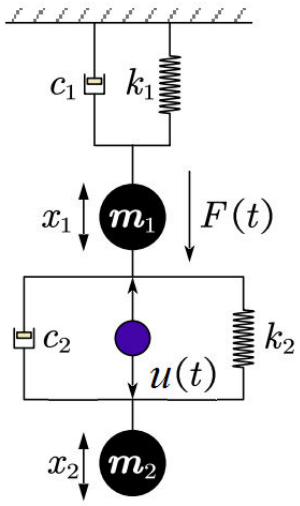

Figure 1 Simplified model of cable and vibration absorber

$$F(t) = F_0 \cos(\omega t)$$

where F_0 is the amplitude, and ω is the angular frequency of excitation. The control force $u(t)$ is considered in the simple form of a PD controller:

$$u(t) = Px_1(t) + D\dot{x}_1(t)$$

The control parameters are determined from the excitation frequency. When the excitation frequency is equal to the natural frequency of the 1DOF system modelling the cable, then the addition of the absorber reduces the vibration amplitude of the mass m_1, and no further control is necessary. For other values of the excitation frequency, the proportional gain P is chosen so that together with the spring stiffness k_2, they provide the same effect. The vibration control works without differential gain D for small absolute values of the proportional gain P. However, when the excitation frequency is great enough, the attenuation of vibration requires great absolute value of the proportional gain P, and the differential gain D will become necessary for reducing vibration amplitude. The absolute value of the differential gain D increases with that of the proportional gain P, but it should be relatively small. The governing equations of motion of the 2DOF model can be organized in the following form:

$$\dot{\mathbf{x}}(t) = \mathbf{A}\mathbf{x}(t) + \mathbf{b}u(t) + \mathbf{f}(t)$$

The vector **x** includes the coordinates x_1 and x_2 together with their derivatives, the matrix **A** and the vector **b** are determined by the system parameters m_1, k_1, c_1, m_2, k_2 and c_2, and the vector **f** includes the excitation force $F(t)$.

The digital control takes samples of the controlled parameters at short time intervals, and the corresponding control force acts after a short time delay. Assume that the time interval between taking samples and the delay of application of the control force are the same, and that the control force is kept constant in each of these short time intervals. Let τ denote the time delay, then the discrete-time model may be written as follows:

$$\mathbf{x}_{n+1} = \mathbf{A}_\mathbf{d}\mathbf{x}_n + \mathbf{b}_\mathbf{d}u_n + \mathbf{c}_\mathbf{d}\mathbf{f}_n$$

The matrix $\mathbf{A}_\mathbf{d}$ and the vectors $\mathbf{b}_\mathbf{d}$, $\mathbf{c}_\mathbf{d}$ are determined from the matrix **A**, vectors **b**, **f** and time delay τ.

Vibration control of a laboratory model of a suspended cable is simulated as an example. The excitation frequency is 10 Hz, and the value of sampling delay is set to be 10 ms. The comparison of the cable vibration for three cases is presented in Fig. 2. These cases include the vibration (i) without control; (i) with control, time delay neglected; (iii) with control, time delay considered. The application of control reduces the vibration amplitude to almost one third of its value without control, although the reduced amplitude is 20-30% greater with the sampling delay considered. Note that the critical value of delay in this case is 18 ms, i.e. the motion becomes unstable for greater values of the delay. Fig. 3 presents how the critical sampling delay decreases with excitation frequency. This result reveals a limitation of the control applied, which concerns the case of high excitation frequency.

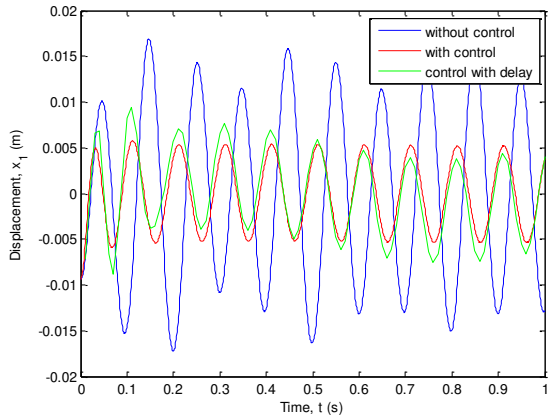

Figure 2 Time histories of vibration of mass modelling the cable

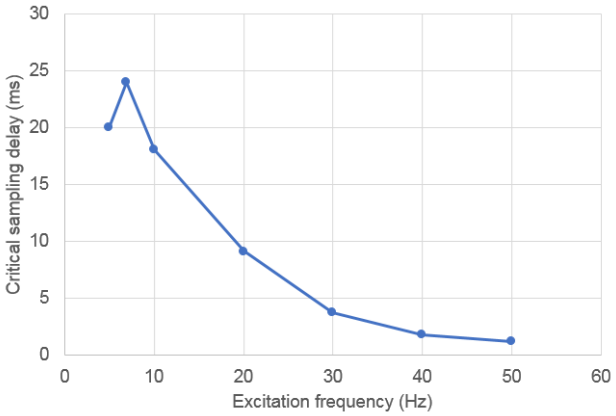

Figure 3 Variation of critical sampling delay with excitation frequency

Development of the vibration control involves further challenges, including the application of control for high-amplitude vibration when the elastic behavior of the cable is nonlinear, or for the case of varying excitation frequency.

ACKNOWLEDGMENTS

This paper was supported by the János Bolyai Research Scholarship of the Hungarian Academy of Sciences. The research was carried out in the frame of the project „EFOP-3.6.1-16-2016-00018 – Improving the role of research + development + innovation in the higher education through institutional developments assisting intelligent specialization in Sopron and Szombathely".

REFERENCES

[1] A. Cigada, G. Diana, M. Falco, F. Fossati, A. Manenti, *Vortex shedding and wake-induced vibrations in single and bundle cables*. Journal of Wind Engineering and Industrial Aerodynamics, 72, 253-263. 1997.

[2] M. Farzaneh, *Atmospheric icing of power networks*. Springer Science and Business Media. 2008.

[3] Y. Meng, L.E. Kollár, *Proposed active control methodologies for aeolian vibration of suspended cables under icing conditions*, Proc. of 18th International Workshop on Atmospheric Icing of Structures, Reykjavik, Iceland, Paper No. 30. 2019.

[4] L. E. Kollar, M. Farzaneh, *Modeling the Dynamic Effects of Ice Shedding on Spacer Dampers,* Cold Regions Science and Technology, 57(2-3), 91-98. 2009.

[5] H.M. Irvine, *Cable Structures*, MIT Press, Cambridge, MA, USA. 1981.

ANALYSIS OF A SPECIAL, 3D METAL-PRINTED HPDC TOOL MATERIAL

[1]KOVÁCS Sándor Endre PhD, [1]VARGA László PhD, [2]SZENTES Zsolt
[1]Faculty of Material Science and Engineering, Institute of Metallurgical and Foundry Engineering, University of Miskolc
E-mail: kovacssandorendre@gmail.com, laszlo.varga.mak@gmail.com
[2]Foundry Solid Kft
E-mail: szentes.zsolt@foundry-solid.com

Keywords: 3D printing, HPDC, tool steel, special alloy, simulation, mechanical testing

High Pressure Die Casting (HPDC) is the most productive metal-casting method of our time. It can produce precise geometries with high cycle numbers, particularly good for making products with fixed or occasionally changed geometries. To achive this great number of cycles, the process requires special tools, which will not react with the casting alloy and can withstand the high temperature during the cycles. These materials must have good heat-resistence and toughness.
Generally, when a HPDC tool is created, the inner cavities (such as cooling channels, ejectors etc) are made by using CNC machning technology. [1] This however, with today's more and more demanding industry can not meet every expectations, because their usage is somewhat limied when it comes to difficult cavity geometries, as shown in Fig 1.

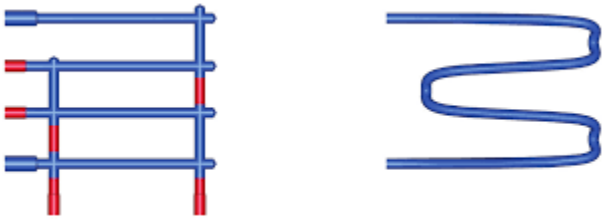

Figure 1 Linear (left) and conformal (right) cooling channels [1]

Conformal cooling channels can cover more of the casting's surface, thus can manage the process' thermophysical properties much better, allowing the HPDC tool an increased lifespan, and causing less downtimes due to repair operations. [2] But these thermal parameters are not only influenced by the cooling channels only [3]. Choosing the right tool material can, with higher heat conductivity, can also improve the quality of the process, and these two points are the main objectives of our work.
With everything said, combining a good heat-conductor steel with a conformal cooling channel sounds a straightforward answer to our question: „How can we improve our HPDC process the most?". So to dive deeper into this question we created a model-simulation with extreme properties to clearly show the difference between the different versions of the simulated version. The four different simulation is shown in Table 1.

Table 1 Simulation methods

	Tool steel	Cooling channel
A	Dievar	Linear / Conventional
B	HTCS	Linear / Conventional
C	Dievar	Conformal
D	HTCS	Conformal

The objective of this comparison was to determine which type of usage is the most favorable for a HPDC production, because there are times when not the most straightforward answer is the best one. We also compared this result with a simulation based on practical use, with the same ideology, but with only the tool material as variable.
Afterwards we conducted the laboratory analysis of the target material. Usually, when one wants to achieve a greater quality towards a specific factor, usually have to sacrifice something else. Here however, the manufacturer promising a great heat-conductivity steel with the same physical properites as a conventional tool steel. Combining this with 3D

printing technology lies the true challenge and our question: „Can the 3D printed tool steel maintain the same physical quality as the one made by conventional methods?".
To answer this question we conducted measurements in tensile strenght, hardness, Charpy-testing, texture analysis, and also made meauserements towards the fuel of the 3D printing process, the powder itself and the structure of the powder is shown in Fig 2.

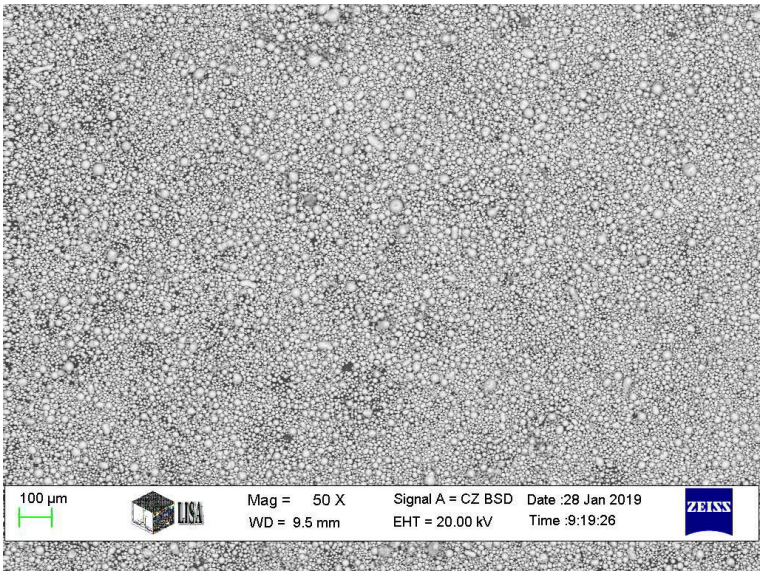

Figure 2 Powder structure under SEM analysis

Every measurement we made in this area was made by using conventional test specimens, but made by 3D printing technology. This kind of analysis was unique, because we were the first ones who printed these test-specimens using this alloy powder.
The results then were collected, then compared with the data sheet made from the same material's specimens but from conventional manufacturing methods.

ACKNOWLEDGEMENTS
The described work was carried out as part of a project supported by the Foundry Solid Kft. The 3D printed test specimens were made in the Széchényi István University, Győr, Hungary, and the measurements were carried out at the University of Miskolc.

REFERENCES
[1] M. Frings, M. Behr, S. Elgeti, *A simplified simulation model for a HPDC die with conformal cooling channels*
[2] B. Zink, F. Szabó, I. Hatos, H. Hargitai és J.G. Kovács *DMLS szerszámbetétek szimulációs vizsgálata*.MŰANYAG- ÉS GUMIIPARI ÉVKÖNYV, 12 (1). pp. 80-87. ISSN 1589-6269, 2014
[3] A. Armillotta, R. Baraggi, *SLM tooling for die casting with conformal cooling channels*

STATE EQUATION OF EQUILIBRIUM AND REARRANGEMENT OF A SET OF CONVEX, RIGID PARTICLE

LÁMER Géza PhD
Faculty of Mechanical Engineering, University of Debrecen
E-mail: glamer@eng.unideb.hu

Keywords: set of grains, balance of grains, and rearrangement of grains

ASSUMPTIONS

During the analysis we assume that the particles are absolutely rigid, strictly convex, there is no friction or adhesion between the particles. We further assume that there is a three-point, in some cases symmetrical, supporting hypothesis, that is, we choose the arrangement of the particles so that the hypotheses are fulfilled. The grains are assumed to be absolutely rigid. For sets placed on the surface, we assume that all the particles in contact with the surface have a (Karman–Bio-type) periodic boundary condition [2,3].
We assume that the size of each particle is nearly the same, that their shape is full, that is, there are no significant differences between their sizes. (This means that they are close to spherical, i.e. they cannot be flat or oblong.) [2]
To set up the equations, we assume that the surface of each particle has an equation and the contact network of the particles is given. It is further assumed that, in the initial situation, the network and the arrangement of the particles are such that the set of particles is in equilibrium under self-weight.
We consider the loads and their nature to be known - conservative or follower.
Boundary conditions, whether the container or support or the free surface, are known.

THE EQUATIONS THAT DETERMINE THE BALANCE OF THE GRAINS

The system of equations to be written is nonlinear; unknown quantities cannot be explicitly highlighted in the first approach. The equations can only be written in a specific order so that the system of equations can be solved.
Determining the coordinates of the contact points of the particles:

$$F_i(\mathbf{O}_i\mathbf{x}+\mathbf{R}_i)=F_j(\mathbf{O}_j\mathbf{x}+\mathbf{R}_j), i, j=1,2,...,n_{sz}.$$

The geometry is used to determine the coordinates of all contact points. The location vector of the intersection point of the *i*-th and *j*-th particles in global coordinates is denoted by $\mathbf{R}_{ij}$.
Determination of the coordinates of the points of contact of the granules and the boundary ("pot") surfaces:

$$F_i(\mathbf{O}_i\mathbf{x}+\mathbf{R}_i)=F_p(\mathbf{O}_p\mathbf{x}+\mathbf{R}_p), i=1,2,...,n_{sz}, p=1,2,...,n_p.$$

The geometric arrangement determines the coordinates of all points of contact between the particles and the boundary ("pot") surfaces. The location vector of the point of intersection of the *i*-th grain and the *p*-th edge in global coordinates is denoted by $\mathbf{R}_{ip}$.

$$\mathbf{R}_{it}=F_i(\mathbf{O}_i\mathbf{x}+\mathbf{R}_i)_{|\mathbf{x}_t}, i=1,2,...,n_{sz}, t=1,2,...,n_{i,t}.$$

The geometric arrangement determines the coordinates of the points of attack of the loads. The location vector of the *t*-point of the *i*-th particle in global coordinates is $\mathbf{R}_{it}$.
Direction of forces acting on the system:

$$n_{is}=\left(\frac{\partial F_i}{\partial X_1^{(i)}},\frac{\partial F_i}{\partial X_2^{(i)}},\frac{\partial F_i}{\partial X_3^{(i)}}\right)_{|P=P_s}, i=1,2,...n_{sz}, s=j,p,t.$$

$$\mathbf{X}^{(i)}=\mathbf{Q}_i\mathbf{x}+\mathbf{R}_i,\ i=1,2,\ldots,n_{sz}.$$

The direction vector of the contact forces, reaction forces and load are determined at the points of contact of the particles ($s=j$), the points of contact of the particles and the boundary ("pot") surfaces ($s=p$) and the points of contact of the loads ($s=t$). The outward directions of the grains are considered positive.
Equilibrium equations. The balance equations of moment are written at the centre of gravity of the grain.
Equilibrium of the contacting particles:

$$-\sum_j S_{ij}\cdot\mathbf{n}_{ij}+\mathbf{P}_{\ddot{o}i}=\mathbf{0},\hat{i}=1,2,...,n_{sz}.$$

$$\sum_j (S_{ij}\cdot\mathbf{n}_{ij})\times(\mathbf{R}_i-\mathbf{R}_{ij})=\mathbf{0},\hat{i}=1,2,...,n_{sz}.$$

Equilibrium of the particles in contact with the boundary („pot”):

$$-\sum_j S_{ij}\cdot\mathbf{n}_{ij}-\sum_p S_{ip}\cdot\mathbf{n}_{ip}+\mathbf{P}_{\ddot{o}i}=\mathbf{0},\bar{i}=1,2,...,n_{sz}.$$

$$\sum_j (S_{ij}\cdot\mathbf{n}_{ij})\times(\mathbf{R}_i-\mathbf{R}_{ij})+\sum_p (S_{ip}\cdot\mathbf{n}_{ip})\times(\mathbf{R}_i-\mathbf{R}_{ip})=\mathbf{0},\bar{i}=1,2,...,n_{sz}.$$

Balance of free surface loaded (and non-contacting with the boundary („pot”)) particles:

$$-\sum_j S_{ij}\cdot\mathbf{n}_{ij}-\sum_t T_{it}\cdot\mathbf{n}_{it}+\mathbf{P}_{\ddot{o}i}=\mathbf{0},\bar{i}=1,2,...,n_{sz}.$$

$$\sum_j (S_{ij}\cdot\mathbf{n}_{ij})\times(\mathbf{R}_i-\mathbf{R}_{ij})+\sum_t (S_{it}\cdot\mathbf{n}_{it})\times(\mathbf{R}_i-\mathbf{R}_{it})=\mathbf{0},\bar{i}=1,2,...,n_{sz}.$$

REFERENCES

[1] Á. Kézdi, *Talajmechanika I. Negyedik kiadás.* Tankönyvkiadó, Budapest, 1972. *Talajmechanika II. Második, átdolgozott kiadás.* Tankönyvkiadó, Budapest, 1970.

[2] G. Lámer, *Az anyagi viselkedés folytonos és diszkrét modellezésének kérdései.* In: Török Á. – Vásárhelyi B. szerk.: Mérnökgeológia-Kőzetmechanika 2010. Konferencia (Budapest, 2010. március hó 25.), [A Mérnökgeológia-Kőzetmechanika Kiskönyvtára 8. kötet], pp. 123-146, Műegyetemi Kiadó, Budapest, 2010.

[3] G. Lámer, *Egy szemcse egyensúlya: kinematikai határozatlanság és statikai határozottság*. In: Pokorádi László szerk., Műszaki Tudomány az Észak-Alföldi régióban 2010. (Nyíregyháza, 2010. május hó 19.), pp. 53-58, Debreceni Akadémia Bizottság Műszaki Szakbizottsága, Debrecen, 2010.

[4] G. Lámer, *Száraz, vizes, kötött szemcsék és a folytonos közeg, avagy a szemcsétől kontinuumig*. In: Török Á. – Vásárhelyi B. szerk., Mérnökgeológia-Kőzetmechanika 2008. Konferencia (Budapest, 2008. november hó 26.), [A Mérnökgeológia-Kőzetmechanika Kiskönyvtára 7. kötet], pp. 271-286. Műegyetemi Kiadó, Budapest, 2008.

[5] G. Lámer, *Erőeloszlások szabályosan elrendezett szemcsehalmazban és folytonos közegben*. Geotechnika (Ráckeve, 2016. október hó 10-12.) Konferenciakiadványa, pp 120-131, 2016.

[6] G. Lámer, Symmetry and asymmetry, or regularity and irregularity in the force distribution in the heaped bodies. *Culture and Science. Ed.: Darvas Gy.* 17:221–233, 2006.

[7] G. Lámer, A szemcsék és a szemcsehalmazok geometriai és topológiai jellemzése. In: Műszaki Tudomány az Észak-kelet Magyarországi Régióban (Miskolc Egyetemváros, 2011. május hó 18.). Szerk.: Pokorádi L. ISBN 978-963-7064-25-8. pp.273-285. 2011.

[8] Лойцанский, Л.Г. – Лурье, А.И. *Курс теоретической механики. Т. I.* Наука, Москва, 1982.

[9] K. Bagi, *Szemcsehalmazok mikroszerkezetének vizsgálata.* Akadémiai Doktori Értekezés (Kézirat), Budapest 2005.

[10] G. Lámer, *Szemcsehalmazok egyensúlyának és átrendeződésének az állapotegyenlete*. A XI. Magyar Mechanikai Konferencia (Miskolc, 2011. augusztus hó 29-31.) Konferenciakiadványa. Szerk.: Baksa A. – Bertóti E. – Szirbik S. 65. cikk. 11 oldal, 2011.

FORCE DISTRIBUTION IN A SET OF REGULARLY ARRANGED, CONGRUENT, CONVEX, RIGID PARTICLES

LÁMER Géza PhD
Faculty of Mechanical Engineering, University of Debrecen
E-mail: glamer@eng.unideb.hu

Keywords: set of regularly arranged balls or columns, force lines, force distribution in the set of grains, side pressure in the set of grains

ASSUMPTIONS

During the analysis, we assume that the balls are all the same diameter and the columns are congruent, all bodies are absolutely rigid, there is no friction or adhesion between the balls or the columns. We also assume that there is a three-point, in some cases symmetrical supporting hypothesis, that is, we choose the arrangement of the balls and columns so that the hypotheses are fulfilled [1,2].
In this abstract, we only look at results for sets of balls.

FORCE DISTRIBUTION IN THE SET OF BALL ARRANGED IN REGULAR PYRAMID

From balls of equal size, assuming a periodic boundary condition, three regular pyramids can be formed: rectangular, triangular, and hexagonal. A rectangular pyramid has four “edges” and a triangular pyramid has three. The hexagon-based pyramid does not have an “edge”. Note that the layout of the triangle-based pyramid is the same, while that of the hexagon-based pyramid varies from layer to layer. (See Figures 1.2 and 1.3.)

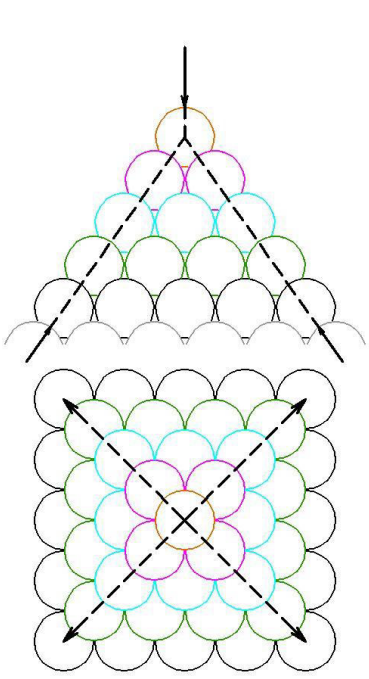

Figure 1.1
Pyramid with rectangular base

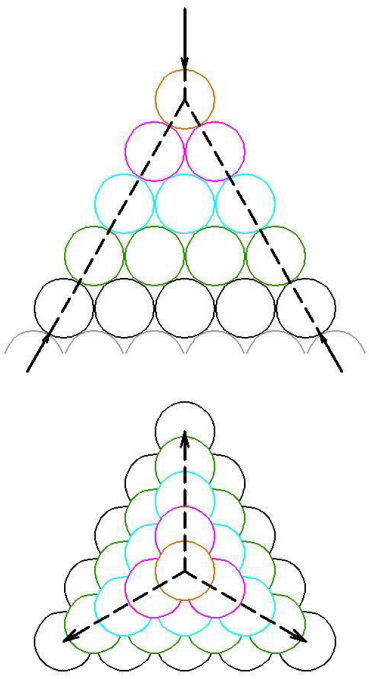

Figure 1.2
Pyramid with triangle base

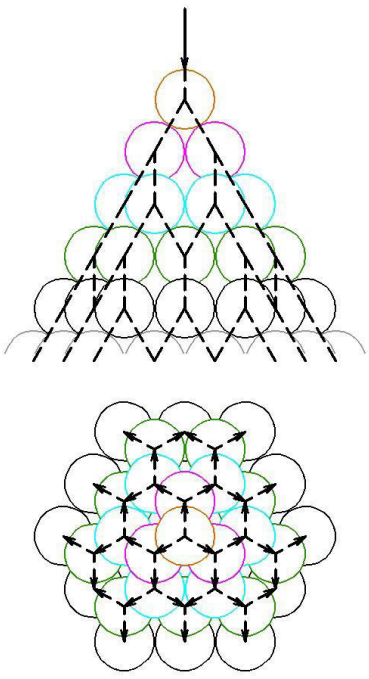

Figure 3.3
Pyramid with hexagon base

Figure 1 Force distribution in the set of ball arranged in regular pyramid

SIDE PRESSURE IN THE SET OF BALLS ARRANGED REGULARLY IN A POT

The arrangement according to the relative position of the layers may be as follows.

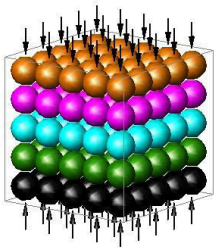

Figure 2.1. Vertical arrangement

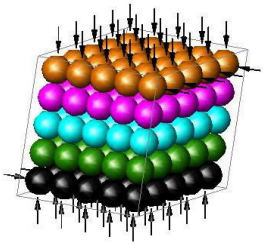

Figure 2.2. Slanted hanging arrangement

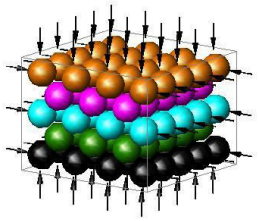

Figure 2.3. Plane mesh arrangement

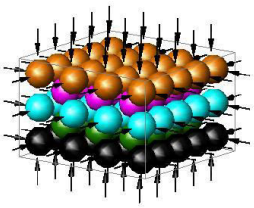

Figure 2.4. Spatial mesh arrangement

Figure 2 The arrangement according to the relative position of the layers

In a planar section, we review the geometric condition for the existence of side pressure and the dependence of side pressure on the line angle defined by the centres of the superimposed balls. (Angles refer to a plane problem.)

No side pressure and no horizontal reaction force	No side pressure, but horizontal reaction force	Side pressure occurs	The interval of the existence of the side pressure	The side pressure and the horizontal reaction force are also eliminated

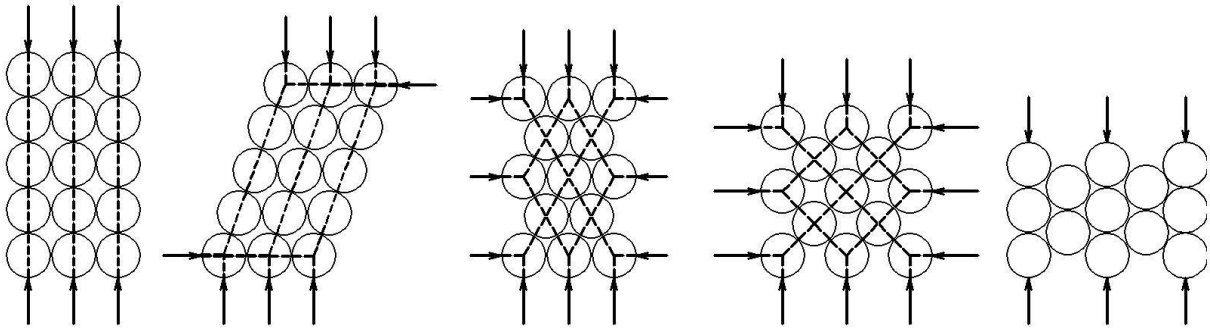

α = 90º | 90º > α > 60º | α = 60º | 60º > α > 30º | α = 30º

Figure 3 The geometric condition for the existence of side pressure (in a plane)

REFERENCES

[1] Lámer G. *Az anyagi viselkedés folytonos és diszkrét modellezésének kérdései*. In: Török Á. – Vásárhelyi B. szerk.: Mérnökgeológia-Kőzetmechanika *2010. Konferencia* (Budapest, 2010. március hó 25.), [A Mérnökgeológia-Kőzetmechanika Kiskönyvtára 8. kötet], pp. 123-146, Műegyetemi Kiadó, Budapest, 2010.

[2] Lámer G.: *Egy szemcse egyensúlya: kinematikai határozatlanság és statikai (túl)határozottság*. In: Pokorádi László szerk., Műszaki Tudomány az Észak-Alföldi régióban 2010. (Nyíregyháza, 2010. május hó 19.), pp. 53-58, Debreceni Akadémia Bizottság Műszaki Szakbizottsága, Debrecen 2010.

[3] Kézdi Árpád. *Talajmechanika I. Negyedik kiadás.* Tankönyvkiadó, Budapest, 1972. *Talajmechanika II. Második, átdolgozott kiadás.* Tankönyvkiadó, Budapest, 1970.

[4] Lámer G.: *Száraz, vizes, kötött szemcsék és a folytonos közeg, avagy a szemcsétől kontinuumig*. In: Török Á. – Vásárhelyi B. szerk., *Mérnökgeológia-Kőzetmechanika 2008. Konferencia* (Budapest, 2008. november hó 26.), [A Mérnökgeológia-Kőzetmechanika Kiskönyvtára 7. kötet], pp. 271-286. Műegyetemi Kiadó, Budapest, 2008.

[5] Lámer G.: *Erőeloszlások szabályosan elrendezett szemcsehalmazban és folytonos közegben*. Geotechnika 2016. (Ráckeve, 2016. október hó 10-12.) Konferenciakiadványa, pp 120-131

[6] Lámer G.: S*ymmetry and asymmetry, or regularity and irregularity in the force distribution in the heaped bodies.* Culture and Science. Ed.: Darvas Gy. 17:221–233, 2006.

[7] Budó Ágoston. *Mechanika. Ötödik kiadás.* Tankönyvkiadó, Budapest, 1972.

[8] Lámer G.: *Erővonalak edényben szabályosan elrendezett golyók halmazában*. A XI. Magyar Mechanikai Konferencia (Miskolc, 2011. augusztus hó 29-31.) Konferenciakiadványa. Szerk.: Baksa A. – Bertóti E. – Szirbik S. 64. cikk. 12 oldal

COMPLIANT MECHANISMS IN PROGRESS AND DEVELOPMENT OF MODERN TECHNOLOGY

[1]LATEŞ Daniel PhD, [2]CĂŞVEAN Marius
[1]Pharmacy, Science and Technology of Târgu Mures, iFOR Res. and development center of IRUM, University of Medicine
E-mail: lates.upm@gmail.com, daniel.lates@irum.ro
[2]Accesa IT Systems, Cluj-Napoca, Cluj
E-mail: marius.casvean@yahoo.com

Keywords: compliant mechanism, compliant joints, compliant devices, compliant micro mechanisms, displacement, geometry

There are many types of mechanisms nowadays. A mechanism is a device to transfer or transform motion, force or energy. Traditional rigid body mechanisms consist of rigid links connected at movable joints. Whatever machines you see in your day to day life has some underlying mechanisms that govern its motion to produce the desired output. The energy is transfered from the input to the output. Compliant mechanisms have been used for decades in different fields and industries. In particular, robotics, medical or aerospace have been using such mechanisms for some 50 years now, even more. These mechanisms depend on some parameters, like elastic deformations, to provide precise and smooth motions. It is essential to develop an accurate model to quatify the deformation for kinetic analysis and parameter optimization.


Figure 1 Compliant tweezers


Figure 2 Displacement inverter mechanism

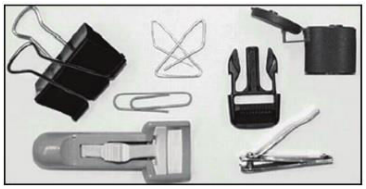
Figure 3 Common compliant devices


Figure 4 Compliant torsional spring

Compliant mechanisms are monolithic structures where the movement is given by the flexibility of the structure rather than the presence of joints and pins. The absence of joints allows the construction of compliant mechanisms in microscale.
This kind of mechanism transfer motion, force or energy. Unlike rigid-link mechanisms, compliant mechanism gain at least some of their mobility from the deflection of flexible members rather than from movable joints only. Basically not all the links of the mechanism need to be flexible for it to be named as a compliant system but some important links must be flexible. Fully compliant mechanisms are very unstable and unreliable.
Also, these mechanisms rely upon elastic deformation to perform their function of transmitting and transforming motion and force. From an overall perspectve that consider performance, economy of material, scalability to micro and nano sizes, etc., compliant mechanisms are preferable over rigid body mechanisms.

INTERNATIONAL PAPERS

A large number of papers exists, regarding the compliant mechanisms. It is not the concept that can be treated as something new, but it is the role that can be assigned to it. And the shape may looks always simple, but there is invested a large amount of time to investigate how this should look like for doing the proper desired functionality. Optimizations are welcome anytime.
For a continuum topology design problem, the optimal solution is a structure that is composed of only one material and voids, which means that a 0-1 decision is used to determine whether the material should be placed at a point within the design domain.
Other papers can bring a short overview of some mechanical structures and their performance characteristics. One of them presents three concepts of force amplifiers and results from simulations are discussed. The specific design of the linear motion force amplifier/motion reduction for a high accuracy positioning device with large payload capacity is studied.

REPRESENTATIVE PAPERS WITH IMPACT IN MODERN INDUSTRY

Compliant mechanisms have made an enormous contribution in various fields. Several methods have being conceived to analyze and design these compliant mechanisms that gain part of their motion from deflection of flexible members rather than movable joints, as conventional mechanisms. Recently, many familiar example of compliant mechanisms have been designed and widely used in various field as automotive industry, aerospace industry, MEMS, Medical devices, Robotic arm with minimal impedance and assistive mechanisms. For adaptive structures, components in transportation, etc., the largest challenge is to analyze and design these mechanisms.

Consider the compliant over-running clutch and its rigid body counterpart. Considerably fewer components are required for the compliant mechanism than the rigid mechanism. The reduction in part count may reduce manufacturing and assembly time and cost. Compliant over-running clutch is an example for application of compliant systems in automotive industry, apart from that the car wiper, steering parts, gears, breaks are other examples. The compliant mechanisms and systems are also used in (new age) industry like aerospace, mechanism amplification for sensors and actuators or for microsurgery suturing device, etc.

Morphing aircraft structures can significantly enhance air vehicle performance. The aerodynamic benefits are exploit. Computational tools are being developed to design structures that deform into specified shapes given simple actuators inputs. These synthesis methods seeks to optimize the stiffness of the structure to minimize actuator effort and maximize the stiffness with respect to the environment.

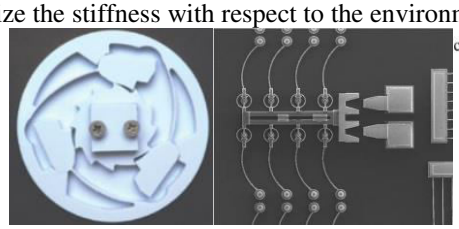
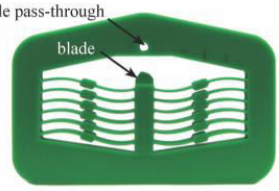

Figure 5 Over-running clutch *Figure 6* Micro mechanisms *Figure 7* The cutter non-explosive release mechanism *Figure 8* The pointer device

Mechanisms that possess distributed compliance, as opposed to lumped compliance, are much more fatigue resistant and easier to manufacture. Several computational approaches have been developed to design compliant mechanism for desired force-displacement characteristics and more recently for generalized shape change.

Compliant mechanisms offer undisputable advantages, in term of reliability and performance and as such can be a great ally in the search for enhanced quality. The potential for dramatic reduction in the total number of parts required to accomplish a specific task.

ACKNOWLEDGMENTS

We would like to express our gratitude to SC IRUM SA for the moral and financial support for the realization of this article. We also want to thank the organizers of the event for organizing such a scientific conference that helps us publish articles on engineering.

REFERENCES

[1] Muqing Niu, Bintang Yang, Yikun Yang, Guang Meng,(2018),*Two generalized models for planar compliant mechanisms based on tree structure method*,Precision Engineering, vol.51, pag.137-144

[2] Cicero R. de Lima, Glaucio H. Paulino, (2019), *Auxetic structure design using compliant mechanisms: A topology optimization approach with polygonal finite elements*, Advances in Engineering Software, vol. 129, pag. 69-80.

[3] M. P. Bendsoe, O. Sigmund, (2004), *Topology Optimization: Theory. Methods and Applications*, Springer.

[4] Jaroslav Hricko, Stefan Havlik, Compliant mechanisms for motion/force amplifiers for robotics, Advances in Intelligent Systems and Computing (AISC), vol. 980.

[5] Pandiyan Arumugam, Arun Kumar, (2016), *Design methods for compliant mechanisms used in new age industry – a review*, Istrazivanja i projektovanja za privredu, vol. 14, pag. 223-232.

[6] Sridhar Kota, Joel Hetrick, Russell Osborn, Donald Paul, Ed Pendleton, Peter Flick, Carl Tilmann, (2003), *Design and application of compliant mechanisms for morphing aircraft structures*, Proceedings of SPIE – The International Society for Optical Engineering.

[7] Lateș, D., (2014), *Cercetări teoretice și aplicative privind mecanismele compliante folosite în mecatronică,* Teza de Doctorat, Cluj-Napoca.

[8] J. Agnus, N. Chaillet, C. Cl´evy, S. Demb´el´e, M. Gauthier, Y. Haddab, G. Laurent, P. Lutz, N. Piat and M. Rakotondrabe, (2013), *Robotic Microassembly and micromanipulation at FEMTO-ST* (https://gjlaurent.github.io/assets/papers/Agnus2013robotic.pdf).

[9] Shannon A. Zirbel, Kyler A. Tolman, Brian P. Trease, Larry L. Howell, (2016), *Bistable Mechanisms for Space Applications*, PLOS ONE | DOI:10.1371/Journal.Pone.0168218

STRUCTURAL AND ECONOMIC ASSESSMENT OF HYBRID COMPOSITE MATERIALS USING EXCEL DATA ANALYSIS

[1]LISBOA SOUZA Vinicius, [1]PÁLINKÁS Sándor PhD, [2]DA SILVA Luís PhD
[1]*Institute of Mechanical and Vehicle Engineering*
E-mail: viniciuslisboasouza@gmail.com, palinkassandor@eng.unideb.hu
[2]*Institute of Mechanical Engineering*
E-mail: charles.silva@ufv.br

Keywords: composite, hybrid, data analysis

Composite materials have been gaining ground in engineering uses over the years, especially about their structural applications. Thus, the following definition can be followed: "A composite material can be defined as a combination of two or more materials that results in better properties than those of individual components when used separately" [1]. Applications of such materials are due to their versatility and modellable properties according to the utility of the final piece to be produced, since the choice of constituent materials will dictate the properties of the resulting composite. Therefore, knowing the properties of the constituent materials and how they interact with each other is fundamental for the realization of a cohesive, safe and well-dimensioned project. The physical and mechanical properties of the reinforcements mentioned are different, resulting in composites with different properties even when the same polymeric matrix is used. However, such constituents can be applied in similar structural uses and are extensively used in today's transportation industry, mainly the aerospace and electrical vehicle ones. Such use is mainly due to the properties such as low density and high mechanical strength, essential for aerospace and electrical vehicles uses.
Glass fiber is known to be the most commonly used reinforcement in most commercial composites because it has low cost and reasonable mechanical properties when compared to high-performance fibers such as carbon fiber or Aramid. Thus, the use of high-performance reinforcements, such as carbon fiber, for example, offers a high relationship between mechanical strength and density, which favors the use in high-performance applications.
From this point, economic considerations become essential, as the cost difference between fibers is considerable and becomes a crucial factor in the cost-effectiveness of the entire project. Therefore, a study was made of the cost ratio for each reinforcement mentioned with the mechanical properties of the components produced, always paying attention to the resulting density, considering that the study is focused on the optimization of such material by Excel data analysis. That is why the purpose of the research program was the investigation of the relation of mechanical properties and specific price for hybrid composite materials using statistic methods utilizing Excel data analysis techniques. This research provided a clear relationship between these properties and using such information, it would be possible to Project Engineers or Structural Engineers consider the use of composites, aiming the improvement of some properties or the decreasing in the price for some components.
The research started with the collection of data related to these materials, this data is informed by the provider or by the manufacturer of such materials. After that, this information was used to the construction of models, using Excel, analyzing the materials from the theoretical method for composite materials [2][3]. Using the technique, it is possible to analyze composites with a wide range of configurations, and after that plot the relation between different configurations and the properties, mechanical and economical ones.
For the hybrid composite strength, that the hybrid has a resistance dependent on the number of layers of each fibrous phase (n), the resistance of each separate phase (σ) and the thickness of each layer (t) [4]. Equation 8 demonstrates such a relationship, with h, c, and g being the subscripts referring to hybrid, carbon fiber layers, and fiberglass layers, respectively.

$$\sigma_h = \frac{n_c \cdot \sigma_c \cdot t_c + n_g \cdot \sigma_g \cdot t_g}{n_c \cdot t_c + n_g \cdot t_g} \quad (8)$$

Such properties refer to a single layer of the composite. To predict the properties of the laminate, specifically the stress-strain relationship, some other hypotheses are required. A matrix relation measures the properties of the orthotropic laminate, that is, that at least one of the 3 conditions can be fulfilled: 1-Composed only by layers θ = 0 ° or θ = 90 °; 2-For each layer + θ there is a layer –θ; 3- a combination of the two conditions above, theta being the orientation of the fibers according to a reference [3]. Equation 9 below presents such a relationship.

$$\begin{bmatrix} \sigma_1 \\ \sigma_2 \\ \tau_{12} \end{bmatrix} = \begin{bmatrix} Q_{11} & Q_{12} & 0 \\ Q_{12} & Q_{22} & 0 \\ 0 & 0 & Q_{66} \end{bmatrix} \cdot \begin{bmatrix} \varepsilon_1 \\ \varepsilon_2 \\ \gamma_{12} \end{bmatrix} \quad (9)$$

Since the first matrix refers to normal and shear stresses, the third to normal and shear deformations, and the second to relations dependent on the properties of each layer and which effectively dictate the stress-strain relationship, shown below.

$$Q_{11} = \frac{E_1}{1-v_{12}\cdot v_{21}} \qquad Q_{22} = \frac{E_2}{1-v_{12}\cdot v_{21}} \qquad Q_{12} = \frac{v_{21}\cdot E_1}{1-v_{12}\cdot v_{21}} \qquad Q_{66} = G_{12}$$

With the terms of matrix Q, relating stress and strain, it is possible to find the properties for the laminate according to the following relations.

$$E_x = A_{11} - \frac{(A_{12})^2}{A_{22}} \qquad E_y = A_{22} - \frac{(A_{12})^2}{A_{11}} \qquad v_{xy} = \frac{A_{12}}{A_{22}} \qquad v_{yx} = \frac{A_{12}}{A_{11}} \qquad G_{xy} = A_{66}$$

Being $A_{ij} = \frac{1}{t}\sum Q_{ij}(\theta)(h_k - h_{k-1})$. The terms interior to the sum represent the values of Q_{ij} for layers with varying fiber orientation angles and the thickness of each layer within the laminate. The term t represents the final thickness of the entire laminate.

This data collection was made following standards which are stated by specific bibliography related to Excel data analysis. The first step is to choose the type of data to be collected, which in this case is ratio data [5]. It came from different sources, like for example academic bibliographies, material suppliers, MatWeb, and others. The most important point during this process is to keep the consistency about the type of data, what requires a refined knowledge about these materials. The second step is the creation of a model, in this case a symbolic model characterized by a symbolic representation.

Thus, it is noted that the hybrids have values for the modulus of elasticity 32% lower than the values of carbon components, but are 91% larger than the components made of fiberglass, the which may mean greater tolerance to deformation and consequently greater structural stability.

For resistance, hybrids are only 10% less resistant than pure carbon components, and 14% stronger than entirely fiberglass components. These values may differ from the actual values, as the ultimate stress values used for the glass fibre refer to data from the MatWeb platform and other sources, and it is not possible to know exactly the value provided by the manufacturer.

It is also noted that the different types of epoxy systems basically do not change the properties decisively, presenting similar values when used with the same types of fibers. Therefore, the choice of epoxy systems should be based mainly on their costs, in addition to other constructive properties, such as mixing time, cure time and viscosity.

Regarding weight, hybrids are 17% heavier than carbon fiber laminates and 13% lighter than glass fibre components. However, the most notable difference is cost, as the hybrid is 53% cheaper than a laminate of the same weight made of carbon fiber alone

ACKNOWLEDGMENTS

The described work was carried out as part of a project supported by Talent Management Programme of the University of Debrecen and by the Federal University of Viçosa as part of the requirements of the Institutional Program for Scientific Initiation PIBIC/FAPEMIG.

REFERENCES

[1] F.C. Campbell, *Introduction to Composite Materials*. ASM International, 2010.
[2] F. Ashby, F. Michael, *Seleção De Materiais No Projeto Mecânico*. 4 ed. Rio de Janeiro: Elsevier, 2012.
[3] A. Baker, S. Duton, D. Kelly, *Composite Materials for Aircraft Structures*. 2 ed. Blacksburg: AIAA, 2004.
[4] Bittencourt, P. Ana Paula *Estudo Comparativo de Processos de Compósitos fibra de vidro/poliéster*. Joinville, 2015. 68p. Bachellor project–Naval Engineering, Universidade Federal de Santa Catarina.
[5] H. Guerrero, *Excel Data Analysis: Modeling and Simulation*. Springer, 2019.

THE VARIATION OF GAS PRESSURE IN FURAN NO-BAKE SAND CORES

MÁDI Laura, BUDAVÁRI Imre, VARGA László PhD
Faculty of Materials Science and Engineering, Foundry Institute, University of Miskolc
E-mail: madi.laura.johanna@gmail.com, budavari1987@gmail.com, laszlo.varga.mak@gmail.com

Keywords: gas defects, gas pressure, sand grain size, furan binder, acid hardener

Expendable sand molds and cores can be used to produce the desired quality of castings. Most of the sand molds and cores are produced using organic binders for bonded sand grains. In the casting manufacturing process several casting defects can be attributed to poor quality of molds and cores and inadequate control of process variables. During pouring, molten metal interacts with the sand mold/core. Because of the heat exposure of metal, a variety of complex degradation reactions may occur in the sand mold/cores. Several gaseous products are evolved from the decomposition of binder that may cause different kinds of gas defects. Gases evolved from the mold/core must be allowed to escape from the mold cavity through core print, artificial vent etc. In some cases high gas pressure may be generated at the mold/metal interface. If the casting skin is not solidified before the gas could pass through the semi-solidified metal skin could be blown away from the mold/metal interface. This kind of gas defect is called blowholes, which can be described as an individual or groups of cavities with smooth walls at the surface of the casting. Blowholes may be occurred by the low gas permeability of core sand, the high amount of binder, insufficient core venting, etc. To prevent the formation of gas defects it is important to control and minimize both the gas evolution rate as well as the amount of the produced gases. Since the usage of organic resin binder in the mold -, and core making process, a lot of research was conducted to determine factors that influence the volume and pressure of gases released from mold and core.
The aim of this article is to investigate the impact of the grain size of base sand, the amount of resin binder and the amount of acid hardener on the gas pressure of released gases from no-bake furan resin sand cores. Cores were made out of commercially available refractory silica sands (SH32 and SH34) having different grain size distribution. The amount of furan resin binder was 1.0%, 1.4% and 1.8% based on sand weight. For curing the binder, acid hardener (benzol sulphuric acid) was prepared in 40% and 80% based on the weight of the binder. Total of 12 different compositions of core mixtures were made using a laboratory mixer. First, the acid hardener was added to the base sand then the furan binder. The stirring time was 1 minute after each component was added to the silica sand.
Cores were prepared in steel core – box with constant compacting energy and approximately the same bulk density (1.5 – 1.6 g/cm^3). The setting time of the core mixtures was 4 hours. The geometry of the cylindrical test bars was Ø28x134.3 mm. In order to collect the released gases from the sand core, steel pipe with geometry of Ø6x300mm was placed 5 mm away from the top of the test bars during core making. The completed test bar can be seen in Figure 1.

Figure 1 The cylinder test bar in the cores - box

The mold was prepared using green sand mixture with 8 % bentonite and 4 % water based on the silica sand. Molds were produced with a Multiserw Morek sand muller mixer. Approximately 50 kg of the green sand mixture was necessary for each forms. The size of the drag box was Ø330x200 mm and the size of the cope box was Ø330x140 mm. Casting was carried out simultaneously using a tangential gating channel in a three-cavity form that was made with cone-shaped wooden patterns (Ø70x150mm, draft: 4°). For the experiments 720°C foundry aluminium alloy was poured into the mould cavity. The released gases passed through a silicone tube to a pressure transducer. Three Baumer type pressure transducers were used for measuring the gas pressure. The device was designed for low-pressure measurement (0-0.1 bar with ±0,5% accuracy). The data acquisition was carried out using HBM QuantumX-MX840B universal 8 channel amplifier module, which is connected to a computer with an HBM Catman software. The sampling rate was 20 Hz.

The gas pressure curves of the released products obtained at 5 mm from the core/metal interface can be seen in Figure 2a – 2d. In every case, two maximum were observed on the gas pressure curves. The first main pressure increase was at 5-10 seconds because of the fast heating up and the expansion of the air, trapped in the pores. Thereafter, the amount of gas produced due to the high-temperature gradient of the mould wall, fills the pores and the gas evolve is started. During the heat exposure of core sand mixture, the velocity of gas production is getting faster until the gas pressure reaches its maximum.

Based on Fig 2a and Fig 2b it can be observed that cores containing SH34 silica sand show a peak pressure ranging from 20 – 28 mbar depending on the resin content. The amount of resin also affects the time at which the gas pressure reaches up its maximum value. The amount of the acid hardener determines the size of the area under the gas pressure curve.

Cores based on SH34 silica sand have higher gas pressure due to the low gas permeability, which leads to low gas discharge. The probability of casting defects (like blowholes) caused by gas penetration is also increased. The gas pressure of cores made out of SH32 silica sand can reach up to 8 - 10 mbar (see Fig 2c and Fig 2d). In this case, evolved gases can be discharged through larger pores between sand grains. The coarser the sand grains the higher the gas permeability. The effect of resin content and acid hardener on the gas pressure of cores were smaller comparing cores with SH34 silica sand.

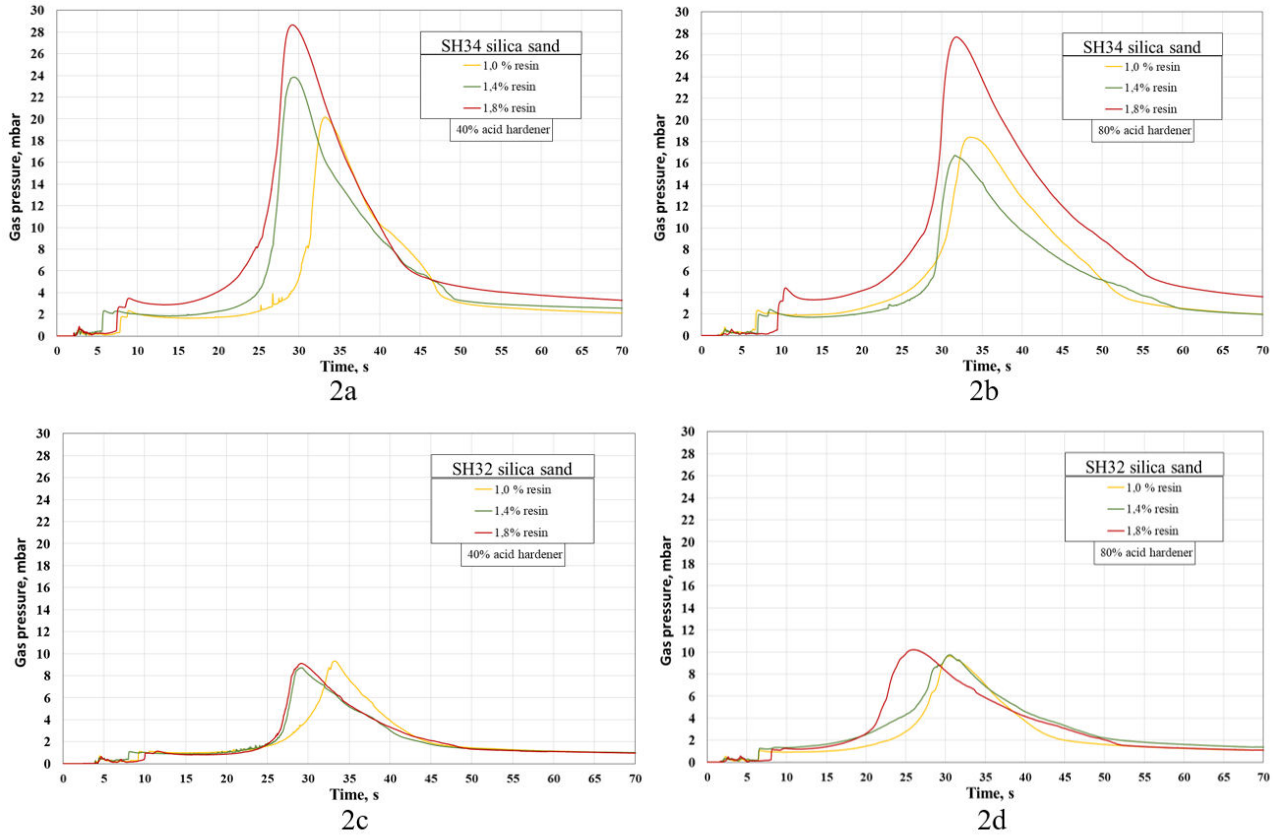

Figure 2 Variation of gas pressure in furan no-bake resin sand cores

From the results it can be established that the grain size is the main factor influencing the core gas pressure. The finer sand grains improve the surface quality of the cores, but also decrease the gas permeability. Because of that released gases can't be discharged through the pores thus increasing the probability of casting defects. During the experiment, every aluminium alloys made with cores based on SH34 silica sand have gas blowholes at the core/metal interface. The extent of the defect was determined by the amount of resin and acid hardener of the core.

THE PRESSURE CHARACTERISTICS OF THE RELEASED GASES FROM SAND CORES

MÁDI Laura, BUDAVÁRI Imre, VARGA László PhD
Faculty of Materials Science and Engineering, Foundry Institute, University of Miskolc
E-mail: ontlaura@uni-miskolc.hu, budavari1987@gmail.com, laszlo.varga.mak@gmail.com

Keywords: casting, sand cores, core gas, gas pressure, binders, resin content

The examination of the gas and its pressure generated from sand cores is a matter of priority. The intense gas release from the core can result in blowholes. If the gas pressure exceeded the metal head pressure, the gas would bubble through the molten aluminum. The composition of the produced gases is an important environmental issue, as the regulations are getting stricter. The intense gas release from the core can result in blowholes, while the metal can also penetrate the sand. The relation of the speed of the produced and released gas determined the gas pressure in the core.
The pressure of the gases released is influenced by various factors. Higher pressure area also for cores with long distance to core prints, and for cores that decompose to produce higher viscosity gases. The gas evolution rate and viscosity increase with immersion temperature. Sands with higher thermal conductivity would allow heat to penetrate more quickly into the core and develop a higher gas pressure. The pressure in the core decreases with an increase in the core print area and core permeability. The pressure increases linearly with distance and unless the metal is poured rapidly to produce higher head pressures or unless the permeability coefficients of the sand are increased, gas can be expected to bubble through the castings. Increasing core permeability significantly decreases the pressure in the core. There is an asymptotic decrease in internal gas pressure for the geometry being considered with an increase in permeability. [1]
The aim of this article is to investigate the impact of the quantity and quality of resin binder and the temperature of the core and the casting on the gas pressure of released gases from sand cores. The test bars were prepared with various resin qualities (no-bake phenol, HB-phenol, and HB-furan). The amount of resin used is usually 0.9-1.2%, based on sand weight. Catalyst levels generally are from 30 to 50 %, based on the weight of the binder. The binder content recommended by the manufacturer and cores containing 30% less and 30% more binder is also examined. The geometries of the test bars were as follows one core had a diameter of 28.85 mm and a length of 126.16 mm and another diameter of 26.2 mm and a length of 117 mm. The cores were prepared with constant compacting energy and approximately the same bulk density (1.3 g/cm^3).
The measurement is similar to the actual production conditions. Stainless steel tube (Ø6x300mm) were used as pressure probes; they were placed in the axial center of the core and so that their ends were 5 mm from the mold-metal interface, the closest distance at which the molten metal would not plug the tube. In the literature, the pressure of the gases was measured at a distance of 0.635 cm (0.25 in.) from the mold-metal interface. [2] The form was prepared using a bentonite mixture containing 8% bentonite and 4% water. The fire-resistant matrix of the form was silica sand. The drag box was Ø330x200 mm and the cope box was Ø330x140 mm. The casting was carried out simultaneously using a tangential access channel in a three-cavity form. Approximately 50 kg bentonite mixture was necessary for each form which was produced with a Multiserw Morek low-speed mixers. The mould cavities were made with a cone-shaped wood pattern (Ø70x150mm, draft: 4°). 720 °C foundry aluminium alloy was used for casting. The cores with the steel tubes and the thermocouples in the drag box were placed and poured around with liquid metal. The gating system was formed in the cope box. preparation steps of the waste mould can be observed in Figure 1. The produced gases passed through a silicone tube to a pressure transducer. Three Baumer-type pressure transducers were used for the experiments.

Figure 1 The experimental moulding box, a) lower part with the cone-shaped wood pattern, b) tangential access channel without cores and c) with core, d) drag and cope box with weight on

During core making and casting, the composition of the sand cores may not be uniform, so it is also necessary to test the cores with different resin contents. In the case of HB-furan resin cores, the effect of different amounts of resin on the pressure of the gases evolved from the cores is shown in Figure 2.

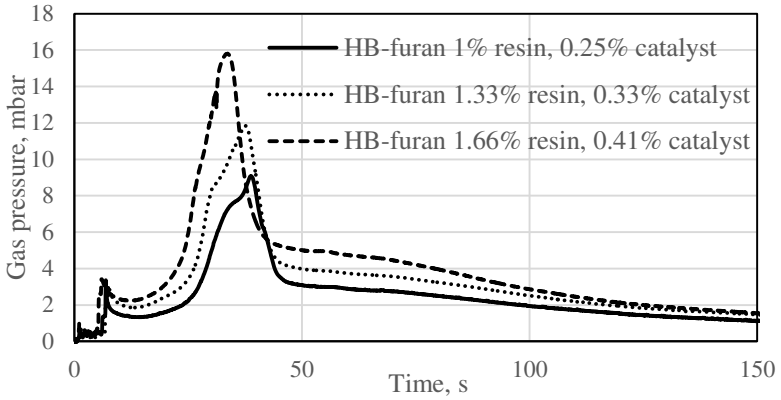

Figure 2 The effect of resin quantity on the pressure of the released gases

As the resin content increases, core gas pressure increases significantly and gas pressure peaks appear earlier in time. Temperature measurements are also required to investigate the causes of the above phenomena and to connect pressure values to thermophysical processes. The melt temperature was measured 10 mm from the parting line and 10 mm from the mold wall, the core temperature was measured 5 mm from the core surface and 8 mm from the core edges using a K-type chromium-aluminum thermocouple. The temperature measurement results are shown in Figure 3.

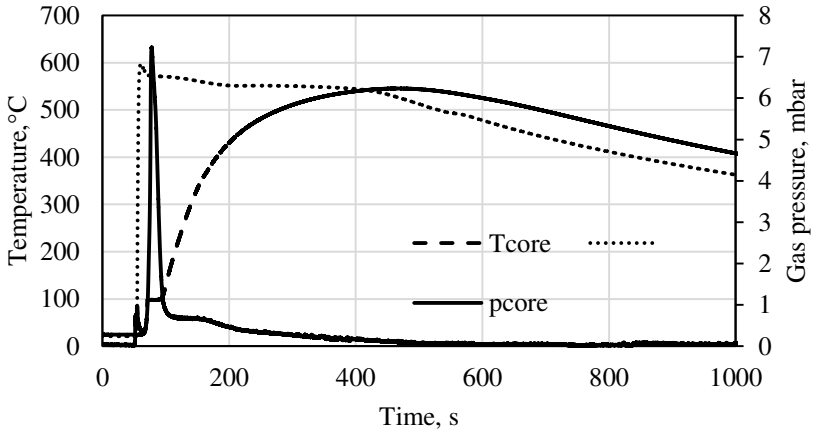

Figure 3 Relationship between melt cooling curve, core temperature, and core gas pressure

When metal initially contacts the mold, there is a huge increase in temperature, and the condensed water near the interface vaporizes, expanding in volume over 1000 times. [3] This rapid expansion displaces the air originally in the mold. The maximum gas pressure is observed at the time the core is heated to 100 ° C, which is explained by the release of vapor/gas (water vapor, ethanol, propanol, solvent) from polycondensation processes.

ACKNOWLEDGMENTS
The research was also supported BY the ÚNKP-17-3 New National Excellence Program of the Ministry of Human Capacities.

REFERENCES

[1] L. Winardi, H.E. Littleton, C.E. Bates, *Gas Pressure in Sand Cores*- AFS Trans., 07-062(04), 303-312, 2007.
[2] S.Ravi, J. Thiel, *Prediction of Core Gas Pressure from Chemically Bonded Sand Molds Using Process Simulation Software*-AFS Transactions, 17-097 v125, 2017.
[3] R. Pattabhi, A.M. Lane, T.S. Piwonka, *Cast Iron Penetration on Sand Molds, Part III: Measurement of Mold-Metal Interfacial Gas Composition*- AFS Trans. 96-208, 1259- 1264, 1975.

DESIGN OF CLAMPING DEVICES FOR DIFFERENT MILLING AND DRILLING OPERATIONS

MOHAMMAD Alkhateeb, BODZÁS Sándor PhD
Department of Mechanical Engineering, University of Debrecen
E-mail: mohammad5atib@gmail.com, bodzassandor@eng.unideb.hu

Keywords: milling operations, clamping device, fixture, workpiece, machine table, jaw, self-centering chuck

The clamping system is essential in the milling and drilling operation, since the CM (Clamping Device) (fixture) is responsible for holding the workpiece into the table of the milling machine. Clamping device should be installed with the machine table, to assure maximum accuracy and quality of the work done. Direct clamping with the table of the machine should be avoided.
The main considerations when designing a clamping device are: the fixture should be stronger than the frame of the machine, the ability to be fastened solidly to the table of the milling machine, capability of holding the workpiece against the forces developed during operating and the possibility to hold different shapes of workpieces.
The aim of this study is to design and manufacture clamping devices. These devices should be able to hold various shapes and dimensions of a workpiece, and should be portable, capable to joint with different types of milling and drilling machines, and easy to assemble and disassemble. In this project we have designed four different clamping devices in order to compare them regarding the advantages, disadvantages, and the different shapes of clamping possibilities.

First Clamping Device: Four Jaw clamping device.

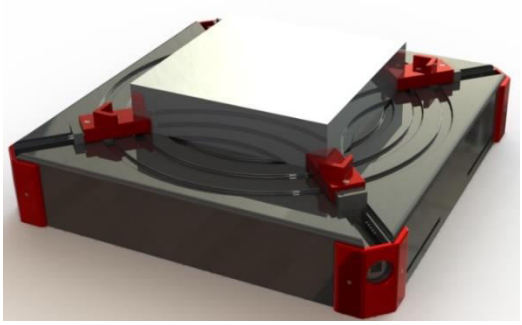

Figure 1 Four Jaw clamping device.

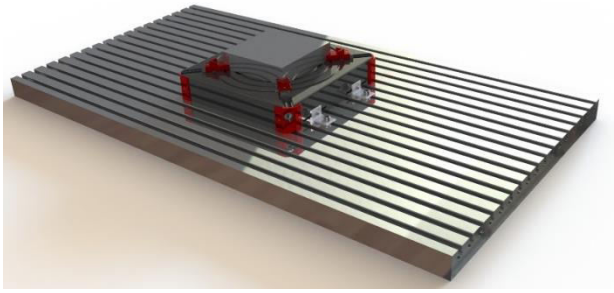

Figure 2 Clamping device installed to machine table.

Second Clamping Device: Fixed Base rotary arm clamping device.

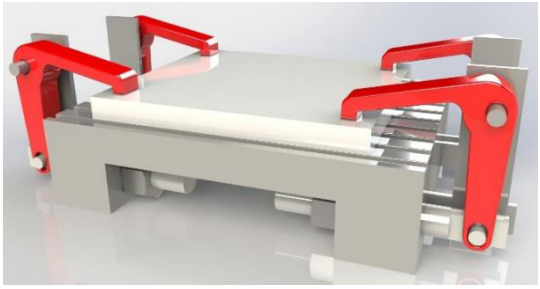

Figure 3 Fixed Base rotary arm clamping device with demonstration.

Usage / Advantages: Suitable for drilling operation and simple working principle.
Disadvantages: limitations regarding the (Height, Length, width and the working area) of the workpiece.

Third Clamping Device: Sliding Base rotary arm clamping device.

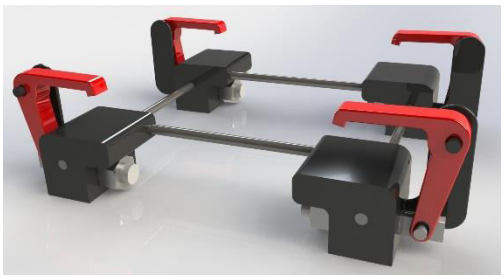

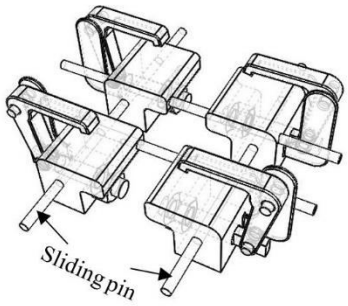

Figure 4 Sliding Base clamping device with demonstration.

Usage / Advantages: Suitable for drilling and milling operations.
Disadvantages: limitations regarding the Height of the workpiece.

Fourth Clamping Device: four jaw chuck self-centering clamping device.

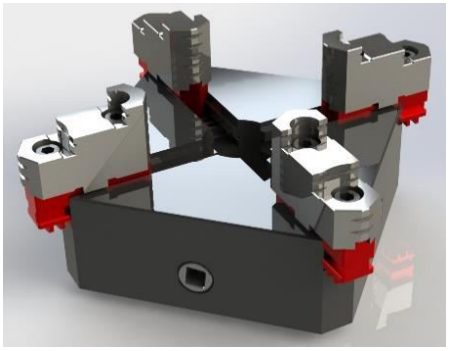

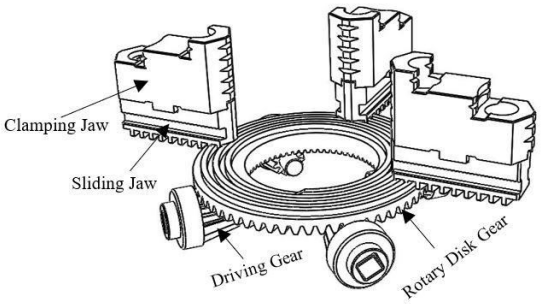

Figure 5 self-centering clamping device with demonstration.

Usage / Advantages: Suitable for drilling and milling operations, all the clamping jaws moves together due to gear connections and this device is applicable for various heights.
Disadvantages: this device is only capable to clamp cylindrical and equilateral shapes.

In this section, we will explain the clamping possibilities, components, advantages and disadvantages for the first clamping device (Four Jaw clamping device).

1	Device Frame	5	Slider Jaw	9	L-Joint
2	Edge Cover	6	Clamping Jaw	10	Sliding Nut
3	Driving Screw	7	Holding Screw	11	Sliding Screw
4	Holding Pin	8	Device Base		

Components:
Table 1 Components names for the clamping device.

Usage / Advantages: Suitable for drilling and milling operations, Portable and can be installed to various types of milling machines.

Disadvantages: each clamping jaw should be moved separately.

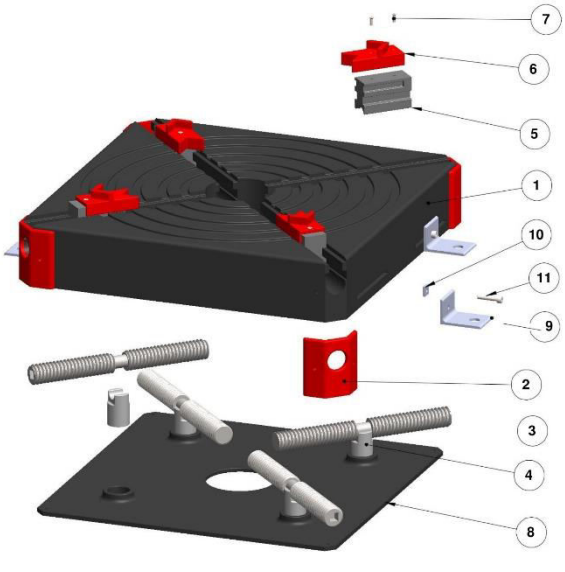

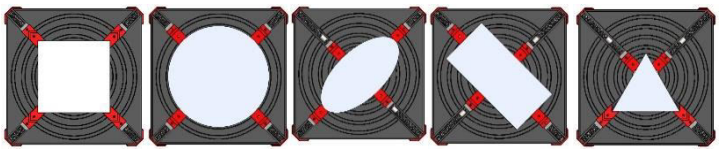

Clamping possibilities: this device is capable to clamp different shapes and heights such as:

Figure 7 Different Clamping possibilities.

Figure 6 Components for the clamping device.

THERMAL SPRAYED NICRBSI LAYER REMELTING WITH MIXED LASER PROCESS

[1]MOLNÁR András PhD, [2]BALOGH András PhD, [3]BARKÓCZI Péter PhD, [4]FAZEKAS Lajos PhD, [5]BATTÁNÉ GINDERT- KELE Ágnes PhD
[1,2]Faculty of Mechanical Engineering and Informatics, University of Miskolc
E-mail: metspray@uni-miskolc.hu, metweld@uni-miskolc.hu
[3]Institute of Metallurgy Plastizzation and Nanotechnology, University of Miskolc
E-mail: fembarki@uni-miskolc.hu
[4,5]Department of Mechanical Engineering, Faculty of Engineering, University of Debrecen
E-mail: fazekas@eng.unideb.hu , battane@eng.unideb.hu

Keywords: NiCrBSi coatings, HVOF spraying, Flame spraying, Coating, Heat treatment, Ck45, Microstructure, Microhardness

INTRODUCTION

Ni-based coatings are mainly used to form surface layers exposed to corrosion and abrasion at elevated temperatures [1]. The B and Si contents of the Ni-based alloys facilitate the scattering and melting process. The presence of Si and B increases the thinness of the Ni-based alloy and the melting and crystallization heat intervals. The presence of B (about 3.6% by weight) promotes the formation of a hard phase [2]. Increasing the Si content to improve the fluidity of the dispersed layer did not yield any results. Cr plays an important role in the application of NiCrBSi alloys by increasing the hardness and mechanical properties of the deposited and melted coat and also increases its wear resistance [3].
Various NiCrBSi alloys have been developed to produce coatings to improve mechanical properties and to determine the coating's abrasion behavior with sufficient precision [4]. Due to the discontinuities in the coating (porosity, unmelted particles, oxide inclusions), the spray coating is not perfect. [5]. Laser beam melting applied to form a flawless, compact layer helps to completely eliminate porosity and thus completely coat the coating [6]. Due to the fine structure of the layer, the mechanical properties of the coating will be improved and the abrasion resistance will be significantly improved. Laser beam curing, coupled with concentrated heat input, can cause cracks in the solidifying metallic coating, which can be avoided by preheating and controlled cooling of the specimen or workpiece.

RE-MELTING OF THE THERMAL SPRAY APPLIED LAYER WITH LMD HEAT SOURCE

For the first experiments in mixed laser re-melting technology, we have selected a basicbody that allows operation in a wide melting band. The flat specimen is more suitable for the melting conditions.
Considering that there was no practical experience with the chosen method for re-melting the coated NiCrBSi layer, the design of the re-melt and setting of the technological characteristics given in. The upper temperature of the melting gap of the given NiCrBSi alloy. The re-thawing of the NiCrBSi layer applied by thermal spraying was performed using a laser head mounted on a Fanuc robot (as shown in Figure 1), which was connected to the laser diode unit apparatus by an optical cable.
SEM - EDXMA analysis was performed with a ZEISS MA 10 SEM electron microscope in the Laboratory of Complex Image Analysis and Structure Analysis (LISA) of the Institute of Metallurgy, Image Processing and Nanotechnology, University of Miskolc.

Figure 1 Re-melting of the sprayed layer with a mixed diode laser heat source mounted on a Fanuc robot

The average thickness of the re-melted layer was measured during SEM and was 436 µm. In the transitional zone, approx. A 10 µm thick iron enriched zone is present. The Cr and Si fluctuations in the line analysis suggest a uniform distribution of the hard phases. The clear portion is a dendritic Ni solid solution; the darker, evenly distributed, high Cr-containing eutectic hard phase.
In the EDS analysis, the high Cr content of the layers is striking, indicating the presence of hard phases - chromium carbides and borides (mainly Cr7C3 and CrB Thermal input plays an important role in the re-melting of the layer, which can be achieved by properly adjusting and fine-tuning the LMD heat source parameters.
If the heat input is too low, the layer will not or partially melt and will not properly bond with the parent metal. Excessive heat input results in dilution of the layer with the parent metal - limiting the usefulness of the component (e.g., not achieving the desired abrasion resistance.

CONCLUSIONS

In this work, a NiCrBSi coating thermally dispersed and remelted by laser beam (using LMD heat source) was introduced in this work.
• In the re-melted coating, a fine, evenly distributed hard phase is observed.
• The coating tested is characterized by a dendritic matrix Ni solid solution.
• Studies show that re-melting using the LMD heat source promotes dendritic microstructure and significantly reduces the porosity of the coating.
• Re-melting the coating using an LMD heat source allows for a more compact, finer texture and crack-free coating.
• In addition to the many benefits of re-melting a layer using an LMD heat source, keeping heat input to a minimum - and slowly cooling the workpiece - is very important.
• In the re-melted coating, various hard phases are observed which are in the Ni matrix (Cr, Fe)$_7$C$_3$, CrB, and Ni$_3$B (Cr, Fe)$_7$C$_3$, CrB, and Ni$_3$B.

REFERENCES

[1] Gómez-del Río, T., Garrido, M. A., Fernández, J. E., Cadenas, M., Rodríguez, J., *Influence of the deposition techniques on the mechanical properties and microstructure of NiCrBSi coatings*. Journal of materials processing technology 204 304–312, 2008.
[2] Cordia, M., Delogu, P., Nenci, F., *Microstructural aspects of wear-resistant stellite and colmonoy coatings by laser processing.* Wear 119 (2), 137–152., 1987.
[3] Zhang, D.W., Lei, T.C., Zhang, J.G., Ouyang, J.H., *The effects of heat treatment on microstructure and erosion properties of laser surface-clad Ni-base alloy.* Surf. Coat. Technol 115, 176–183. 1999.
[4] Li, Q., Zhang, D., Lei, T., Chen, C., Chen, W., *Comparison of laser-clad and furnace-melted Ni-based alloy microstructures.* Surf. Coat. Technol. 137, 122–135., 2001.
[5] Kim, H.J., Hwang, S.Y., Lee, C.H., Juvanon, P., *Assessment of wear performance of flame sprayed and fused Ni-based coatings.* Surf. Coat. Technol. 172, 262–269, 2003.

ADVANCED LASER BEAM PROCESSES IN SURFACE TREATMENT

[1]MOLNÁR András PhD, [2]DRASKÓCZI László, [3]CSABAI Zsolt PhD, [4]BUZA Gábor PhD, [5]PÁLINKÁS Sándor PhD
[1]*Faculty of Mechanical Engineering and Informatics, University of Miskolc*
E-mail: metspray@uni-miskolc.hu
[2]*Bubenlaser Ltd.*
E-mail: draskoczi@t-online.hu
[3]*Dr.Csabai Pharma Ltd.*
E-mail: mailto:dr.csabaizs@gmail.com
[4]*ATI Bay Zoltan Institut*
E-mail: gabor.buza@bayzoltan.hu
[5]*Department of Mechanical Engineering, Faculty of Engineering, University of Debrecen*
E-mail: palinkassandor@eng.unideb.hu

Keywords: laser beam, LMD process, heat souce, diode laser, mixed laser

The heat source of the mixed laser beam process is a beam obtained by collecting the light energy of a coherent light emitting diode bundle in a range of wavelengths of different wavelengths, passing through various filters and prisms through an optical cable to the medium to be heated. There are eight pieces of laser beams of four different wavelengths (940, 980, 1030 and 1060 nm). Mixed laser heat source created by superimposing the energy of the laser diode unit can be used for heat treatment, welding, re-melting and surface alloying and not for the rebuilding of 3D parts - of course, with various additional accessories. In this paper, the authors would like to report on our experience with this heat source.

THEORETICAL STRUCTURE OF THE LMD HEAT SOURCE

The LMD process means the initials of the English term, which in Hungarian translates as a mixed diode laser designation, which indicates that the laser beam heat source itself utilizes the energy of several laser diode units of different wavelengths. The abbreviation LMD was first used by the Fraunhoffer Institute in Dresden and by Laserline, referring to the equipment they developed [1-3].

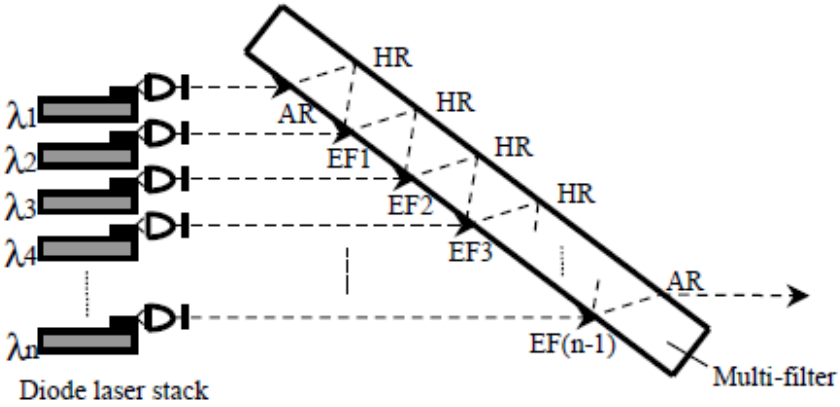

Figure 1 Generation of Mixed Laser Beam by Switching N Number of Diode Stacks of Different Wavelengths

By concentrating the LMD heat source on the heating of the thermally sprayable powder, it is possible to create a more compact and reliable layer (Figure 1) [4].

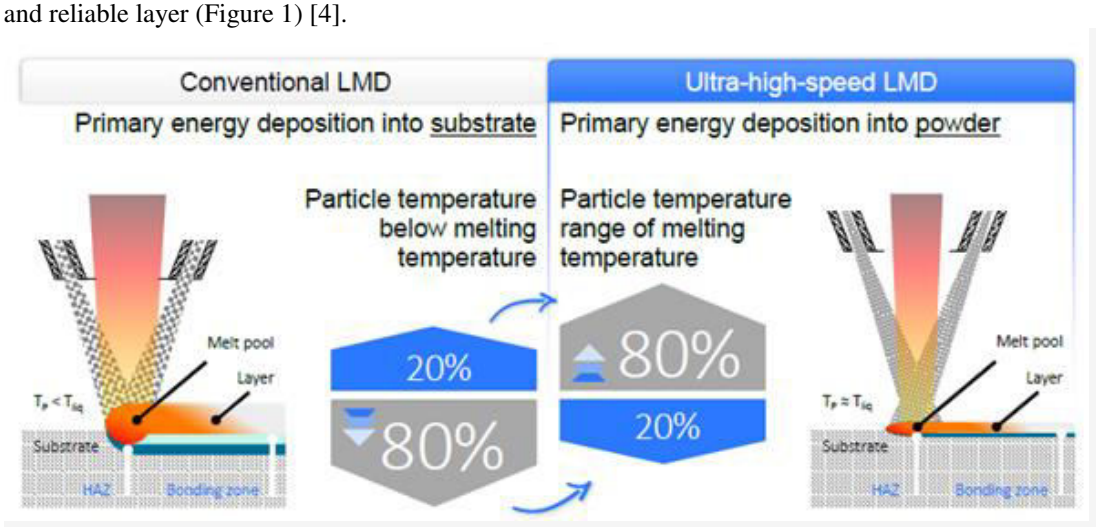

Figure 2 Comparison of different LMD laser beam methods (Convencional vs. Ultra High-speed LMD

The difference between the two procedures is described in Figure 2. The material needed to coat the hydraulic piston with a conventional laser beam process is 0.843 kg NiCrBSi powder and can be made in 1.75 h at a cost of 270 Euro. The ultra-high speed process consumes just 0.373 kg and 0.3 h at a much lower cost of 70 Euro. Figure 9 illustrates the difference between the two processes (particularly important in economic terms) [5].

SUMMARY, RESULTS

The use of laser beam technologies to create surface layers is a new, state-of-the-art technology that will gain more and more space in the future. - When using laser beam heat sources, the heat input is well controlled, the workpiece is hardly deformed and the heat treatment state of the workpiece does not change. On the other hand, a laser beam of CO_2 or Nd: YAG, a very small diameter, high-jet jet, allows excessive heat input. When using these heat sources, very narrow melting bands (3 to 5 mm) and dilution with higher raw material (above 10%) were observed. The use of blended laser beam heat sources opens up new perspectives in the field of coating as the heat input is highly controllable and, as a result, the dilution of the layer with the substrate is better controlled.

REFERENCES

[1] Lim, J. J., Sujecki, S., Senior, L. L., Zhang, Z., Paboeuf, D., Pauliat, G., Lucas-Leclin, G., Georges, P., Roderick, MacKenzie, C. I., Hasler K. H., Sumpf, B., Wenzel, H., Gotz, E., Thestrup, B., Petersen, P. M., Michel, N., Krakowski, M., and Larkins, E. C., *Design and Simulation of Next-Generation High-Power, High-Brightness Laser Diodes*, Journal of Selected Topics in Quantum electronics, Vol. 15, No. 3, p. 993. May/June, 2009.

[2] Strohmaier, S. G., Erbert, G., Rataj, T., Meissner-Schenk, A. H., Loyo-Maldonado, V., Carstens, C., Zimer, H., Schmidt, B., Kaul, T., Karow, M. M., Wilkens, M., Crump, P.: *Forward development of kW-class power diode laser bars,* High-Power Diode Laser Technology XVI, 1051409, 7 May 2018.

[3] Buza, G., *Lézersugaras technológiák I.* EDUTUS Főiskola, 2012.

[4] Bitay, E., *Lézeres felületkezelés és modellezés,* Erdélyi Múzeum Egyesület, Kolozsvár, 2007.

[5] Hecht, J., *Short history of laser development* Optical Engineering pp.49-99, 091002,September, 2010.

A STUDY OF EVOLUTION OF FRICTION TEMPERATURE FOR SEVERAL COMPOSITE MATERIALS BY A PIN-ON-PLATE SYSTEM

MUHANDES Hasan, KALÁCSKA Gábor DSc
Institute of Mechanical Engineering Technology, Szent István University
E-mail: hasanmuhandes@gmail.com , kalacska.gabor@gek.szie.hu

Keywords: pin-on-plate, abrasive wear, composite materials

To improve the performance of the Agricultural machinery, several composite materials were suggested as replacements of critical fast-wearing steel parts. These materials were examined by a pin-on-plate system with sliding abrasive cloths.
Five types of composite materials were suggested to replace these steel parts. We chose (ESD PA6 G, HD1000, PA6E, PA6G and PA66GF30) as test materials.
The test was done by Pin-on-plate system test device, which can be found in our institute's workshop in Szent István University, Gödöllő, with the temperature of the room as 23℃, and this system is apparent in the following figure.

Figure 1 Pin-on-plate wear device

Simple apparatus assembled and sensors were fixed on the device and connected to a computer data collecting interface. The interface was converting the sensor signals into digital values and provided the data to a computer that was recording the values.
During the entire tests, the computer registered the wear, friction forces, and the temperature of the specimens from a close point of the contact area between the samples and the abrasive wear.
This device can give us a nonstop wear interface and furthermore a possibility to control several parameters:

1. Opportunity to control the speed of the interface wear.
2. Possibility to use several wear interfaces
3. Opportunity to add a load over the specimens.
4. Opportunity to observe the evolution of the temperature in the contact area.
    - Two types of wear interfaces were used (P60 and P150).
    - Two speeds are used which are (20%=0.032 m/s and 40%=0.056 m/s)
    - And we used Three loads (9.81 N, 29.43 N and 49.05 N)

As a result of these variables that we can control, we have 12 tests. In figures 2 and 3, we show the extreme cases that we have. During test 1, the load was 9.81 N, and the speed was 0.032 m/s. While in test 6, the load was 49.05 N and the speed was 0.056 m/s.

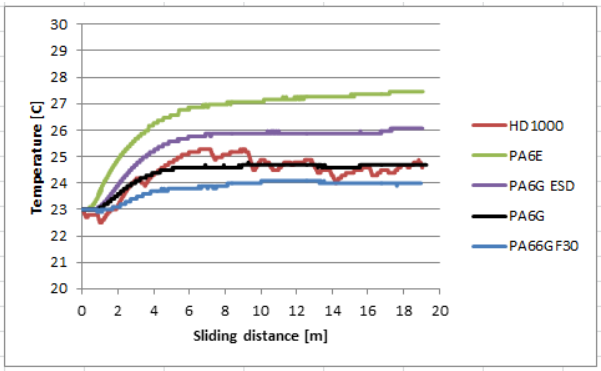

Figure 2 The temperature of test 1

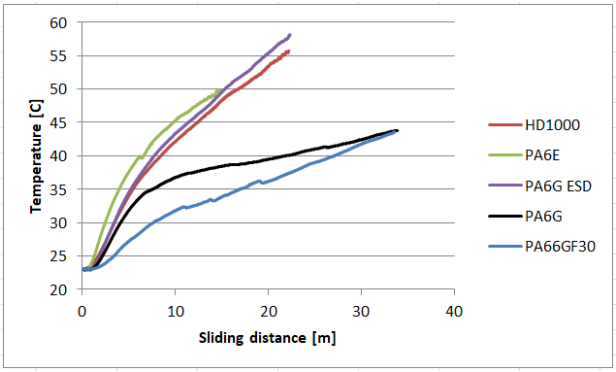

Figure 3 The temperature of test 6

These results were compared to the thermal properties of the tested materials which are shown in Table 1.

Table 1 Thermal properties of the tested materials

	PA6E	PA6G ESD	PA6G	HD1000	PA66GF30
Thermal conductivity [*W/(K.m)*]	0.37	0.29	0.38	0.41	0.39
Melting temperature [ºC]	220	216	216	135	260
Glass transition temperature [*ºC*]	45		40		48
Specific heat [*J/(g.K)*]	1.7		1.7	1,9	1.2
Max. allowable service temperature in air, short term [*ºC*]	160	170	170	130	170
Max. allowable service temperature in air, long term [*ºC*]	100	110	100	80	110
Min. allowable service temperature in air, long term [*ºC*]	- 40	- 40	- 40	- 250	- 20
Heat deflection temperature [*ºC*]	75	100	95	80	150

As we can see in the diagrams that PA6E had the highest temperature and that what can be explained by the value in the table, where PA6E has:

- The lowest heat deflection temperature
- High specific heat

While PA66GF30 had the lowest temperature that what can be explained by the value in the table, where PA66GF30 has:

- The highest heat deflection temperature
- Low specific heat

LIGHTWEIGHT MANUFACTURING OF AUTOMOTIVE PARTS

[1]WADAS Tatiane, [2]TISZA Miklós PhD
Department of Materials Science and Engineering, University of Miskolc

Keywords: manufacturing, automotive, steel

All over the world there is a competition among car manufacturers to reduce the weight of cars. Sheet metal forming is one of the most important key technologies in automotive industry concerning material and energy consumption, as well as the overall cost efficiency. To keep this role in manufacturing industry a continuous development is necessary concerning materials, the development of new innovative forming process and the tooling and manufacturing equipment. The increasing requirements stated by the automotive industry is the main driving forces behind sheet metal forming innovations.

Recently, the big challenge is to balance mass, costs and CO2 emissions, depending on the vehicle segment under consideration. The competition in car manufacturing is extremely strong leading to larger model variety and shorter model cycles. The increased competition also leads to a very intense development activity to increase productivity. Some of these requirements are arising from the customers' side and from legal requirements, e.g. increased safety and increased environment protection.

The new design concepts are required, which require new materials, new innovative forming process and new tooling concepts. The increased competition also requires shortening the lead times from the concept to final realization and to reduce the lead times the application of various methods of computer Aided Engineering CAD, CAM, CAE and FEM techniques are inevitable.

Some decades ago, design engineers focused more on structural and dimensional stability, but in recent years the focus is on the reduction of fuel consumption with increasing comfort requirements what lead to development of new materials. Enhanced stiffness together with weight reduction resulted in the development and wide application of various grades of high strength steels. Nowadays, several micro-alloyed and phosphorous-alloyed steels with and without bake hardening are frequently used. An increasing use of interstitial-free (IF) steels, dual-phase and TRIP-steels, as well as the ultra-low and super ultra-low carbon steels can also be observed in Figure 1 concerning the last 30 years.

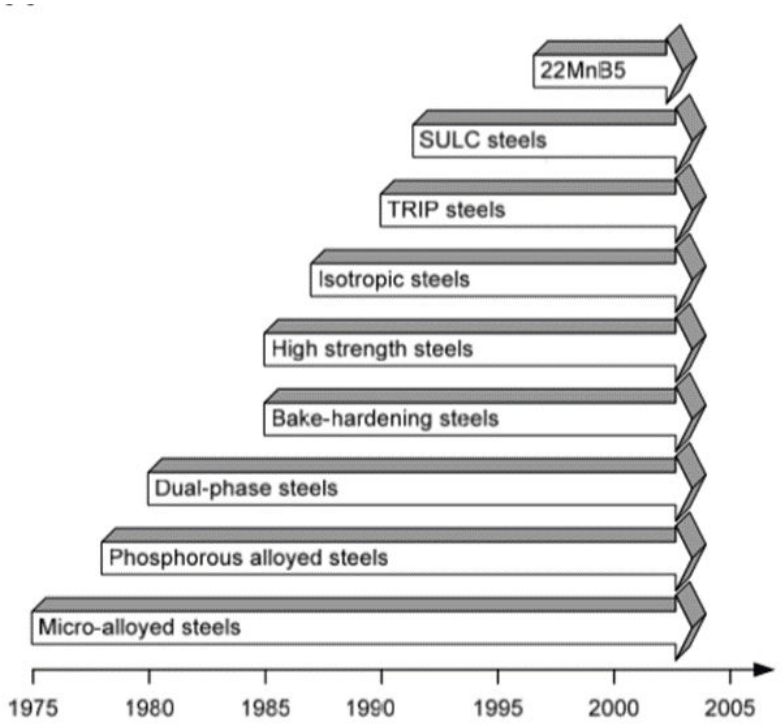

Figure 1 Time horizon of steel development in the automotive industry in the last 30 years

It can be observed that from the elaboration of various micro-alloyed steels in the mid-seventieth of the last century, there is a continuous pressure on material development leading to the appearance of new advanced steel materials practically in each five years.

In this paper, we will analyse these car-making concepts both from the side of new, innovative materials and from the side of manufacturing processes.

TURNING SIMULATION WITH FINITE ELEMENT METHOD

[1]NEMES Csaba, [2]LUBOMIR Javorek PhD, [3]BODZÁS Sándor PhD, [4]PÁLINKÁS Sándor PhD
[1,3,4]Department of Mechanical Engineering, Faculty of Engineering, University of Debrecen
E-mail: csabanemes94@gmail.com, bodzassandor@eng.unideb.hu, palinkassandor@eng.unideb.hu
[2]Department of Manufacturing Technology and Quality Management, Technical University in Zvolen
E-mail: lubomir.javorek@tuzvo.sk

Keywords: cutting force, turning, machining, measurement, depth of cut

We carried out the measurement of the three components of the cutting force as a function of the modification of the depth of cut during the longitudinal turning process. The results show that if we increase the depth of cut, all three components of the cutting force shows increasing tendency, regardless of how much the cutting speed and feed speed were performed during the measurements.

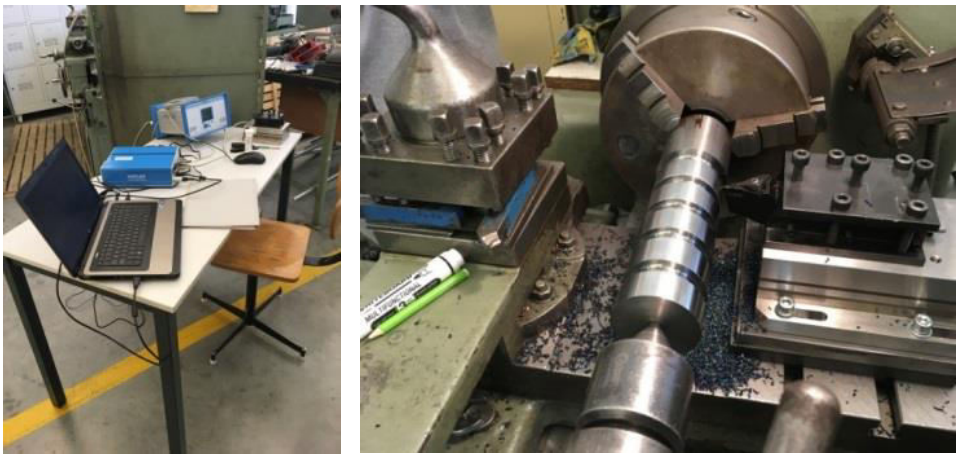

Figure 1 The lathe (E-400) and the instruments

We used the following measuring instruments:

- Kistler Type 9257B
- Kistler Data Acquisition System Type 5697A 22003583
- Kistler Multichannel Charge Amplifier Type 5070

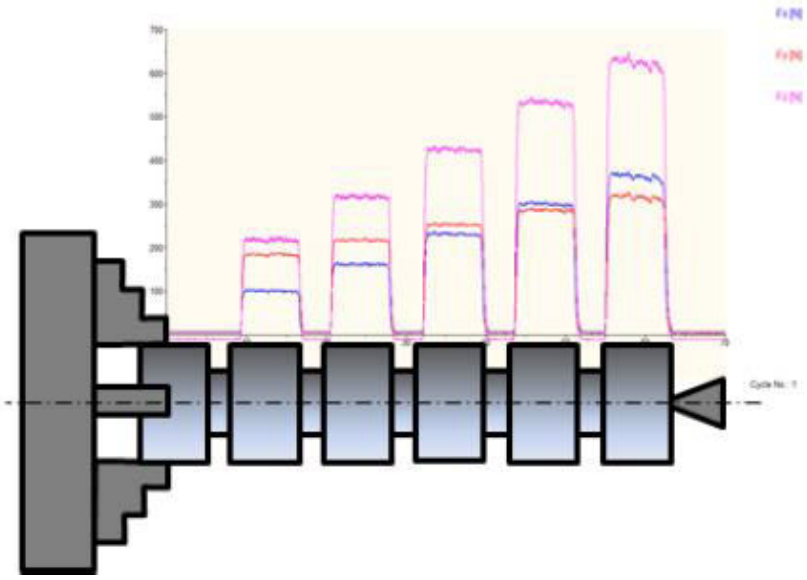

Figure 2 Schematic illustration

Then we use the Ansys software, and made five simulations.
The formula for calculating:

$$F_c = C_1 \cdot f^x \cdot e^y \cdot \sigma^n \cdot R^p \cdot \kappa^s \cdot {v_c}^b \cdot K_\gamma \cdot K_k \cdot K_h \cdot K_a \cdot K_\lambda$$

F_c: main cutting force
C_1: chipping factor
f: depth of cut
x: exponent of depth of cut
e: feed
y: exponent of feed
σ: tensile strength
n: exponent of tensile strength
R: corner radius
p: exponent of corner radius
κ: major tool cutting edge angle
s: exponent of major tool cutting edge angle
v_c: cutting speed
b: exponent of cutting speed
K_γ: tool rake dependent factor
K_k: tool wear dependent factor
K_h: tool cooling dependent factor
K_a: tool clearance dependent factor
K_λ: tool inclination angle dependent factor

The formula for simulation (**Johnson-Cook**):

$$\sigma = \left(A + B \cdot \varepsilon_p^n\right)\left[1 + C \cdot \ln\left(\frac{\dot{\varepsilon}}{\dot{\varepsilon}_0}\right)\right]\left[1 - \left(\frac{T - T_r}{T_m - T_r}\right)^m\right]$$

The results (Measured cutting force, calculated cutting force (with hand, traditional formulas), and FEM simulation):

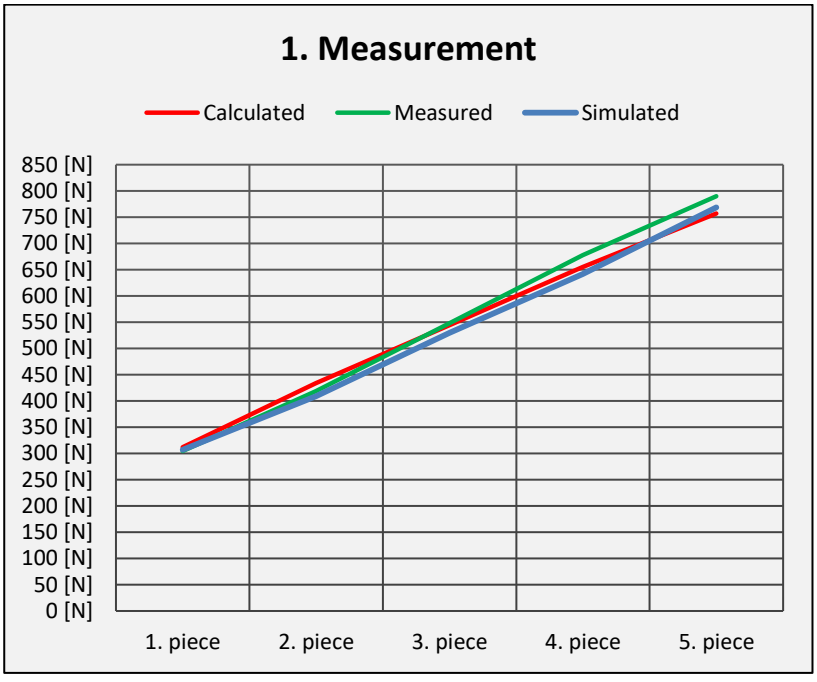

Figure 3 Results

1. piece: $a_p = 0{,}5\ mm$
2. piece: $a_p = 0{,}75\ mm$
3. piece: $a_p = 1\ mm$
4. piece: $a_p = 1{,}25\ mm$
5. piece: $a_p = 1{,}5\ mm$

ACKNOWLEDGMENTS
The project was implemented by the Ministry of Human Resources through the New National Excellence Program of the Higher Education Master's Degree Researcher's Scholarship. Project number: ÚNKP-18-2-I-DE-100.

EMBERI ERŐFORRÁSOK MINISZTÉRIUMA

ANALYSIS OF CONCEPTUAL SOLUTIONS OF UNIVERSAL HELICAL GEAR REDUCERS

RACKOV Milan PhD, KUZMANOVIĆ Siniša PhD, KNEŽEVIĆ Ivan, ČAVIĆ Maja PhD, PENČIĆ Marko
Faculty of Technical Sciences, University of Novi Sad
E-mail: racmil@uns.ac.rs, kuzman@uns.ac.rs, ivanknezevic@uns.ac.rs, scomaja@uns.ac.rs, mpencic@uns.ac.rs

Keywords: universal gear reducer, helical gears

Gear reducers are mechanisms designed to reduce the number of revolutions using gear elements and nowadays they present one of the most commonly used types of mechanical transmissions in mechanical engineering. Due to the different shapes of gear elements, there are different types of gear transmissions: helical, bevel, worm, special and combined transmissions. This paper analyses only helical gear transmissions, since there is a great extent of whole this matter. Helical transmissions are analysed only with external helical gearing, since internal gear pairs represent a special and very large group of gears. Within the external helical gear transmissions, only torque transmissions are analysed, while the transmissions of motion are not analysed and they represent another large group of transmissions. Only universal gear reducers with axial, or almost-axial, parallel shafts are considered (two-stage and three-stage transmissions). Although, single-stage gear reducer produced with parallel shafts are not considered by the paper in order to reduce the area of researching. Gear reducers are most commonly delivered to customer with electric motor, known as motor gear reducer, and they are studied here extensively. Gear reducer can be also delivered without motor, only with input shaft. The basic aim of this paper is to present all characteristics and specificities of motor gear reducer in one place.
Nowadays, universal motor gear reducers with helical gears have an extremely large application in mechanical engineering. It is only because of their simple construction, high adaptability, high reliability, high power rationality and relatively low production and maintenance costs. Universal gear reducers can be also delivered without electric motor. However, it is a rarely required and only in the case when the customers want to install standard IEC electric motor (Fig.1) or when they want to base the motor separately (if the space is limited and/or the motors are large and heavy).

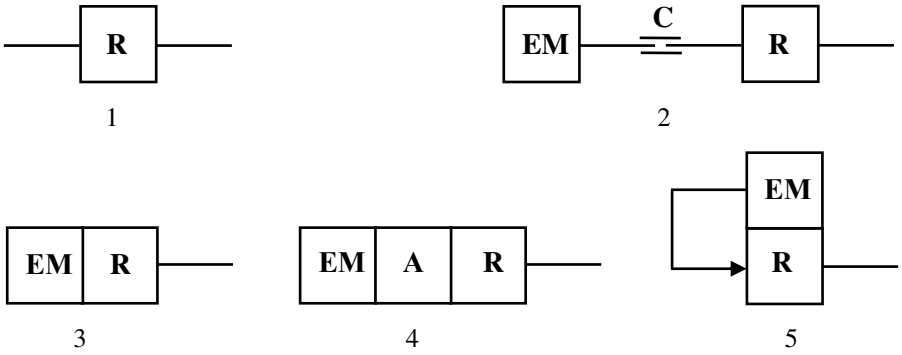

Figure 1 Schematic review of characteristic construction ways of universal gear reducer: 1 – input shaft reducer (R), 2 - input shaft reducer connected by coupling (C) with standard IEC electric motor (EM), 3 – motor gear reducer, 4 - motor gear reducer with adapter (A) which connect IEC motor and reducer and 5 - motor gear reducer where IEC motor is connected by belt transmission with the reducer [1]

Universal gear reducers are produced as single-stage, two-stage, three-stage and multistage units. Based on the conducted research of realised solutions of almost all leading producers of universal motor gear reducers with helical gears, it can be concluded that their production program contains universal units of very different conceptual solutions.
Most of manufacturers of gear reducers produce single-stage units, although there are some manufacturers which do not produce them since they cover these small gear ratio by belt transmission and there is no need for producing single-stage units (for example companies ROSSI [2], BEGE [3] etc.). If small gear ratio is required, these manufacturers use two-stage reducers and with their lowest gear ratio cover the gear ratio area of single-stage units. With this approach, they simplify and make cheaper their production. However, they certainly lose a part of the market, despite the selling of low-speed two-stage gear reducers at a slightly lower price in order to be competition with manufacturers of single-stage reducers.
Great number of smaller manufacturers produces two-stage gear reducers in special case for two-stage gear unit, while three-stage reducers are built by connecting two-stage and single-stage gear units. Therefore, their three-stage gear units are slightly more expensive then gear reducers built in the universal case for two-stage and three-stage gear reducer. By this approach, they achieve emphasis on two-stage gear reducers and achieve slightly lower production costs then manufacturers who produce two-stage gear units in universal housings for two-stage and three-stage gear reducers. At

the same time, manufacturers with high gear ratios of two-stage gear reducer try to capture as much of the customers who are interested for three-stage gear units.
Most manufacturers of three-stage gear reducers produce three-stage gear units in universal housing for two-stage and three-stage units. In that case, the emphasis is on three-stage units, which gives them a major advantage in the area of three-stage gear units over the manufacturers who build their three-stage gear units by connecting two-stage and single stage gear reducer. Any weakness of their two-stage gear reducers is compensate by this operation.

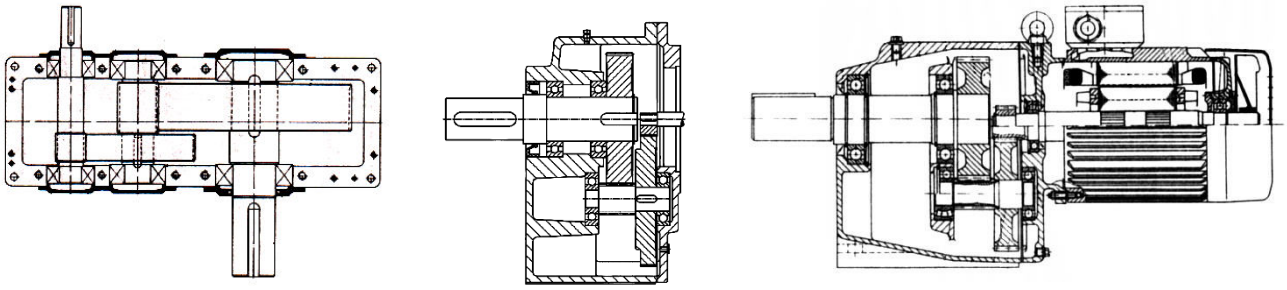

1 2 3

Figure 2 Characteristic solutions of a two-stage universal gear reducers: Nord (1), Lenze (2) and Winsmith (3)

Based on the given analysis, it is evident that modern solutions of gear units are made in different variants in order to ensure providing as simple and low cost as possible manufacturing and assembling. Gear reducers with special housing for two-stages gear units and gear reducers with universal housing for two-stage and three-stage gear unit are almost equally exploited. Today, one-piece housings are required almost in all cases in order that manufacturing become easy, no matter the assembly will be more complex. One-piece housing makes possible ideal axial consistecy of bearings and so far the providing of regular and proper gearing. This is very important for long-lasting and reliable operation of gear reducers. Additionaly, one-piece housings provide greater rigidity of the unit, which also has beneficial effect for the gear reducer lifetime. One-piece housings are also better hermetically closed, which is also important for gear units. Of course, radial mounting allows the mounting of large gears, with a slightly more complex assembling, i.e. certain subassemblies are not possible to assemble outside of the reducer and to be then mounted into the housing.

ACKNOWLEDGMENTS
This paper is part of a research on project "Research and Development of a New Generation of Wind Generators of High Energy Efficiency" TR 35005, supported by the Ministry of Education and Science, Republic of Serbia.

REFERENCES

[1] M. Rackov, S. Kuzmanović, M. Blagojević, Z. Đorđević, *Motor gear Units with Helical Gears*. (monograph publication, in Serbian), University of Novi Sad, Faculty of Technical Sciences. 2019.
[2] S. Kuzmanović, M. Vereš, M. Rackov, *Product Design as the Key Factor for Development in Mechanical Engineering*, Mechanical Engineering in XXI Century, University of Niš, Faculty of Mechanical Engineering, Niš, Serbia, 25-26 November 2010, str. 113-116, ISBN 978-86-6055-008-0. 2010.
[3] M. Rackov, I. Knežević, S. Kuzmanović, M. Čavić, M. Penčić, *Analysis of Housing Models of Modern Single-Stage Universal Gear Reducers*, IOP Conference Series: Materials Science and Engineering, Vol. 393, pp. 012048-1– 012048-9, 2018., Publisher: IOP Publishing, Bristol, United Kingdom, ISSN: 1757-8981., 2018.
[4] S. Kuzmanović, M. Rackov, *Directions of Development of Universal Speed Reducers*, International Conference General Machine Design 2009, Rousse, Bulgaria, 15-16. October 2009, ISSN 1313-9193; University of Ruse „Angel Kanchev“ / Transport Faculty of University of Ruse / Union of Scientists – Branch Rousse; pp. 31-34., 2009.
[5] https://www.rossi.com/en/products-category/gear-reducers-and-gearmotors
[6] https://www.bege.nl/downloads/catalogues/BEGE%20G-DSG%202017-10%20NL%20DE%20GB%20FR.pdf
[7] https://www.nord.com/cms/media/documents/bw/G1000_IE3_50Hz_EN_2317.pdf
[8] https://www.rehfuss.com/de/
[9] https://www.lenze.com/de-de/produkte/vorgaengerprodukte/getriebe/stirnradgetriebe-gst/
[10] https://www.bege.nl/de/hochwertige-produkte/?filter=&brand=Str%C3%B6ter,
[11] https://www.motive.it/p-13-coassiali-robus-a.html

STRUCTURAL INVESTIGATION OF GRANULAR COMPOSITES BY MODERN METHODS

RÁTHY Istvánné PhD, PINKE Péter PhD, FÁBIÁN Enikő Réka PhD, NAGYNÉ Halász Erzsébet
Donát Bánki Faculty of Mechanical and Safety Engineering, Óbuda University
Email:rathy.istvanne@bgk.uni-obuda.hu

Keywords: granular composites, structural investigations, SEM, CT X-ray

Structural investigations of granular composites were carried out using modern test methods. Composite sheets of different compositions and with different injection molding speeds were prepared and used. Polypropylene (PP) matrix was mixed with glass beads of three different size ranges (0-75 μm, 75-125 μm, 125-250 μm) and in three weight percentages (10 , 25, 40 wt %). During our investigations, scanning electron microscopy (SEM) and industrial computer tomography (CT) were used as modern diagnostic tools.

A scanning electron microscope is an electron-optic device that scans a defined area of the subject′s surface with a directional thin electron beam. Signals from the interaction between an electron beam and an object are sensed by suitable detectors and after proper processing and synchronization with the movement of the electron beam, they are visualized [1]. In our case, the amount and size of glass beads were examined at predetermined locations of the obtained sample plates (80x80x2 mm).

The computer tomographic device generates a 2D X-ray image sequence of the object under examination, in which the sample rotates in series with a defined small angle value [2]. This is repeated until the specimen is completely rotated, and an X-ray image is produced at each angle. Based on 2D images 3D reconstructions can be made with appropriate software [3].

Figure 1 shows SEM images from the fracture surface of a granular composite (at 40 wt% glass beads content). The images can be used to determine the size and volume fraction of glass beads. The images show that the surface adhesion is good between the matrix and the glass beads, the PP matrix adheres to the glass beads and the fracture occurred in the matrix. The SEM images also show that the distribution of glass beads is not considered to be uniform. When analyzing a large number of SEM images, it is only possible to draw conclusions about the glass bead content and size distribution of the glass beads in a given composite.

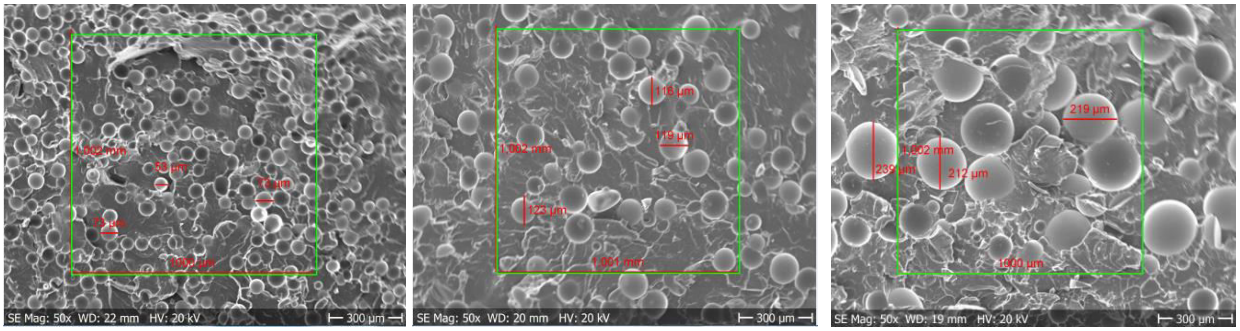

a) 4007520-08-01b sample b) 4012520-12-01a sample c) 4025020-08-03b sample

Figure 1 SEM images of PP composites containing different bead sizes (40 wt% glass bead content)

Figure 2 shows 2D CT images of complete composite sheets (at 10 wt%, 25 wt% and 40 wt% glass beads content). The injection rate resulted in different bead distributions ranging from homogeneous distribution through ”tunnel” shape to ”volcanic” shape. The darker regions on the images indicate the density increase of the glass beads. The distribution of glass beads at a test region on a sample plate after 3D reconstruction shows Figure 3. The distribution of glass beads is inhomogeneous, with two narrow bands of glass beads clearly visible. It can be seen that by 3D reconstruction the internal structure of the investigated composite can be well mapped.

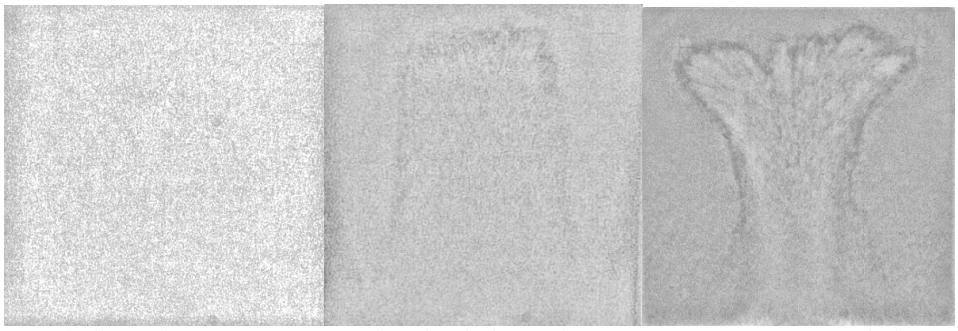

a) 1007505 sample b) 2507505 sample c) 4007505 sample

Figure 2 2D CT images of PP composite samples containing different glass bead content (10, 25, 40 wt%) produced at the same injection molding speeds

3D CT measurements can be used to determine the location of areas rich and poor in glass beads. This gives an accurate overview of the distribution of the glass beads along the injection molding path. The CT investigation method can be an effective tool for designing filler material (size, volume) and injection molding parameters of particulate composites to ensure uniform filler distribution.

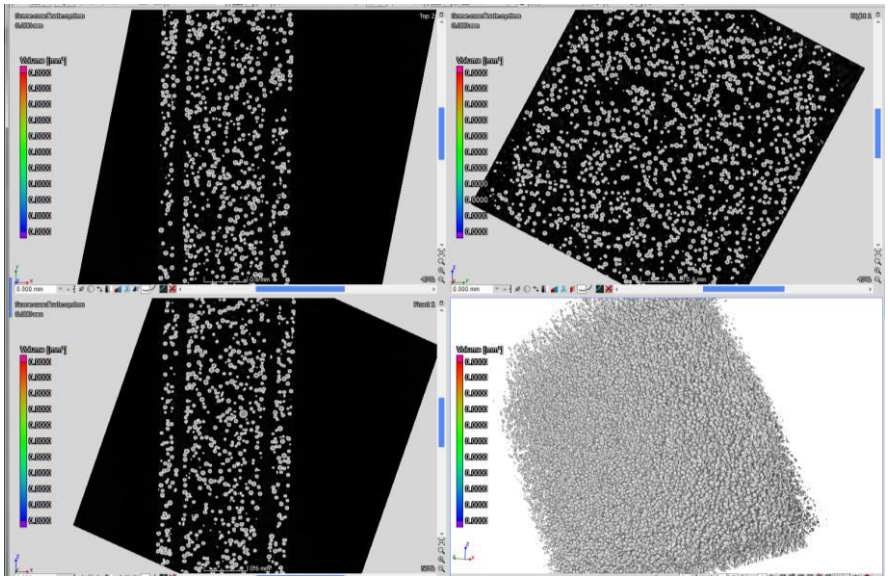

Figure 3 PP composite samples 4007520_07 / 9E after performing the inclusion analysis (the bottom right corner shows the 3D distribution of the glass beads, the top left and the right and the bottom left the 2D sectional views of the 3D pattern in the xy, yz, and xz planes respectively)

ACKNOWLEDGMENTS

The described work was carried out as part of a project supported by the National Competitiveness and Excellence Program – NVKP_16-1-2016-0038.

REFERENCES

[1] J.I. Goldstein, *Scanning Electron Microscopy and X-Ray Microanalysis.* Springer International Publishing, 4th ed., Germany, 2018.

[2] S. Carmignato, W. Dewulf, R. Leach, *Industrial X-ray Computed Tomography.* Springer International Publishing, Germany, 2018.

[3] C. Reinhart, *VG Studio MAX: Application examples from science and industry*, High-Resolution X-ray CT Symposium, Dresden, Germany, 2010.

THE EFFECT OF ALUMINIUM DROSS ON FOAM GLASSES PREPARED FROM CATHODE-RAY TUBE (CRT) AND BOTTLE GLASS (BG)

SASSI Meriem, SIMON Andrea PhD
Institute of Ceramics and Polymer Engineering, Miskolc University
E-mail: qkosassi@uni-miskolc.hu, femandi@uni-miskolc.hu

Keywords: waste management, CRT, Aluminium dross, Glass foam

The intensive use of non-renewable resources which has triggered a growing environmental concerns and social responsibility have served to boost the recycling activity especially in the construction sector to achieve efficiency as regards to energy and also, to reduce the associated emissions. Improving the mechanical and thermal properties of construction materials and using sustainable sources, based on waste material can improve the building energy consumption and decrease heat transfer coefficient. This will be implemented by employing eco-friendly materials such as glass foam which is a porous material having appropriate strength and low thermal conductivity. This study deals with the investigation of glass foam based on recycled material to reach the optimal characteristics by varying raw material composition and material formulation (proportion of the components, foaming agent details, particle size). The materials used are recycled bottle glass, cathode-ray tubes (CRT) glass and aluminium dross. Silicon carbide was added as a foaming agent.

Cathode-ray tubes, found in computer monitors and TV sets, are considered as electronic waste. Over the century, this kind of waste has increased exponentially. CRT glasses are complicated to recycle, as they contain hazardous components (e.g. Ba, Sr, Pb) requiring special treatment for safety [1]. However, there is a few CRT recycling facility in Europe and the rest of the world but its low value and the limitations of market make it difficult to recycle into new products. Managing this problem is critical from the viewpoint of creating functional WEEE treatment systems [2].

The other material being investigated is aluminium dross resulting from the hot (thermo-mechanical) processing based on the application of a relatively large amount of salt flux. This material is officially categorized as hazardous according to the European Catalogue for Hazardous Wastes [3]. Therefore, it may entail a severe financial burden for the mandatory handling. Its disposal is prohibited in many countries of the EU. A major problem is reactivity with water and even with the humidity in ambient air, leading to the formation of some toxic and even potentially explosive gases, such as NH_3, CH_4, PH_3, H_2 and H_2S [4].

In this study, the effect of dross and CRT glass on the mechanical strength, thermal conductivity and microstructure of the glass foams was determined. CRT glass with particles sizes of D90=63 μm were added in quantities of 5 to 10 wt%. Aluminium dross was washed with water 3 times and added in quantities of 10 wt%, 20 wt%, and 30 wt%. The foaming agent (SiC) was added in quantities of 2 wt%. Weighted mixtures were homogenized in a laboratory mixer for 10 minutes at 200 rpm and poured in a cylindrical mold and pressed under 11 MPa. Composition of the samples is listed in Table 1.

Table 1 Composition and foaming temperature of the mixtures

Sample Code	Composition *(wt%)*				Foaming temperature *(°C)*
	Dross	SiC	CRT63	Bottle glass	
BG		2		98	960
CRT10D	10	2		88	897
CRT20D	20	2		78	862
CRT30D	30	2		68	896
5CRT10D	10	2	5	83	965
5CRT20D	20	2	5	73	897
5CRT30D	30	2	5	63	890
10CRT10D	10	2	10	78	915
10CRT20D	20	2	10	68	894
10CRT30D	30	2	10	58	880
5CRT		2	5	93	970
10CRT		2	10	88	947

The first digit in sample coding means the quantity of CRT added in wt%, BG refers to Bottle Glass and the last number indicate the amount of dross added in wt%.

To characterize the thermal behaviour, heating microscopy was used for the mixtures. Foaming temperature was determined by analysing HSM curves. The density and thermal conductivity of the samples was conducted in order to obtain light weight product with high thermal insulation. Microstructure and pore size distribution were analysed using optical microscopy. To determine the mechanical behaviour of the samples, compressive strength was measured. Finally, chemical stability was determined using leaching test.

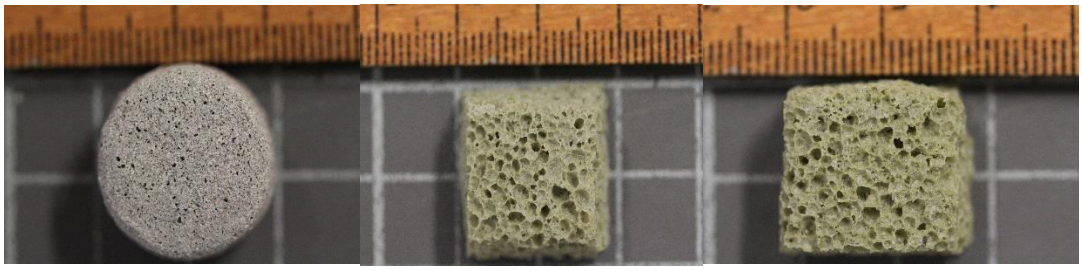

Figure 1 Foamed samples

The heating microscopy results of mixtures containing 0, 10, 20 and 30 wt% dross, shows that as we increase the dross content the foaming temperature decreases. This behaviour is explained by the presence of salts (CaF_2, NaCl, KCl) used as a flux to reduce the melting point, and in our case used to decrease the foaming temperature.

ACKNOWLEDGMENTS

The research work is supported by the GINOP2.2.1-15-2016-00018 project in the framework of the New Széchenyi Plan of Hungary, co-financed by the European Social Fund. The described study was carried out as part of the EFOP-3.6.1-16-2016-00011 “Younger and Renewing University – Innovative Knowledge City – institutional development of the University of Miskolc aiming at intelligent specialisation” project implemented in the framework of the Széchenyi 2020 program. The realization of this project is supported by the European Union, co-financed by the European Social Fund.

REFERENCES

[1] E. Restrepo, R. Widmer and M. Schluep, *Leaded glass from cathode ray tubes (CRTs)*, Step Green Paper Series. 2016.

[2] F. Méar, P. Yot, M. Cambon, M. Ribes, *The characterization of waste cathode-ray tube glass*, Elsevier, Waste Management 26, pp. 1468-1476, 2016.

[3] P. Tsakiridis, *Aluminium salt slag characterization and utilization*, Journal of Hazardous Materials 217-218, Elsevier, pp. 1-10., 2012.

[4] M. Mostafa, A. Ali, *Enhanced alumina recovery from secondary aluminum dross for high purity nanostructured alumina powder production: Kinetic study*, Journal of Environmental Management 212, pp. 278-291., 2018.

SIMULATION OF PRODUCTION PROCESS OF MOULD FOR DIE CASTING BY EDM TECHNOLOGY

STRAKA Ľuboslav PhD, DITTRICH Gabriel
Technical University of Kosice, Slovakia
E-mail: luboslav.straka@tuke.sk, gabriel.dittrich@tuke.sk

Keywords: Electrical Discharge Machining (EDM), progressive technology, mould, simulation

An integral part of every modern manufacturing company is the implementation of highly sophisticated production processes and technologies into the production process. Their main task is, first of all, to increase production efficiency. These advanced progressive technologies include EDM. This progressive technology is characterized by high product quality that can only be achieved with the full support of computing. The aim of the paper is therefore to demonstrate the process of manufacturing a die-casting mould using EDM technology using computer simulation. Since the production of die-casting moulds is predominantly prototypes, the task of computer simulation is to assist, in particular, in identifying possible tool collisions with the workpiece, thus avoiding insufficient quality of the functional parts of the mould or more precisely preventing damage to the machine or tool.

INTRODUCTION

The scope of application of conventional machining technologies is limited, on the one hand, by the mechanical properties of the material being machined, and on the other hand, by the complexity of the final shape of the machined surface of the product. For this reason, it is preferable to apply progressive machining technologies to machining materials with specific mechanical properties, such as treated high-alloy steels, carbides and the like. As a rule, they use some of the physical or physico-chemical principles of material removal in machining [1]. At the same time, when machining complicated product contours, locally limited edge breaking or more precisely material removal in a certain sequence or in precisely defined layers is often required. As a rule, these specific requirements require the application of multiple tools and equipment, resulting in an increase in machining time.

DESIGN OF MOULD FOR DIE CASTING OF METALS

Nowadays, we can hardly imagine the design of a die-casting mould without modern computer technology [2]. Before its actual production, it is appropriate to have made model in digital form, which significantly reduce the risk of errors of individual pressure mould. There are several CAD programs for its digitization. These allow, in addition to the design of the functional part of the mould cavity, also the design of the other parts of the mould which serve for its attachment, closing / opening, cooling and the like.

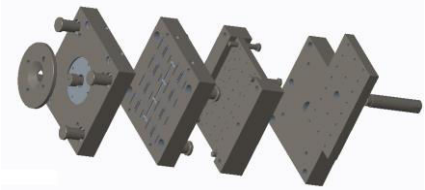

Figure 1 CAD design of individual functional parts of die casting mould

DESIGN OF ELECTRODES FOR PRODUCTION OF MOULD CAVITY BY EDM

Another important step in designing the manufacturing process of the functional part of the mould cavity is the specification of the tool electrodes. These must be designed not only for their functionality, but also for the practicality and economic efficiency of their application. In this case too, modern procedures require the application of computer support. When designing, it is possible to use several programs, for example Creo 3.0.

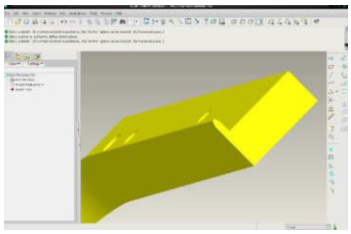

Figure 2 Design of tool electrode for EDM cavity moulds in Creo 3.0. software

An essential part of every production process is also the creation of drawing documentation. Therefore, both the design of the individual parts of the mould and the design of the tool electrodes require drawing documentation. Again, there are several software for its creation. For example, Creo 3.0. software allows you to create 2D drawings using a standard Drawing module from pre-created 3D models. This module also enables the creation of drawings for individual mould parts and tool electrodes as well as for their assemblies.

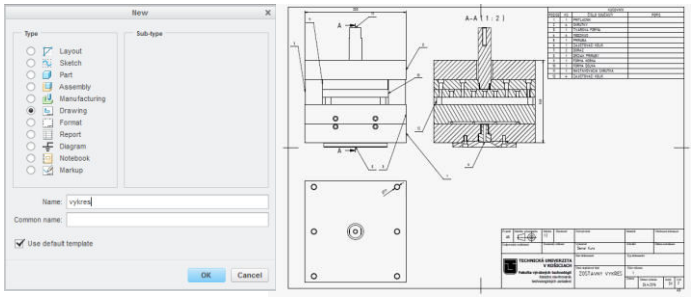

Figure 3 Creation of drawing documentation of individual parts of die casting mould

SIMULATION OF THE MANUFACTURING PROCESS FOR DIE-CASTING MOULD USING TECHNOLOGY EDM

The last step before the actual production of the tool electrodes and the individual parts of the die casting is the simulation of their production. The task of the simulation is first of all to propose suitable technological parameters, which gives us information about the total production time of the mould. Simulation is also possible to detect possible hidden shortcomings, but also to assess the efficiency of the production process of the mould as a whole. Again, there are several software applications to simulate the production process. In the above Creo 3.0. software this feature is enabled by the Manufacturing module.

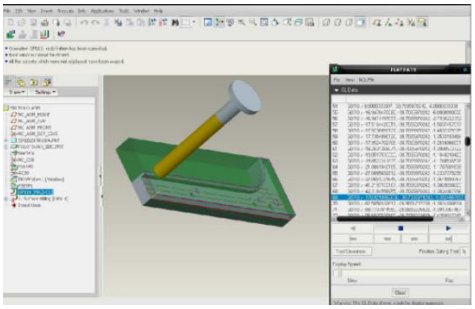

Figure 4 Simulation of production of a certain part of the die cavity by means of a cylindrical tool electrode

By simulating the production of the electrodes as well as the individual parts of the die casting mould, several alternatives can be made. Consequently, based on the chosen optimization criterion [3], which may be e.g. minimizing production time, maximizing production accuracy, etc., we can opt for the most suitable production method.

CONCLUSION

The task of computer simulation and the use of CAD / CAM software in technical practice is primarily to save the work of engineers and to prevent the occurrence of spoilage. Since die casting is almost always a prototype, its production cannot be tuned to test specimens. At the same time, due to complicated repair procedures or, in some cases, even impossible correction of defects in any of its parts, the simulation of the die casting process has an important position.

ACKNOWLEDGMENTS

The described work was carried out as part of a project supported by the VEGA 1/0205/19.

REFERENCES

[1] H.A. Firouzabadi, J. Parvizian, A. Abdullah, *Improving accuracy of curved corners in wire EDM successive cutting*. International Journal of Advanced Manufacturing Technology, 76, 447-459., 2015.

[2] S. Hašová, Ľ. Straka, *Design and verification of software for simulation of selected quality indicators of machined surface after WEDM*. Academic Journal of Manufacturing Engineering, 14(2), p. 13-2., 2016.

[3] A.T. Salcedo, P.I. Arbizu, C.J.L. Perez, *Analytical modelling of energy density and optimization of the EDM machining parameters of Inconel 600*. Metals, 7(5), 166., 2017.

THE INFLUENCE OF MPT AT WEDM OF TOOL STEEL ON WORKPIECE SURFACE QUALITY

STRAKA Ľuboslav PhD, DITTRICH Gabriel
Technical University of Kosice, Slovakia
E-mail: luboslav.straka@tuke.sk, gabriel.dittrich@tuke.sk

Keywords: Main Technological Parameters (MTP), tool steel, wire electrode, Wire Electrical Discharge Machining (WEDM)

The aim of the paper is to describe the results of experimental research focused on the assessment of the impact of the main technological parameters for WEDM on the quality of machined surface. The samples were made of tool steel ENX155CrVMo12-1 using an electroerosion equipment SODICK AQ535. As wire tool electrode was used brass cutting wire 0.25mm diameter with the designation ELECUT BRASS CuZn37 and a tensile strength *Rm*=980N/mm^2.

INTRODUCTION

Unlike conventional technologies, progressive technologies normally use energy sources other than purely mechanical energy. These technologies include WEDM, which uses the physical principle of material removal. The removal of material particles occurs by cyclically repeating electrical discharges between the tool and the workpiece which is immersed in the dielectric. The final quality of the machined surface depends on the intensity of the electric discharges. In general, the lower intensity of electrical discharges during WEDM has a positive impact on the quality of the workpiece [1]. However, too low a value of the intensity of the electric discharges leads to a substantial loss of the electroerosion process, making this process economically inefficient [2]. Therefore, it is necessary to find a compromise between the achieved quality of the machined surface and the productivity of the electroerosion process itself [3].

MATERIAL AND METHODS OF WORK

SODICK AQ535 (Fig.1) electroerosion equipment was used for production of samples in the experiment. It is a multi-axis CNC machine used in practice for cutting materials It is mainly used for the production of moulds, shearing tools, electrodes, etc. made of very hard materials, respectively products with complicated shapes.

Figure 1 Electroerosion cutter SODICK AQ535

Laboratory measuring devices were used to measure the qualitative indicators of the prepared samples in terms of roughness and geometric accuracy. A Mitutoyo Surftest SJ 400 contact profilometer (Fig. 2a) was used to measure the roughness of the eroded surface. The CNC contact coordinate machine ThomePräzision with software Metrolog XG (Fig. 2b) was used to measure the deviations of the geometric accuracy of the eroded surface.

a)  b) 

Figure 2 Measuring equipment used to identify qualitative indicators of eroded surface of experimental samples

In the experiment, brass wire 0.25mm diameter manufactured by ELERO s. r. o. with the designation ELECUT BRASS CuZn37 was used for the production of samples. It is a standard type of compact wire electrode having a relatively high tensile strength Rm=980N/mm2 with a 63% Cu content and a 37% Zn content. This type of wire electrode is able to ensure the required quality of the machined surface with high productivity and at the same time favorable economic efficiency of the electroerosion process. The samples were made of Böhler tool steel with the designation

ENX155CrVMo12-1. It is highly alloyed ledeburitic chromium - molybdenum - vanadium steel, which is characterized by high abrasion resistance, wear resistance and good toughness. At the same time, it has also excellent hardenability and dimensional stability. Its basic chemical composition is shown in Tab. 1.

Table 1 Basic chemical composition of tool steel marked EN 155CrVMo12-1

Steel marking	Percentage of elements (%)							
	C	Si	Mn	Cr	Mo	V	P	S
EN ISO X155CrVMo12-1	1.55	0.25	0.35	11.80	0.80	0.95	max 0.030	max 0.030

The sample material it was be heat treated before to erosion. The heat treatment of the sample material consisted of a two-stage heating to an austenitization temperature of about 1040°C and a hardening to oil followed by tempering at a temperature of about 520°C to a secondary hardness of 56HRC. In the following Fig. 3 are shown made experimental samples.

a)  b) 

Figure 3 Experimental samples made

In the first case (Fig. 1a) it was a cylinder 8.0mm diameter with a length of 40.0 mm, in the second case (Fig. 1b) a prism with dimensions 8.0×8.0×40.0 mm.

RESULTS OF EXPERIMENTAL MEASUREMENTS

Based on the results of experimental measurements, graphical dependencies were subsequently constructed describing the influence of MTP on the machined surface quality in terms of roughness parameters *Ra*, *Rz* (Fig. 4a) and geometric deviations of the machined surface (Fig. 4b) for WEDM tool steel ENX155CrVMo12-1 wire electrode 0.25mm diameter with the designation ELECUT BRASS CuZn37.

a) 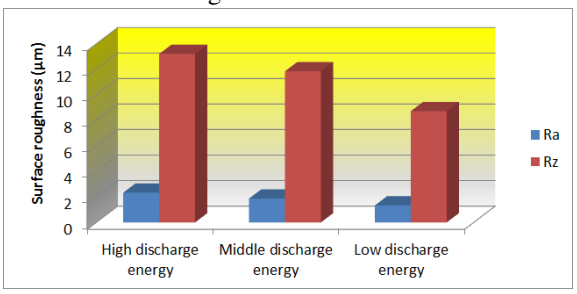

b) 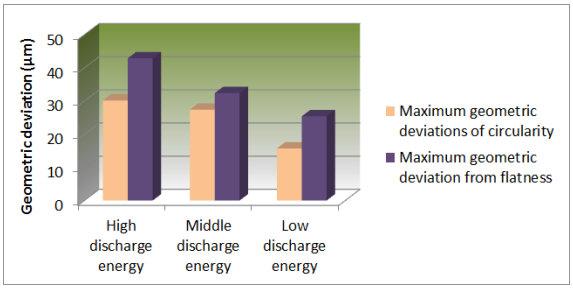

Figure 4 Dependence of roughness parameters *Ra*, *Rz* and maximum geometric deviations of machined surface on MTP for WEDM tool steel EN ISO X155CrVMo12-1

CONCLUSION

The aim of the paper was to identify the influence of MTP on machined surface quality from the point of view of roughness parameters *Ra*, *Rz* and geometrical deviations machined for WEDM tool steel. Based on the results of experimental measurements, it was found that with the decreasing intensity of the discharge energy, which is represented by a lower value of peak discharge current and duration of discharge, while higher value of the duration of pauses between discharges occur to a significant improvement in both quality indicators machined surface.

ACKNOWLEDGMENTS

The described work was carried out as part of a project supported by the VEGA 1/0205/19.

REFERENCES

[1] A. Mičietová, M. Neslušan, M. Čilliková, *Influence of surface geometry and structure after non-conventional methods of parting on the following milling operations.* Manufacturing Technology, 13(2), 199-204., 2013.

[2] Ľ. Straka, I. Čorný, J. Piteľ, S. Hašová, *Statistical Approach to Optimize the Process Parameters of HAZ of Tool Steel EN X32CrMoV12-28 after Die-Sinking EDM with SF-Cu Electrode.* Metals, 7(2), 1-22., 2017.

[3] A.T. Salcedo, I.P. Arbizu, C.J. Luis Pérez, *Analytical modelling of energy density and optimization of the EDM machining parameters of inconel 600.* Metals, 7(5), 1-21., 2017.

SOME ASPECTS OF THE RELIABILTY OF VIBRATION MONITORING OF ROTATING MACHINERY WITHIN THE FRAMEWORK OF THE NEW INDUSTRIAL REVOLUTION

[1]SZABÓ József Zoltán PhD, [2]DÖMÖTÖR Ferenc PhD
[1]Donát Bánki Faculty of Mechanical and Safety Engineering, Óbuda University
E-mail: szabo.jozsef@bgk.uni-obuda.hu
[2]Faculty of Transport Engineering and Vehicle Engineering, Budapest University of Technology and Economics
E-mail: ferenc.domotor@gjt.bme.hu

Keywords: Predictive maintenance, new industrial revolution, vibration diagnostics

The basic condition for an effective operation of the manufacturing plant in the new industrial revolution is the reliability of the information provided by the sensors and devices. This is related not only to the pure measurement data, but to the processed data used in rules for decisions in expert software. This is the case e.g. in the case of evaluation of vibration spectra recorded on rotating machinery. The various mechanical faults have different typical spectral features. These faults can be identified using these spectra, as they are like fingerprints. In this paper we had the goal to test some typical, artificially generated problems (static and dynamic balancing, misalignment of shaft/coupling) and check whether the spectral fingerprints they follow the pattern determined in the literature.

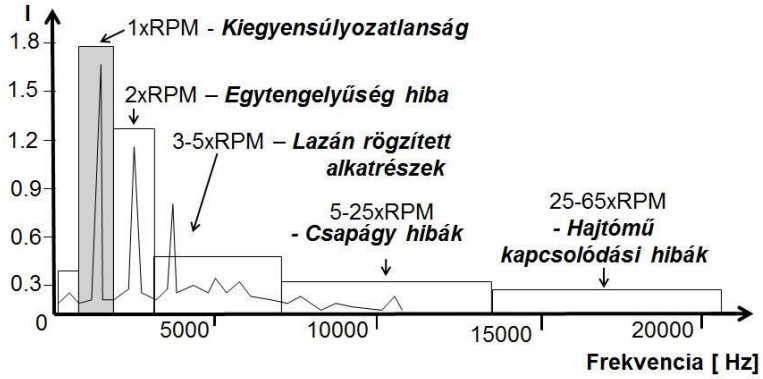

Figure 1 Typical vibration spectra of rotors with different faults

Two series of experiments had been carried out. The one was a test with the goal to identify the response function a vibrating rotor having static unbalance on one hand and dynamic unbalance on the other hand. This test has been repeated several times with different trial weights, and different rotational speeds. The other series of test had the goal to identify/check the response of the stationary part of the machine, excited by a shaft misalignment.

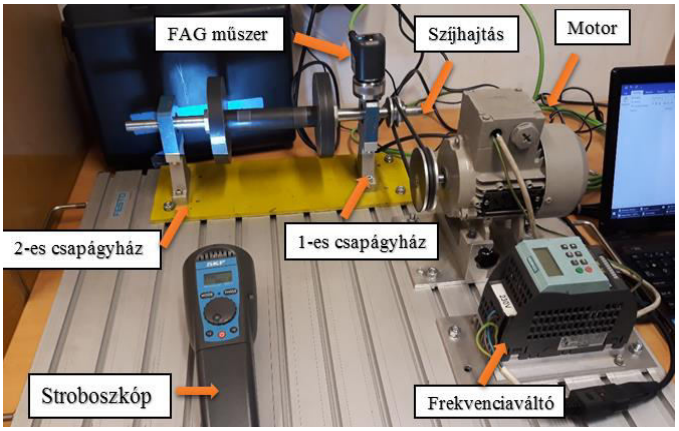

Figure 2 Test rig in the laboratory

For the tests the following intruments were used:

• FAG SmartCheck vibration measuring instrument, SmartWeb and SmartUtility software applications.
• SKF TKRS 10 strobe light (for mesuring the rotational speed),
• Vibrotester test rig (internal development),
• Fixtur Laser shaft alignment system,
• Personal computer
• Scale (weight)

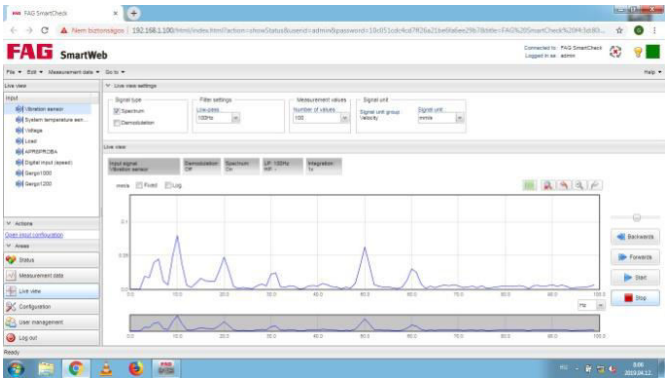

Figure 3 Typical vibration spectrum

During the tests it has been found, that - despite of the expectations – the amplitudes of the 1X and 2X components have risen, but not as much, as expected. Consequently a linear function could not be determined between the extent of misalignment and the severity of the vibration. Results, got during the tests of unbalance are somewhat disappointing, too. In case of static unbalance the amplitude of the 1X component is increasing linearly with the weight. However, in case of dynamic unbalance this is not the case. Measurement results are spreading strongly.

On the other hand the change of the speed – probably due to the natural frequencies – has no unambigous rule, at all and is not proportional to the square of the rotational speed. This is very important, because we had nearly ideal conditions (unlike in industrial plants), and despite of this we had no clear results. To be honest, we expected a quadratic function and this could not be found.

ACKNOWLEDGMENTS
The described work was carried out as part of a project supported by the Óbuda University, the Schaeffler Hungary and the Fixtur laser Hungary companies.

REFERENCES
[1] J.E. Berry, *Predictive Maint. and Vibration Signature Analysis*, Technical Associates of Charlotte, USA 1995.
[2] L. Juhász, and L. Pokorádi, *Relations between the Internet of Things and the Maintenance Nowadays (in Hungarian)*, Gradus Vol 5, No 1 (2018) 99-106, ISSN 2064-8014, 2018.
[3] SmartCheck product description, Schaeffler Technologies AG & Co. KG (Schweinfurt, Germany
[4] Fixtur Laser product description, ACOEM AB, Box 7, SE-431 21 Mölndal, Sweden

EFFECT OF THE MEAN TEMPERATURE DIFFERENCE IN THE HEAT AND MASS TRANSFER MODEL OF FLUIDIZED BED DRYERS

SZABÓ Viktor PhD, POÓS Tibor PhD
Department of Building Services and Process Engineering Budapest University of Technology and Economics
E-mail: szabo.viktor@mail.bme.hu, poos@mail.bme.hu

Keywords: fluidized bed dryer, mean temperature difference, heat and mass transfer model

Heat and mass transfer models using the volumetric heat transfer coefficient were developed for fluidized bed dryers. These models are suitable to determine the change in the moisture content and temperature of the particles, in the temperature and the absolute humidity of the drying gas versus drying time, and the change in the temperature and absolute humidity of the drying gas along the dryer. In the case of the model describing the heat and mass transfer as a function of the drying time, the differential temperature change of the particles [1]:

$$dT_P = (\alpha a)\frac{A_d L}{m_P c_P}\Delta T_{G-P}dt + \frac{m_{dP} r_F}{m_P c_P}\frac{dX}{dt}dt\,,$$

where ΔT_{G-P} is the mean temperature difference between the drying gas and the particles. The aim of our research is to investigate the effect of the mean temperature difference value on the results of the heat and mass transfer model. In drying processes the logarithmic mean temperature difference is generally used [2]. The general equation of the logarithmic mean temperature difference (ΔT_{lm}) is shown in Table 1.
The logarithmic mean temperature difference has caused inconveniences in several applications [3]. In the literature, there are many replacements for ΔT_{lm}, mostly in heat exchanger applications. The summary of the equations of the mean temperature differences is shown in Table 1. ΔT_A indicates the difference of the temperature between the drying gas at the inlet of the dryer and the temperature of the particles, and ΔT_B means the difference of the temperature between the drying gas at the outlet of the dryer and the temperature of the particles. During fluidized bed drying generally $\Delta T_B \ll 1°C$ at steady state condition. The purpose of this study is to propose a valid equation to determine the mean temperature difference in fluidized bed dryers, when the temperature of the drying gas at the inlet and at the outlet of the dryer, and the temperature of the particles are known

Table 1 Expressions to calculate the mean temperature difference

Name	Equation	Reference
ΔT_{lm}	$\frac{\Delta T_A - \Delta T_B}{ln\frac{\Delta T_A}{\Delta T_B}}$	[3]
$\Delta T_{Underwood}$	$\left(\frac{\Delta T_A{}^{1/3} + \Delta T_B{}^{1/3}}{2}\right)^3$	[4]
$\Delta T_{Paterson}$	$\frac{\frac{\Delta T_A + \Delta T_B}{2} + 2\sqrt{\Delta T_A \Delta T_B}}{3}$	[5]
ΔT_{Chen}	$\sqrt[3]{\frac{\Delta T_A + \Delta T_B}{2}\sqrt[3]{\Delta T_A \Delta T_B}}$	[6]

The difference between the expressions can be illustrated graphically. Figure 1 shows the variation of the ratio of the mean temperature differences (ΔT_{G-P}) and the greater temperature differences (ΔT_A) in the function of the smaller temperature differences (ΔT_B) for the four equations presented. The value of ΔT_A was set to 100 °C in this example.

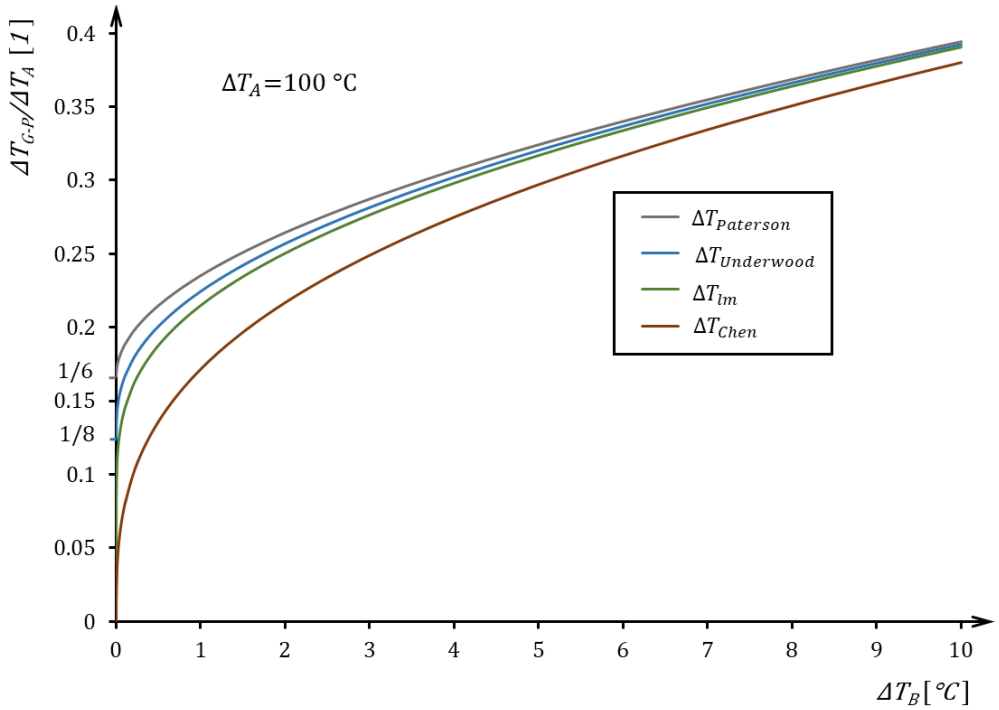

Figure 1 Variation of the ratio of the mean temperature differences and the greater temperature differences in the function of the smaller temperature differences

According to Figure 1, there is a divergence between the functions calculated with the mean temperature difference equations below $\Delta T_B < 10\ °C$. This uncertainty results inaccuracies in the heat and mass transfer models. The limits of the mean temperature differences calculated with the referred equations are summarized in Table 2, when $\Delta T_B \to 0$.

Table 2 Limits of the referred mean temperature differences

$\lim_{\Delta T_B \to 0} \Delta T_{lm} = 0$	$\lim_{\Delta T_B \to 0} \Delta T_{Underwood} = \frac{1}{8}\Delta T_A$	$\lim_{\Delta T_B \to 0} \Delta T_{Paterson} = \frac{1}{6}\Delta T_A$	$\lim_{\Delta T_B \to 0} \Delta T_{Chen} = 0$

The heat and mass transfer model is sensitive to the calculation method of the mean temperature difference. Since the outlet temperature of the drying gas and the product are nearly the same, the limits of each mean temperature differences cause a significant error in the description of the drying process. Measuring the actual value of the mean temperature difference should help to decide, which equation is appropriate to calculate the mean temperature difference of the fluidized bed dryer system.

REFERENCES

[1] V. Szabó, *Modeling of heat and mass transfer in fluidized bed dryers*. PhD Thesis, Budapest, 2019.
[2] A. Iguaz, A. Esnoz, G. Martinez, A. Lopez, P. Virseda, *Mathematical modelling and simulation for the drying process of vegetable wholesale by-products in a rotary dryer*. Journal of Food Engineering, 59(2), 151-160., 2003.
[3] A. Zavala-Río, R. Femat, R. Santiesteban-Cos, *An analytical study of the logarithmic mean temperature difference*. Revista Mexicana de Ingeniería Química, 4(3), 201-212., 2005.
[4] A.J.V. Underwood, *Simple Formula to Calculate Mean Temperature Difference*. Chemical Engineering, 77, 192, 1970.
[5] W.R. Paterson, *A replacement for the logarithmic mean*. Chemical Engineering Science, 39(11), 1635–1636, 1984.
[6] J.J.J. Chen, *Comments on Improvements on a Replacement for the Logarithmic Mean*. Chemical Engineering Science, 42, 2488–2489, 1987.

INTRODUCTION OF A NEW INDUSTRIAL PROCESS FLOW FOR TOPOLOGY OPTIMIZATION THROUGH A CASE STUDY OF A BRACKET

[1]SZALAI Enikő, [2]JÓNÁS Szabolcs
[1]Department of Machine and Product Design, Budapest University of Technology and Economics
[1]E-mail: Eniko.Szalai@knorr-bremse.com
[2]Knorr-Bremse Rail Systems Budapest, Hungary
[2]E-mail: Szabolcs.Jonas@knorr-bremse.com

Keywords: topology optimization, method, design process

ABSTRACT
The importance of incorporating Computer Aided Optimization (CAO) into the design process lies in providing the fastest possible solution to a technical problem, within the given structure.
Therefore, we have created a design process with topological optimization as an integral part to save time and resources in practice.

INTRODUCTION
With the advancement of computers, the solutions for complicated engineering computing problems have accelerated. Such engineering calculations are algorithmic optimization and finite element analysis based on numerical methods [1].
Optimization is used in engineering practice when it is necessary to create a more favorable design for a particular task.
In the design process of optimizing a *new product* it appears in the preparation phase of the design variants, in the case of an *existing product*, it means the modification of the finished part according to the purpose.
The starting point in both cases is a geometry (consisting of design and nondesign space), and knowledge of loads, boundary conditions and constraints of the component.
In the case of traditional intuitive optimization, based on the information described above, the designer begins to remove material from the design space based on his/her experience. After a finite element analysis of this first-generation design additional material is taken or reconstructed by the designer, which is followed by another check. All this iteration process takes place until the shape of the part has met the expectations.
In case of (Computer Aided) optimization, after the import of design and nondesign space, adjustment of constraints and loads, and addition of finite element mesh, the software creates a geometry according to the purpose of optimization (mass minimization, compliance minimization, etc.). Several optimization algorithms have been developed, the most commonly used by software is the SIMP method.

METHODOLOGICAL RESEARCH
We believe that incorporating computer aided topology optimization into the design process will speed up component design time, which saves time and energy and, last but not least, provides a better solution to the problem than we would have received through intuitive optimization.
Experimentally, during the optimization of an example part, we collected the information needed to assemble the design process. We first optimized the component intuitively and then used Inspire 2018.3 and Ansys WB 19.2 (this allowed us to compare the speed and efficiency of the traditional and CAO) we used Creo 4.0 for modeling, and ANSYS WB 19.2 for finite element analysis of the models.
The practical experience gained in this way has provided a wealth of useful information about the capabilities and limitations of each software, from which we have already developed the design process.

Design space and software-generated raster model *Finished optimized design*

Figure 1 Optimization result example (Inspire)

DEVELOPED OPTIMIZATION PROCESS

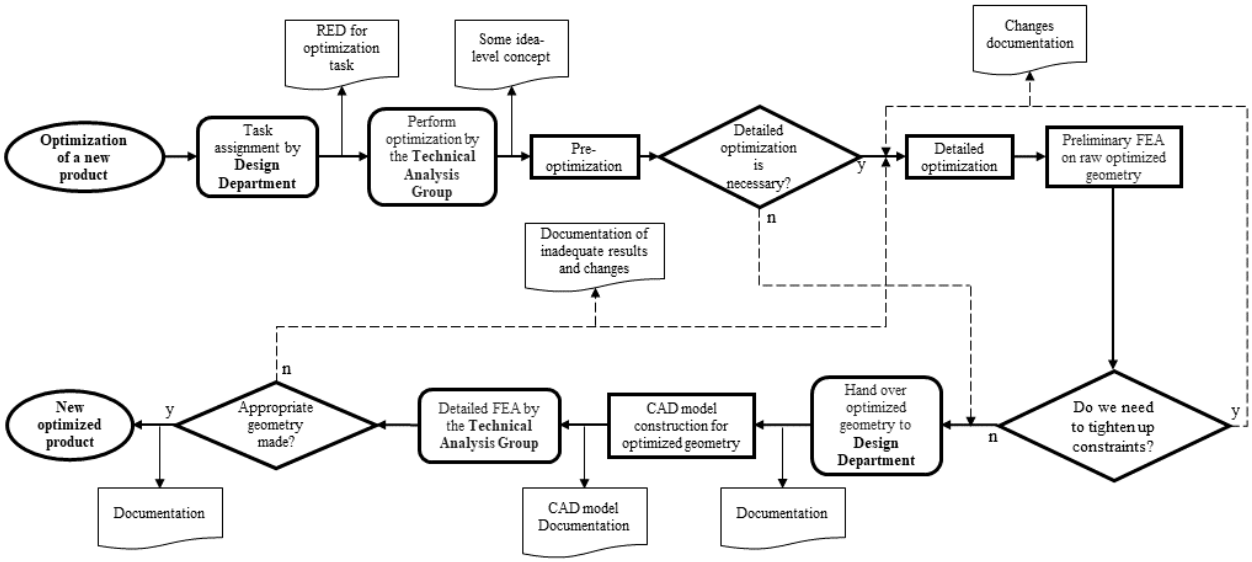

Figure 2 Optimization process

The flowchart contains iteration loops that, at each decision, can feed back to an earlier event (which means repeating the previous process knowing some new information) or omitting some unnecessary steps in decision places.
Output elements appear in the flowchart after some steps to indicate the documentation of a particular subprocess or its recordable form. They are basically designed to streamline communication between the two groups (Design Department and Technical Analysis), to exchange data and information in such a way that it remains trace and retrievable in the future.

PRACTICAL APPLICATION

Figure 3 Optimization result based on the developed process

All in all, the optimization process can be significantly accelerated with the help of software, and we can remove remarkable more unnecessary material from each structure. At the same time, it should not be overlooked that it is essential to study the operation of individual software. The time it takes to acquire this knowledge is significantly less than collecting the engineering experience needed to achieve the same amount of weight reduction through intuitive optimization.

REFERENCES

[1] M.P. Bendsoe, O. Sigmund, *Topology optimization; Theory, methods and applications,* 2003.
[2] M.Q. Osvaldo, V. Mariano, C. Alonso, M. Pascual, *Topology Design Methods for Structural Optimization,* 2017.

PARAMETER ESTIMATION OF DRAG COEFFICIENT AND ROLLING RESISTANCE OF VEHICLES BASED ON GPS SPEED DATA

SZÁNTÓ András, HAJDU Sándor PhD
Department of Mechanical Engineering, Faculty of Engineering, University of Debrecen
E-mail: andras.szanto.0503@gmail.com, hajdusandor@eng.unideb.hu

Keywords: parameter estimation, vehicle, Simulink

Parameter estimation [1] is a key method in model-based design (MBD) [2]. In MBD, we need validated mathematical models of the parts of a system (and the assembly of the system also needs to be validated). The mathematical models are usually lumped-element models [3] instead of distributed-parameter models [4]. Parameter estimation is needed when the constant parameters of the lumped-elements cannot be computed directly from the measurement data. This happens when the accessibility of measurement devices is limited. In this case, parameter estimation is applied which is an optimization process: a cost function is calculated based on the difference of the measurement data and the same data in the mathematical model, and the variables of the optimization are the appropriate constant parameters of the elements in the model. The estimation is successful if the fit of the curves is acceptable. Then, the estimated parameters need to be validated with different measurements. The main environments for lumped-element modelling and parameter estimation (and a lot of other things and methods) are MATLAB, Simulink and Simscape, all of them developed by MathWorks.

In this paper, the above-mentioned parameter estimation process is applied to estimate the drag and rolling resistance coefficients of a vehicle (which is currently a bicycle). In fact, a constant-force parameter (*c_const*) and a velocity-square-force parameter (*c_square*) are in the model, and these result in the sum force (*fz_Model*) applied along the translational DOF that models the vehicle (this vehicle model has only 1 DOF). It is only an assumption that the constant force is the rolling resistance and the force proportional to the square of the velocity is the drag force of the air.

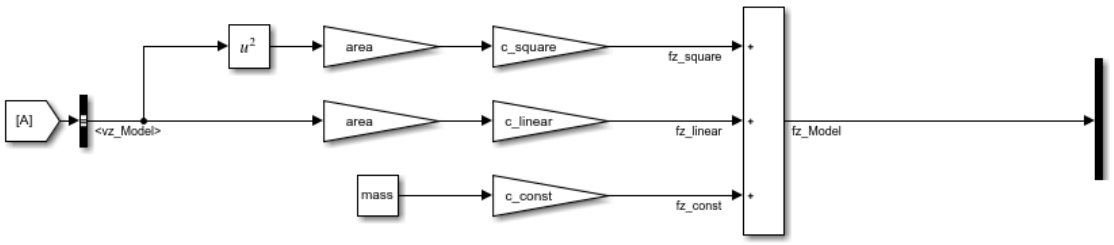

Figure 1 Forces applied to the vehicle model

The names of the loss forces are not sure to be important. A simple experiment is shown in the following two figures. Two parameter estimations are done with and without the rolling resistance force (*c_const* parameter) in the model, and the best fits are in the figures. This experiment can prove the existence of a constant force (most likely the rolling resistance). The iterations of different models to estimate the parameters can be applied without knowing the name of the forces: then the model with the best fit needs to be applied for modelling the part. Of course, in the case of vehicles, all forces are well-studied and have their own names. Not only the rolling resistance loss but other wheel forces and torques are modelled by the Pacejka wheel models [5]. The authors previously researched lumped-element vehicle models in Simscape based on the Pacejka semi-empirical model, and its application for modelling a theoretical ABS algorithm [6].

In the paper, the method of applying the parameter estimation and the results are described in details. The conclusion is that parameter estimation is a valid alternative when expensive measurement devices are not accessible: a wind tunnel in the case of this research.

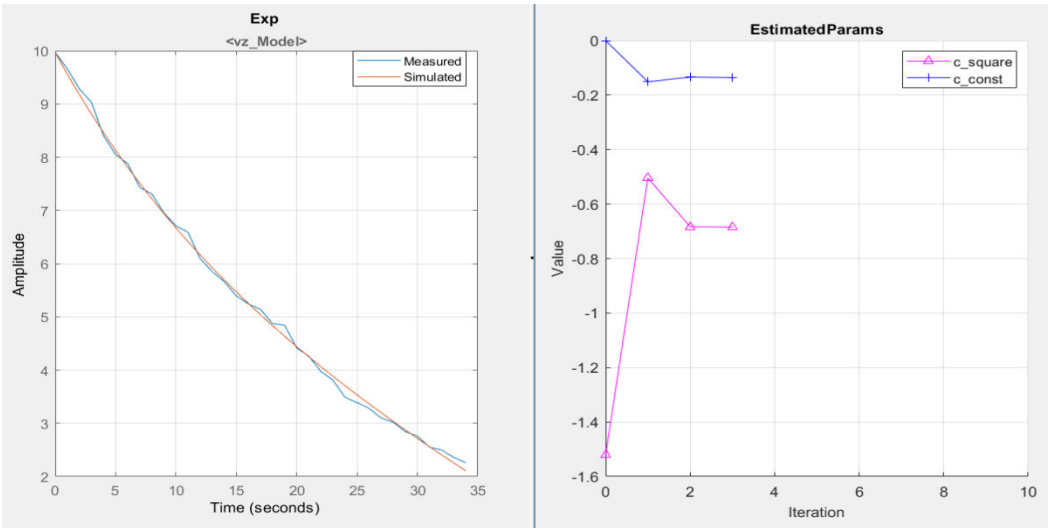

Figure 2 Estimation of 2 variables (c_const and c_square). The measured and modelled velocity curves fit well with a cost function value of 0.0035.

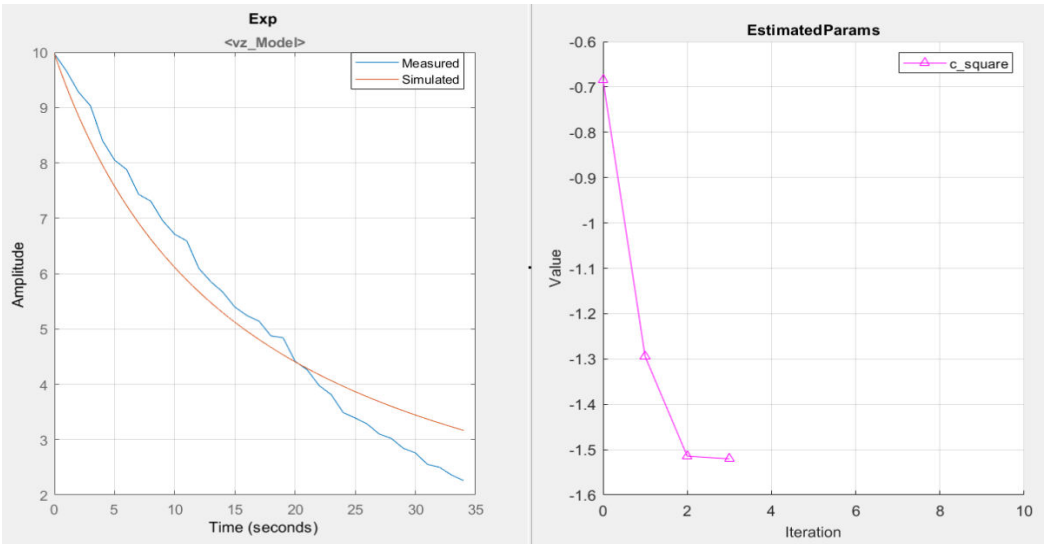

Figure 3 Estimation of 1 variable (c_square), other parameters are set to zero. The measured and modelled velocity curves fit mediocre with a cost function value of 0.097 (28 times larger than that of the pervious model).

ACKNOWLEDGMENTS

SUPPORTED BY THE ÚNKP-19-2 NEW NATIONAL EXCELLENCE PROGRAM OF THE MINISTRY OF HUMAN CAPACITIES

REFERENCES

[11] https://www.mathworks.com/help/sldo/parameter-estimation.html (downloaded: 10/25/2019)
[12] https://en.wikipedia.org/wiki/Model-based_design (downloaded: 10/25/2019)
[13] https://en.wikipedia.org/wiki/Lumped-element_model (downloaded: 10/25/2019)
[14] https://en.wikipedia.org/wiki/Distributed_parameter_system (downloaded: 10/25/2019)
[15] H. Pacejka, *Tire and vehicle dynamics.* Elsevier, 2005.
[16] A. Szántó, S. Hajdu, *Vehicle Modelling and Simulation in Simulink.* International Journal of Engineering and Management Sciences (IJEMS) Vol. 4. (2019). No. 1 DOI: 10.21791/IJEMS.2019.1.33., 2019.

PARETO OPTIMIZATION OF THERMOELECTRICALLY COOLED HEATSINK FOR A GIVEN DESIGN CONDITION

SZODRAI Ferenc PhD, KUTHY Árpád
Department of Building Services and Building Engineering, Faculty of Engineering, University of Debrecen
E-mail: szodrai@eng.unideb.hu

Keywords: CFD, TEC, Pareto, heatsink, optimization

Nowadays the improvement of energy efficiency and the reduction of the energy demands is getting more and more crucial. The reduction of the energy demand is needed at every field of engineering. Air cooling can be used for electronics cooling or for personal ventilation systems which power demand is usually low. Air cooling under 1 kW power demand can be solved with heat buffering if robust thermodynamic machines are used. However, thermoelectric devices also known as "TEC" can provide small amount of cooling power and smaller volume is required. To describe the working method of the TEC devices works by both Lineykin and Ben-Yaakov and Al-Rubaye et.al. were used, where they described every essential parameter of the cooling devices with only details provided by manufacturers. [1, 2]
The goal was to find an optimal heatsink geometry that could cool down a 32 °C warm 4 m s^{-1} airflow to 26 °C with the most effective way and to showcase how was it obtained. The examined cooling device consisted of two type TEC1-12710 Peltier device that was a placed in a 40 mm x 40 mm x 140 mm large tunnel. Between the two TEC1-12710 a copper heatsink was placed. It was assumed that the cooling devices most crucial point was the geometry of the heatsink. Finned construction of heatsink was examined and it was expected that if it had densely placed fins, it could cause large pressure change while it produces significant cooling; also if it had less fins in the tunnel it could produce less cooling.
To find out which geometry was the best for the task 33 independent geometries were examined. The geometry was created with parametric algorithm where the width of the fin and the number of the fins were varied. The width (v) of the fins changed between 0.5 mm and 6 mm, the number of fins was limited by how many of the fins could be physically placed between the two TEC devices.

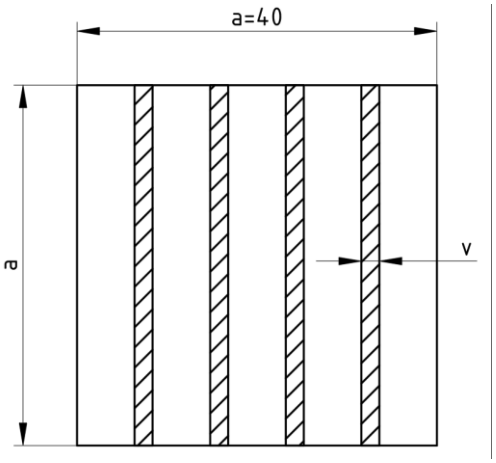

Figure 1 scheme of the heatsink

The examination was done with commercially available CFD software (ANSYS 2019 R2), to showcase, that with CFD software it is possible to optimize before the manufacturing process and find the optimal solutions. This method also reduces the waste and helps us solve complex thermodynamics and fluid mechanics problems such as the heatsink temperature distribution, the thermal transmittance and the pressure increase by the heatsink. Since the heatsink and the airflow of the tunnel was modelled, the fluid simulation was coupled with a thermal finite element simulation. For the fluid modelling k-ε turbulence model was used with scalable wall function. This turbulence model was used in the work of Seo et. al. with an accurate result [3].
In the evaluation Pareto diagram was utilized which is a known method for multi objective optimizations [4].
Pareto diagram is a Cartesian coordinate diagram where the y and x axis represent optimization parameters. If it is assumed that the minimum of the parameters are preferred, then the ideal case can be found at the origin of the diagram. If the maximum of the parameter is preferred, then to apply the same methodology the inverse of the parameter is needed. Every calculated case was a point on the Pareto diagram and the one with the shortest vector length from the origin point was chosen to be the favoured optimal case. The optimization parameters can be normalized measurement

values or dimensionless numbers. With normalized measurement values the maximum optimum length is $2^{0.5}$ and the ideal is 0. This method makes the two parameter change equal and with multiplier coefficient one of the parameter importance can be increased, however the change of normalized values is dependent on the measurement range, that is why the measurement range has to be chosen carefully. The normalized values were created from the results of the simulations. The values were put in a box plot and the values that were not in the quartiles was disregarded. Without the peak values the change in the optimized parameters was more important.
With normalized values the vector length for a case can be calculated with the following equation, if the pressure difference (p) [Pa] and the cooled air temperature (T) [K] is known optimizing parameters.

$$L_{oi} = \left(\left((p_i - p_{min}) \cdot (p_{max} - p_{min})^{-1} \right)^2 + \left((T_i - T_{min}) \cdot (T_{max} - T_{min})^{-1} \right)^2 \right)^{0,5}$$

For dimensionless number evaluation the valve loss factor and the inverse of the Bosnjakovic factor was used. With the two method similar results occurred. In further research where there is no known dimensionless number the vector length method can be used.
In our research, it was concluded that in the thermoelectrically cooled heatsink optimization crucial factors are the cooled air temperature, the static pressure increase and also the lowest temperature of the heatsink. The lowest temperature of the heatsink was sometimes lower than the TEC device was capable of.
In the thermodynamic model this result could be considered to be correct, though knowing the performance limit of the TEC device, those cases had to be disregarded. Since at that level of heat flux the device cannot cool down to the desired temperature.
The optimal geometry was when 5 pieces of 5 mm thick fins were used in the tunnel. The simulation was verified with theoretical power demand calculation and the error was less than 10%. This error also included the fin efficiency.

REFERENCES

[1] S. Lineykin, S. Ben-Yaakov, *User-friendly and intuitive graphical approach to the design of thermoelectric cooling systems*, International Journal of Refrigeration, 1. 30, pp. 798-804, 2007.
[2] A. Al- Rubaye, K. Al-Farhany, K. Al-Chlaihawi, *Performance of a portable thermoelectric water cooling system*, International Journal of Mechanical Engineering and Technology, 1. 9, 1. 8, pp. 277-285, 2018.
[3] Y.M. Seo, M.Y. Ha, S.H. Park, G.H. Lee, Y.S. Kim, Y.G. Park, *A numerical study on the performance of the thermoelectric module with different heat sink shapes*, Applied Thermal Engineering, 1. 128, pp. 1082-1094, 2018.
[4] J. Michanan, R. Dewri, M.J. Rutherford, *Understanding the Power-Performance Tradeoff through Pareto Analysis of Live Performance Data,*in IEEE, Dallas, TX, USA, 2014.
[5] M.G. Prakash, M.-H. Sayer, S. Mukhopadhyay, S. Kumar, *Ultrathin Thermoelectric Devices for On-Chip Peltier Cooling*, IEEE TRANSACTIONS ON COMPONENTS, PACKAGING AND MANUFACTURING TECHNOLOGY, 1. 1, 1. 9, pp. 1395-1405, 2011.

WETTABILITY CHANGING EFFECT OF FEMTOSECOND LASER IMPULSES ON DP STEELS

TAJTI Ferenc, BERCZELI Miklós
Department of Materials Technology, John Von Neumann University
E-mail: cbfferi@gmail.com

Keywords: high strength steel, laser, surface treatment, wettability, surface tension

As a result of stricter environmental and safety standards, vehicle manufacturers have to reduce the weight of the vehicles, because 10% weight loss cause 8-10% reduction of fuel consumption. To reduce car's weight and increase safety, vehicle manufacturers use high-strength steels. Further weight reduction can be achieved by using corresponding adhesive technologies and optimizing these technologies can increase the strength of the joints. According to literature research, the improvement of interface properties has a large effect on adhesive technologies. In order to improve interface properties, we can use multiple surface treatments. In our research we investigate the effects of femtosecond laser surface treatment on high strength steels. In order to detect the effect of surface treatment, we investigate the wettability of the treated and untreated steels. In our research we measure the surface tension of treated and untreated steels. Our main goal is to improve wettability properties thus the adhesive technology.

In our research we used DP 600 high strength steel sheet with the thickness of 1 mm. We cut the steel sheet to 25mm wide and 55mm long workpieces. Before the surface treatment, the workpieces had to be cleaned and degreased using methanol. We searched for parameters that do not cause any visible changes on the surfaces. Among the parameters of the treatment we were able to change the output power of the laser. We used contact angle measurement to examine the wettability. We used distilled water to the contact angle measurement. On the untreated workpiece we measured 89°contact angle on distilled water and we found that the contact angles decreased with the increase in laser output power as seen on Figure 1.

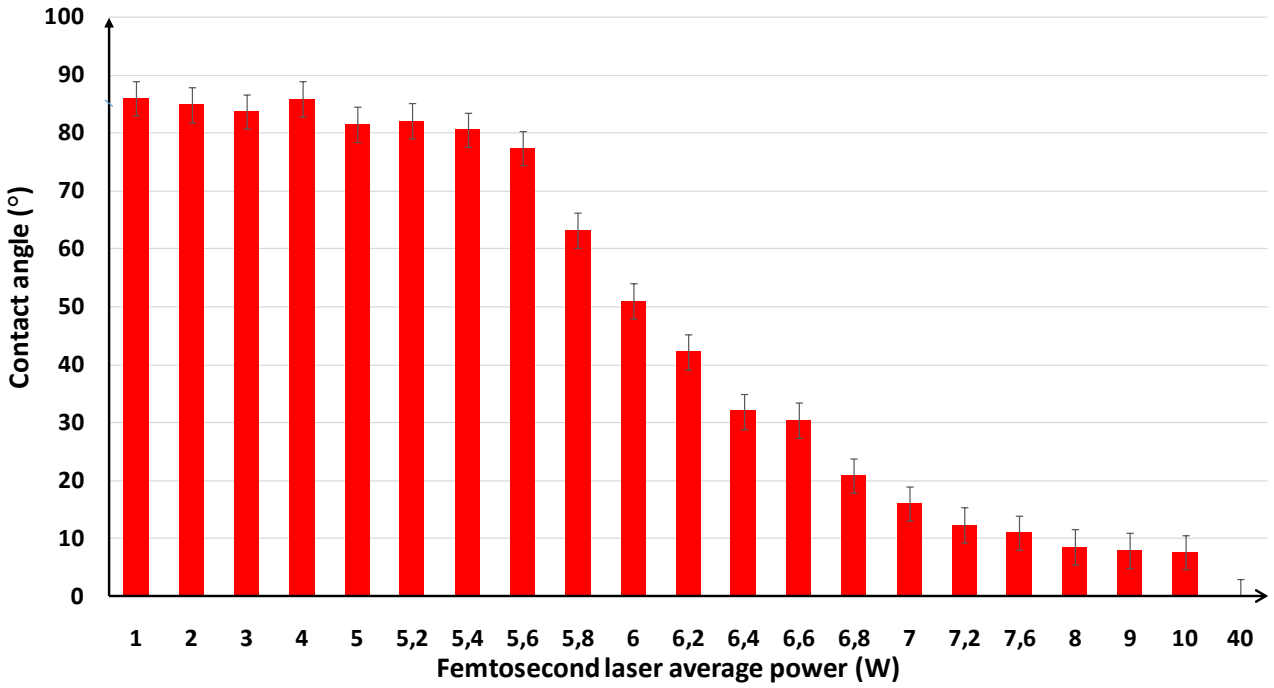

Figure 1 Distilled water contact angles on laser treated surface

We also investigated how long the surface treatment effect lasts as seen on Figure 2.

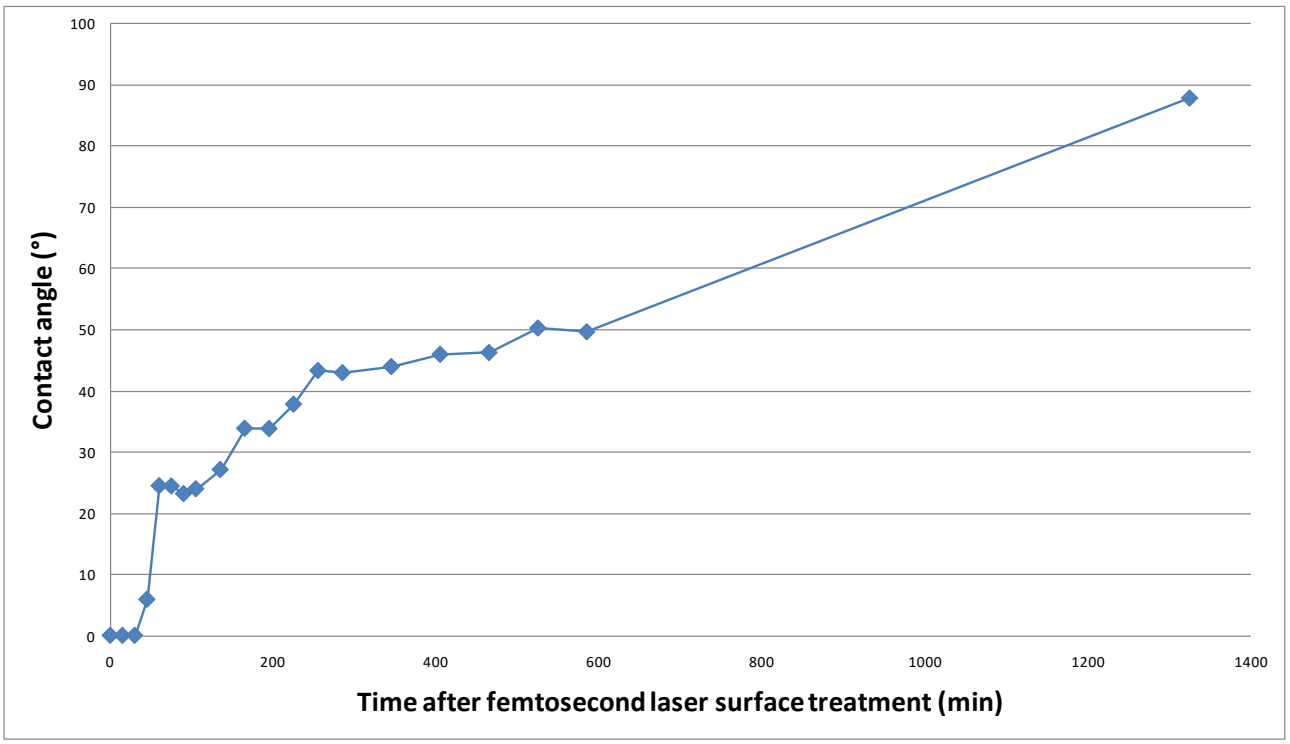

Figure 2 Contact angle changing after surface treatment

We found that femtosecond laser surface treatment can improve the wettability of high strength steels thus joints strength should improve.

ACKNOWLEDGMENTS
This research was supported by EFOP-3.6.1-16-2016-000014. The Project is supported by the Hungarian Government and co-financed by the European Social Fund.

ZEOLITE FILLED PLA (POLYLCATIC-ACID) AND THEIR PROPERTIES

TAMÁSI Kinga PhD, KOVÁCS Annamária, IBRAHIM Jamal Fadoul Mohammed PhD
Institute of Ceramic and Polymer Engineering, University of Miskolc
E-mail: polkinga@uni-miskolc.hu, kovacs.annamaria.uni@gmail.com, jamalfadoul@gmail.com

Keywords: PLA, zeolite filler, biodegradable, nanocomposites

We studied the effect of one type of zeolite ($NaAlO_2$) in biodegradable poly(lactic acid)(PLA), with a particular interest in the improvement of mechanical-surface properties [1, 2]. Using the zeolite filler of a two different size fraction: under 160 µm and above 160 µm sizes, in 3 different contents: 5; 10 and 20 phr. Samples are prepared the meltmixing process by means of a Brabender mixer. We started by characterizing the mechanical properties (Shore D hardness test and tensile strain by INSTRON), surface and morphology test were determined by a stereoregular microscope and a FT-IR spectroscope (Bruker Tensor 27). Then a comparative study on the mechanical and surface properties of these two type of composites has been conducted. It was shown that these two families present almost similar properties. The strongpoint of the nanocomposites was their good mechanical properties (high tensile strength), in front of the surface-homogenity properties.

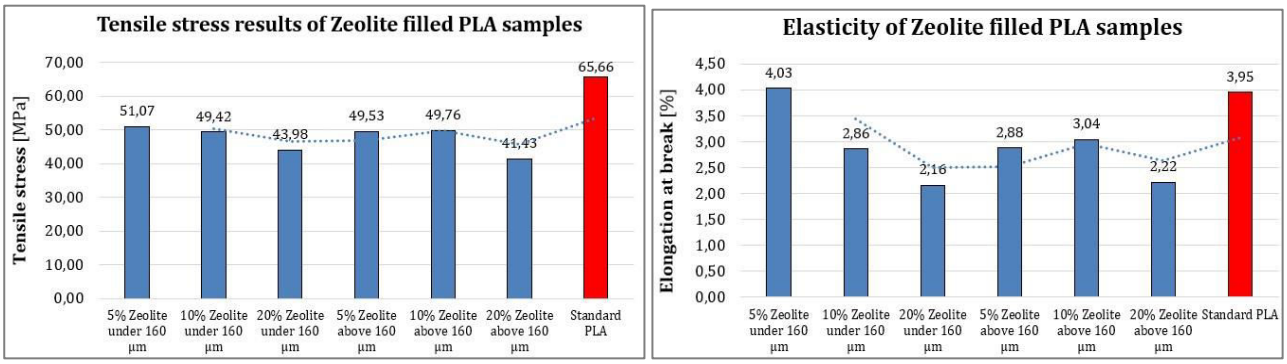

Figure 1 Mechanical properties of Samples

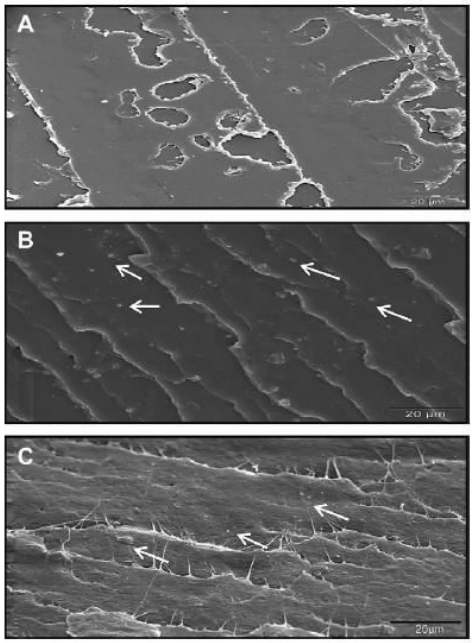

Figure 2 SEM images of PLA and PLA/zeolite composites.
A: PLA magnification: 1000x, scale bar 20 mm;
B: PLA/type 4A magnification:1000x, scale bar:20 mm;
C: PLA/chabazite magnification:1000x scale bar: 20 mm. Arrows indicate the zeolite particles [1]

ACKNOWLEDGMENTS
"The described article/presentation/study was carried out as part of the EFOP-3.6.1-16-00011 "Younger and Renewing University – Innovative Knowledge City – institutional development of the University of Miskolc aiming at intelligent specialisation" project implemented in the framework of the Szechenyi 2020 program. The realization of this project is supported by the European Union, co-financed by the European Social Fund".

REFERENCES
[1] I.E. Yuzay, R. Auras, H. Soto-Valdez, S. Selke, *Effects of synthetic and natural zeolites on morphology and thermal degradation of poly(lactic acid) composites,* Polymer Degradation and Stability, 95, 1769-1777., 2010.
[2] D. Bendahou, A. Bendahou, Y. Grohens, H. Kaddami, *New nanocomposite design from zeolite and poly(lactic acid)*, Industrial Crops and Products, 2015.

THERMAL RESPONSE OF A BRICK FILLED WITH PCM COMPOSITE

THALMAIER György PhD, COBÎRZAN Nicoleta PhD
Technical University of Cluj-Napoca, Romania
E-mail: Gyorgy.Thalmaier@sim.utcluj.ro, Nicoleta.Cobarzan@ccm.utcluj.ro

Keywords: Clay brick, PCM composite, Paraffin wax, Aluminum chips

Paraffin is the most commonly used commercially available organic, low temperature phase change materials (PCM) for latent heat storage. Its main advantage is its low cost good thermal energy storage density, thermal behaviour and varied phase change temperature. Paraffin waxes are a group of saturated hydrocarbons with general formula C_nH_{2n+2}. By varying the chain length, the melting temperature the specific heat of fusion, densities and specific heat capacities differs also. The main drawback of the paraffin waxes is their reduced thermal conductivity, its conductivities reported in literature are between 0.15 and 0.36 W/mK [1]. These low values reduce the paraffin waxes reaction times during their phase change [2, 3]. The heat can be delivered or extracted from a phase change material without a significant change in temperature. Thus, phase change materials (PCMs) can be used to stabilize the interior temperature in a building.
The thermal conductivity can be enhanced by adding high conductivity materials or particles into the PCM material The present study goes this way and adds a new feat by using metallic recycled aluminum alloy particles to enhance the conductovity and test the PCM composites functionality inside a real clay brick.
Thus, in this respect, the behaviour of two bricks one filled with PCM composite material and an identical, empty brick was compared. The PCM paraffin composite with a melting temperature of 52 °C containing ~ 30% volume aluminium particles to increase the thermal conductivity. The addition of 30% aluminium particles was chosen in order to get between the metallic particles a mechanical contact and to limit their sinking in the liquid PCM. The two bricks were insulated from each other and from the outside environment with 100 mm thick expanded polystyrene. They had only the front and back side open to the environment to assure a well-controlled heat flux. The assembly was heated on the front surface with a heat flux of about 0.7 W / m^2. The schematics of the experimental setup used is presented in the figure 1.

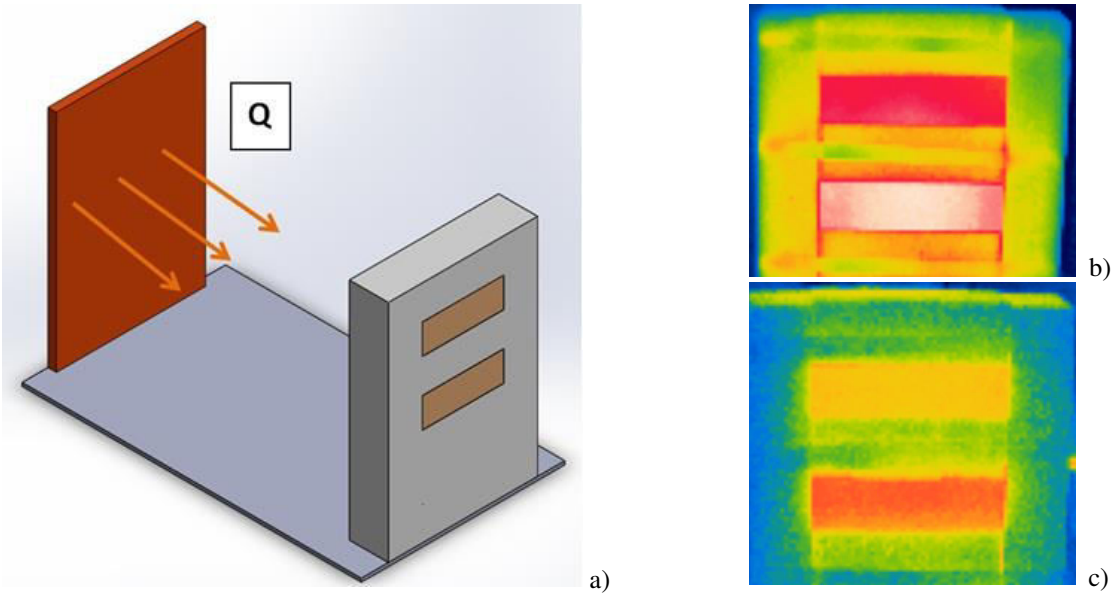

Figure 1 Experimental setup a) and sample IR images: b) front side and c) back side

The temperature variation was monitored by non-contact IR thermal imaging. Images were taken every 15 minutes on the front and back side of the bricks. The obtained images were analysed and the temperature variation with time was evidenced.

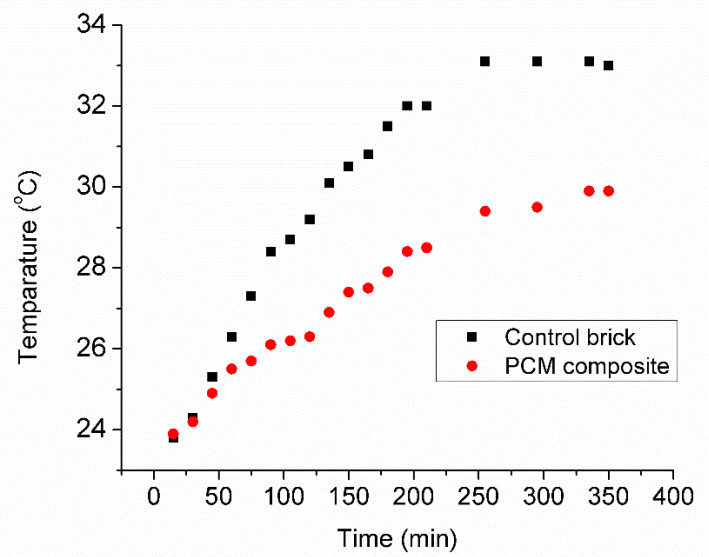

Figure 2 The temperature variation with time on the bricks back side

During the experiment a slower temperature increase of the bricks containing the PCM composite was observed on both the heated face and the unheated side. When the bricks temperature exceeded 25 °C the heating rate was lowered initially by the PCM's higher heat capacity and later by its phase change. A maximum of 3 °C temperature difference was measured after 6 h of heating. This temperature difference can lead to important savings in cooling costs in summer.
Further optimisation is envisaged in order to improve the PCM composites effect.

ACKNOWLEDGMENTS
This work was supported by the Romanian National Authority for Scientific Research and Innovation, CNCS/CCCDI – UEFISCDI, project number PN-III-P2-2.1-BG-2016-0203 within PNCDI III; 71BG/2016.

REFERENCES
[1] K. Sasaguchi and R.J. Viskanta, *Energy Resources Technol*., 111, 43, 1989.
[2] M. Akgun, O. Aydin, K. Kaygusuz, *Energ. Convers. Manage.*, 48, 669, 2007.
[3] Z. Gu, H. Liu and Y. Li, *Appl. Therm. Eng.*, 24, 2511, 2004.

LITERATURE OVERALL OF FATIGUE ANALYSIS APPROACHES OF VEHICLE COMPONENTS MADE OF RUBBER

TOMPOSNÉ SZÜLEI Veronika
Department of Applied Mechanics, University of Széchenyi István
E-mail: szule.veronika@sze.hu

Keywords: fatigue analysis, influences of temperature, prediction models, thermo-viscoelastic-damage coupling

Generally, the most frequently used structural materials are metals which have high strength and stiffness. However, there are many cases when other important properties come to the front, as well as high deformation capacity with elastic behavior, high viscosity namely good damping effect. Due to its above-mentioned properties, rubber is widely used in vehicle and automotive industry. Vehicle components made of rubber usually exhibit large deformations. Cyclic finite deformations generate temperature in hyperelastic materials. Furthermore it is necessary to take into consideration the effects of ambient temperature. The mechanical properties of rubber depend on temperature and temperature changes can accelerate chemical alteration processes which lead to the material deterioration and fatigue processes.
Research on fatigue behavior and fatigue properties of rubber has a great significance for predicting fatigue life and improving durability of rubber products. There are several studies on the fatigue behavior of rubber-based materials, but there is less research in the fatigue life prediction considering the influence of temperature and temperature changes.
The first purpose of this paper is summarizing the influence of temperature and temperature changes on the fatigue behavior of rubber. The second purpose of this study is to provide an overview of the state of the art on the fatigue life prediction of rubber with primary focus on the different methods (prediction models using finite element method and experimental results) available for prediction of fatigue life under the influence of temperature and temperature changes. This study is the basis of the following research which will include the modeling of the temperature-changing induced fatigue behavior and fatigue life prediction of rubberlike materials by using self-developed finite element code.
The fatigue life decreases when temperature increases due to the effects of working temperature and heat in rubber material. Two main approaches can be distinguished for analyzing fatigue life in rubber components. These are the crack nucleation approach and crack growth approach. Elevated temperature has a deleterious effect on rubber, both on crack nucleation life, and on fatigue crack growth rate. For rubber during displacement controlled test, fatigue life drops significantly as the temperature increases 100 °C [1,2]. These temperature effects occur independently of any chemical processes that may occur due to aging. The effect of temperature on the mechanical and fatigue behavior of rubber will be discussed in Table 1 [3,4].

Table 1 Effect of temperature on the mechanical and fatigue behavior/properties of rubber

Framework	Investigated property	Consequence
Lu et al, Lake and Lindley	Fatigue resistance	decreases when temperature increases.
Zhang et al.	Thermal-oxidative ageing (sulfur bond failure and recombination)	accelerates when temperature increases and it leads to decay its antifatigue property.
Ruellan et al.	Material stiffness increases	when temperature increases
Zhang et al.	Elastic response of rubber	decreases SIC (strain induced crystallization)
Mars and Fatemi	Rate-independent hysteresis	depends on temperature.
Le Chenadec	Lifetime reinforcement	decreases as temperature increases

Fatigue life prediction due to temperature changes has a substantial significance for rubber components to ensure their reliability and safety. There are several studies on the fatigue life of rubber materials, but there is less research into fatigue life prediction considering temperature factors. Table 2 contains and summarizes the fatigue life prediction methods for rubber materials and fatigue life prediction methods in consideration of the effects of temperature [5,6].

Table 2 Fatigue life prediction methods of rubber

Framework	Prediction method
Mars and Fatemi	Investigated that the fatigue life of rubber material changes with temperature.
Neuhaus et al.	Carried out fatigue tests to study the influence of chemical an thermal ageing.
Shangguan et al.	Established three kinds of fatigue life prediction models at different temperatures using the engineering strain as damage parameter.
Fatemi et al.	Applying damage criterion: maximum principal strain and Miner's linear cumulative damage rule and using FEA.
Woo et al.	FEA and life prediction of rubber composites by using Green-Lagrange strain as fatigue damage parameter
Suryatal et al.	Predicted the fatigue life of a railway elastomeric pad by combining the experiment of material properties and using the Mooney-Rivlin model for FEA. Maximum first principal elastic strain was selected as fatigue damage parameter.
Seichter et al.	Summarized the advantages of fatigue crack growth theory.
Wang et al.	Computed three fatigue damage parameters by finite element method, namely: logarithmic principal strain, Cauchy principal stress and starin energy density for fatigue life. Their prediction model is based on the least-square method.
Shangguan et al.	Predicted the fatigue life of rubber isolator by choosing and analysing different fatigue damage parameters.
Zhang et al.	Proposed a prediction model with temperature as the dependent variable and predicted the fatigue life of rubber materials at different temperatures.
Le Saux et al.	Heat build-up protocol and micro-tomography measurements, by relationship between temperature rise and maximum principal strain to explain fatigue behavior.
Guo et al.	Developed a new thermo-viscoelastic-damage approach, in accordance with thermodynamic principles and the proposed model was implemented into a finite element program.

There are some questions in which future progress can be made: Guo et al. developed a new approach which is able to predict the fatigue thermomechanical response in rubbers, and in which the authors used the Arruda-Boyce model to determine free energy functions. The first question is raised what are the results of this approach using other models to predict the fatigue thermomechanical response. This paper presented the properties which are affected by temperature. One of these properties is SIC. Another question is what are the conditions of fatigue-induced SIC?
This study summarized the influence of temperature and temperature changes on the fatigue behavior of rubber and made an overview of the state of the art on the fatigue life prediction of rubber with primary focus on the different methods available for prediction of fatigue life under the influence of temperature.

ACKNOWLEDGMENTS
„SUPPORTED BY THE ÚNKP-19-3-III-SZE-7 NEW NATIONAL EXCELLENCE PROGRAM OF THE MINISTRY FOR INNOVATION AND TECHNOLOGY"

REFERENCES

[1] J. Zhang, F. Xue, Y. Wang, X. Zhang, S. Han, *Strain energy-based rubber fatigue life prediction under the influence of temperature* Royal Society Open Science, 5(10), 1-13., 2018.
[2] B. Ruellan, J.B. Le Cam, I. Jeanneu, F. Canévet, F. Mortier, E. Robin, *Fatigue of natural rubber under different temperatures*, International Journal of Fatigue, 124, 544-557., 2019.
[3] P. Behroozinia, S. Taheri, R. Mirzaeifar, *A review of fatigue and fracture mechanics with a focus on rubber-based materials,* Proceedings of the Institution of Mechanical Engineers Part L Journal of Materials and Aplications, 4(2017), 1-16., 2017.
[4] J.T. Bauman, *Fatigue, Stress, and Strain of Rubber Components*. Hanser Publishers, Münich, 2008.
[5] W.V. Mars, A. Fatemi, *A literature survey on fatigue analysis approaches for rubber,* International Journal of Fatigue, 24, 949-961., 2002.
[6] Q. Guo, F. Zairi, X. Guo, *A thermo-viscoelastic-damage constitutive model for cyclically loaded rubbers,* International Journal of Plasticity, 101, 106-124., 2018.

EFFECT OF COPPER-SULFATE AND HUMATE MODIFIED CELLULOSE SHEETS ON THE SHELF-LIFE OF BERRIES

TÓTH Annamária, HALÁSZ Katalin PhD
Simonyi Károly Faculty, Institute of Wood Based Products and Technologies, University of Sopron
E-mail: toth.annamaria@phd.uni-sopron.hu, halasz.kata@uni-sopron.hu

Keywords: composite, cellulose, copper(II)-sulfate, humate, antimicrobial

Shelf life of packaged foods is mainly influenced by the presence of microorganisms, fungi and bacteria. The most serious disease is caused by Listeria genera among the bacteria that cause deterioration which can reproduce under chilled conditions, and modified atmosphere packaging (MAP) does not inhibit its reproduction either. So, even frozen vegetables can be a source of human listeriosis. In 2018, several frozen vegetables were recalled by the European Food Safety Authority (EFSA) and the European Center for Disease Prevention and Control (ECDC) to curb an epidemic caused by an aggressive bacterial variant of Listeria monocytogenes (EFSA 2018).
Humic acid can be extracted from mineral coal (Dogan et al., 2015; Erdogan et al., 2007; Kumar et al., 2013). Alkali humates, the water-soluble salts of humic acids are prepared by alkaline extraction from lignite of high humic acid content. The most commonly used bases for extraction are potassium hydroxide and sodium hydroxide. The alkaline humates thus prepared are potassium humate and sodium humate. These alkali humates bind well to metals through their carboxyl and hydroxyl, and can also bind well to cellulose fibers.
The aim of our research was to develop an active, cellulose-based packaging that is both antimicrobial and economical to produce. Using humate and adding copper sulfate, linter cellulose based test plates were prepared. There was also a differentiated control sheet, a sheet made with copper sulphate only, a sheet with potassium humate only, and a sheet made with humate and copper sulphate. The prepared paper sheets were examined for the shelf life, elemental composition and surface morphology of raspberry grains, as well as the amount of Cu ion released from the sheets.

RESULTS

Raspberry placed on non-$CuSO_4$ test sheets deteriorated most rapidly. Raspberry deterioration was slowed down by sheets made with the addition of copper sulphate (Figure 1). Sample containing Cu-cellulose and humate was the most effective in slowing down the rashberry deterioration. Compared to the control sample, the test sheets slowed the mold growth and fermentation of raspberries.

Figure 1 Photographs of deteriorating raspberries

CONCLUSIONS

During the examination, there were obvious differences between the fermented raspberry grains. Based on the results it can be concluded that the sheet made with the addition of copper sulfate and humate has antimicrobial effect and increases the shelf life of the fruit. In the future, it would be worth examining the effects of sheets on other vegetables and fruits, as well as examining the gas-binding capacity of the test sheets, especially for deterioration stimulating gases (ethylene, oxygen, etc.).

REFERENCES

[1] A. Ricci, A. Allende, D. Bolton, M. Chemaly, R. Davies, B. Nørrung, *Listeria monocytogenes contamination of ready-to-eat foods and the risk for human health in the EU*, EFSA Journal, 16(1), e05134., 2018.

[2] H. Dogan, M. Koral, A. Vatansever, T. Inan, M. Ziypak, Z. Olgun, Ü. Beker, *New Method for the Production of Barium Humate from Turkish Coal*, Advances in Chemical Engineering and Science, 5(3): 290., 2015.

[3] S. Erdogan, A. Baysal, O. Akba, C. Hamamci, Interaction of Metals with Humic Acid Isolated from Oxidized Coal. Journal of Environmental Studies, 16: 671-675., 2007.

[4] D. Kumar, A.P. Singh, P. Raha, A. Rakshit, P. Kishor, C.M. Singh, *Potassium Humate: A Potential Soil Conditioner and Plant Growth Promoter,* International Journal of Agriculture, Environment and Biotechnology, 6(3): 441-46., 2013.

HYBRIDIZED, DUAL-MIXED VARIATIONAL FORMULATION FOR THE DEVELOPMENT OF *hp*-SHELL-FEM: MATHEMATICAL MODEL AND CONVERGENCE BEHAVIOR

TÓTH Balázs PhD
Institute of Applied Mechanics, University of Miskolc
E-mail: mechtb@uni-miskolc.hu

Keywords: hybridized variational formulation, dual-mixed *hp-version* FEM, shells of revolution, dimensional reduction

The developed *hp*-version finite element method (FEM) is based on a three-field, dual-mixed (DM) variational formulation, using weakly imposed symmetry conditions for the stress tensor components along the thickness. This complex approach yields an indefinite linear algebraic system of equation [1, 2]. These structural FEMs provide locking-free numerical results, the solution of the resulting equation system can become a computationally expensive procedure [1, 2]. To circumvent this drawback, a new vector is introduced as hybrid, interface variable living only on the mesh skeleton. In this case the effective system matrix can be effectively inverted elementwise, decreasing the computational cost. This means that the original three-field variational form is transformed into a discretized, hybrid-DM one with a bit larger number of degrees of freedom (DOF) [3].

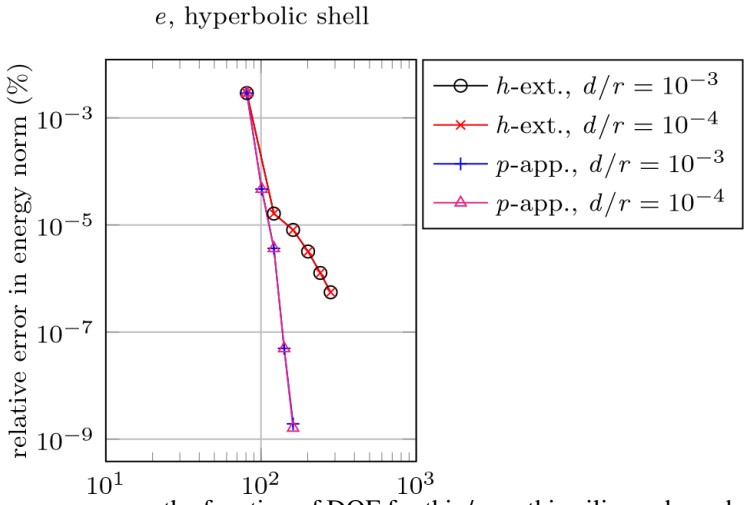

Figure 1 Relative error convergence as the function of DOF for thin/very thin silicone hyperboloid shell with free ends

Based on this latter detailed hybrid-mixed variational formulation, a new, *hp*-version, dimensionally reduced, general axisymmetric shell FEM will be presented for the boundary value problems of thin, linearly elastic shells of revolution. The computational performance of the constructed hybrid-mixed *hp*-shell-FE is tested through some representative bending-shearing problems (including extension-compression) for different shell geometries: singly- and doubly curved shells with positive and negative Gaussian curvature. Through these numerical computations it has been verified that the presented *hp*-shell-FEM is shear- and membrane locking-free, i.e., gives realiable and robust (uniformly convergent) results not only for the displacements but also for the stresses in the case of both membrane- and bending-dominated situations [3], see, for example, the convergence histories of the relative error measured in energy norm for *h*-extension (classical mesh refinement strategy) and *p*-approximation in Figure 1. Of course, the *p*-convergence is much faster than the *h*-convergence.

A nice feature of the suggested *hp*-FEM is that it can be applied to modeling not only thin but also moderately thick shell structures with considering transverse shear deformations. Besides, both the through-the-thickness variation and the membrane stress normal to the shell mid-surface have been retained as independent variables, making it much easier to build up shell models for contact problems of shells, later. This latter ascertainment has arisen from the particular feature of the presented dimensional reduction process dictated/guided by the hybrid DM variational formulation [3], i.e., these results can not be considered as any modification or improvement of the existing theoretical models appearing in the scientific literature. In Figure 2, the von Mises effective stress is plotted on the deformed shell mid-surface for a moderately thick silicone hyperboloid shell, using a very small number of element (two-element mesh) and a very high polynomial degree (p=10), thereby illustrating the efficiency of the *p*-version approximation technique.

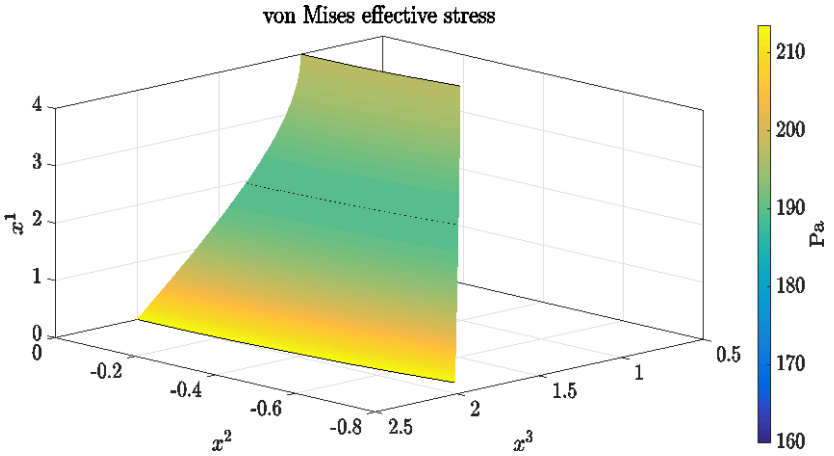

Figure 2 Von Mises effective stress for moderately thick silicone hyperboloid shell with free ends

ACKNOWLEDGMENTS

The described work was carried out as part of the EFOP-3.6.1-16-2016-00011 "Younger and Renewing University - Innovative Knowledge City - institutional development of the University of Miskolc aiming at intelligent specialisation"
project implemented in the framework of the Szechenyi 2020 program. The realization of this project is supported by the
European Union, co-financed by the European Social Fund. Besides, this research was supported by the National Research, Development and Innovation Office NKFIH under Grant No. K115701.

REFERENCES

[1] W. Qiu, L. Demkowicz, *Mixed hp-finite element method for linear elasticity with weakly imposed symmetry*. Computer Methods in Applied Mechanics and Engineering, 198, 3682-3701, 2009.
[2] B. Tóth, L.G. Kocsán, *Comparison of dual-mixed h- and p-version finite element models for axisymmetric problems of cylindrical shells*. Finite elements in Analysis and Design, 65, 50-62., 2013.
[3] B. Tóth, *Hybridized dual-mixed hp-finite element model for shells of revolution.* Computers and Structures, 218, 123-151., 2019.

ANALYSIS OF METHODS TO DETECT BEARING FAILURES

TÓTH Dániel, TAKÁCS György PhD, SZILÁGYI Attila PhD
Department of Machine Tools, University of Miskolc
E-mail: toth.daniel@uni-miskolc.hu, takacs.gyorgy@uni-miskolc.hu, szilagyi.attila@uni-miskolc.hu

Keywords: condition monitoring, bearing, fault detection

Bearings can be found widely in industrial and domestic applications. They are vital components of most mechanism and their working conditions influence the operation of the entire machinery directly. Even if bearings are being used under optimal conditions, sooner or later material fatigue will occur. Among other things poor operating environment, contaminated or peculiarly moist areas and improper handling practices induce untimely bearing failures. Bearing faults may cause machine breakdown and might even lead to catastrophic failure. In order to prevent unexpected events, bearing defects should be detected as early as possible.

Failure modes with characteristics / Possible causes			Operating conditions					Environmental factor					Lubrication					Mounting							Other					
			Overload	Overspeed	Excessive freq. of load/speed changes	Vibrations	Shaft/housing deflection	Temperature too high/low	Dust and dirt ingress	Water ingress	Electrical leakage	Wrong viscosity	(Consistency) additives selection	Lack of lubricant	Excess of lubricant	Impurities	Incorrect handling (shock loads)	Mounting procedures	Fit too tight	Fit too loose	Tilting/misalignment	Incorrect setting	Incorrect locating (clamping)	Storage	Transportation (vibration/shock)	Bearing selection	Equipment design	Manufacturing concerns	Material concerns
Fatigue		Flaking, spalling, peeling	•				•	•				•	•	•			•	•	•		•	•			•	•	•	•	•
		Burnishing, microcracks		•	•	•		•	•	•	•	•	•	•	•	•		•				•		•		•	•		•
Wear	Abrasive	Excessive wear		•	•	•	•	•	•	•	•	•	•	•		•				•	•	•	•			•			•
		Scratches, scores		•	•				•				•			•	•	•							•				
	Adhesive	Seizing marks, smearing	•		•		•	•				•	•	•	•			•	•	•	•					•	•	•	•
		Hot runners	•	•	•		•	•				•	•	•	•			•	•		•	•	•			•	•	•	•
Corrosion		Moisture corrosion								•			•			•		•						•	•		•		
		Fretting corrosion	•		•	•	•													•	•	•	•			•	•	•	
		False brinelling			•	•							•							•				•	•	•			
Electrical erosion		Craters, fluting									•																•		
Plastic deformation		Depressions	•				•	•							•		•	•	•		•	•	•	•	•	•			•
		Debris indentation							•							•	•	•									•	•	
		Nicks, gouges															•	•										•	
Fracture & cracking		Forced fracture	•	•				•									•	•	•		•	•	•			•	•	•	•
		Fatigue fracture	•	•	•	•	•													•	•	•	•			•	•	•	•
		Thermal cracking	•	•	•			•				•		•	•			•	•			•					•		•

Figure 1 Bearing faults and causes [1]

Each failure creates its own typical mark. Defects can be divided into primary or secondary ones in several cases. Primary failures are for example the corrosion, wear, indentations, smearing, surface distress and the passage of electric current. Even these defects may lead to scrapping the bearings in consequence of noise, low efficiency, vibration and so forth. Secondary defects such as flaking and cracks are rooted in primary ones. A defective bearing often indicates a combination of secondary and primary failure.
Condition monitoring is one possibility of a preventive maintenance program. The information collected can be used to specify machinery problems and corrective actions can then be implemented. Several methods are used for the detection

and diagnosis of bearing failures. These methods are acoustic measurements, lubricant analysis, temperature monitoring, lubricant analysis, vibration analysis etc.

Table 1 Fault groups and condition monitoring methods [3]

	Hard-particle contamination	Lubrication faults	Water-contamination	Electric faults	Surface faults	Subsurface faults
Acoustic emissions	X	X	-	X	X	X
Lubricant analysis	X	X	X	-	-	-
Thermal imaging	X	X	-	X	X	X
Vibration analysis	X	X	-	X	X	X

An investigation via lubricants is capable of revealing any kind of defects originated from the abrasion process. If this procedure is performed frequently, valuable pieces of information can be obtained on the remanent lifetime of the bearings. The extent of the defect rooting in the corrosion can be estimated numerically by the investigation of the physical and chemical properties of the lubricants. Since, as the result of the investigation, there are several interfering output parameters to be analyzed, even the companies specialized on such an assessment has to apply computerized expert systems. Since the noise emitted by bearings is composed of all the types of defects developed during the manufacturing process and the working time of the bearings, the effective values of certain noise quantities enable quick lifetime estimation. However, in the lack of sound-proofing, the noise from the background decreases the effective noise detection significantly, so this method needs to be performed in a dead room. The AE transducer is sensitive about high natural frequencies. The transducer signal is processed by a band-filter built in the preamplifier. The AE process is capable of detecting defects forming deep inside the material, even before it would propagate out to the surface [2]. When the assessment of a bearing is performed by vibration analysis, several signal processing techniques can be considered. Among these processes the spectral analysis is perhaps the most widely spread one. A bearing is supposed to be a flexible part with the capability of producing vibrations at certain natural frequencies and along certain directions. Once the spectrum diagram of such vibrations has been detected and analyzed, then the natural frequencies can be „visualized", and finally, the defected bearing parts can be identified. As the intensity of the defects develop in time, the spectral diagram keeps on being modified. Vibration based methods are well established for the condition monitoring of bearings, although they are not so effectual in detecting early defects in the bearing. Acoustic emission is receiving increasing attention as a complementary method for condition monitoring of bearings as acoustic emission is enough sensitive to initial defects.

ACKNOWLEDGMENTS
Supported by the ÚNKP-19-3 New National Excellence Program of the Ministry for Innovation and Technology.

REFERENCES

[1] Railway technical handbook, *Volume 1*, SKF, 2011.
[2] N. Tandon, A. Choudhury: *A review of vibration and acoustic measurement methods for the detection of defects in rolling element bearings.* Tribology International 32 469-480., 1999.
[3] R. Schulz, S. Verstockt, J. Vermeiren, M. Loccufier, K.S. Stockman, V. Hoecke, *Thermal Imaging for Monitoring Rolling Element Bearings*. QIRT, 2014.

FUNCTIONAL EXAMINATION OF MACHINE TOOL SLIDEWAY WITH HYDRAULIC RELIEF

TÓTH Sándor Gergő, TAKÁCS György PhD
Department of Machine Tools, University of Miskolc
E-mail: toth.sandorgergo@uni-miskolc.hu, takacs.gyorgy@uni-miskolc.hu

Keywords: machine tools, slideways, hydraulic relief

Machine tool guideways are one of the most important components of machine tools, because they support moving components (carriages, rams etc.) so that they can achieve high accuracy and high speed during positioning or machining. In addition to the well-known types of guideways (sliding, rolling and hydrostatic), theoretical research of combined guideway types has recently begun. Partially floating sliding guideways are one of sub-type of these combined guide systems. If the hydrodynamic slides provide high stiffness and rapid damping, they have high frictional resistance. On the other hand, although the frictional resistance of hydrostatic guideways is low, there are difficulties, especially in the feed direction. In order to improve both stiffness and damping capability, a new design can be used that allows for an adequate amount of contact between the sliding surfaces, while retaining some of the benefits of non-contact operation typical of hydrostatic guides. The slideways with hydraulic relief is a construction in which a pressurized lubricant such as lubricant oil is placed between the sliding surfaces to reduce the load on the sliding surface, thereby allowing a heavy body to move smoothly with minimal friction loss. The term "partially floating guide" derives from this characteristic of mixed lubrication, where part of the sliding surface slides non-contact while the other surfaces contact each other [1].

Figure 1 The assembled measuring device of the slideway with hydraulic relief

The maximum value of unloading is not yet determined, and according to an empirical equation, up to 70% unloading can be achieved [2]. A measuring device was assembled for functional testing of the guideway. The trial pads are located on the ground side surfaces of a central rectangular beam so that each guide surface has 2 to 2 pads. The 4-4 trial pads are mounted on each board in a "V" shape (negative prism shape). One of the baseplates is fixed to the stand and the other to the beams on the lower base. The boards are surrounded by load rings. The trial pads are supplied with oil from a common hydraulic line, so each pressurized recess will have the same pressure, and each support pads have the same hydraulic force. The leakage flow collecting channels are separately discharged per pads, so it is easy to observe when leakage starts at any of the pads. The force applied to each pair of opposing pads can be generated by tensioning a steel ring supported in the pocket at the hydraulic pads' center of loading. The amount of load applied to

the support pads can be adjusted by the tightening torque of the support bolts, the force generated by the elastic deformation of the ring. The deformation of the ring can be measured by strain gauge filament on its circumference. During the measurement, it has been investigated that if the pressure of the pressure recess specimens is gradually increased, then what is the significant pressure reduction in the feed force at the recess pressure. The feed force is calculated from the measured chamber pressure of the hydraulic cylinder actuator. During the test, the tightening torque of the support bolts was adjusted with a torque wrench. The cylinder pressure of the feed cylinder is measured by pressure transmitters connected to the hydraulic connections of the cylinder.

Table 1 3000 kN preloaded cylinder's chamber pressures at given recess pressures and recorded statements during observations

Recess pressure [bar]	Cylinder pressures [bar]				Leakage intensity	Statement
	+ direction (push)		- direction (pull)			
	p1	p2	p1	p2		
0	12,7	2,7	3,2	12,2	No	Starting pressure: 20 bar
5	12,7	2,7	3,2	12,2	It starts dripping weakly on some tubes	Standing, then starts slowly
	10,5	3	4,2	10,8	Dripping on each tube	Strongly slips in the + direction, Slips weaker - in the direction
10	4,2	7,5	2,7	2,7	Flow on the lower pads	Smooth moving

Measurements have shown that by installing hydraulic recesses, the load on the friction guideway can be reduced by the amount of hydraulic force applied to the effective surface of the support pads. The trial slideway system is very sensitive to system defects in parallel conductor surfaces, with a few µm errors leading to the appearance of leakage oil. The amount of leakage oil increases with increasing recess pressure. This is partly due to the greater pressure that drives the flow through the existing gap, and partly to the greater deformation of the loading rings due to the higher loading force induced by higher pressure, which increases the gap size. Furthermore, much more force is needed to start the carriage than to keep it moving.

ACKNOWLEDGMENTS
The described article/presentation/study was carried out as part of the EFOP-3.6.1-16-00011 "Younger and Renewing University – Innovative Knowledge City – institutional development of the University of Miskolc aiming at intelligent specialisation" project implemented in the framework of the Szechenyi 2020 program. The realization of this project is supported by the European Union, co-financed by the European Social Fund.

REFERENCES
[1] T. Saito, *Development of Machine Tool's Guideways- Dynamically Pressurized, Statically Pressurized and Partially Floated Guideways*. JTEKT Engineering Journal English Edition No. 1001E, 57-64., 2006.
[2] N.K. Mehta, *Machine Tool Design and Numerical*. Tata McGraw-Hill Education, 220-221., 1996.
[3] F.M. Stansfield, *Hydrotatic Bearings* The Machinery Publishing Co. LTD., 37-122., 1970.

USING OF THE STATISTICAL METHOD FOR MACHINING PROCESS ANALYZE

JAVOREK Ľubomír
Faculty of manufacturing technology, Technical University in Zvolen
E-mail: lubomir.javorek@tuzvo.sk

Keywords: routing, force, design of experiment, multifactor analyse

The creation of each product which is characterized by shape, dimensions, surface parameters and that would be accepted by potential customer – it is the aim of every production process.
It means, that all parameters of product are defined by technical drawings and must be realized acceptable setting of production process parameters (factors); for machining it is for example cutting speed, feed speed, revolutions, depth of cut, tool geometry etc. The detail information of production process, i.e. the analyze of individual factors and its influence to process are the basic of controlling and the acceptable goal. The statistical methods must not be used for controlling only at the last stage of production, but may by efficient tool for setting or modification these factors before, or during process, bur relevant values must be obtain earlier, usually from experiments.
Design of Experiment (DOE) is an experimental or analytical method that is commonly used to statistically signify the relationship between input parameters to output responses, where by a systematic way of planning of experiments, collection and analysis of data is executed. DOE has wide applications especially in the field of science and engineering for the purpose of process optimization and development, process management and validation tests. A mathematical model has been developed by using analysis techniques such as ANOVA and regression analysis whereby the mathematical model shows the relationship between the input parameters and the output responses.

DESIGN OF EXPERIMENT

The design of experiments and procedures are as follows:

a. Definition of the problem and identification of noise factors.
b. Selection of response variables and selection of control parameters and their levels.
c. Identification of control factor interactions.
d. Selection of the orthogonal array and conducting the matrix experiments.
e. Analysis of the data and prediction of optimum level.

APPLICATION OF DOE IN ROUTING

DOE method was used in routing of aluminium alloy used in automotive and aerospace industry and the aim of experiment was estimate the influence of variables to final force and its components. DOE was applied as a part of process considering monitoring of process and to mark way for minimize of routed part deflection. Purpose was to determine key input factors and their optimal level for a machining process. We realized an experiment with 3 - factor and 2-level, where n factors are studied, each of them with 2 levels. Lower level is marked as -1 and upper level +1. In this case the design of experiment involves all possible combinations of factors and their levels. The number of experiments k with n factors is 2n. Design matrix represents all combination of possible experiments by using both levels of determined factors.

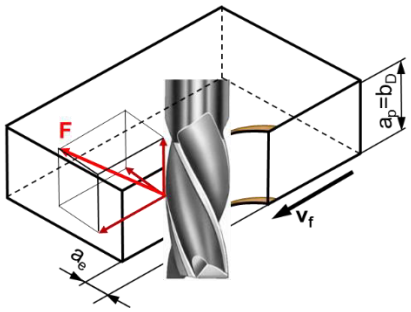

Figure 1 The scheme of machining

As input factors with influence on output characteristics were determined the following factors and their levels:

- revolution speed: the lower limit 4000 rpm and the upper limit 6000 rpm;
- working engagement of a cutting edge a_e: the lower limit – 1 mm; and the upper – 3 mm;
- back engagement of a cutting edge a_p: the lower limit – 5 mm; and the upper – 15 mm.

Design matrix was presented for process of machining (Table 1), individual experiments were realized in random order and each experiment was repeated 3 times.

Table 1 The marking of input factors

	Factor	Units	Symbols		Limits of factors	
			Original	Coded	Lower -1	Upper +1
1	Revolutions	1/min.	n	A	4000	6000
2	Working engagement of a cutting edge a_e (mm)	mm	a_e	B	1	3
3	Back engagement of a cutting edge a_p (mm)	mm	a_p	C	5	15

RESULTS AND DISCUSION

This paper has discussed the influence of cutting parameters like the cutting speed, working engagement of a cutting edge a_e (axial dept of cut) and back engagement of a cutting edge a_p (radial depth of cut), respectivelly using design of experiment method for estabilish the influence of variables to the cutting force components in routing.

Regarding the results were found the most important parameter (respectively sequence of parameters) for the predictions of the final cutting force; in our case it is axial depth of cut, very closely followed by radial depth of cut. The influence of revolutions is not so expressive, but it is by reason of smaller difference between the lowest and the highest value – 50%; in case of axial and radial depth of cut it is 200%.

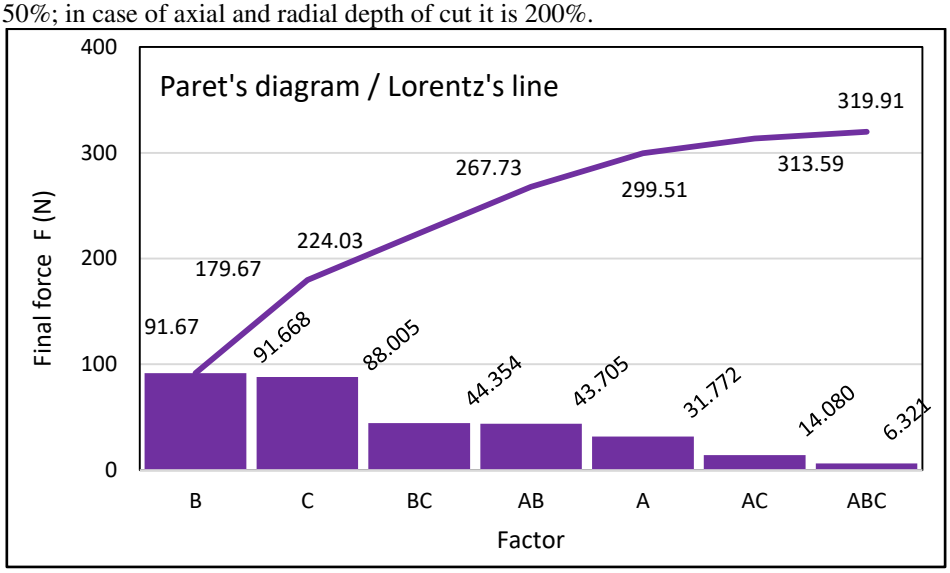

Figure 2 Paret's diagram and Lorentz's line for final force F

ACKNOWLEDGMENTS

This work was supported by the Slovak Research and Development Agency under the contract No. APVV-16-0177 and by the Scientific Grant Agency of the Ministry of Education SR and the Slovak Academy of Sciences Grant No. 1/0822/17.

REFERENCES

[1] Ľ. Javorek, J. Svoreň, M. Kučerová, *Závislosť výslednej sily of otáčok a rýchlosti posuvu obrobku pri pílení buka. (The dependence of results force from revolutions and feed speed during beech sawing).* In Acta facultatis technicae. Zvolen. ISSN 1336-4472. Vol. 22, No. 2, p. 159-167. 2017.

[2] S.P. Kondapalli, S.R. Chalamalasetti, N.R. Damera, *Application of Taguchi based Design of Experiments to Fusion Arc Weld Processes: A Review.* In.: International Journal of Technology and Management. ISSN 1927-9000 | Vol. 2 No. 1, pp. 1-8 2013.

[3] M. Kučerová, M. *Uplatnenie metódy plánovania experimentov v manažérstve kvality (Using methods of design of experiments in quality management.)*Trnava. AlumniPress. p. 92. ISBN 978-80-8096-112-1. EAN 9788080961121, 2010.

[4] T.S. Lee, Y.J. Lin, *A 3D Predictive cutting-force model for end milling of parts having sculptured surfaces.* Int J Adv Manuf Technol 16:773–783. Springer-Verlag London Limited, 2000.

[5] G.W. Vickers, K.W. Quan, *Ball-mills versus end-mills for curved surface machining,* Transactions ASME Journal of Engineering for Industry. 111. pp. 22–26. 1989.

DESIGN OF CHIP CONVEYOR

SZABÓ Kristóf
Faculty of Mechanical Engineering and Informatics, Department of Machine Tools, University of Miskolc
e-mail: szgtszab@gmail.com

Keywords: screw conveyor, design theory, methodology

INTRODUCTION

A drastic increase can be perceived in the operation of the production tools, so the automation of machining processes requires that the auxiliary processes should be performed automatically by structural units and equipment without direct human intervention [1][2]. Screw handling unit is one of the most used machines with continuous operation with some theoretical questions from János Benkő and Sándor Verdes [3][4]. The University of Miskolc, Faculty of Mechanical Engineering and Information Technology boasts a wealth of knowledge in the design methodology of various machines and equipment that was utilized in this topic [5][6][7][8][9].

METHODOLOGY

Before the design process the amount of material separated by the machine was determined. By the multiplication of the amount of separated material by the volumetric factor of the chip, the volumetric flow rate of the actual chip volume to be discharged in one minute could be obtained [10]. The bulk density of the material being transported was determined as it is required to be known to be able to calculate the transport capacity in terms of [tonne per hour].
In case of screw conveyors, the geometric scaling of the screw element could be determined based on formulas used for the definition of the expected transport capacity and maximum speed [11]. The obtained result was rounded up to a standard value. Being aware of the diameter of the screw conveyor, the minimum speed was calculated as a function of the expected capacity. To determine the proper operating parameters of the material handling unit, the maximum carrying capacity at maximum speed should be calculated.
In case of the design of the body elements, where it was important to seek the proper shaping of the bearing and fixing points, the mechanical connections to the bed were designed at the first stage. It was investigated and identified where the material should be counted, as suitable collecting elements should be placed at appropriate points. If the purpose is the transportation and separation of materials with different consistency, the appropriate design solutions should be provided to ensure that these functions can be performed during machine operation. A well-designed chamber at the material transfer points was created to ensure a smooth flow of the process. Suitable structural elements were provided for connection to geared motors and ancillary components. The appropriate filtration and collection of the separated liquids was ensured by means of a container. Being aware of the structural elements formed, the resulting geometrical and different connection dimensions could be determined. Based on the previous correlation, it is possible to determine the required length of the auger rows.
In the following phase, standard parts, such as bearings for geared motors and clutches can be selected. In terms of bearing, it is advisable to select from the range of pre-assembled bearing units, however, where the bearings are surrounded by flowing material, it is preferable to choose a plain bearing to utilize the advantageous installation dimensions. To achieve proper operation, in the case of the motors with worm geared motors, it is advisable to select the low speed and high torque. It is advisable to connect the driving and driven shafts with a flexible coupling.
The control of the parts is necessary because it shows whether the parts have been selected correctly. The motors are checked based on the power required to drive each auger line, which depends on static and dynamic loads. Based on the differential equation of the mass point moving on the helical axis [3], the components of forces acting in each direction could be determined. By applying the parameters defined so far, the power required to move the material, the power requirement due to friction, and the power needed to overcome the material's acceleration resistance can be determined.
The motors are suitable if their rated power is greater than the power requirement of the screw. The selected clutches were checked at the maximum permissible torque [12]. For plain bearings, the check was based on permissible surface pressure [13].

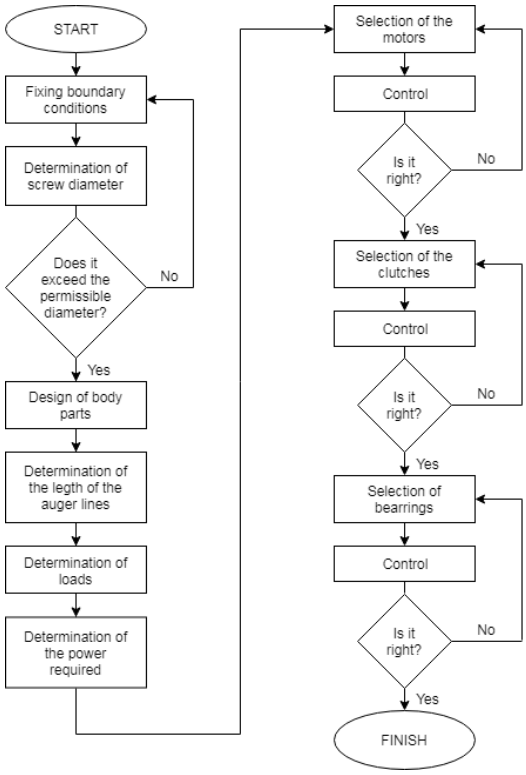

Figure 1 Applied designing method

The applied designing method can be successfully used to define the geometric scaling and designing of screw conveyors. Based on the developed dimensions, the method can be used to accurately determine the static and dynamic loads of the auger lines, which can be used to select and check commercially available standard parts.

ACKNOWLEDGMENTS
The described article was carried out as part of the EFOP-3.6.1-16-00011 "Younger and Renewing University – Innovative Knowledge City – institutional development of the University of Miskolc aiming at intelligent specialisation" project implemented in the framework of the Szechenyi 2020 program. The realization of this project is supported by the European Union, co-financed by the European Social Fund.

REFERENCES

[1] Ch. Bührdel, G. Frömmer *Automata forgácsoló szerszámgépek,* Műszaki Könyvkiadó, 1984.
[2] Gy. Takács, A. Szilágyi, P. Demeter, A. Barak, *Forgácsoló szerszámgépek*, Nemzeti Tankönyvkiadó, 2009.
[3] J.A. Benkő *szállítócsigák néhány elméleti kérdése, Gépgyártástechnológia*, XXXIV (7-8). pp. 274-282. ISSN 0016-8580, 1994.
[4] Verdes, S. *Anyagmozgatás és gépei*, Pannon Egyetem, 2012.
[5] Á. Szombatfalvy, *Szerkezeti elemek tervezésének technológiai szempontjai*, Műszaki Könyvkiadó, Budapest, 1981.
[6] Gy. Hegedűs *A módszeres géptervezés alkalmazása ipari mérőgép fejlesztése estén, Doktoranduszok Fóruma* 2002: Gépészmérnöki Kar szekciókiadványa. 2002.
[7] L. Kamondi, F. Sarka, Á. Takács *Fejlesztés- módszertani ismeretek,* Nemzeti Tankönyvkiadó, Miskolc, 2011.
[8] G. Pahl, W. Beitz, J. Feldhusen, K.-H. Grote *Engineering Design – A Systematic Approach*, London: Springer-Verlag, ISBN 978-1-84628-318-5, 2007.
[9] Gy. Takács, Z. Zsiga, I. Szabóné, Gy. Makó Hegedűs *Gyártóeszközök módszeres tervezése,* Nemzeti Tankönyvkidó, Miskolc, 2011.
[10] T. Kulcsár, *Gépipari technológiai ismeretek,* Pannon Egyetem, 2012.
[11] J. Benkő, Z. Nagy *Tervezési segédlet szállítócsigákhoz,* Szent István Egyetem, Gödöllő, 2013.
[12] G. Németh *Biztonsági tengelykapcsoló méretezése* (Oktatási segédlet), Miskolci Egyetem, Miskolc, 2013.
[13] J. Péter *Géptervezés alapjai,* Miskolci Egyetemi Kiadó, Miskolc-Egyetemváros, 402 old. ISBN 978-963-661-837-7. 2008.

SUPPORTING COMPANIES

THE ISCAME 2019 CONFERENCE AND THE 7th MECHANICAL ENGINEERING INDUSTRIAL EXHIBITION, DEBRECEN

Company name	Website	Location
Coloplast Hungary Kft.	www.coloplast.hu	Nyírbátor
Diehl Aircabin Hungary Kft.	www.diehl.com	Debrecen, Nyírbátor
DKV Debreceni Közlekedési Zrt.	www.dkv.hu	Debrecen
Electrolux Lehel Kft.	www.electrolux.hu	Nyíregyháza
Emerson Automation Solutions	www.aventics.com	Eger
Enterprise Communications Magyarország Kft.	www.enterprisegroup.hu	Budapest
EREDŐ Garázsipari Kft.	www.eredo.hu	Debrecen
EuroSolid Kft.	www.eurosolid.hu	Budaörs
FAG Magyarország Ipari Kft.	www.schaeffler.hu	Debrecen
GYULAI Irányítástechnikai Kft.	www.gyulaikft.hu	Debrecen
HAJDU Autotechnika Ipari Zrt.	www.hajduautort.hu	Téglás
HAJDU Hajdúsági Ipari Zrt.	www.hajdurt.hu	Téglás
Henkel Magyarország Operations Kft.	www.henkel.hu	Körösladány
HOYA Szemüveglencse Gyártó Magyarország Zrt.	www.hoya.com	Mátészalka
KEVIÉP Kft.	www.keviep.hu	Debrecen
KITE Zrt.	www.kite.hu	Nádudvar
Manz Hungary Gépgyártó Kft.	www.manz.com	Debrecen
Promatech Célgépgyártó Kft.	www.promatech.hu	Nagytarcsa
Robert Bosch Automotive Steering Kft.	www.bosch.hu	Eger, Maklár
S&T Consulting Hungary Kft.	www.snt.hu	Budaörs
SPM Instrument Budapest Kft.	www.spminstrument.com	Budapest
TRUMPF Hungary Kft.	www.trumpf.com	Vecsés
Unilever Magyarország Kft.	www.unilever.hu	Nyírbátor
Vitesco Technologies Hungary Kft.	www.continental-corporation.com	Budapest
ZF Hungária Kft.	www.zf.com	Eger

COLOPLAST HUNGARY KFT.
Address: 4300 Nyírbátor, Coloplast út 2.
Phone: +36-42-886-300
Webpage: www.coloplast.hu

About the company

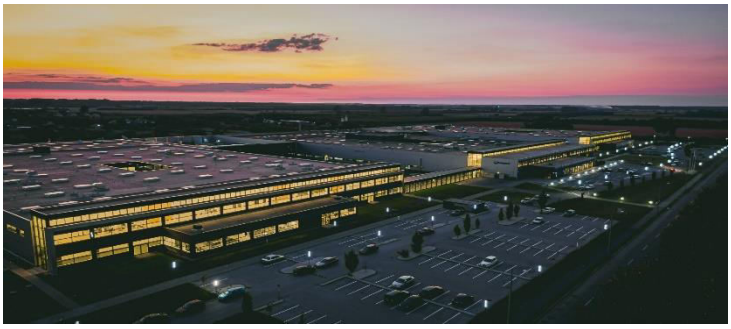

Coloplast develops products and services that make life easier for people with very personal and private medical conditions.

Working closely with the people who use our products, we create solutions that are sensitive to their special needs. We call this intimate healthcare.

Our business includes Ostomy Care, Continence Care, Wound & Skin Care and Interventional Urology. We operate globally and our organization is about 12,000 people strong.

Most of us want to work for a company that makes a difference. Well, in Coloplast you can. Our purpose is to make life easier for people with intimate health care needs. Once you have experienced the impact our products can have, not only on a person's life, but for that person's entire family, you know that you are making a difference.

Why to join?

We are more than 12,000 people in 41 countries. A mix of different nationalities and cultures working together in many languages. But we are also much more. At Coloplast we want you to be you.

Only through a diverse workforce can we innovate and respond to the challenges of our users. Listening means being open to things that are different. We employ the same strategy with our people. If you share our values and see yourself committing to our purpose, we want you to join our company!

Our colleagues are professional experts in their filed, together with being genuinely nice people. They will do what they can to help you succeed and grow and they will expect you to do the same. At Coloplast, being ambitious is about working together to achieve the best results. In total, we might be over 12,000 people, but you will never be lost in the crowd.

For more information please visit our website: www.coloplast.hu!

ELECTROLUX LEHEL LTD.
Address: 4401, Nyíregyháza, Ipari Park
Phone: +36-42-594-856
Webpage: www.electrolux.hu

SHAPE LIVING FOR THE BETTER

Electrolux shapes living for the better by reinventing taste, care and wellbeing experiences, making life more enjoyable and sustainable for millions of people. Through our brands, including Electrolux, AEG, Anova, Frigidaire, Westinghouse and Zanussi, we sell more than 60 million household and professional products in more than 150 markets every year.

WHO WE ARE

Electrolux Lehel Ltd. is one of the subsidiaries of the Swedish Electrolux, the world's leading producer of domestic appliances. Our factory in Nyíregyháza is one of the Group's leading European manufacturing bases, and its main profile is the manufacturing of high-end refrigerators. Electrolux is sustainable and innovative. Continuously developing its operation, our factory also aims at operating optimally taking into account the entire life cycle of the product from production to manufacturing, use, recycling and re-production, using its resources as optimally as possible, as well as minimizing the environmental impact. As an innovative company, we are already working on the introduction of Industry 4.0 digital, industrial automation and robot technologies around the world, and our Nyíregyháza plant will be renovated in the coming years.

Electrolux Nyíregyháza Refrigerator Factory started operations in 2005, and in October this year, we have reached a new milestone: our 10,000,000th product rolled off the production line.

WE BELIEVE

We believe that outstanding taste experiences should be easy for everyone. That there is always a better way to care for our clothes to make them look and feel new longer. That the home should be a place for wellbeing, a place to care for ourselves and our loved ones. To succeed, we continuously rethink and improve our ways of working - internally, and together with our customers and partners. By creating desirable solutions and great experiences that enrich peoples' daily lives and the health of our planet, we want to be a driving force in defining enjoyable and sustainable living.

This is us - at Electrolux we shape living for the better.

Electrolux Nyíregyháza
Nyíregyháza, Nyíregyháza Ipari park, 4400

www.electrolux.hu
www.electroluxgroup.com

EMERSON AUTOMATION SOLUTIONS
Address: 3300 Eger, Bánki Donát u. 3.
Phone: +36-36-531-600
Webpage: www.aventics.hu

Emerson (NYSE: EMR), headquartered in St. Louis, Missouri (USA), is a global technology and engineering company providing innovative solutions for customers in industrial, commercial, and residential markets. Our Emerson Automation Solutions business helps process, hybrid, and discrete manufacturers maximize production, protect personnel and the environment while optimizing their energy and operating costs.

As part of Emerson Automation Solutions, AVENTICS™ is one of the world's leading product brands for pneumatic components and systems. The pneumatic engineering brand provides products and services for industrial automation, as well as the food, packaging, medical, and energy technology industries. For our pneumatics brand, we also develop solutions for the commercial vehicles, marine, and railway technology sectors.

The Emerson pneumatics manufacturing base in Eger produces high quality products. Compressed air cylinders and valves are used, inter alia, in production lines and industrial applications, including large multinational companies operating mainly in the mechanical, shipping, printing, packaging, food, textile and metallurgical industries.

The Emerson plant in Eger is not a mass production company in the classic sense, but rather a specialist in the pneumatic industry specializing in custom solutions. No matter how complex or out of the ordinary, customers' ideas ensure that they are realized - even in very small series. They are particularly well-suited for their unique complexity of handling 1300-1500 customer orders per day, 60% of which cover 1-5 pieces, ready to be delivered on the 7th day after ordering. In addition, the factory offers 25,000 products to its partners, using over 32,000 parts from over 800 suppliers.

The factory is constantly modernizing its machinery fleet, operating a comprehensive quality management system, developing its suppliers and paying great attention to improving delivery accuracy. It also manages occupational safety and the environment through certified systems. By integrating electronics, using high-tech materials and focusing on machine safety and the Internet of Things (IIoT), it is a pioneer in applied and environmentally friendly solutions.

The Emerson pneumatics plant in Eger is aware of the importance of supplying professionals and the growing importance of alternative energy sources. The company combined these two aspects when it announced the first Pneumobil competition in 2008. Student teams of Hungarian and foreign higher education institutions undertake the construction of air-powered vehicles year after year. Preparations for the 13th race in 2020 are under way.

Emerson is actively involved with the University of Debrecen, the University of Miskolc, and the Eszterházy Károly University of Eger in order to provide quality professionals, participate in dual training, provide internships for students.

The Eger plant has become one of the most prestigious and attractive workplaces in the city for many years. Its professional performance is marked by the growing volume of production and the expanding product range. Several Hungarian colleagues of the factory are commissioned to carry out central purchasing, quality and financial activities for the Group. The International Financial Services Center now accounts internationally for its Emerson Group subsidiary in 11 European countries, based in Eger.

ENTERPRISE COMMUNICATIONS MAGYARORSZÁG LTD.
Address: H-1138 Budapest, Váci str. 117-119.
Phone: +36-1-471-2380/ext.2
Webpage:www.enterprisegroup.hu/plm

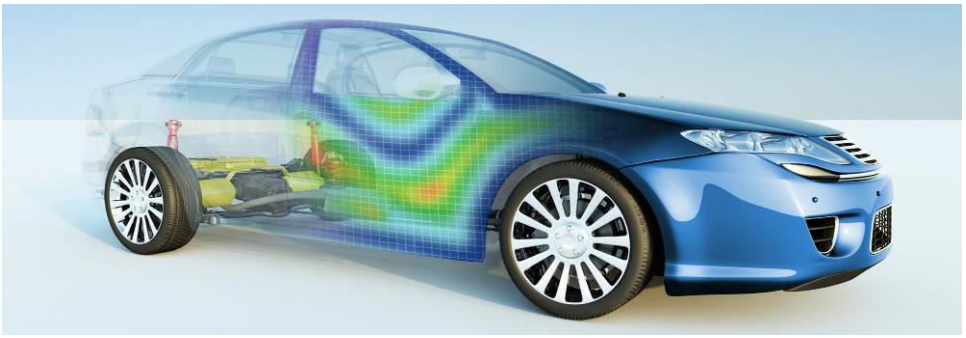

Enterprise Group PLM Business Unit – Engineering Solutions

CAD/CAM solutions and product lifecycle management (PLM) from design to implementation

Our PLM division provides complex engineering solutions and IT services for companies that operate in the field of industry. The market-leading solutions of Siemens PLM and Vero Software cover the entire lifecycle of products - from the original concept, through the design process, all the way to manufacturing - and support product development and recycling. Our team of experts, with decades of experience in engineering, IT and industry related projects, coupled with the stable corporate background of the Enterprise Group, ensures that our clients will always receive reliable solutions that are customised to meet their own particular requirements.

PLM is a complex process which facilitates the management of a product's entire lifecycle. It includes computer-aided design (CAD) and manufacturing (CAM) solutions, but it is more complex than that, as it encompasses the full lifecycle of products. PLM offers advantages such as time-to-market acceleration, product quality improvements, prototype production cost reductions, rapid identification of potential sales opportunities and overall cost savings by recycling previously obtained data and by fully integrating engineering work processes.

Our PLM division supplies the well-known products developed by Siemens PLM Software, as well as their connected services. The division is ready to serve existing and future clients as a distributor of Solid Edge, NX, Tecnomatix-RobotExpert-Process Simulate, Teamcenter, Femap and Preactor..

With solutions from Vero Software, the world's largest CAM-oriented CAD/CAM developer, the division is capable of comprehensively satisfying all the requirements of manufacturing companies. Among these solutions, Edgecam is recommended for production machining, Radan for sheet metal manufacturing tasks, and Alphacam for the wood and stone industries. For the Mould and Die industries, we offer Visi, as an integrated CAD/CAM solution and WorkNC, as the market leading automatic CAM software solution for 2 to 5-axis milling of complex 3D models.

Besides supplying the market's well-known Siemens PLM and Vero Software products and solutions, Enterprise Group's PLM division also helps partners with the introduction of new software, as well as support and updates, training programs and constant availability. Our staff can also call on the knowledge of Enterprise Group's other divisions and rely on the smooth operational background of the company when implementing their own projects.

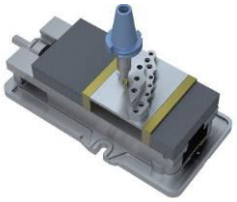

EUROSOLID LTD.
Address: Budapest, 1117 Szerémi út 7/B
Phone: +36-20-222-0454
Webpage: www.eurosolid.hu

EuroSolid Ltd. has been dealing with the introduction and installation of CAD/CAM/PLM/MDC systems, process optimization, education and support of technical, engineering and manufacturing softwares for 20 years in Hungary. Since its foundation, our company was driven by one goal which is to help companies in product development and manufacturing fields in the most efficient way and at the highest professional standards to tackle their technical challenges.

Today EuroSolid Ltd is one of the market leaders and has more than 800 partners with references such as Michelin, Aloca, Coloplast, GE or Linamar.

Our company is the sole and exclusive distributor of SOLIDWORKS softwares in Hungary plus the only qualified education and support centre in the country. As the representative of SOLIDWORKS, our activities include professional client support, data management system installation, delivering and solving engineering tasks and performing different simulation tests with our softwares.

SOLIDWORKS is the market leading and the most integrated software system available. In the past 25 years the CAD software has grown out to become the foundation of a wide ranged product portfolio which not only includes engineering design and simulation but also electrical design, data management, quality management for inter- and post production processes, sheet-less sketch creation, rendering, technical documentation modules and so much more.

Our goal is to deliver solutions with the excellent tools, quickly-to-adapt and easy-to-learn systems of SOLIDWORKS and with the new technologies supporting design and manufacturing that ensure profitable investment and increasing productivity with optimized workflow for our clients.

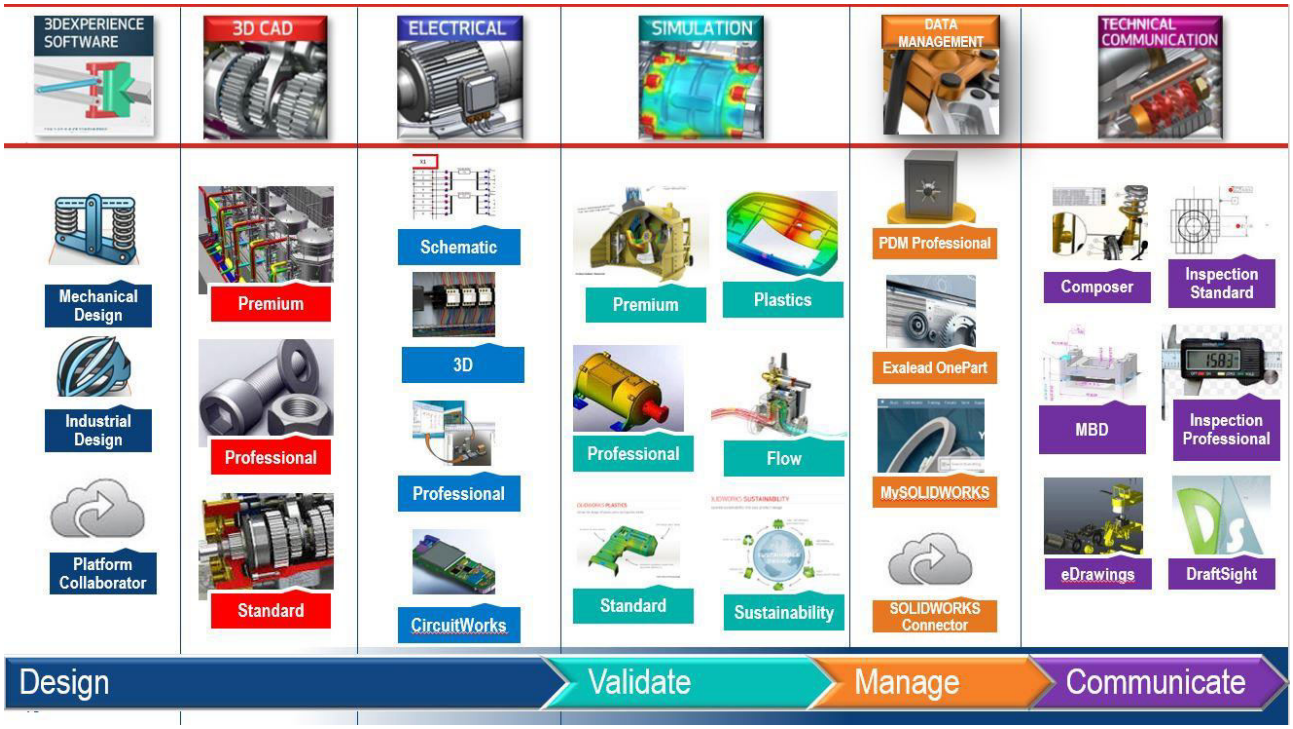

GYULAI IRÁNYÍTÁSTECHNIKAI KFT.
Address: 4030 Debrecen, Álmos utca 5-7.
Phone: +36-52-470-500
Webpage: www.gyulaikft.hu

GYULAI Irányítástechnikai Kft.
IPARI ELEKTROMOS MEGOLDÁSOK

GYULAI Irányítástechnikai Kft.
ELECTRIC SOLUTIONS FOR THE INDUSTRY

OUR OPERATING PROFILE:

- Wholesale trading of power-current and specialized industrial, automation and control engineering parts, devices, equipment
- Design and installation of power-current energy distributors, phase correctors
- Design and installation of control engineering and automation distributors, programming and implementation of the underlying processes (PLC controls)
- Automation of machines and technological processes, systems

WHOLESALE TRADING

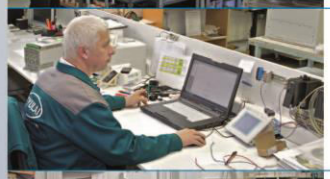

DESIGN

INSTALLATION
OF ELECTRIC DISTRIBUTORS

MANUFACTURING
AND OVERHAUL OF MACHINES

STANDARDIZED
CONSUMPTION-METERING BOXES

HOYA LENS MANUFACTURING HUNGARY PRIVATE CO.
Address: H – 4700 Mátészalka, Ipari út 18.
Phone: +36-44-502-831
Webpage: www.hoyavision.com

HOYA Corporation is a diversified, multinational company and leading supplier of innovative and indispensable high-tech and healthcare products. HOYA is active in two main business segments: The Life Care segment encompasses health care areas such as eyeglass lenses and the operation of contact lens retail stores, as well as medical related areas such as intraocular lenses for cataract surgery, medical endoscopes, surgical equipment and artificial bones and implants. HOYA´s Information Technology segment focuses on electronics products for the semiconductor industry and LCD panels, glass disks for HDDs and optical lenses for digital cameras and smartphones. The HOYA Group comprises over 100 subsidiaries and affiliates and over 34,000 people worldwide.

Life Care

HOYA has diversified its business portfolio with its optical technologies providing indispensable products to people´s lives. We strongly believe that by providing enduring solutions that meet needs in areas closely connected to people's lives, such as endoscopes, eyeglass lenses and intraocular lenses, it will be able to bring about changes in the quality of those lives.

Life Care Segment, Health Care

HOYA provides products and services to care for that most important sensory organ- the eye. HOYA started manufacturing eyeglass lenses in 1962 and contact lenses in 1972. Based on the optical and material technologies acquired since 1941, HOYA continues to contribute quality high value-added vision products to people around the world.

Eyeglass lenses

As a global manufacturer of eyeglass lenses, HOYA has passionately driven optical technology innovation with the aim of finding only the best vision solutions.

HOYA´s unparalleled technology creates a profoundly clear vision experience for the progressive lens wearer.
Integrated Double Surface Design (iD), HOYA´s patented, award-winning design technology, separates the surface geometry of progressive lenses into two components: vertical and horizontal, positioned individually on each of the two lens surfaces. Thanks to this technology, HOYA´s premium progressive lenses can be individually designed; each patient´s unique visual and lifestyle requirements can be integrated in the lens design to provide them with the most comfortable and accurate vision, tailored to their individual needs.

HOYA Vision Care Company is a global organization covering 52 countries with a network of over 12,000 employees and over 64,000 active accounts globally.

HOYA Lens Manufacturing Hungary private Co., Mátészalka

HOYA Lens Manufacturing Hungary private Co. is the largest unit of Hoya group in Europe based on the headcount and production volume as well. The past of the company and the nearness of the European market give a geopolitical advantage and stabile future for the company. A Belgian investor bought 50% of Optikai Művek factory's unit in 1991. In 1994 with total ownership the enterprise with mass production has been called Buchmann Optical Művek for 8 years. Hoya has bought the Buchmann-group in 1994, so the plant in Mátészalka also became a member of the japan lens production company. By now the company do partial serving of all affiliated companies in Europe.

TRUMPF HUNGARY KFT.
Address: 2220 Vecsés Lincoln u. 1.
Phone: +36-29-999-100
Webpage: www.trumpf.com

Our mission is to further develop and digitally connect production technology, to make it even more efficient, precise and future-proof. In doing so, we want to make manufacturing and its upstream and downstream processes more efficient. This is how we build the industrial world of tomorrow. We are market and technology leaders in machine tools and lasers for industrial manufacturing, and work with our innovations in almost every sector. Our software solutions pave the way to the Smart Factory, allowing us to implement high-tech processes in industrial electronics.

Our principles

We are a family-owned company. A readiness to fully commit oneself to the company in good times as well as bad is something that applies in equal measure to everyone who works for the company. We want to remain independent, and growth by our own efforts is decisive in this regard. Geographical proximity to our customers is also essential. Nevertheless, a powerful headquarters is necessary. All our dealings are characterised by fairness, moderation and trust.

Our objectives

We want to satisfy our customers, employees, owners and society in equal measure. In each of our sectors of activity and in all of our products and services, we are leaders on a world scale in terms of both technology and organisation. We strive to achieve continuous growth that is far above average for the sectors in which we are active. We aim for a return on sales that enables us to afford our high expenditure on research and development as well as investments made by our own efforts.

The Department of Mechanical Engineering is responsible for the mechanical engineering education on bachelor (BSc) and master (MSc) levels. The research activity of the department covers the mechanical engineering scientific area starting from the materials science to the specific fields (diagnostics, material handling, etc.). From 2015 we have introduced the dual training. At the moment we cooperate with 19 industrial partners.

DEPARTMENT STAFF

Tamás MANKOVITS PhD associate professor head of department *mechanics* *finite element method* 	**Sándor BODZÁS PhD** associate professor vice head of department *manufacturing,* *machine elements* 	**Sándor HAJDU PhD** associate professor vice head of department *material handling,* *mechanics* 
Lajos FAZEKAS PhD college professor *logistics,* *machine repairing* 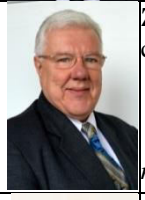	**Zsolt TIBA PhD** college professor *machine elements* 	**†Ágnes BATTÁNÉ GINDERT-KELE PhD** associate professor *manufacturing,* *machine elements* 
Levente CZÉGÉ PhD associate professor *process analysis,* *machine elements,* 	**György JUHÁSZ PhD** associate professor *machine elements,* *hydraulics and pneumatics* 	**László MOLNÁR** associate professor *finite element method* 
Sándor PÁLINKÁS PhD associate professor *materials science,* *manufacturing* 	**József MENYHÁRT PhD** assistant professor *process analysis,* *computer aided design* 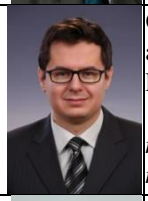	**Gábor BALOGH** assistant lecturer PhD student *materials science,* *manufacturing* 
Zsolt BÉKÉSI assistant lecturer PhD student *machine elements* 	**Krisztián DEÁK** assistant lecturer PhD student *diagnostics,* *mechanics* 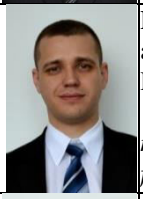	**Dávid HURI** assistant lecturer PhD student *mechanics,* *finite element method* 
András GÁBORA department engineer PhD student *materials science,* *technology* 	**Márton LÉVAI** department teacher *materials science,* *technology* 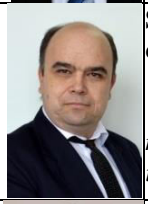	**Sándor ANDRÁSKÓ** department teacher *materials science,* *technology* 
Tibor PÁLFI department teacher *machine elements,* *computer aided design* 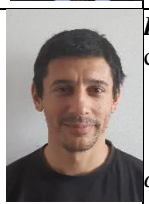	***Dániel NEMES*** department engineer *computer aided design* 	**Zoltán Gergő GÉRESI** CNC technologist *manufacturing* 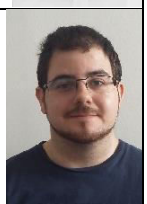
Lilla CSONKÁNÉ DÓRÓ administrative assistant 	**Szandra SITKU** administrative assistant 	**Department of Mechanical Engineering** **Faculty of Engineering,** **University of Debrecen** 4028 Hungary, Debrecen, 2-4 Ótemető Tel.: +36-52-512-900 E-mail: gepeszmernok@eng.unideb.hu Website: www.mecheng.unideb.hu 

Mechanical Engineering BSc Program

Automotive Production Process Control Specialization

The aim of the teaching program includes preparing engineers to improve quality and use lean tools in the vehicle industry, enabling them to gain an understanding of the complete product development (from the supplier to the customer) and lead project teams. In cooperation with local vehicle suppliers students learn about completing cost estimation, utilizing computer software to solve manufacturing problems.

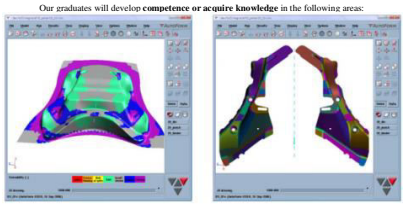

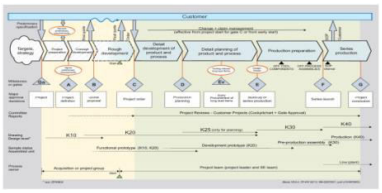

- introducing and applying modern technologies, computational engineering methods and systems (manufacturing technologies, CAE)
- operating and developing mechatronical systems (electrotechnics and electronics, measuring and automatics, hydraulics and pneumatics)
- designing and redesigning plant layouts, checking KPI systems robot technology, automation, etc.
- planning material handling and manufacturing processes
- analyzing, controlling and optimizing production processes
- applying modern manufacturing management philosophies (Lean management) in the vehicle industry

The **curriculum** contains the following **subject modules**:

Basic science subjects: 48 credits

- Mathematics, Technical Mechanics, Engineering Physics, Operation and Theory of Machines, Thermodynamics and Fluid Mechanics, Technical Chemistry

Economics and humanities subjects: 20 credits

- Economics for Engineers, Microeconomics, Basics of Quality Management, Management for Engineers, State Administration and Law, Introduction to Ethics

Professional subjects: 117 credits

- Informatics, Machine Elements, CAD and CAE, 3D Computer-Aided Design, Materials Science, Technology of Structural Materials, Electrotechnics and Electronics, Thermal and Fluid Machines, Manufacturing Processes, Logistics, Industrial Safety, Computational Engineering Methods and Systems, Measuring and Automatics, Hydraulics and Pneumatics, Mechanical System Engineering, Quality Management, Safety Engineering, Material Handling and Robotics, CAM, Manufacturing Planning, Maintenance Engineering, PLC.

Optional subjects: 10 credits

Thesis: 15 credits

Duration of studies: 7 semesters, Contact hours: 2.352

ECTS credits: 210, Internship: 6 weeks

Final exam:

- Defending the thesis (oral presentation and discussion)
- Exam in two subject areas chosen by the student
  - Production Process and Control, Production Optimization, Logistics
  - Assembling Technology, CAM, Quality Management

Mechanical Engineering BSc Program

Operation and Maintenance Specialization

The aim of the teaching program is to train mechanical engineers who are able to operate and maintain machines and mechanical devices, introduce engineering technologies and apply them, organize and control work phases, mechanical developments, solve the general problems of research and planning as expected by the labor market. Those having completed the specialization have in-depth theoretical knowledge to continue their studies in the second cycle.

Our graduates will develop **competence or acquire knowledge** in the following areas:

- introducing and applying modern technologies and computational engineering methods and systems (manufacturing technologies, CAE)
- operating and developing mechatronical systems (electrotechnics and electronics, measuring and automatics, hydraulics and pneumatics)
- operating and maintaining machines and mechanical devices (mechanical system engineering, heat and fluid machines)
- organizing and controlling operational processes, mechanical developments
- planning the construction and designing of the machine parts, devices and apparatus (machine element, CAD, finite element method)
- solving the general problems of research and planning as expected by the labor market (studies of administration and law, basics of quality assurance, management for engineers, safety engineering)
- carrying out diagnostic testing, assessing the reliability of machines and devices (fracture mechanics, non-destructive testing and diagnostics)

The **curriculum** contains the following **subject modules**:

Basic science subjects: 48 credits
- Mathematics, Technical Mechanics, Engineering Physics, Operation and Theory of Machines, Thermodynamics and Fluid Mechanics, Technical Chemistry

Economics and humanities subjects: 20 credits
- Economics for Engineers, Microeconomics, Basics of Quality Management, Management for Engineers, State Administration and Law, Introduction to Ethics

Professional subjects: 117 credits
- Informatics, Descriptive Geometry, Technical Drawing, Machine Elements, CAD and CAE, 3D Computer-Aided Design, Materials Science, Technology of Structural Materials, Electrotechnics and Electronics, Measurements and Automatics, Thermal and Fluid Machines, Manufacturing Processes, Logistics, Industrial Safety, Steel Constructions, Hydraulics and Pneumatic Machines, Fracture Mechanics, Manufacturing Planning, Diagnostics, FEM, PLC, Material Handling and Robotics, Drivetrain Optimization, Machine Repairing, Maintenance Engineering.

Optional subjects: 10 credits
Thesis: 15 credits
Duration of studies: 7 semesters, Contact hours: 2.352
ECTS credits: 210, Internship: 6 weeks

Final exam:
- Defending the thesis (oral presentation and discussion)
- Exam in two subjects chosen by the student
  - Machine Repairing,
  - and one subject chosen by the student:
    - Material Handling and Robotics
    - *or* Maintenance Engineering

Mechanical Engineering MSc Program

Production Engineering Specialization

The aim of the teaching program is to train engineers who are able to design and elaborate production processes and the conceptions of manufacturing technologies as well as can be responsible for modelling, designing, operating, maintaining, supervising and organizing production tasks. They are capable of providing the conditions of precise and up-to-date production and its processes (optimizing and developing production processes; designing and implementing devices and systems serving the production). The specialization considers the needs of the partner industrial companies.

Our graduates will develop **competence or acquire knowledge** in the following areas:

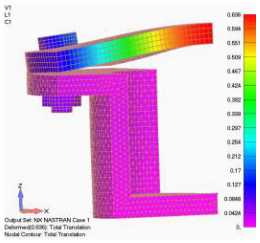

- applying modern computational engineering methods (CAD, CAM, CAE)
- supporting, optimizing and developing production systems and processes;
- designing of manufacturing and material handling systems,
- applying management methods and systems,
- supervising and organizing in production environment,
- applying expert systems (diagnostics and condition monitoring).

The **curriculum** contains the following **subject modules**:

Basic science subjects: 22 credits
- Mathematics, Applied Statistics, Modern Physics, Dynamics of Mechanical Systems, Thermodynamics and Fluid Mechanics, Advanced Material Science

Economics and humanities subjects: 16 credits
- Basics of Management, Quality Management, Financial and Advanced Economic Knowledge, Research Methodology

Professional subjects: 46 credits
- Measurement, Signal Processing and Electronics, Design of Engineering Structures, Engineering Modelling and Simulation, Manufacturing Equipments, Design and Quality Assurance of Manufacturing Processes, Assembly Automation, Design of Material Handling Systems, Production Logistics, Maintenance and Machine Repairing Technologies, Diagnostics and Condition Monitoring, Lean Production

Optional subjects: 6 credits
Thesis: 30 credits
Duration of studies: 4 semesters, Contact hours: 1.428
ECTS credits: 120, Internship: 4 weeks

Admission requirements for the Mechanical Engineering MSc program

Unconditional admission: Mechanical Engineering BSc:
Conditional admission by prescribing pre-master courses:
Materials Engineering BSc, Safety Engineering BSc, Energy Management BSc, Civil Engineering BSc, Industrial Design Engineering BSc, Vehicle Engineering BSc, Light Industrial Engineering BSc, Environmental Engineering BSc, Transportation Engineering BSc, Mechatronics Engineering BSc, Earth Science Engineering BSc, Technical Management BSc, Chemical Engineering BSc, Electrical Engineering BSc, Mechanical Engineering in Agriculture and Fodd Industry BSc
Final exam:
- Defending the thesis (oral presentation and discussion)
- Exam in two topics chosen by the student :
  - Production systems and processes (Design of Material Handling Systems, Production Logistics, Lean Production)
  - Manufacturing systems and processes (Manufacturing Equipments, Design and Quality Assurance of Manufacturing Processes)
  - Maintenance and operation (Maintenance and Machine Repairing Technologies, Diagnostics and Condition Monitoring)

Welcome in Debrecen for the

8^{th} International Scientific Conference on Advances in Mechanical Engineering (ISCAME 2020)

and

8^{th} Mechanical Engineering Exhibition

The Department of Mechanical Engineering
Faculty of Engineering, University of Debrecen